Manoeuvreergedrag van containerschepen in slibrijke vaarwateren

Manoeuvring Behaviour of Container Vessels
in Muddy Navigation Areas

Guillaume Delefortrie

Promotor: prof. dr. ir. M. Vantorre
Proefschrift ingediend tot het behalen van de graad van
Doctor in de Ingenieurswetenschappen: Scheepsbouwkunde

Vakgroep Mechanische Constructie en Productie
Voorzitter: prof. dr. ir. J. Degrieck
Faculteit Ingenieurswetenschappen
Academiejaar 2006 - 2007

UNIVERSITEIT
GENT

ISBN 978-90-8578-146-2
NUR 969, 974
Wettelijk depot: D/2007/10.500/20

MANOEUVRING BEHAVIOUR OF CONTAINER VESSELS IN MUDDY NAVIGATION AREAS

by

Guillaume Delefortrie

Promoter: prof. dr. ir. Marc Vantorre

Examining Board:

- prof. dr. ir. Ronny Verhoeven
  (Ghent University, chairman)
- prof. dr. ir. Jan Vierendeels
  (Ghent University, secretary)
- dr. David Clarke
  (University of Newcastle upon Tyne, UK)
- prof. dr. ir. Julien De Rouck
  (Ghent University)
- dr. ir. Katrien Eloot
  (Flanders Hydraulics Research, Belgium)
- Dr.-Ing. Andreas Gronarz
  (Entwicklungszentrum für Schiffstechnik und Transportsysteme, Germany);
- prof. dr. ir. Jean Marchal
  (Université de Liège, Belgium)
- prof. dr. Anthony Molland
  (University of Southampton, UK)
- prof. dr. ir. Marc Vantorre
  (Ghent University, promoter)

The experimental research and initial modelling (Chapters 4 – 8) was part of the research project *Determination of the nautical bottom in the harbour of Zeebrugge: Nautical implications*, carried out co-operatively by Ghent University and Flanders Hydraulics Research (2001-2004) and commissioned by T.V. Noordzee & Kust (Ostend, Belgium) – a joint venture of NV Baggerwerken Decloedt & Zoon, NV Dredging International and NV Ondernemingen Jan De Nul – in the frame of the optimisation of the maintenance dredging contract for the harbour of Zeebrugge, financed by the Department Maritime Access of the Flemish Authorities, Mobility and Public Works. The author performed his doctoral research as an assistant at Ghent University (2002-2007).

Flanders
Hydraulics
Research

Ghent University, Faculty of Engineering

PREFACE

This dissertation summarizes a five years long exciting research odyssey, which I could not have completed without the help of many persons.

In de eerste plaats wil ik de promotor van dit onderzoek, professor MARC VANTORRE, bedanken voor de interessante uitdagingen die me geboden werden. Evenzeer ben ik hem niet alleen dankbaar voor het vele nalezen van dit werk en ook van publicaties en rapporten, maar vooral voor het aanleren van de vele aspecten die scheepshydrodynamica behelzen.

I would like to thank the members of the examining board for having read this dissertation with interest and attention, so thank you professor MOLLAND and doctor CLARKE. *Vielen dank für Doktor GRONARZ. Un grand merci pour professeur MARCHAL. Dank voor de professoren VERHOEVEN, DE ROUCK en VIERENDEELS en doctor ELOOT.*

Building mathematical models would not have been possible without the experimental research in which the following persons had an important share. *Bedankt LUC VAN OSTAEYEN en LEONID VERZHBITSKIY (спасибо вы) voor het aanleren van de finesses van bediening van de sleepwagen of nog om je samen met me op te winden over dioc time outs en bulten in de bekleding. Bedankt GREET VAN KERKHOVE voor het verder opvolgen van de proeven eens het experimentele onderzoek op dreef was. Eveneens wil ik mijn voorganger BART WACKENIER bedanken voor het vele aankoopwerk en technische beslommeringen op zich te nemen die gepaard gaan met de opstart van experimenteel onderzoek.*

The processing of results and the setup of the adequate mathematical models has been possible thanks to the following persons. *KRISTIEN SEYNAEVE en* ELLADA *VERZHBITSKAYA (спасибо вы)*, *bedankt voor het schrijven van (vervelende en moeilijke) macro's in Excel en ander programmeerwerk. KATRIEN ELOOT, bedankt voor het inzicht in de wiskundige modellering.*

Carrying out simulation runs could not have been possible without the work of the following persons. *ERIK LAFORCE, bedankt voor je gedrevenheid in het nautische onderzoek. KAREL VANDEN BROECK, bedankt voor het delen van je kennis, niet enkel voor de simulator, maar nog meer voor de sleeptank. WERNER MARCHANG en GILLES VAN AVERBEKE wens ik te bedanken voor de grafische hoogstandjes die ze op het scherm toveren. Verder wil ik ook een speciale vermelding voor de loodsen van de haven van Zeebrugge (DABL) zonder wie de simulatorvaarten niet mogelijk zouden geweest zijn, eveneens een woord van dank voor TIM GODDERIS voor de bediening van de sleepboten.*

Of course a huge project comes with lots of administrative work. I would also like to thank these persons. *FRANS DEPUYDT, bedankt om het tekenwerk op u te willen nemen. Eveneens bedankt voor de soms welgekomen babbel, zodat ik niet al te veel in mijn onderzoek zou verdwalen. KARINE DE GRAUWE, bedankt voor de hulp bij het organiseren van de workshop Nautische Bodem.*

Parts of this investigation, such as the second real-time simulation programme and the analysis and preliminary modelling have been carried out by *SIMON VANDER DONCKT, hiervoor is een welgemeend proficiat op zijn plaats.*

I would like to mention my other colleagues at the Maritime Technology Division, for also having a share in this research, varying from tips in word processing, reporting or ship resistance and knowledge interchange for (non-financial) bank effects (*bedankt EVERT LATAIRE*), programming work (*HOANG-TRI TRAN, cảm ơn lắm*) or asking difficult questions during exercise classes (JEROEN VERWILLIGEN).

Doctoral research is a typical activity that is not restricted to office hours. Therefore some words of thanks for the people I see beyond 8 to 5. I would like to thank my wife ELISA for the time she spent alone while I went to classes to improve this thesis. Moreover I cannot quantify the support she gave me, even in the most difficult moments. *DOMINIQUE en FRANÇOISE (ook gekend als pa en ma) merci voor de continue steun in hetgeen ik doe. Dankzij jullie ben ik bijvoorbeeld nog op tijd in Gent geraakt voor het toelatingsexamen burgerlijk ingenieur. Het kan van heel kleine dingen afhangen ;-). Bedankt ook GENEVIÈVE, SÉBASTIEN en MARIE-LAURE om iets minder lawaai te maken gedurende de examens, maar nog meer voor het plezier dat we beleefden gedurende de welverdiende vakanties. JULIO, REBECA, ANDREA y SANTIAGO muchas gracias por los momentos divertidos que pasamos juntos en Argentina y Perú que me permitieron ponerme las pilas para seguir adelante con mis investigaciones. Bedankt FREDERIK en KADIR voor het samen maken van programmeerprojecten.*

I am also very proud that part of my research has been honoured by the Japanese Society of Naval Architects and Ocean Engineers ありがとお ございます。

Finally I want to thank YOU, reader, for the interest you have in this research, I hope you will enjoy the reading.

SUMMARY

Scope

To asses the navigability in muddy navigation areas the nautical bottom concept was introduced, according to the International Navigation Association:

The nautical bottom is the level where physical characteristics of the bottom reach a critical limit beyond which contact with a ship's keel causes either damage or unacceptable effects on controllability and manoeuvrability.

The nautical bottom is mostly determined based on a density value as critical limit. The choice of the critical parameter is merely based upon the feasibility to continuously monitor the density of a mud layer, however, it is only a surrogate for the so-called rheological transition. Moreover, according to the nautical bottom criterion knowledge on ship behaviour in muddy areas is also needed.

Experimental research

A common practice to gather knowledge on ship behaviour is the execution of model tests. One of the major problems when a mud layer is involved is the search for an accurate model for the mud behaviour. Mud behaves rather complexly and is subjected to time dependence. Furthermore its characteristics vary with the depth. The model tests that have been carried out mostly use an artificial mud layer. Because of the time dependence of the mud layer it is difficult or even impossible to repeat several tests under the same natural mud conditions.

In most cases an artificial mud layer was used having a constant density and viscosity in function of the depth. One research institute, SOGREAH (1989), included a gradient for the density. The early research programs were however limited in time or technology. MARIN (1976) only carried out some captive manoeuvring runs, while Flanders Hydraulics Research (1984-1989) did not even have a towing tank. Those three research institutes were the only ones that performed experimental research on muddy navigation conditions.

Hence, the results of these programs cannot be generalized, however some common interesting observations were made such as the occurrence of undulations of the water-mud interface and the drop in the speed-propeller rate characteristic, which can be ascribed to the decreased propeller efficiency due to the undulations that disturb the inflow of the propeller.

An additional problem in the execution of model tests are the scaling effects. Froude's law is commonly chosen to scale ship models. In this case both model and full scale density are equal. A scaling correction is determined for the ship resistance according to the ITTC 1978 recommendations. To take the effect of the mud layer into account a weighted Reynolds number has been used, based on the amount of wetted hull surface in contact with the mud layer. Other methods are also possible, such as:

- The determination of a weighted frictional resistance coefficient based on the amount of wetted hull surface in contact with the mud layer. This however yields larger reductions in case of low density mud layers;
- The determination of the resistance coefficient based on the vertical velocity distribution in water and mud layer.

The experimental research can be supported by theoretical calculations which show that a shallow water approach can be used to model the effect of a mud layer.

Because of the limited character of the research programs carried out in the past, a new research program was initiated, consisting of captive manoeuvring tests in Flanders Hydraulics Research shallow water tank and both fast- and real-time simulation runs. The mud layer was simulated with a mixture of chlorinated paraffins and petroleum. A wide range of viscosities and densities has been tested covering the typical mud viscosities and densities in the harbour of Zeebrugge. The artificial mud layer was however chemical aggressive so that a special coating in the tank was needed.

Tests were carried out with three ship models: a model of a 6000 TEU container carrier, a 8000 TEU container carrier and a bulk carrier. Most runs were carried out with the first ship model as this one was the standard type of vessel for the harbour of Zeebrugge at that time. Mud layer thicknesses were varied from 0.75m till 3.00m and under keel clearances referred to the water-mud interface from -12.2% till +21% of draught.

Mathematical modelling

With the results of the captive manoeuvring runs a four quadrant harbour manoeuvring model has been built in three stages. The mathematical model is a modular one and takes the physical background as much as possible into account. In a first stage a separate set of coefficients was determined for each combination of under keel clearance, mud composition and mud layer thickness. With this mathematical model simulation runs have been carried out.

The disadvantage of a separate set of coefficients for each condition, is that only mud layers corresponding with the ones of the experimental program could be simulated. To tackle this problem a new mathematical model has been built. The second stage lead consequently to a mathematical model that took the under keel clearance effect into account. Starting from this mathematical model the real depth was replaced by a so-called hydrodynamically equivalent depth in a third stage. The hydrodynamically equivalent depth takes the watery behaviour of the mud layer into account by means of a newly defined fluidization parameter. With the fluidization parameter the manoeuvring behaviour of a 6000 TEU container carrier above a whole range of mud layers, whose conditions are within the boundaries of the experimental program, can be modelled.

It is even possible to predict the manoeuvring behaviour of thinner mud layers by using an interpolation formula. Prediction of the manoeuvring behaviour

above mud layers of lower viscosity and density is also possible, but as the undulations of the interface are likely to behave differently, the prediction precision will not be that accurate. Finally the fluidization parameter based on the regression analysis with a 6000 TEU container carrier, can be applied to any deep drafted vessel, with known mathematical model in function of the under keel clearance.

Simulation runs

Both fast- and real-time simulation runs based on the first stage of the mathematical model have been carried out. With the assistance of the Zeebrugge pilots a redefinition of the nautical bottom criterion resulted possible. Ship manoeuvring behaviour in the harbour of Zeebrugge was subjected to the following constraints:

- Sufficient speed development;
- Sufficient controllability by own means;
- Sufficient tug assisted controllability.

The assessment of the criteria lead to a new critical limit of 1.20 ton/m³, if at least 2x45 ton bollard pull tug assistance is available. However the penetration of mud layers of a lower density is also restricted to:

- 0% under keel clearance for assistance of 2 tugs of 30 ton bollard pull and less;
- -7% under keel clearance if 2x45 ton bollard pull tug assistance is available;
- -12% under keel clearance in case of 2x60 ton bollard pull tug assistance.

These conclusions are only valid in moderate wind conditions for 6000 TEU container carriers. However the methodology can be applied to any vessel or harbour. The new critical limit lead to the admittance of deeper drafted vessels and an optimization of the maintenance dredging works in the harbour Zeebrugge, without jeopardizing the safety.

SAMENVATTING

Probleemstelling

Om het probleem van de manoeuvreerbaarheid in slibrijke vaarwateren aan te pakken werd door de International Navigation Association het concept nautische bodem ingevoerd:

De nautische bodem is het niveau waar de fysische karakteristieken van de bodem een kritische limiet bereiken. Overschrijding van deze limiet leidt tot schade of tot onaanvaardbare effecten voor de controleerbaarheid en manoeuvreerbaarheid.

Als kritische limiet om de nautische bodem te definiëren wordt meestal een densiteitswaarde gekozen. Die keuze steunt voornamelijk op het gemak om continue metingen van de slibdensiteit te kunnen uitvoeren. Anderzijds is de densiteit veeleer een surrogaat voor de rheologische gedragsovergang in de sliblaag. Bovendien is op basis van het concept nautische bodem eveneens kennis omtrent het scheepsgedrag in slibrijke vaarwateren nodig.

Experimenteel onderzoek

Het verzamelen van kennis door het uitvoeren van modelproeven is een frequente praktijk om het scheepsgedrag te achterhalen. In het geval van sliblagen is één van de grootste problemen het zoeken van een adequaat model om het gedrag van slib te voorspellen. Slib gedraagt zich immers complex en tijdsafhankelijk. Daarenboven variëren de slibkarakteristieken met de diepte. Derhalve werden de meeste modelproeven uitgevoerd boven een kunstmatige sliblaag. Wegens de tijdsafhankelijkheid van de sliblaag is het moeilijk of zelfs onbegonnen werk om modelproeven te herhalen boven gelijkblijvend natuurlijk slib.

In de meeste gevallen werd kunstmatige slib gebruikt met een constante densiteit en viscositeit in functie van de diepte. Eén onderzoeksinstituut, SOGREAH (1989), paste een densiteitsgradiënt toe. De vroegere onderzoeks-programma's waren gelimiteerd in tijd of technologie. MARIN (1976) heeft maar enkele gedwongen manoeuvreerproeven uitgevoerd, terwijl het Waterbouwkundig Laboratorium (1984-1989) zelfs geen sleeptank ter beschikking had. Dit waren de enige drie onderzoeksinstituten die experimenteel onderzoek verricht hadden naar het manoeuvreergedrag in slibrijke vaarwateren.

Gezien de beperkingen zijn de resultaten van deze onderzoeksprogramma's niet algemeen toepasbaar. Wel waren er enkele interessante bevindingen, zoals het optreden van oscillaties van de water-slib interface en de afname in de snelheids-rpm-karakteristiek, hetgeen een gevolg is van een verminderd schroefrendement door een verstoring van de aanstroming van de schroef veroorzaakt door de rijzingen van de interface.

Een bijkomend probleem bij het uitvoeren van modelproeven zijn de schaaleffecten. Scheepsmodellen worden doorgaans opgeschaald volgens de wet van Froude, hetgeen leidt tot een zelfde slibdensiteit op modelschaal als in werkelijkheid. Een opschalingcorrectie voor de weerstand kan bepaald worden aan de hand van de ITTC 1978 procedure. Om het effect van de sliblaag mee op te schalen werd een gewogen Reynoldsgetal gebruikt dat gebaseerd is op de verdeling van het natte scheepsoppervlak in contact met de sliblaag. Andere methoden zijn eveneens mogelijk, zoals:

- Het gebruik van een gewogen wrijvingsweerstandcoëfficiënt gebaseerd op de verdeling van het natte scheepsoppervlak in contact met de sliblaag. Dit geeft echter aanleiding tot merkelijk hogere reducties in het geval van sliblagen van een lage densiteit;
- Het begroten van de weerstandscoëfficiënt gebaseerd op de verticale snelheidsverdeling in de water- en in de sliblaag.

Het experimenteel onderzoek wordt ondersteund door theoretische berekeningen die aantonen dat een ondiep water benadering gebruikt kan worden om het effect van een sliblaag te voorspellen.

Wegens het beperkte karakter van de onderzoeksprogramma's uit het verleden, werd een nieuw experimenteel programma opgestart, bestaande uit gedwongen manoeuvreerproeven in de sleeptank van het Waterbouwkundig Laboratorium evenals fast- en real-time simulatieruns. De sliblaag werd gemodelleerd door een mengsel van gechloreerde paraffines en petroleum. Een groot bereik aan viscositeiten en densiteiten, zoals die voorkomen in de haven van Zeebrugge, werd beproefd. Het kunstslib was echter chemisch agressief, zodat een speciale bekleding nodig was voor de sleeptank.

Proeven werden uitgevoerd met drie scheepsmodellen: een model van een 6000 TEU containerschip, een 8000 TEU containerschip en een bulk carrier. De meeste proeven werden uitgevoerd met het eerste schip, aangezien dit in die tijd het standaardschip was voor de haven van Zeebrugge. De sliblaagdiktes werden gevarieerd van 0.75m tot 3.00m en de kielspelingen ten opzichte van top slib van -12.2% tot +21% van de diepgang.

Wiskundige modellering

Met de resultaten van de gedwongen manoeuvreerproeven kon een vier kwadrantenmodel voor havenmanoeuvres gebouwd worden in drie stappen. Het wiskundige model is van het modulaire type en tracht de fysische achtergronden zoveel mogelijk in rekening te brengen. In een eerste stap werd een aparte set coëfficiënten bepaald voor iedere combinatie van kielspeling, slibsamenstelling en sliblaagdikte. Met dit wiskundige model werden dan de simulatieruns uitgevoerd.

Het nadeel van een aparte set coëfficiënten voor iedere conditie, is dat enkel de sliblagen, die overeenstemmen met deze uit het experimentele programma, gesimuleerd konden worden. Dit probleem werd opgelost door een nieuw wiskundig model. De tweede stap leidde dus tot een wiskundig model dat de

kielspeling in rekening bracht. Op basis van dit model werd dan gedurende de derde stap de werkelijke diepte vervangen door de hydrodynamisch equivalente diepte. De hydrodynamisch equivalente diepte houdt rekening met het waterige gedrag van een sliblaag door middel van een nieuw gedefinieerde fluïdizatieparameter. Met de fluïdizatieparameter kan het manoeuvreergedrag van een 6000 TEU containerschip voorspeld worden boven, en in contact met, een ganse reeks sliblagen, waarvan de eigenschappen binnen de grenzen van het experimentele programma liggen.

Het is zelfs mogelijk om het manoeuvreergedrag boven dunnere lagen te voorspellen aan de hand van een interpolatieformule. Het voorspellen van het manoeuvreergedrag bij sliblagen van lagere viscositeiten en densiteiten dan de experimenteel bepaalde is eveneens mogelijk, maar aangezien het gedrag van de rijzingen van de interface anders zal zijn, impliceert dit een lagere nauwkeurigheid. Tot slot kunnen de fluïdizatieparameters, bepaald aan de hand van regressieanalyses met het 6000 TEU containerschip, toegepast worden op eender welk diepstekend schip waarvan het wiskundige model in functie van de kielspeling boven een vaste bodem gekend is.

Simulatieruns

Zowel fast- als real-time simulatieruns, gebaseerd op het wiskundige model van de eerste stap, werden uitgevoerd. Met de hulp van de loodsen van de haven van Zeebrugge bleek een nieuwe definitie van de kritische limiet van de nautische bodem in de haven van Zeebrugge mogelijk. De voorwaarden voor een veilig manoeuvreergedrag in de haven van Zeebrugge waren:

- Voldoende snelheidsopbouw;
- Voldoende controleerbaarheid met de eigen middelen van het schip;
- Voldoende controleerbaarheid met sleepboothulp.

Het beoordelen van deze criteria heeft geleid tot een nieuwe kritische limiet van 1.20 ton/m³, op voorwaarde dat minstens 2x45 ton bollard pull sleepboothulp voorhanden is. Daarenboven is de indringing van sliblagen van een lagere densiteit eveneens beperkt tot

- 0% kielspeling als 2x30 ton bollard pull sleepboothulp of minder voorhanden is;
- -7% kielspeling als 2x45 ton bollard pull sleepboothulp voorhanden is;
- -12% kielspeling als 2x60 ton bollard pull sleepboothulp voorhanden is.

Deze besluiten gelden enkel bij matige wind en voor containerschepen met een lengte van 300 m. De gebruikte methodiek kan echter algemeen toegepast worden. De nieuwe kritische limiet heeft geleid tot het toelaten van schepen met een grotere diepgang en tot een optimalisatie van de onderhoudsbaggerwerken in de haven van Zeebrugge, zonder dat de veiligheid in het gedrang kwam.

TABLE OF CONTENTS

NOMENCLATURE

A	coefficient of σ^2	(kg^2m^2)
A_0	propeller disc area	(m^2)
A_R	rudder area	(m^2)
a_H	share of the hull in the rudder induced hull force	(-)
B	mud of density 1.18 ton/m^3 and viscosity 0.10 Pa.s	(-)
	Ship beam	(m)
	coefficient of σ	(kg^2m)
C	mud of density 1.15 ton/m^3 and viscosity 0.06 Pa.s	(-)
	coefficient of σ^0	(kg^2)
	resistance coefficient	(-)
C_B	block coefficient	(-)
C_D	drag coefficient	(-)
C_L	lift coefficient	(-)
C_Q	propeller torque coefficient	(-)
C_T	propeller thrust coefficient	(-)
C_u	bottom adhesion parameter	(kN/m^2)
D	ship model (6000 TEU container)	(-)
	mud of density 1.10 kg/m^3 and viscosity 0.04 Pa.s	(-)
$D_{(P)}$	propeller diameter	(m)
D_R	drift force acting on the rudder	(N)
d	discriminant	(#[1])
E	ship model (bulk carrier)	(-)
	mud of density 1.26 ton/m^3 and viscosity 0.28 Pa.s	(-)
F	force	(N)
	mud of density 1.20 ton/m^3 and viscosity 0.11 Pa.s	(-)
F_N	perpendicular force acting on the rudder	(N)
$F_{n(h)}$	Froude number	(-)
F_T	tangential force acting on the rudder	(N)
F_X	longitudinal force acting on the rudder	(N)
F_Y	lateral force acting on the rudder	(N)
G	mud of density 1.25 ton/m^3 and viscosity 0.33 Pa.s	(-)
H	mud of density 1.21 ton/m^3 and viscosity 0.19 Pa.s	(-)
h	depth	(m)
h*	hydrodynamically equivalent depth	(m)
I_{PP}	polar moment of inertia around the propeller shaft	(kgm^2)
I_{zz}	moment of inertia about the Z-axis	(kgm^2)
J	advance	(-)

[1] Dimension depends of the context.

K	propeller coefficient	(-)
K_Q	propeller torque coefficient	(-)
K_T	propeller thrust coefficient	(-)
$K_{1,2}$	parameter for selecting quadrants	(-)
k	form factor (Prohaska)	(-)
k_{HR}	straightening coefficient	(-)
L, L_{PP}, L_{OA}	ship length	(m)
L_R	lift force acting on the rudder	(N)
m	mass	(kg)
N	yawing moment	(Nm)
N_i	hydrodynamic derivative ($i = \dot{v}, \dot{r}$, uv, ur)	(#)
N'	non dimensional yawing moment	(-)
n	propeller rate	(rpm)
n_0	nominal propeller rate	(rpm)
$\dot{n}$	propeller acceleration	(1/s²)
Q_E	engine torque	(Nm)
$Q_{(P)}$	propeller torque	(Nm)
$Q_{R(udder)}$	rudder torque	(Nm)
P_D	propeller power	(W)
P_T	thrust power	(W)
r	yaw rate	(°/s)
$\dot{r}$	yaw acceleration	(°/s²)
S	wetted surface	(m²)
	cross section	(m²)
	Tug force	(N)
T	draught	(m)
	period	(s)
$T_{(P)}$	propeller thrust	(N)
T_z	dry sediment concentration	(%)
t	time	(s)
	thrust deduction factor	(-)
t_R	rudder deduction factor	(-)
U	ship model (8000 TEU container)	(-)
u	longitudinal velocity	(m/s)
u_P	longitudinal velocity at propeller	(m/s)
$\dot{u}$	longitudinal acceleration	(m/s²)
ukc	under keel clearance	(-)

ukc_{crit}	minimal under keel clearance at which contact between mud and ship occurs	(-)
V	ship velocity	(m/s)
v	sway velocity	(m/s)
$\dot{v}$	sway acceleration	(m/s²)
w_P	wake factor (thrust)	(-)
w_Q	wake factor (propeller torque)	(-)
w_{RX}	wake factor (longitudinal rudder force)	(-)
w_{RY}	wake factor (lateral rudder force)	(-)
X	longitudinal force	(N)
	Longitudinal axis	(-)
X_i	hydrodynamic derivative ($i = \dot{u}, v, r, \dot{v}, vv, rr$)	(#)
X'	non dimensional longitudinal force	(-)
x	longitudinal direction	(m)
x_{pivot}	position of the pivot point	(m)
x_G	longitudinal position of centre of gravity	(m)
x_H	application point of the force $a_H F_Y$	(m)
x_R	longitudinal position rudder stock	(m)
x_{RP}	distance between rudder stock and tip of propeller blades	(m)
x_r	application point sway force due to yawing	(m)
x_v	application point sway force due to sway	(m)
x_Y	application point sway force due to sway	(m)
x_δ	application point sway force due to rudder deviation	(m)
Y	sway force	(N)
	Lateral axis	(-)
Y_i	hydrodynamic derivative ($i = \dot{v}, \dot{r}$, uv, ur)	(#)
Y'	non dimensional sway force	(-)
y	lateral direction	(m)
Z	vertical axis	(-)
z	vertical direction	(m)
	sinkage	(m)
α	inflow angle of the rudder	(°)
	Propagation angle of the water-mud interface undulations	(°)
	parameter	(-)
β	drift angle	(°)
	Damping angle of the rising of the water-mud interface	(°)
	parameter	(-)
γ	yaw angle	(°)
	parameter	(-)

	shear rate	(1/s)
γ^*	apparent hydrodynamic angle	(°)
δ	rudder angle	(°)
δ_0	rudder asymmetry correction	(°)
ε	hydrodynamic angle	(°)
ε^*	apparent hydrodynamic angle	(°)
ζ	amplitude of a rising	(m)
η	dynamic viscosity	(m²s)
η_P	propeller efficiency	(-)
η_0	propeller open water efficiency	(-)
η_R	relative rotative efficiency	(-)
μ	dynamic viscosity	(Pa.s)
μ'	non-dimensional dynamic viscosity	(-)
ν	kinematic viscosity	(m²s)
ξ	proportion coefficient	(-)
	under keel clearance coefficient or function	(-)
Π	keel penetration parameter	(-)
ρ	density	(kg/m³)
σ	stability index	(1/s)
τ	shear stress	(Pa)
τ_0	initial rigidity	(Pa)
Φ	fluidization parameter	(-)
φ	phase shift	(°)
	solid material fraction in mud	(-)
φ^*	apparent hydrodynamic angle	(°)
χ	correlation angle	(°)
ψ	course, angle of the yawing table	(°)
ω	oscillation frequency	(1/s)
ω'	non dimensional oscillation frequency	(-)
ϑ	mud property	(-)

subscripts

1	water layer
2	mud layer
H	hull
P	propeller
R	rudder
S	tugs

superscripts

N	nature
m	model

In the world there is nothing more submissive and weak than water. Yet for attacking that which is hard and strong nothing can surpass it.

Lao-Tzu

CHAPTER 1

SHALLOW WATER RESEARCH

1.1 Challenges

1.1.1 Overseas trading

Mankind has always chosen to live in the vicinity of water, for the many advantages the location offers. Cities emerged alongside rivers or near shores. Soon emerged the idea of crossing the river or exploring the sea to meet new territories or engage trading activity with overseas populations, a process that has been going on until now. Trading is important as some resources can only be found in one country, while another nation may need them urgently. If the sea is between them the only option for a long time had been the transportation by ship.

In the last century the plane came in as a secondary option for overseas trading, but the ship offers a more economic mean of transportation, although a ship is remarkably slower than an airplane. One of the utmost advantages of transportation by ship is the massive capacity of goods that can be transported, combined with a small transport cost (in ton/mile) and a low emission per transported ton. Cargo can be transported either in bulk (wheat, petroleum,…), by container or in separate packages, but for all transportation types the highest efficiency is reached when transporting as many goods as possible in one trip.

The last decennia the vessel size has consequently been increasing significantly. Modern container carriers can transport up till 11 000 TEU[1] and even larger ships are being built. To provide this higher capacity the outer dimensions of the vessel are continuously expanding. On the other hand the dimensions of access channels and harbours cannot easily follow the expansion rate of the vessels. As a result larger vessels have to manoeuvre through relatively small access channels. The economic advantages result actually in scientific challenges that need to be resolved so that safety can be guaranteed any time. Some of those challenges are resumed in the next paragraphs.

Figure 1.1. Emma Maersk, the largest container carrier ever built, having a capacity of 11000 TEU, started sailing in September 2006.

[1] TEU: Twenty feet Equivalent Unit: size of a standard container: 20x8x8 ft³, 1 ft = 0.3048 m.

1.1.2 Shallow water

As stated in the previous paragraph the depth of the navigation area is closely related to the vessel dimensions. A small fishing boat will be comfortable in a navigation area having a depth of 25 m, while a large crude carrier will already feel the effect of the restricted depth. To make a distinction between deep and shallow water the ship's draught is used. PIANC for instance proposes the following classification **[1.4]**:

- 3.0 < h/T — deep
- 1.5 < h/T < 3.0 — medium deep
- 1.2 < h/T < 1.5 — shallow
- 1.0 < h/T < 1.2 — very shallow

As vessels need to manoeuvre in shallow water the difficulty of the manoeuvre will increase. This is easily understandable when analysing the blockage, which is the proportion of the cross section of the vessel to the cross section of the channel.

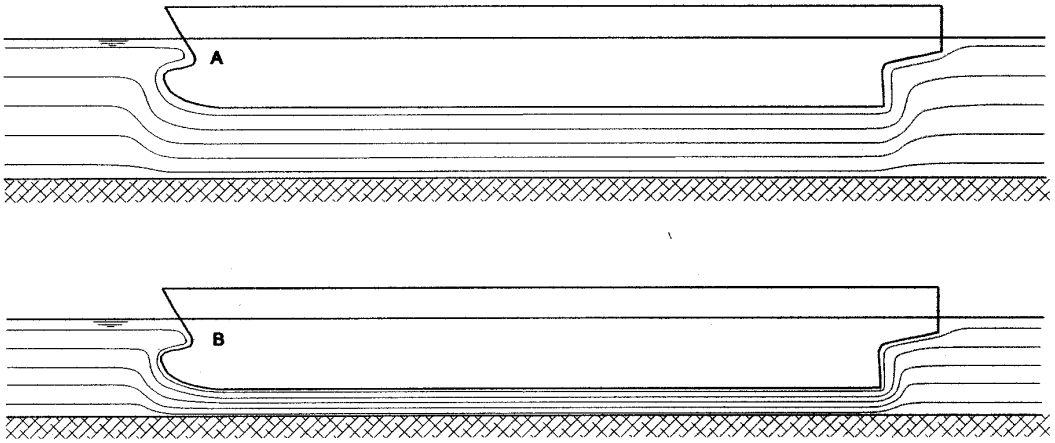

Figure 1.2. Influence of the under keel clearance on the flow lines.

A ship that is navigating has to push the water out of its way. When navigating in open seas there is plenty of space for the water to evacuate. In the case of rivers or channels the space is rather limited. When both ships in Figure 1.2 navigate at the same speed, the flow rate of the water is equal, but as the under keel clearance for ship B is smaller, the flow lines converge and the flow speed increases. According to Bernoulli's equation:

$$p_1 + \rho g z_1 + \frac{\rho V_1^2}{2} = p_2 + \rho g z_2 + \frac{\rho V_2^2}{2} \qquad (1.1)$$

an increase of flow speed at location 1 results in a decrease of pressure at location 1. One of the consequences of this pressure drop is a decrease of the water plane near the ship. To counteract this loss of buoyancy the ship will sink deeper into the water. As common ships do not have athwart symmetry the loss of buoyancy will be different between fore and aft of the ship, resulting in a

different sinkage and thus a trim. This combination of sinkage and trim is referred to as squat. The squat will be larger in shallow water and the probability of bottom touching will increase.

Another effect of the changed blockage is that due to the dropped pressure the hydrodynamic forces will increase. The manoeuvring behaviour of the ship will be more difficult:

- The size of the ship's turning circle increases with decreasing depth;
- The straight-line stability of the ship decreases with the water depth in the medium deep water range, but will increase significantly with the water depth in the (very) shallow water range;
- The lateral deviations during a stop are larger in shallow water.

1.1.3 Lateral boundaries

The navigation is not only restricted in a vertical sense, but also in lateral sense. When navigating in the middle of a symmetric access channel the water can as easily evacuate along the starboard side as it would do along the port side. However when the ship draws closer to one of the channel boundaries the flow around the hull will be influenced by the presence of this boundary, and consequently the hydrodynamic forces acting on the ship will be affected.

According to **[1.6]** the effects of the presence of a lateral boundary can be classified as follows:

- *Bank effects* due to a ship's motion parallel to the bank and/or propeller action;
- *Cushion effect*: the lateral force acting on a ship hull moving laterally at constant speed towards a solid boundary increases with decreasing bank clearance;
- Lateral restrictions influence a ship's frequency domain characteristics and, therefore, hydrodynamic *memory effects* occurring in case of large accelerations or decelerations.

1.1.4 Ship-ship interaction

With increasing shipping traffic, the manoeuvring behaviour is also affected by other lateral boundaries such as encountering and overtaking ships. The effect is equal as the lateral boundary of a bank, but in case of ship-ship interaction the forces are not constant, but transient in time. The time dependence results in a sequence of repulsion and attraction for the forces acting on both ships during the manoeuvre.

This is also of importance when a ship is passing a moored ship. Mooring lines can possibly break due to the ship-ship interaction forces and consequently jeopardize the safety.

Figure 1.3. Huge shipping traffic near the harbour of Singapore.

1.1.5 Waves

Whereas in protected navigation areas the effect of waves can be omitted such is not the case in near shore conditions at sea. To reach the ports of Zeebrugge (see Appendix F for the port map) and Antwerp ships have to travel through the Scheur, see Figure 1.4, which depth is not unlimited. Due to the waves the ship is subjected to heave and pitch (see Figure 1.5 for the different degrees of freedom), consequently a ship with an increased draught will have - in the same condition as other vessels – a higher probability to touch the bottom.

Figure 1.4. Satellite picture of the northern Belgian North sea coast with the Scheur (3-4), the access channel to Zeebrugge harbour: Pas van het Zand (5) and the Scheldt estuary (6). Readers can also appreciate the differences in rural planning between Belgium and The Netherlands. ©Eurosense Belfotop NV.

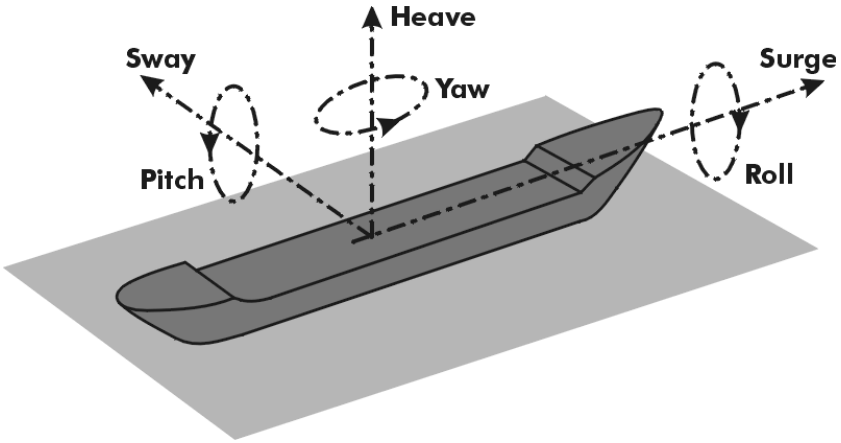

Figure 1.5. Six degrees of freedom of a vessel.

1.1.6 Muddy bottom

Until now the bottom of a harbour or access channel was considered to be solid. In reality this is not always the case. Due to the erosive effect of the current in rivers, particles are transported over a certain distance until they settle again. If those settlements are concentrated at a certain position the formation of a mud layer is possible, depending on the grain size. To avoid excessive formation of mud layers maintenance dredging works are needed so that a minimal under keel clearance can be guaranteed.

The question arises how much of the present mud layer has to be dredged. The mud layer consists of a material which characteristics change with the depth. In general the mud characteristics like viscosity or density increase with increasing depth. Therefore the upper part of the mud layer can rather be considered as black water. If the ship's keel touches this upper part it is unlikely that any damage can occur, on the other hand when a ship navigates above a mud layer an undulation of the water mud interface can be observed. This undulation can possibly have adverse effects on the manoeuvring behaviour of the vessel.

For these reasons PIANC has introduced the nautical bottom concept **[1.5]**:

The nautical bottom is the level where physical characteristics of the bottom reach a critical limit beyond which contact with a ship's keel causes either damage or unacceptable effects on controllability and manoeuvrability.

The nautical bottom concept can be applied to any bottom so that safety and manoeuvrability for the shipping traffic can be guaranteed.

1.2 Research on manoeuvring behaviour in restricted waters

Research on the manoeuvring behaviour in restricted waters is one of the main research topics of the Maritime Technology Division at Ghent University. This research is carried out in close collaboration with Flanders Hydraulics Research (FHR), Flemish Authority, Antwerp. Both institutions aim to gather a thorough knowledge on ship manoeuvring behaviour in restricted water, a common condition in Belgian waterways and harbours.

The nautical research at FHR took a huge step forward in 1989 with the installation of a ship manoeuvring simulator. In 1992 a shallow water towing tank was built to provide the ship manoeuvring simulator with realistic shallow water data. Both the towing tank and the simulator have been refurbished at several occasions to guarantee and enhance the quality of the data. The development of mathematical models is therefore mainly based on captive model testing.

In the future both institutions aim to gather further knowledge by converting the captive manoeuvring towing tank in a way that free running tests can be carried out as well. The main objective for both research institutes in the following years will remain the safe and economic access to the Belgian harbours.

1.2.1 Towing tank

1.2.1.1 Overview

The shallow water towing tank of Flanders Hydraulics Research **[1.7]** is equipped with a planar motion carriage, a wave generator and an auxiliary carriage for ship-ship interaction tests. Its main dimensions are:

- Length over all 88.0 m;
- Useful length 67.0 m;
- Width 7.0 m;
- Maximum water depth 0.5 m;
- Ship model length 3.5 - 4.5 m.

The dimensions of the ship models are preferably as large as possible to avoid scale-effects (see Appendix E). Ship models with a length of 300 m can be modelled at a scale of 1 to 75. A general layout of the tank can be found in Figure 1.6. The dimensions of the towing tank are rather small in comparison with other tanks. The main purpose of bigger towing tanks is the determination of resistance. Larger ship models, higher speeds and thus a larger run-up are needed. In case of manoeuvring tests, speeds are usually lower and smaller ship models can be used. The maximum water depth is also sufficient, as it allows depth to draught ratios up till 250%, which is more than enough to perform runs in shallow water conditions.

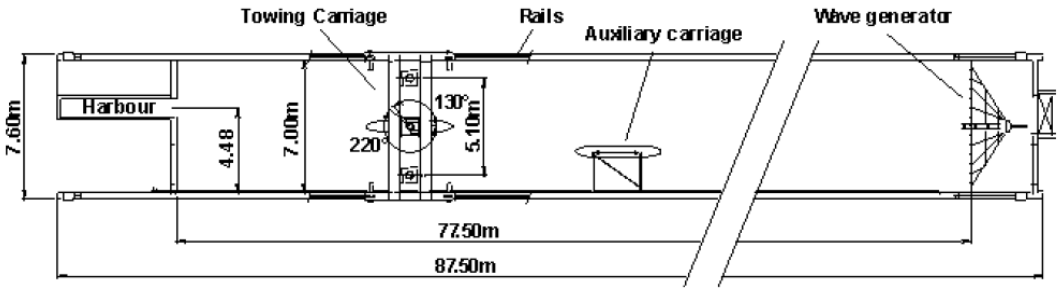

Figure 1.6. Flanders Hydraulics Research: general layout of the towing tank

The instrumentation of the tank is as follows (see Figure 1.7):

- 4 x 2 dynamometers for longitudinal and lateral forces (20, 50, 100, 200 N);
- dynamometers for roll moment;
- measurement of propeller rpm;
- 2 propeller thrust and torque dynamometers (30 N, 0.5 Nm);
- measurement of vertical motion (due to squat or wave action) at 4 measuring posts;
- measurement of rudder angle;
- 2 rudder force and moment dynamometers (50 N, 2 Nm);
- wave height measurement devices.

1 rudder mechanism
2 rudder control system
3 leakage pump
4 battery
5 thrust & torque meter
6 propeller motor
7 propeller rate of turn meter
8 amplifier
9 sinkage measurement (4x)
10 long. dynamometer (2x)
11 lateral dynamometer (2x)
12 roll moment measurement
13 propeller control
14 leakage alarm
15 limit vertical motion (4x)
16 vertical guidance
17 pitch and roll mechanism

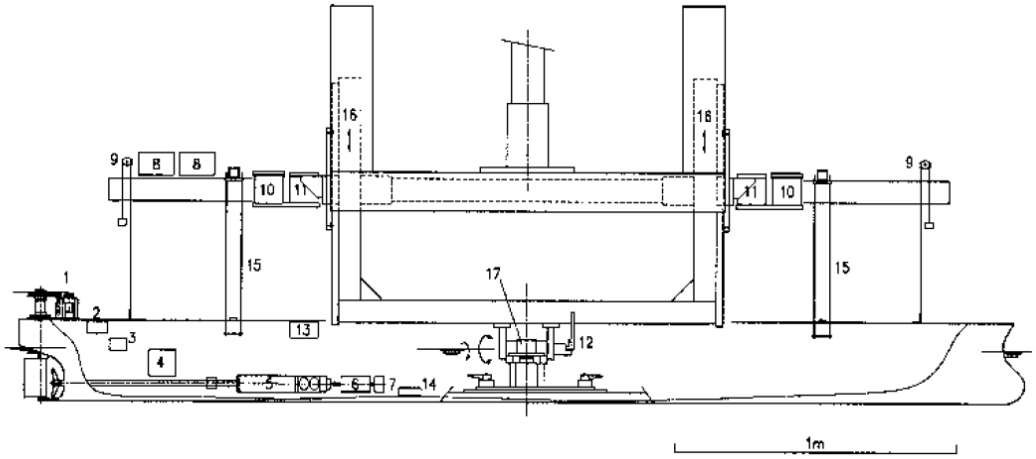

Figure 1.7. Ship model instrumentation

The installation is fully computer controlled, so it can be operated unmanned 24/7.

Carriage

The rails on which the carriage moves are aligned with high accuracy: the level difference of both rails and the lateral deflection of the guiding rail are less than 0.5 mm. The main carriage is a rectangular frame, composed of two wheel girders, connected by two box girders. A lateral carriage is guided between the transversal girders and carries a slide in which a yawing table is incorporated. This slide can be positioned in vertical sense over 0.4 m to take account of the water level. The ship model is connected to the carriage by means of a mechanism which allows free heave and pitch; roll can be restrained or free. In the horizontal plane, a rigid connection is provided.

The computer reads the trajectories, i.e. the positions of the vessel in function of time, and steers up to four 7.2 kW servomotors for the main carriage, a 4.3 kW servomotor for the lateral carriage and a 1.0 kW servomotor for the yawing table.

The maximal longitudinal speed is 2 m/s at a maximal acceleration of 0.4 m/s². An overview of all the characteristics of the movement is given in Table 1.1.

Table 1.1 Characteristics of the movement of the carriage

Movement	Position		Velocity		Acceleration
	minimal	maximal	minimal	maximal	maximal
longitudinal	0.000 m	67.000 m	0.050 m/s	2.000 m/s	0.40 m/s²
lateral	-2.550 m	2.550 m	0.000 m/s	1.300 m/s	0.70 m/s²
yawing	-130.0°	220.0°	0.000°/s	16.000°/s	8.00°/s²

Wave generator

The piston type wave maker, allowing generation of both regular and irregular waves, is driven by an electro hydraulic unit with following kinematics:

- Stroke: 0.3 m;
- Velocity: 0.6 m/s;
- Acceleration: 4.4 m/s².

Auxiliary carriage

In order to carry out ship-ship interaction tests, the tank is equipped with an auxiliary carriage allowing a second ship model to perform a prescribed speed history along a straight trajectory, with a maximum speed of 1.2 m/s.

Control and data acquisition

The three motion modes, the wave generator, rudder, propulsion, the auxiliary carriage and other external devices are controlled by a PC and six DIOCs (Direct Input Output Control). The DIOCs also assure the sampling of the analogue input signals:

- Number of channels 6 x 8;
- Resolution 12 bit;
- Max. sampling frequency 40 Hz.

1.2.1.2 Execution of tests

Test runs are executed in batch mode. After each run a waiting time, varying from 20 to 40 minutes, is included so that the water in the tank – or the underlying mud layer – can settle down to its initial calm state.

Input files for the computer on the carriage can be created offline and basically tell the computer how the kinematical parameters, propeller and rudder angle vary during a test run. Each run is validated with a checksum, so that the ship model cannot collide with the tank boundaries or any obstacles placed into it. Before execution the checksum will be validated online. In order to operate safely in an unmanned way, additional controls are included, such as a monitoring of unacceptable forces. Those controls can abort the execution of the run before any harm to the installation occurs.

During tests the following data is registered:

- Longitudinal force fore: X_{fore} [N]
- Longitudinal force aft: X_{aft} [N]
- Sway force fore: Y_{fore} [N]
- Sway force aft: Y_{aft} [N]
- Sinkage fore, starboard: z_{fore_sb} [mm]
- Sinkage fore, port: z_{fore_p} [mm]
- Sinkage aft, starboard: z_{aft_sb} [mm]
- Sinkage aft, port: z_{aft_p} [mm]
- Propeller rate: n [rpm]
- Rudder deflection: δ [°]
- Propeller thrust: T_P [N]
- Propeller torque: Q [Nmm]
- Longitudinal rudder force: X_{rudder} [N]
- Lateral rudder force: Y_{rudder} [N]
- Rudder torque: Q_{rudder} [Nmm]

In some cases the undulations of the water layer and the water-mud interface were measured too, which adds the following data:

- Rise of the water layer [mm]
- Undulation of the water-mud interface [mm]

To generate the input files the user of the towing tank makes ASCII files (with extension .geg) telling what the carriage should do. An example of such a file is given in Figure 1.8.

```
TYPE STATX0 (type of the test run)
BTCWACHT 2000 (waiting time in seconds before the run should start)
BTCNAAM QXCA (name of the batch)
TWACHT   1 (additional waiting time in seconds before start)
TIJK     10   (calibration time in seconds; measure all channels in order to know their offset)
OPTREK    M      9 (acceleration distance in meters)
VX       0.6 (regime velocity)
LCOND    10.5 10.5  (length in meters of the sub trajectories)
TV1        60  100     (code giving the working conditions in the different sub trajectories)
AFREM     M      9 (deceleration distance in meters)
TNAMEET  1 (additional waiting time in seconds before stop)
SCHIP       g:\sleept\resource\shp\schip.SHP (path to retrieve ship-characteristics)
OMGEVING    g:\sleept\resource\omg\SLIBX00.omg (path to retrieve environment)
DT       0.05 (steering pulse in seconds)
DTIJD    0.05 (measure every x seconds)
*    naam       Y        PSI        N       N1     N2  ROER    XBEGIN  ZIN
(    name       Y        PSI    % rpm                  rudder x-start heading)
*
@  QXCA00.tra   0         0        TV1      -      -    0         0     +
*
```

Figure 1.8. Example of a GEG data file.

With the provided .geg-files the program generates trajectory files, which gives the coordinates of the carriage in function of time. An example of such a file can be found in Figure 1.9.

For manoeuvring behaviour purposes the following classification of test types can be made:

1. STATIONARY tests

In this type of tests all kinematical parameters are kept constant during regime. The test can be divided in different sub trajectories in which a different rudder angle and/or propeller rate can be set.

```
* TYPE STATX0 (type of the test run)
* TRAJECT          VUCE58.TRA (name of the trajectory)
* trajectvariable   N1 en N2
* u                +0.456 m/s (longitudinal speed of the vessel)
* u0               +0.458 m/s (longitudinal speed of the carriage)
* dwarspositie     +1.435 m (lateral position of the ship model)
* drifthoek        +5.000 ø (drift angle)
NAAMSHP            U3F.SHP (name of the vessel)
NAAMOMG            OEVER28 (name of the environment)
DT                  0.050 (steering pulse in seconds)
NLIJN                  11 (number of coordinate lines)
*
    0.000  +0.00000000 +1.43500000 +5.00000000 +0.000 +0.000  +0.000 0 0 0 0 0
    1.000  +0.00000000 +1.43500000 +5.00000000 +0.000 +0.000  +0.000 0 0 0 0 1
   11.000  +0.00000000 +1.43500000 +5.00000000 +0.000 +0.000  +0.000 0 0 0 0 1
   59.050 +10.99864500 +1.43500000 +5.00000000 +0.000 +0.000  +0.000 1 1 0 1 1
  100.550 +29.99734500 +1.43500000 +5.00000000 +0.000 +0.000  +0.000 1 1 0 0 1
  126.750 +41.99170500 +1.43500000 +5.00000000 +0.000 +0.000  +0.000 1 1 0 1 1
  168.250 +60.99040500 +1.43500000 +5.00000000 +0.000 +0.000  +0.000 1 1 0 0 1
  198.800 +67.98330000 +1.43500000 +5.00000000 +0.000 +0.000  +0.000 1 1 0 0 1
  199.800 +67.98330000 +1.43500000 +5.00000000 +0.000 +0.000  +0.000 0 0 0 0 0
  199.850 +67.98330000 +1.43500000 +5.00000000 +0.000 +0.000  +0.000 0 0 0 0 0
  199.900 +67.98330000 +1.43500000 +5.00000000 +0.000 +0.000  +0.000 0 0 0 0 0
*
********************** SIGN trajectgeneratie =  17 **************************
* gevalideerd door VALID.BAS REV.1.1  22/8/1997 op 10-12-2006 om 12:20:45 uur.
SIGN 17
```

Figure 1.9. Example of a trajectory file for the towing tank

2. BOLLARD PULL tests

This type of tests, typically carried out to retrieve the propulsion characteristics, is carried out at zero speed and zero acceleration.

3. HARMONIC SWAY TESTS

The sway movement of the vessel is varied harmonically with time, while all the other parameters are kept constant.

4. HARMONIC YAW TESTS

Harmonic yaw tests are identical to harmonic sway tests, but in this case the yaw rate is varied harmonically with time.

5. MULTI-MODAL TESTS

In this case one or more parameters can be varied harmonically with time, while the others remain constant.

To have insight in the manoeuvring behaviour of the vessel, a program consisting of a combination of the above mentioned tests has to be carried out above each combination of under keel clearance and bottom condition (see Chapter 4).

More information about the different test-types can be found in **[1.2]**.

After execution of a test run the measured data is written to a text file with the extension .doc. This file consists of mainly two parts:

- The header contains all information on the run carried out: date, environment, ship, calibration data, etc.
- At each pulse: a line with measured forces, asked and given propeller rate and rudder deviation, sinkage, etc.

A first treatment of this huge amount of data is the computation of files with an extension .krt. These krt-files are the result of several actions:

- The average offset measured per channel during the calibration time is calculated and subtracted from the measured data;
- An average of the measured data is calculated over a larger time span, chosen by the user. For instance if measurements were carried out ten times per second, the average per second can be calculated.

The resulting krt-files contain still a considerable amount of data from a modelling point of view. Therefore dpt-files are computed which contain the following data:

- For stationary tests or bollard pull tests an average of all measured data is calculated per sub trajectory;
- For harmonic sway or yaw tests and for multi-model tests, an average is calculated x times per period[2], where the user may choose the number of times x.

In this work the mathematical models are determined starting from the dpt-files, where for each period 24 averages were calculated. An exception has been made for the calculation of the oscillations occurring in the second and fourth quadrant, which were determined based on the data in the krt-files.

[2] Another possibility is to carry out a Fourier analysis.

1.2.2 Ship manoeuvring simulator

1.2.2.1 Overview

Flanders Hydraulics Research has two full mission bridge simulators **[1.1,1.3]** which comply with the International Convention on Standards of Training, Certification and Watch keeping for Seafarers (STCW 1995). The newer simulator is named SIM360+, because of its 360 degrees horizontal view, with additional possibility of a lateral view of the ship's hull, while the older one has a 255 degrees horizontal view and a rear view: SIM255.

The arrangement of the ship manoeuvring simulator consists of a mock-up of a ship's navigation bridge, an operator's room and a classroom. The bridge has all necessary navigation equipment for steering different vessel types, including digital instruments that can be customized for each ship type, radar and an Electronic Chart Display Information System (ECDIS). The computer-generated perspective image of the surroundings is projected on the transparent screen around the ship's bridge.

Figure 1.10. Flanders Hydraulics Research: bridge of SIM360+.

In a separate room the operator of the simulator has a bridge interface, with visualisation of the ship's instruments and controls, at his disposition. He can select, develop, start and stop the voyages and control target ships, atmospheric conditions, lock doors, tugs, etc. The classroom can be used for the briefing and debriefing of the pilots.

On the simulator bridge, the pilots operate the control units, which emit an electrical signal to a computer. The force balance of the ship is determined at a frequency of 5 Hz, based on a mathematical model of the ship and its environment. The results are sent back to the bridge, so that the visualisation of the ship's instruments can be adapted, and to a graphic's computer which calculates the new surroundings.

Figure 1.11. Flanders Hydraulics Research: operator's room of SIM360+.

1.2.2.2 Mathematical model

A mathematical model resolves the force balance in three degrees of freedom: longitudinal movement, lateral movement and yawing (u,v,r). This set of equations is resolved in a fixed coordinate system.

The mathematical model can take the following parameters into account:

- Water depth;
- Currents;
- Ship hydrodynamics;
- Propeller and rudder forces;
- Bow and stern thrusters;
- Bow rudder forces;
- Wind forces;
- Wave forces,
- Bank effects;
- Collisions with fixed objects as berths;
- Anchor forces;
- Tug forces;
- Ship interaction forces;
- Winches.

1.3 Scope of this work

As can be seen from the comprehensive list in paragraph 1.2.2.2 many of the challenges mentioned in 1.1 have already been investigated thoroughly and partly implemented at the ship manoeuvring simulators at Flanders Hydraulics Research and elsewhere. An exception has to be made for the effects of a muddy bottom. To fill this gap is one of the main purposes of this work.

In Chapter 2 a review of the behaviour of mud layers will be given to offer the reader insight in its complexity. This is followed by the discussion of the state of

the art in Chapter 3. The need for additional research is explained in Chapter 4, as well as the experimental program that has been carried out.

From Chapter 5 on results of the new experimental program will be discussed, starting with the analysis of the undulations of the interface, followed by the construction of a comprehensive harbour manoeuvring mathematical model. The model was built in three stages, each one of it explained in Chapters 6, 9 and 10.

With the results of the mathematical model as described in Chapter 6 fast- and real-time simulation runs were carried out. The results of these runs are discussed in Chapters 7 and 8. Finally the applicability of the new mathematical model is covered in Chapter 11, followed by the conclusions and the opportunities for additional research in Chapter 12.

1.4 References

[1.1] *Beschrijving van de scheepsmanoeuvreersimulator 360+ van het Waterbouwkundig Laboratorium*. Internal document Flanders Hydraulics Research, 2004. (In Dutch)

[1.2] ELOOT K. *Selection, Experimental Determination and Evaluation of a Mathematical Model for Ship Manoeuvring in Shallow water.* Doctoral thesis, Ghent University, Faculty of Engineering, 2006, 414 pp.

[1.3] *Nautical Research – Ship Manoeuvring Simulator.* Internal document Flanders Hydraulics Research, 2004.

[1.4] PIANC. *Capability of ship manoeuvring simulation models for approach channels and fairways in harbours.* Report of Working group no. 20 of Permanent Technical Committee II. Supplement to PIANC Bulletin No. 77, 1992, 49 pp.

[1.5] PIANC/IAPH. *Approach channels – A guide for design, Final report of the joint Working Group PIANC and IAPH, in cooperation with IMPA and IALA.* Supplement to PIANC Bulletin, No. 95, 1997, 108 pp.

[1.6] VANTORRE M., DELEFORTRIE G., ELOOT K. *Modelling of ship-bank interaction forces.* Colloquium "The ship in interaction with the waterway", Duisburg, Germany, 2002.

[1.7] VANTORRE M. *Towing tank for manoeuvres in shallow water. Co-operation Flanders Hydraulics - Ghent University.* Internal document Flanders Hydraulics Research, 2002.

The mind of the people is like mud, from which arise strange and beautiful things.

W. J. Turner

CHAPTER 2

BEHAVIOUR OF MUD LAYERS

In this chapter an overview is given of the characteristics of mud. The aim of this chapter is not the study of the mud itself, but to give an insight in the difficulties that occur in defining the material, measuring it and predicting its behaviour.

2.1 Definition and formation of mud layers

According to **[2.24]** mud is a mixture of cohesive sediments and water. Sediment is matter deposited as a result of a number of processes, which can roughly be classified into natural and anthropogenic. Some examples of natural processes are erosion of soils due to rain, wind or currents. Important anthropogenic processes are waste water and dredging.

Cohesive sediments consist of a flocculated mixture of sand, silt, clay and organic matter. The flocculation depends on **[2.17]**:

- The electrolytic concentration;
- The values of the ions;
- The temperature of the mixture;
- The dimension of the hydrated ion;
- The dielectric constant;
- The pH value;
- The absorption capacity of the anions.

The influence of temperature can explain the seasonal variations that are observed in the mud layer of Zeebrugge, where the biggest variations occur in the winter **[2.8]**. The hypothesis that different organic material with varying seasons can have an influence cannot be confirmed **[2.20]**.

Depending on the proportion of each component in the mixture a different behaviour of the mud layer can be observed. An example of classification based on the distribution of particles can be found in Figure 2.1.

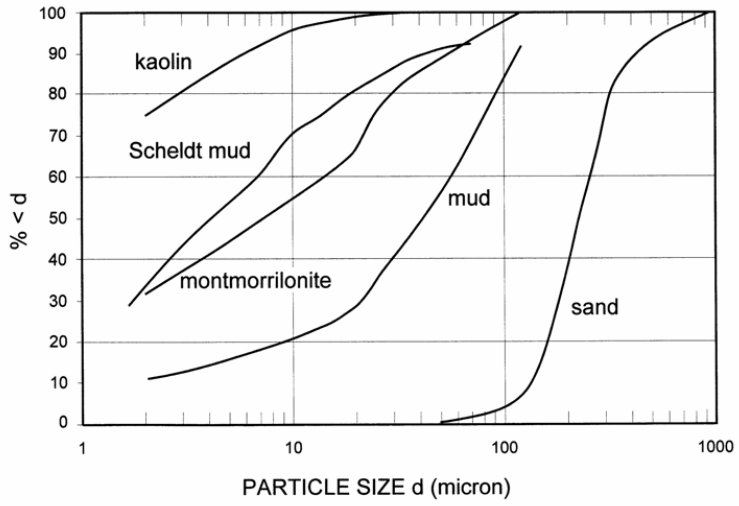

Figure 2.1. Classification of soft bottom layers, based on the distribution of particle size. Adapted from [2.24].

The actual formation of a mud layer depends on various aspects. In the first place transportation of matter must occur until it deposits at some point.

Transportation energy, i.e. kinetic energy, is mainly provided by currents, while gravity leads to settling. Particles are for example transported along a river, but when the river widens the flow will decelerate and gravity will overcome the kinetic energy so that the particles will deposit.

Formation of mud layers consequently occur at the mouth of rivers. Also tidal currents are important. Interaction between saline sea water and fresh water will enhance the deposition of particles. The location of harbours like the harbour of Zeebrugge favours the deposition of particles, so that a formation of a mud layer cannot be avoided. Anthropogenic processes can enhance this formation **[2.25]**.

2.2 Characteristics of a mud layer

In the previous paragraph it has been pointed out that due to a decrease of kinetic energy gravity made the particles settle down to deposit on the bottom of the seabed or channel. If an increasing amount of particles is settling down the base sediment layer will be subjected to increased pressure due to the weight of the upper layers. As a result water is expelled from the base layers and the sediments are compacted. This process is called *consolidation* and depends on the variation of *permeability,* which is the water flux through a unit gross sectional area, and the *effective stress*, which is the total stress minus pore water pressure **[2.1]**.

On the other hand the currents and waves in the upper water layer also affect the mud layer; the proportion of water in the mud layer can consequently increase. This phenomenon results in the opposite effect of consolidation, and is usually called *liquefaction* or *fluidization*, depending on which force weakens the mud layer. The term fluidization will also be used to denominate the proportion of the mud layer that behaves as water, see Chapter 10. The dredging industry also uses fluidization, which is the enhancement of the fluidization process of the mud by injection of air or water in the upper mud layer. The thus resuspended mud can be taken away by existing currents **[2.7]**.

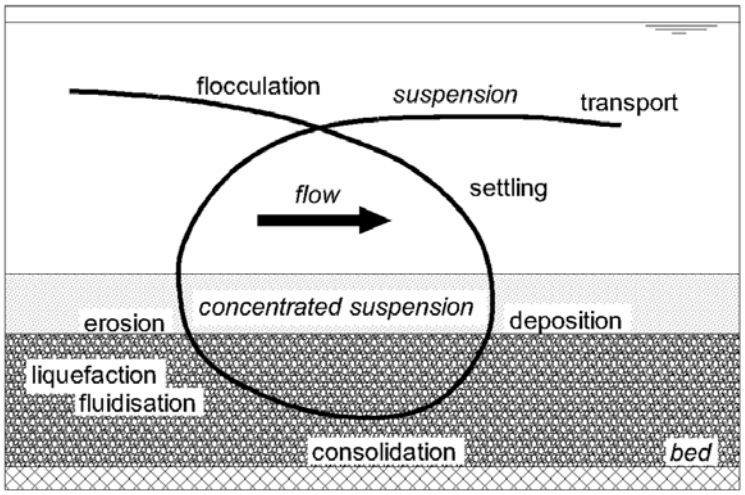

Figure 2.2 The mud cycle. Adapted from [2.24].

Another important aspect is the increase of the mud layer due to erosion. The shear strength of a mud layer is larger than the shear strength of water, so that additional particles will be picked up. Erosion is slower for consolidated mud layers **[2.1]**. The combination of these phenomena with internal transports within the mud layer result in the formation of a mud layer which characteristics change with the depth. The different steps in the cycle of mud-layer formation are shown in Figure 2.2.

Transport of mud due to wave action has been described by several authors. The critical condition at which the mud starts to move due to wave action is closely related to the contact area between elementary sediment particles, the yield stress and density of the mud and the velocity of the waves **[2.12]**.

One important aspect of the different conditions of the mud layer is that its behaviour is location and time dependent. The latter is also known as *thixotropy* and can easily be understood when observing the following example of naval architecture. Consider a vessel navigating in contact with the top of the mud layer. Due to the yield stress caused by the ship's keel, the flocculated suspensions in the top of the mud layer will break down (liquefaction) and will slowly recover after the ship has passed by (aggregation) **[2.23]**. Those break downs and recoveries have different time scales. An aggregation takes more time than liquefaction. It is clear that the mud will always behave in a thixotropic way, taking the many environmental conditions, that have their effect on the mud cycle and its behaviour, into account. The time history of the mud will consequently influence the mud behaviour **[2.29]**.

Thixotropy is also of importance when the rheology of the mud layer has to be measured. This is usually done by measuring the resistance of a rotating cylinder in a mud sample. An example of results is shown in Figure 2.3. Not only the yield stress decreases after several runs, but also a clear hysteresis can be observed. In the first step - increasing the shear rate - the yield stress will be significantly higher in comparison with the second step – decreasing the shear rate. This is caused by the liquefaction that occurs during the measurement. The mud will behave more like a liquid when it has been stirred. The fact that the maximal yield stress is lower after each run shows that the recovery of the mud to its initial condition takes more time than the liquefaction.

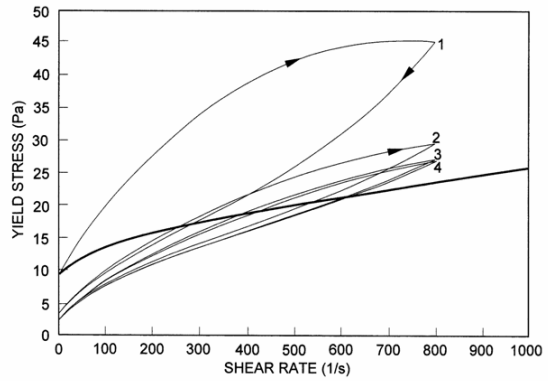

Figure 2.3. Measuring the rheology of hectorite. Adapted from [2.23].

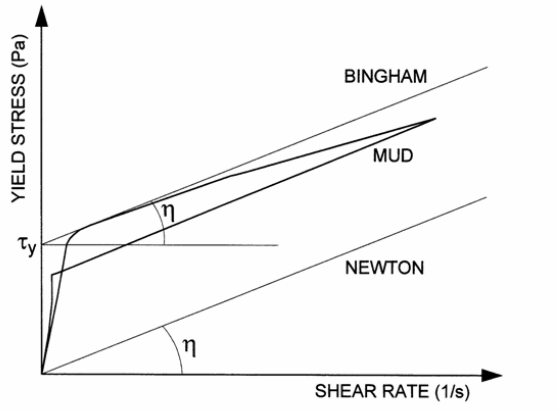

Figure 2.4. Classification of fluids based on their rheology behaviour.

Another point of interest is the initial yield stress or *rigidity*. In order for the mud to move an initial resistance has to be overcome. This is not the case for fluids like water or milk. They behave like a Newtonian fluid, see Figure 2.4. Newtonian fluids have a proportional increase of yield stress with increasing shear rate and there is no initial resistance. Their rheologic behaviour can therefore be characterized by one parameter, which is rate of change of yield stress τ with changing shear rate $\dot{\gamma}$, or the dynamic viscosity η:

$$\tau = \eta \dot{\gamma} \tag{2.1}$$

If an initial resistance needs to be overcome, which is the case for fluids like soup, tomato juice or chocolate sauce, the behaviour can be characterized as a Bingham fluid. Two parameters are needed to describe their behaviour: the initial yield stress or rigidity τ_0 and the dynamic viscosity:

$$\tau = \tau_0 + \eta \dot{\gamma} \tag{2.2}$$

In case of mud, the initial rigidity seems to vary with the dry sediment concentration T_z **[2.10]**:

$$\tau_0 = aT_z^b \tag{2.3}$$

where the coefficients a and b depend on the domain (plastic or liquid).

The Bingham model has often been used to characterize the rheological behaviour of the mud, but the reader should be aware that this is a simplification. More advanced models can be used for hydraulic purposes, such as the Voigt model **[2.15]** or Herschel-Bulkley **[2.24]**. The Bingham model does not take thixotropic effects into account. Moreover as the characteristics of the mud layer change with the depth, so does the rheology.

An additional characteristic of mud layers is *shear thinning*, which means that the viscosity decreases with increasing shear rates **[2.1,2.22,2.31]**. As a result the slope of the curves will decrease with increasing shear rate, see Figure 2.3.

All of the above is appreciably affected by organic matter and sand content **[2.13]**. At a given level of density a sand content of 15% can lead to a rigidity which is 2 to 3 times less than without sand **[2.7]**. However other authors as **[2.18]** state that between 0 and 30% the sand content has little influence on the rigidity, because the mud behaves as a lubricant around the sand particles and only the water content affects the initial rigidity. Only above 30% the sand particles make contact and affect the initial rigidity appreciably, resulting in an increase of initial rigidity.

The amount of organic matter is important in the way that it forms a microbial slime between the particles **[2.31]**. This slime prevents settling of the mud and causes low friction between the particles, resulting into a lower yield point and

lower viscosity. This can be confirmed by **[2.18]** where oxidised mud, i.e. with dead organic matter, gives a rigidity that is 2 to 3 times higher. On the other hand organic matter can interfere with the mineral fraction of the sediment forming aggregates and thus enhancing the cohesion of the suspension, resulting into a higher yield stress **[2.29]**. Biological properties play also a role in erosion **[2.1]**. The amount of organic matter in a mud layer can usually be linked to the 20 μm value **[2.20]**.

Based on the consolidation of the mud layer a rough classification of different types of mud can be made, see Table 2.1 **[2.28]**.

Table 2.1 Influence of consolidation on rheological behaviour and density.

Consolidation stage	Rheological behaviour	Wet sediment density (kg/m³)
Freshly consolidated (1 day)	Dilute fluid mud	1000 - 1050
Weakly consolidated (1 week)	Fluid mud (Bingham)	1050 - 1150
Medium consolidated (1 month)	Dense fluid mud (Bingham)	1150 - 1250
Highly consolidated (1 year)	Fluid-solid	1250 - 1350
Stiff mud (10 years)	solid	1350 - 1400
Hard mud (100 years)	solid	> 1400

The wet sediment density of a mud layer is given by:

$$\rho_2 = (1-\varphi)\rho_1 + \varphi\rho_s \qquad (2.4)$$

In which φ represents the fraction of solid material of a density ρ_s within the mud layer. The water has a density ρ_1.

An increased consolidation means a larger fraction of solid material within the mud layer and thus an increased density. On the other hand the density after consolidation will be proportional with the initial mud density **[2.19]**, however this phenomenon is also affected by the sand proportion, which decreases the ratio of final density versus initial density. A dilute fluid mud layer consists mainly of water. Its behaviour will be close to the behaviour of water and will be similar to any Newtonian fluid. An increase of consolidation results in a more Bingham like behaviour.

A fluid mud layer has a viscous behaviour, while a consolidated soil or *plastic mud* layer has an elastic or visco-elastic behaviour **[2.1]**, however in **[2.31]** fluid mud is also considered visco-elastic. The transition between those two conditions is referred to as the *rheological transition* **[2.7,2.13,2.16]**. As indicated in Table 2.1 this transition occurs at a density range of 1250 to 1350 kg/m³ and is characterized by a sharp increase of shear strength.

From a navigation point of view it can be intuitively seen that contact with plastic mud that behaves as a soil can lead to damage or unacceptable effects on controllability. The rheological transition is therefore an important parameter.

2.3 Measuring the mud layer characteristics

2.3.1 Introduction

The characteristics and behaviour of a mud layer can vary extensively and depend on the location. Every parameter of the mud can be classified and measured to a certain extent. A complete list can be found in **[2.1]**. This paragraph will focus on the measurements of mud layer characteristics that are important from a nautical viewpoint, i.e. for production of nautical charts or survey of dredging works.

For vessels it is important to have a sufficient navigable depth. The aim is then to measure the navigable depth of the mud layer. In spite of the huge range of possible variations in mud layers the rheological transition seems the most important for navigation. The problem then is to locate the point where the yield stress of the mud layer increases sharply over a small depth, see Figure 2.5. This is the methodology that is used in the harbour of Zeebrugge and other harbours.

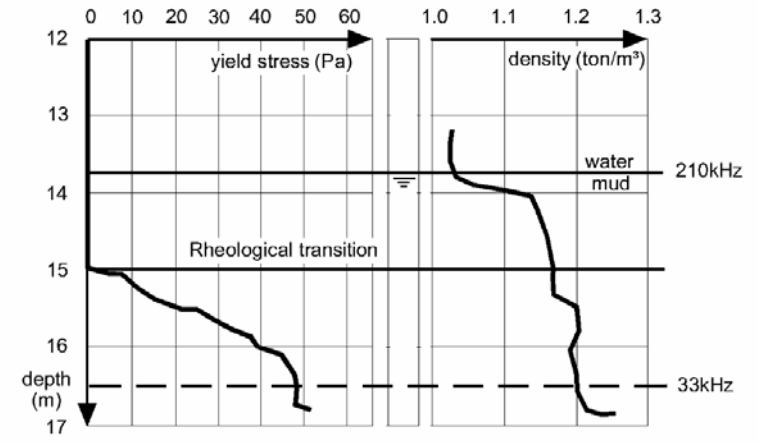

Figure. 2.5. Rheology profile of the mud layer in the harbour of Zeebrugge. Adapted from [2.6].

In some harbours alternative methods are used. In the harbour of Emden **[2.31]** the focus is put on the organic content of the mud layer. By treating the mud layer so that the amount of organic content remains high the mud layer remains fluid. The nautical bottom is there defined at the point where the yield stress is 100 Pa. The problem of measuring the navigable depth is then reduced to the determination of the 100 Pa value. However, this method seems only applicable when the sand content is below 10%.

In **[2.20]** a parameter C_u is introduced, which describes the adhesion between ship and bottom and is measured in Pa. A maximal value for ship navigation is 120 Pa. A strong relationship between this parameter and the mud density has been observed, so that the problem of measuring the navigable depth is reduced to measuring the mud layer density.

In all cases the measurement of mud layer characteristics implies simplifying the mud layer. Most invasive measurement techniques change the characteristics of the mud layers **[2.1]**. Actually, Heisenberg's Uncertainty principle could as well be applied alternatively to mud layers: "The more precisely the characteristic is determined, the less precisely the mud is known".

2.3.2 Echo-sounding

In channels and harbours depth measurements are usually carried out with echo-sounding. In the simplest setup an electromagnetic wave is emitted that reflects at the bottom. The time between emission and reception and the intensity of the received wave is then a measure for the local depth. The frequency of the wave is closely related to its sensitivity for reflection. In case of a soft mud layer on the bottom, a high frequency echo of 210 kHz will reflect on top of the water-mud interface. A lower frequency will reflect at a level somewhat deeper into the mud, see Figure 2.6.

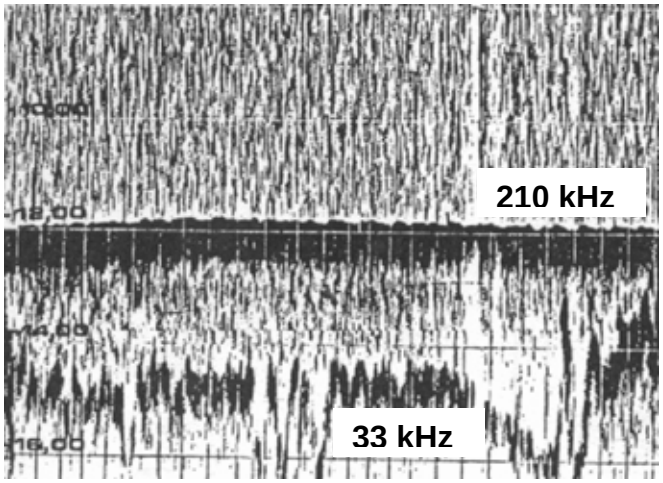

Figure 2.6. Example of an echo-sound result in the harbour of Zeebrugge.

A simple echo-sounder can only emit a fixed frequency wave. Enhancements have been made by installing several echo-sounders on the survey vessel: the multibeam echo-sounding. In this case the different frequencies are emitted at different angles **[2.26]**.

Echo-sounding is very useful to determine the depth in case of a solid bottom. But in case of a muddy bottom there is no certitude which frequency gives the position of the nautical bottom. In Zeebrugge the 33 kHz value is sometimes used to denominate the nautical bottom; in some harbours this is even common practice. But the results are very sensitive and vary in time, so it can only be used when no other measurement equipment is available.

However, some researchers were able to link the results of the echo-sounding to the definition of the nautical bottom. **[2.31]** mentions that in the harbour of Emden the 12 kHz echo-sound corresponds with a yield point of 100 Pa, which is the level of the nautical bottom over there.

Another technique is described in **[2.9]**. An echo-sounding system called Detection of Sediment-Layers and Properties (DSLP) can be used to monitor the nautical bottom:

- All data from an echo-sounding program with a broad frequency range is recorded;
- This data is analysed with a complex signal analysis which allows to recognise the distinct interaction processes between sound and material.

DSLP gives an overview of the different stratified layers based on the separation of the signal due to scatter and the signal due to reflection. However it is not suitable to define a rheological transition.

2.3.3 Monitoring the yield stress

As mentioned before the rheological transition is considered as the critical limit. In order to know its position the yield stress of the mud layer has to be measured. Some common measurement techniques will be presented.

2.3.3.1 Rheological gauge

A rheological gauge **[2.11]** gives the initial rigidity measured by the minimal torque necessary to start the rotor. The response varies according to the stirring the mud undergoes. Different types exist such as the SR10 probe (France), the rheometer (Belgium) and the S3 (The Netherlands).

The measurements have to be carried out in situ whenever possible as the structure of the mud sample depends significantly on the sampling method and treatment of samples **[2.7,2.24]**.

2.3.3.2 Nautisonde

The Nautisonde carries out the measurement of viscosity by mechanical movement of two paddles at it's lower end, see Figure 2.7. The detection of the powers to move the paddles is recorded and is a measure for the viscosity **[2.3]**. By slowly lowering the Nautisonde probe into the system water-column – suspension – sediment a rheological profile is obtained **[2.4]**.

Figure 2.7 The Nautisonde probe [2.4].

2.3.3.3 Wing probe

A wing probe is an instrument to measure the shear strength of the mud **[2.20]**. The wing probe is usually used in laboratory conditions but has been adapted to allow in situ surveys. A rotating head is driven by an electric motor and is controlled electronically by a torque sensor. On the basis of correlations with laboratory experiments it was found that a wing velocity of 6°/min corresponded with the critical C_U value used as a definition for the nautical bottom, see 2.3.1.

2.3.3.4 Towed sled

The disadvantage of the above presented systems is that they can only carry out fixed point measurements. In order to monitor a complete harbour many labour intensive point measurements are needed. Moreover the measurements have to be repeated after a certain period due to the time dependency of the mud layer.

This can be resolved by the principle of a towed sled **[2.22]**. The sled is designed to ride automatically at the navigable depth level. The concept assumes the existence of a physical horizon where the combination of viscous and normal stresses in the mud supports the towed device. In practice the sled can only be towed at a constant density level. The system is therefore quite comparable to the Navitracker, however the latter is capable of measuring the density as well, see 2.3.4.2.

2.3.4 Monitoring the mud density

The mud density is recorded with density probes that can be based on acoustic or nuclear methods. A further classification can be made based on fixed point and towed probes.

2.3.4.1 Acoustic methods

This method is based on the propagation of sound in water, which is related to the density of the fluid **[2.8]**: the velocity of propagation attenuates in function of the density **[2.11]**. The problem however is that there is an ambiguous relationship between sound speed and density and that in the interesting density range of 1 till 1.8 ton/m³ the sound speed only varies with +/- 4%. Moreover the attenuation also depends on physico-chemical characteristics of the mud layer, thus for a different sand content, but equal density another attenuation can be measured.

Acoustic measurements are mostly carried out with fixed point probes. By placing the fixed point probe onto a submarine vehicle a towed probe can be made.

2.3.4.2 Nuclear methods

Due to the severe shortcomings of the acoustic method the nuclear method is more frequently used. The nuclear method is based on the behaviour of gamma-radiation in the mud suspension **[2.8]**. Different techniques exist:

- Compton scattering: scatter of a gamma-photon caused by its collision with an orbital electron in an atom;
- Photo-electric absorption: absorption of a gamma-photon by collision with a tightly bound orbital electron.

[2.14] and **[2.21]** proved that the ratio of the detected intensity to the emitted intensity of the radiation sent through a sediment column of fixed limited thickness depends only on density if the radiation energy is greater than 600 keV. For fixed point probes the scattering method is preferred as source and detector are into one housing and it is consequently easier to enter the mud layer **[2.11]**.

Figure 2.8. Navitracker [2.5].

An example of a towed nuclear probe is the Navitracker **[2.8]**. This is a tow fish containing a high speed nuclear gauge, an intelligent winch controlling the vertical movement of the fish and a computer which controls both echo-sounding and density surveys. Because of its shape the towed body only penetrates in mud up till a certain density. To handle this problem **[2.26]** an H-shaped Vertical Density Profiler was added to the system. The Navitracker is nowadays used in many harbours, among them the harbour of Zeebrugge. Other examples of densimetric probes are JTD3 and JTD4 **[2.2]**.

2.3.5 Presentation of results

The main purpose of monitoring the mud layer in harbours is steering the maintenance dredging works, so that safety of navigation is guaranteed. Some important output in Zeebrugge is **[2.30]**:

- Nautical charts that combine data from a certain density horizon, measured with the Navitracker, and both the 210 kHz and 33 kHz level, see Figure 2.9;
- Differential charts that show the difference between the 210 kHz level and a density horizon (Figure 2.10a) or that show differences between two measurement campaigns (Figure 2.10b);

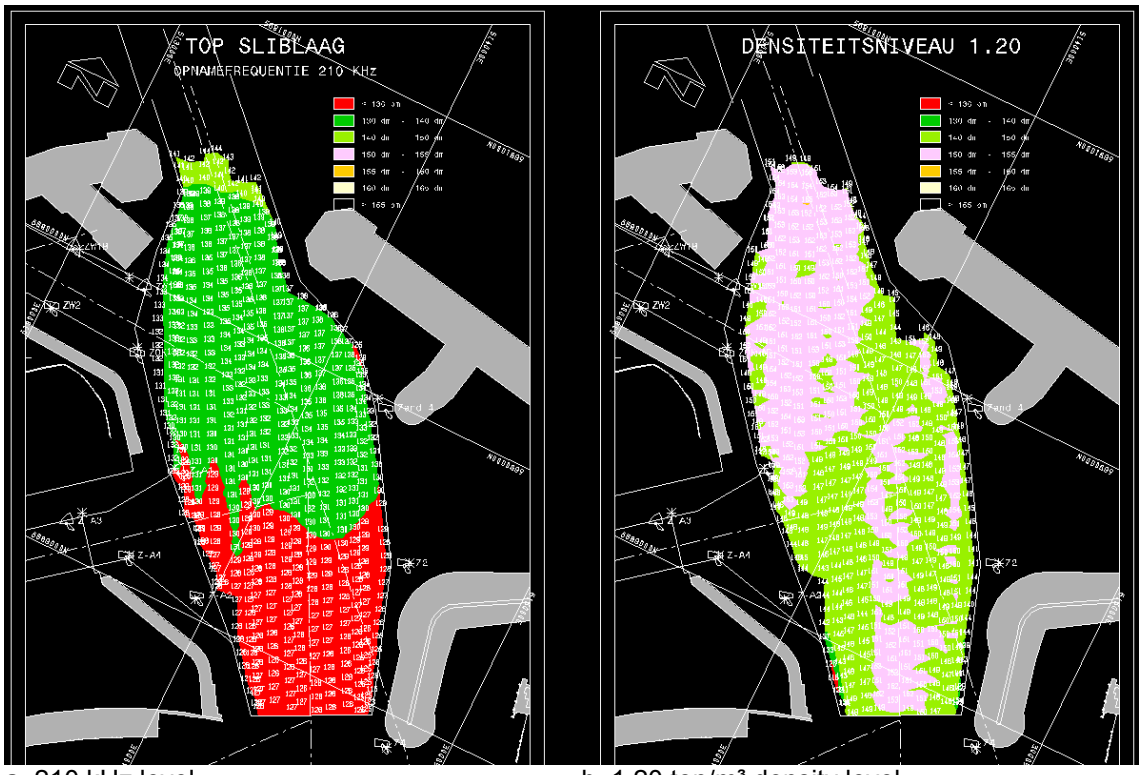

a. 210 kHz level b. 1.20 ton/m³ density level

Figure 2.9. Nautical charts of the central part of the new outer harbour of Zeebrugge [2.27].

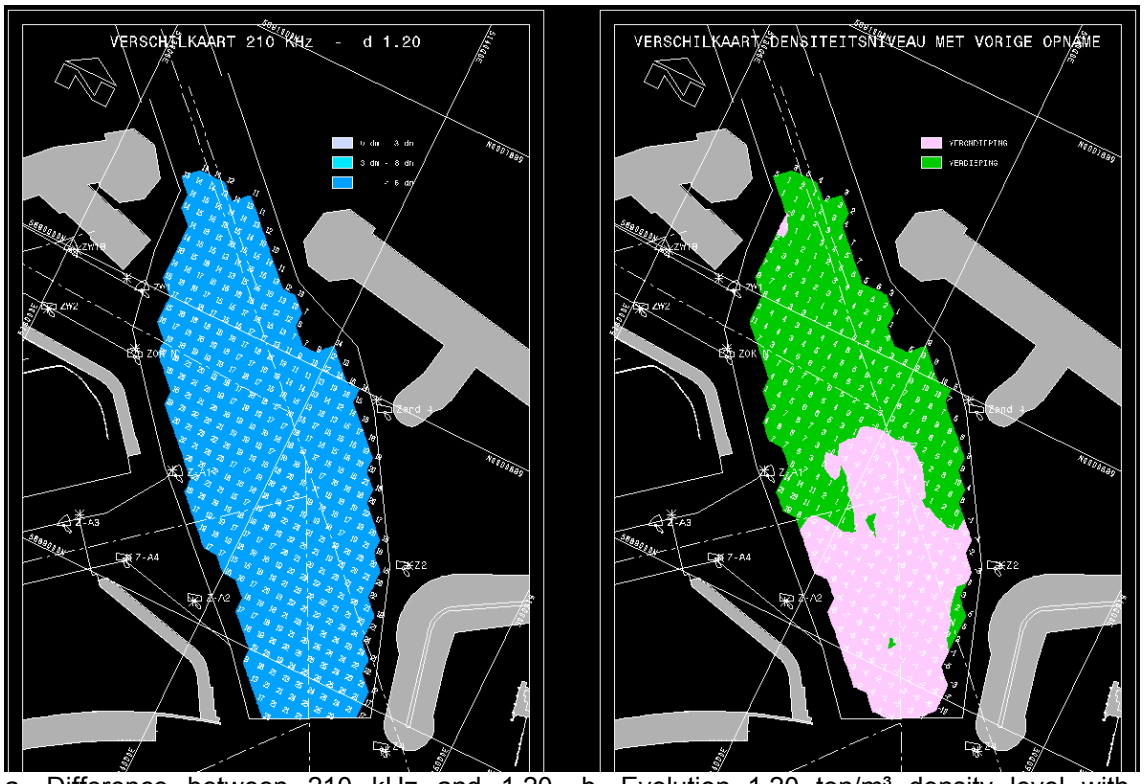

a. Difference between 210 kHz and 1.20 ton/m³ density level b. Evolution 1.20 ton/m³ density level with previous measurement

Figure 2.10. Differential charts of the central part of the new outer harbour of Zeebrugge [2.27].

Other output is:

- The areas to be dredged with respect to the level to be maintained are shown on coloured spot charts, as in Figure 2.11.
- Track plots which represent the dredging vessel's position to indicate the coverage and the intensity of the maintenance dredging (Figure 2.12);

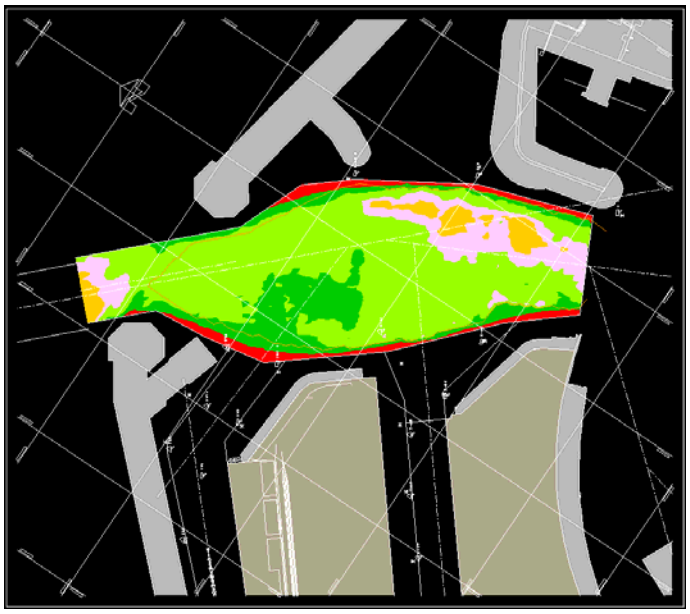

Figure 2.11. Coloured spot chart [2.5].

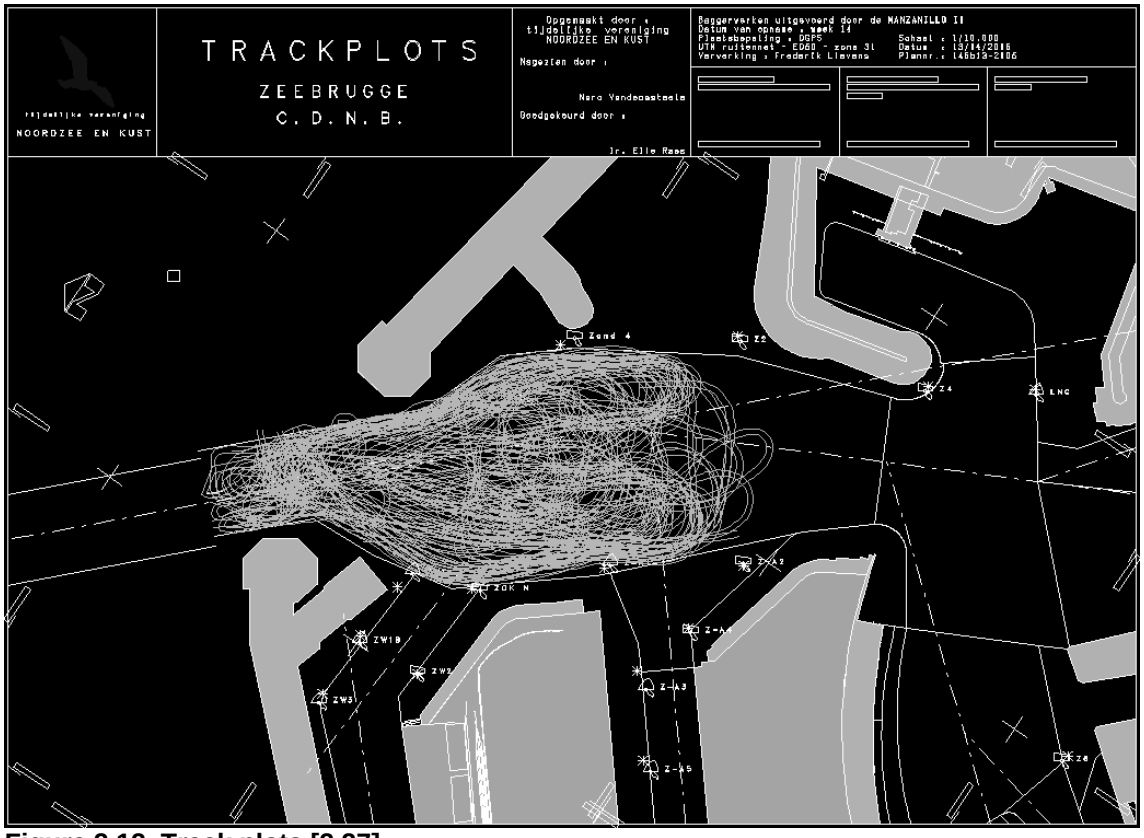

Figure 2.12. Track plots [2.27].

The above charts are updated on a two weekly basis and are mostly oriented to an audience of dredgers and pilots. More extensive measurement campaigns are the quarterly density surveys, see Figure 2.13. These measurements are carried out with fixed point density probes to have an idea of the evolution of the density throughout the mud layer.

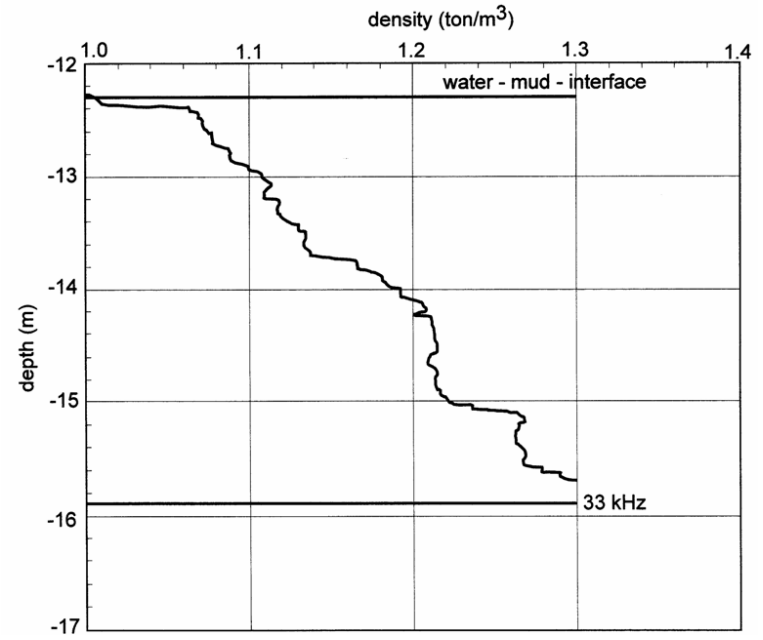

Figure 2.13. Density profile in function of the water depth.

2.4 Practical criterion for the nautical bottom

The reader should by now be aware that mud is not only a material with a highly complex behaviour, but it is also difficult to monitor it in a continuous way. Nevertheless if the nautical bottom concept is used with the definition of PIANC as given in 1.1.6 a critical limit has to be defined within the mud layer. Different approximations are possible, see 2.3.1, but in this project the rheological transition of the mud layer has been chosen as the critical limit.

On the other hand variations of the mud layer with time occur rapidly. As a consequence frequent monitoring of the mud layer is needed in order to follow up the characteristics of the mud layer. To reveal the rheological transition fixed point measurements with rheological gauges have to be carried out. Those measurements, however, are very labour intensive. In the 1980s an extensive program of rheology measurements has been carried out in the harbour of Zeebrugge.[1]

Figure 2.14 represents the behaviour of different mud samples in different concentrations. Two distinct behaviours can be observed, separated by a bend **[2.13]**. For small initial rigidity and viscosity values the rigidity and viscosity are less dependent of the concentration, while they are strongly dependent with higher concentrations. The border between both conditions is represented by the bend in the graphs and is considered the rheological transition. This transition always took place at densities above 1.15 ton/m³. This density was

[1] This program has been repeated in the 1990s and is planned in the near future as well.

therefore considered as a safe value: a rheological transition would always take place at higher densities. As densities are easier to measure in a continuous way with systems as the Navitracker, the critical limit in the nautical bottom definition was therefore linked to a critical density.

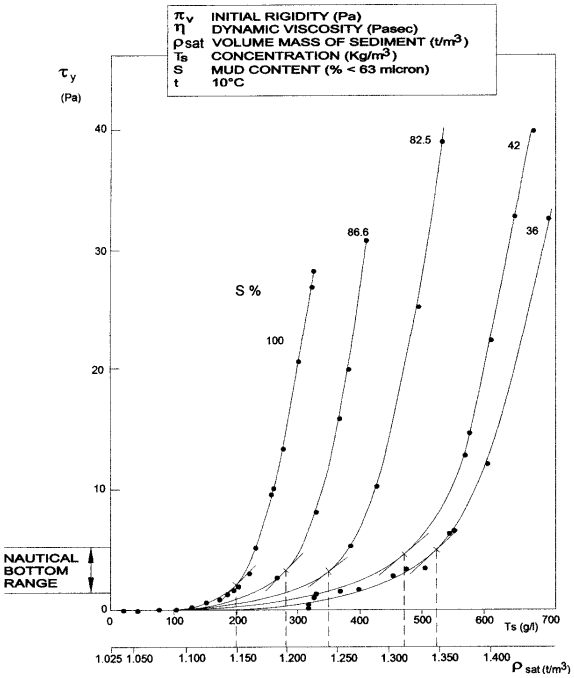

Figure 2.14a. Harbour of Zeebrugge: initial rigidity of mud samples in function of their concentration, density and particle size distribution. Adapted from [2.13].

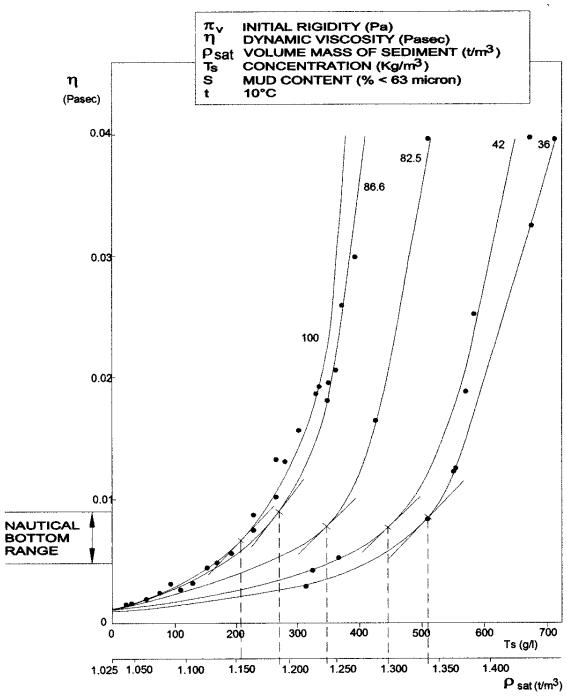

Figure 2.14b. Harbour of Zeebrugge: dynamic viscosity of mud samples in function of their concentration, density and particle size distribution. Adapted from [2.13].

Of course the density is merely a surrogate for the behaviour of the local mud. As density depends on the many characteristics of the mud layer, such as concentration or sand content, different harbours with other mud layers have a different critical density as a definition of the nautical bottom. Examples are Rotterdam (1.20 ton/m³), Nantes (1.20 ton/m³), Maracaibo (1.20 ton/m³), Bangkok (1.23 ton/m³) and Cayenne (1.27 ton/m³).

At the present, investigations are made to be able to measure the rheological transition in a continuous way, which would reflect more the real behaviour of the mud, instead of predicting it by means of the density.

2.5 References

[2.1] BERLAMONT J., OCKENDEN M., TOORMAN E., WINTERWERP J. *The characterisation of cohesive sediment properties.* Journal of Coastal Engineering, **21**, 1993, p 105-128.

[2.2] BROSSARD C., CAILLOT M., GALENNE M., GRANBOULAN J., MIGNIOT M., MONADIER P., ROUDIER J. *Sécurité de la navigation dans les chenaux envasés.* Proceedings 27th International Navigation Congress, PIANC, Osaka, Japan, Section II, Subject 1, 1990, pp. 23-28. (In French).

[2.3] DASCH W. *Die Nautisonde, ein neuer Viskositätssensor.* Hansa – Schiffahrt – SchiffBau – Hafen, Volume 135, No. 9, 1998. (In German).

[2.4] DASCH W., WURPTS R. *Isoviscs as Useful Parameter for Describing Sedimentation.* Terra et Aqua 82, 2001.

[2.5] DE BRAUWER D. *Maintenance dredging and bottom survey in the harbour of Zeebrugge.* Workshop Nautical Bottom, Flanders Hydraulics Research, Antwerp, Belgium, April 29, 2005.

[2.6] DE MEYER C.P., MALHERBE B. *Optimisation of maintenance dredging operations in maritime and estuarine areas.* Terra et Aqua 35, 1987, p 25-39.

[2.7] DE VLIEGER H., *Economic methods of channel maintenance: optimization of maintenance dredging.* Terra et Aqua, June 1991.

[2.8] DE VLIEGER H., DE CLOEDT J. *Navitracker a giant step forward in tactics and economics of maintenance dredging.* Terra et Aqua, December 1987.

[2.9] EDEN H., MÜLLER V., VORRATH D. *DSLP – an innovative echo sounding technology.* Hansa International Maritime Journal, October 2000.

[2.10] GALICHON P., FERAL A., GRANBOULAN J., VIGUIER J. *Variations in rheological properties of muds in the Gironde estuary.* Proceeding of the 22nd Coastal Engineering Conference, Vol. 3, Chapter 222, Delft, The Netherlands, 1990, 14 pp.

[2.11] GRANBOULAN J., CHAUMET-LAGRANGE M. *Data collection and processing.* Terra et Aqua 46, 1991.

[2.12] JIALONG G., XANGLIN L. *The threshold movement of cohesive fine sediment (mud) due to wave action.* Proceedings of Coastal & Port Engineering in Developing Countries, Vol. 1 Edited by Nanjing Hydraulic Research Institute, 1987.

[2.13] KERCKAERT P., MALHERBE B., BASTIN A. *Navigation in muddy areas – The Zeebrugge experience.* PIANC Bulletin 48, 1985, pp. 127-135.

[2.14] KUHN W. *Principal considerations and limiting factors concerning the application of depth and surface equipment for soil density measurements with gamma-rays.* Proceedings of Panel. Meeting: Soil-Moisture and Irrigation Studies. I.A.E.A. Vienna, 1967, pp. 38-53.

[2.15] MAA J.P.Y., MEHTA A.J., *Soft Mud Properties: Voigt Model.* Journal of Waterway, Port, Coastal and Ocean Engineering, Vol. 114, No. 6, 1988, pp. 765-770.

[2.16] MALHERBE B. *Towards a definition of the nautical bed in mud deposits: the concept of rheologic transition RT.* International workshop on cohesive sediments: Towards a definition of "mud", Brussels, Belgium, 1990.

[2.17] MIGNIOT C. *Tassement et rhéologie des vases. Première partie.* La Houille Blanche, no 1, 1989. (In French).

[2.18] MIGNIOT C. *Tassement et rhéologie des vases. Deuxième partie.* La Houille Blanche, no 2, 1989. (In French).

[2.19] MIGNIOT C., HAMM L. *Consolidation and rheological properties of mud deposits.* Proceedings of 22nd Coastal Engineering Conference, Vol. 3, Chapter 225, Delft, The Netherlands, 1990, 9 pp.

[2.20] RECHLIN D. *Definition of the nautical depth in the main muddy areas of the federal waterways board.* PIANC Bulletin 86.

[2.21] TAYLOR D., KANSARA M. *A theory of the nuclear densimeter*. Soil Science, Vol. 104, no. 1, 1967.

[2.22] TEETER A. *Experience with intrusive fluid mud survey systems in coastal channels.* XX International Congress of the International Federation of Surveyors (FIG), Melbourne, Australia, 1994.

[2.23] TOORMAN E. *Mud rheology: implications for navigability.* Workshop Nautical Bottom, Flanders Hydraulics Research, Antwerp, Belgium, April 29, 2005.

[2.24] TOORMAN E. *Coastal and Estuarine Mud. Why we like and dislike it.* ATHENS Short Intensive Course, Hydraulics Laboratory, Leuven, Belgium, March 20-24, 2006.

[2.25] VAN DEN EYNDE D., FETTWEIS M., FRANCKEN F., PISON V., NECHAD B., LAUWAERT B., BACKERS J., DE BLAUWE J.P., POLLENTIER A. *Mud transport modelling and measuring in the Belgian coastal waters in relation with dredging and dumping aspects.* ATHENS Short Intensive Course, Hydraulics Laboratory, Leuven, Belgium, March 20-24, 2006.

[2.26] VAN CRAENENBROECK K., DUTHOO J., VANDECASTEELE M., EYGENRAAM J.A., VAN OOSTVEEN J. *Application of Modern Survey Techniques in Today's Dredging Practice.* Terra et Aqua 72, 1998.

[2.27] VANDECASTEELE M. *Geotechnical, Geophysical and Metocean Expertise Around the World.* Workshop Nautical Bottom, Flanders Hydraulics Research, Antwerp, Belgium, April 29, 2005.

[2.28] VAN RIJN L.C. *Principles of sediment transport in rivers, estuaries and coastal seas*. Aqua publications – I11, Amsterdam, 1993

[2.29] VERREET G., VAN GOETHEM J., VIANE W., BERLAMONT J., HOUTHUYS R., BERLEUR E. *Relations between physico-chemical and rheological properties of fine grained muds.* 3rd International symposium on river sedimentation, Jackson, Mississippi, USA, 1986, p 1637-1646.

[2.30] WARNIER F., DRUYTS M., LEYS E. *Application of new technologies in maintenance dredging.* Proceedings CEDA Dredging days, 1991.

[2.31] WURPTS R., TORN P. *15 Years Experience with Fluid Mud: Definition of the Nautical Bottom with Rheological Parameters.* Terra et Aqua 99, 2005.

If we knew what we were doing it wouldn't be research.

A. Einstein

CHAPTER 3

RESEARCH ON MANOEUVRING BEHAVIOUR IN MUDDY AREAS

3.1 Introduction

The assumption was made that the rheological transition in the mud layer could be defined as the nautical bottom. Based on the measurements of the rheology in the harbour of Zeebrugge the rheological transition was linked to a critical density, because this is the only parameter that can be monitored in a continuous way. However, according to the definition of the nautical bottom by PIANC the manoeuvring behaviour of the vessels should be taken into account. In order to know how vessels react in muddy areas experimental research was needed.

In the past only a few research institutes carried out model tests in muddy conditions. Also a small number of full scale tests has been performed. This chapter describes the setup of these tests and resumes the observations that were made. Additionally some theoretical calculations from literature will be presented to close this chapter.

3.2 Model testing in muddy areas

Before the start of the current research project, only three research institutes carried out model tests:

- MARIN (Wageningen, The Netherlands,1976);
- Flanders Hydraulics Research (Antwerp, Belgium, 1984-1989);
- SOGREAH (Grenoble, France, 1989).

3.2.1 Research at MARIN

The research at Marin has been summarized in **[3.8]**.

3.2.1.1 Motivation

The harbour of Rotterdam has always been a deposit area of sediments due to transports of sediment from the Rhine and transport of sand from the sea. With the venue of large tanker vessels some difficulties arose. Until then the nautical bottom was always located at the top of the water mud interface, but with large drafted vessels the definition was no longer tenable. A research project, consisting of both model and full scale testing (see 3.3.1), was started in order to investigate whether a redefinition of the nautical bottom was possible so that large drafted tanker vessels could safely call the harbour of Rotterdam.

3.2.1.2 Experimental setup

Instead of using real mud in the experimental setup, a mixture of chlorinated paraffin and density regulating kerosene was used as an artificial mud layer. The artificial mud layer was chosen not to be too viscous (ca. 0.03 Pa.s), as the viscosity seemed only of importance in the lower 10% of the mud layer. The density of the model mud layer was in accordance with full scale and was such

to simulate the summer and winter conditions of the mud layer in Rotterdam harbour:

- Winter: ρ_2 = 1140 kg/m³; thickness h_2 = 2.5 m; 1.35 m; 3.85 m;
- Summer: ρ_2 = 1240 kg/m³; h_2 = 2.5 m; 1.35 m;
- Tests without mud as a reference.

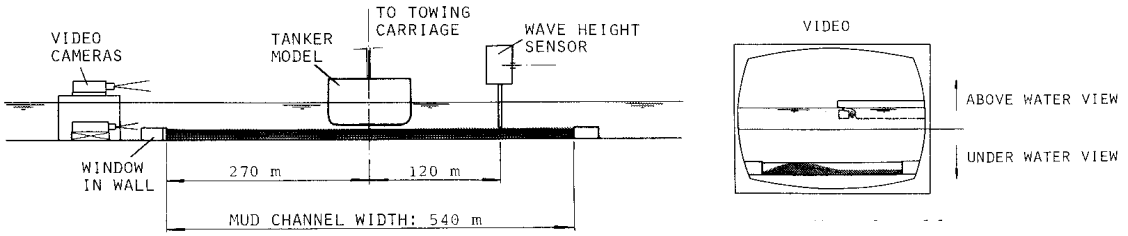

Figure 3.1. Test set-up for observation of the mud layer in Marin [3.8].

Captive manoeuvring model tests, see Figure 3.1, and free running tests were carried out with an 1/82.5 scale model of a tanker (L = 310 m; B = 47.2 m; T = 18.9 m; C_B = 0.85). The under keel clearance referred to the water-mud interface was varied from +0.15T to -0.10T. The program can be found in Table 3.1. The undulations of the water-mud interface were recorded with camera and wave meters.

Table 3.1. Tested conditions. Adapted from [3.8].

Condition	Mud		Ship speed (knots)
	Density (kg/m³)	Thickness (m)	
A	1140	0.13 T	3,5,7
B	1140	0.07 T	5
C	1140	0.20 T	5
D	1240	0.13 T	5
E	1240	0.07 T	5
F	Reference condition: no mud		5

3.2.1.3 Observations

The water-mud interface undulates at a speed of 3 knots or more, see Figure 3.2:

- When the tanker navigates above soft fluid mud a wave is induced, diverging from the aft body and travelling at a critical speed, which depends on the thickness and density of the mud layer;
- The amplitude of the rising increases with the thickness of the mud layer and decreases with decreasing under keel clearance;
- An increase of mud density leads to a decrease of amplitude.

From the free running tests could be observed that in the speed range of 3 to 5 knots the propeller rate in muddy conditions had to be considerably higher to maintain speed, see Figure 3.3. This is especially the case with the winter mud, where large elevations of the interface occur, consequently the speed loss could be ascribed to a loss of kinetic energy to the mud layer. A positive effect is that rudder action will be stronger.

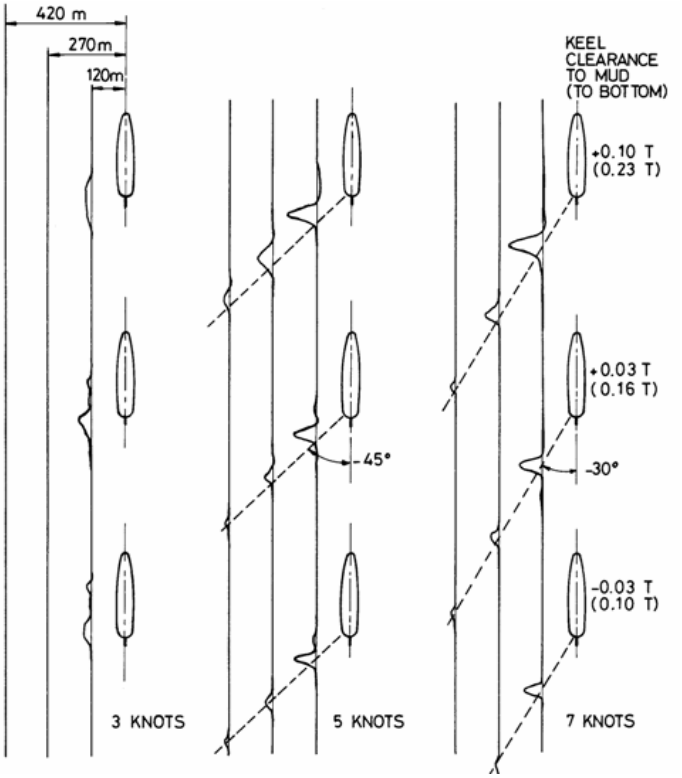

Figure 3.2. Internal wave profiles for a mud layer of 0.13 T thickness and of winter density [3.8].

The sinkage is less above mud in comparison with the solid bottom condition and decreases with increasing layer thickness. The mud density does not seem to have any effect.

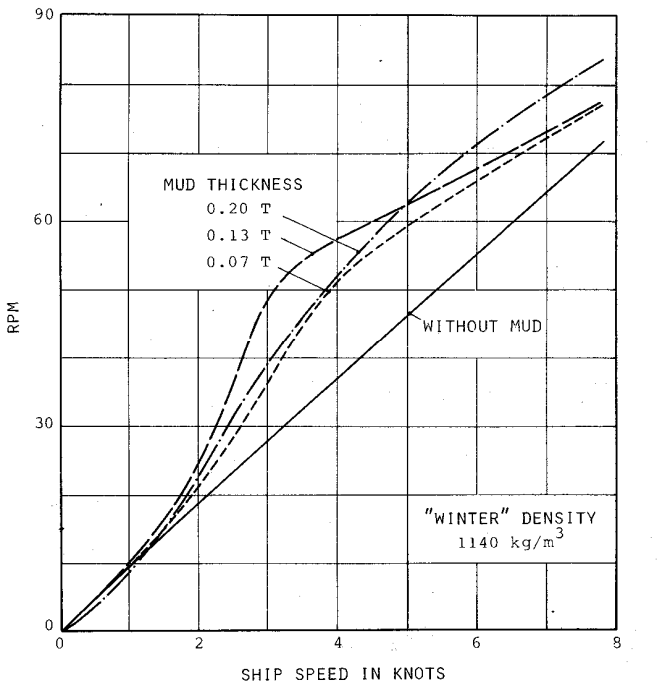

Figure 3.3. Speed-rpm relation for an under keel clearance of 0.10 T referred to the solid bottom [3.8].

3.2.1.4 Modelling and simulating

A mathematical manoeuvring model was developed. The velocity derivatives resulted appreciably higher in muddy conditions (larger damping), while the increase of acceleration derivatives is merely due to the small under keel

clearance and not the effect of the mud layer. Manoeuvres are slower in muddy areas, especially in case of a small positive under keel clearance referred to the water mud interface and when the rising of this interface is high, thus with smaller densities. The mud layer slackens the steady conditions while accelerating the dynamic ones, zigzag tests are for example carried out faster with mud on the bottom, see Figure 3.4, while turning circles are larger in muddy conditions, see Figure 3.5.

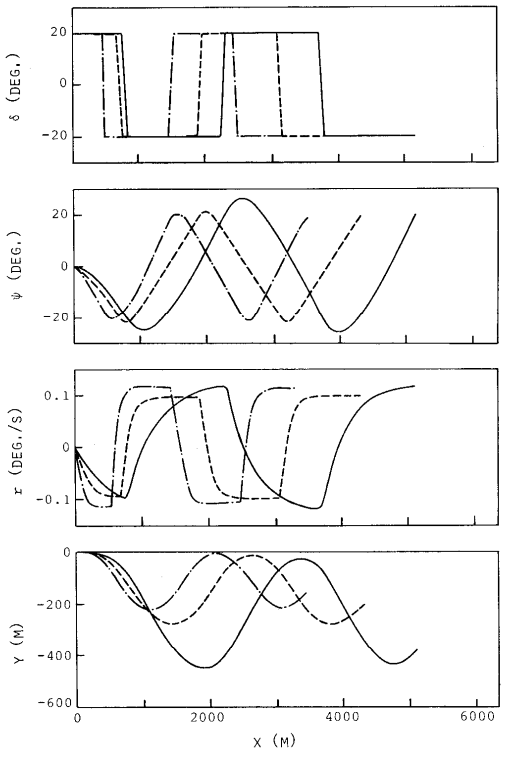

Type of line	Mud		Keel clearance	
	Density (kg/m³)	Thickness	To mud	To bottom
———	0	0	–	0·20 T
-------	1140	0·13 T	0·10 T	0·23 T
—·—·	1240	0·13 T	0·10 T	0·23 T

Figure 3.4. Zig-zag tests [3.8].

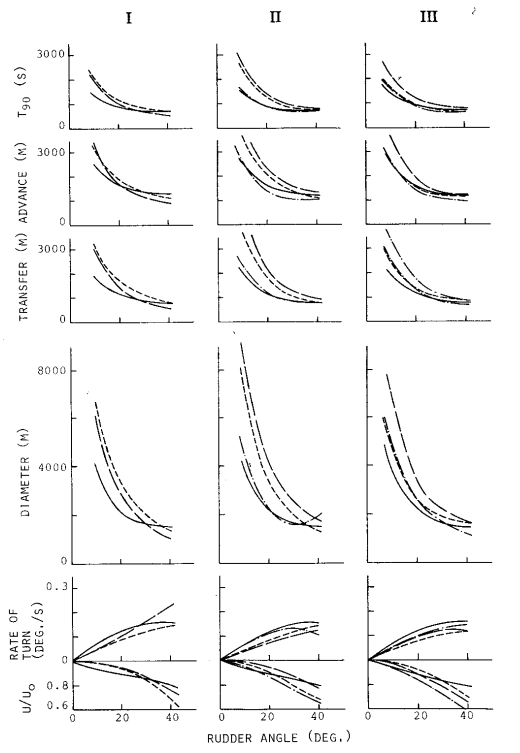

Group	Type of line	Mud		Keel clearance	
		Density (kg/m³)	Thick-ness	To mud	To bottom
I	———	0	0	–	0·20 T
	---------	1140	0·07 T	0·15 T	0·22 T
	— — —	1140	0·13 T	0·10 T	0·23 T
II	———	0	0	–	0·20 T
	---------	1140	0·07 T	0·10 T	0·17 T
	— — —	1140	0·13 T	0·03 T	0·16 T
	—·—·—	1140	0·20 T	–0·03 T	0·17 T
III	———	0	0	–	0·20 T
	---------	1140	0·07 T	0·03 T	0·10 T
	— — —	1140	0·13 T	–0·03 T	0·10 T
	—·—·—	1140	0·20 T	–0·10 T	0·10 T

Figure 3.5. Turning circles: effect of mud thickness [3.8].

3.2.2 Research at Flanders Hydraulics Research

3.2.2.1 Motivation

In **[3.14]** three main reasons were put forward to carry out the research:

- Getting acquainted with experimentation techniques for ship models;

- Selection of an artificial mud layer to simulate the real mud;
- Understanding the physical mechanisms of the ship-mud interaction.

The research activities were mainly a pilot model for the experimental research as described in Chapter 4 to support the nautical bottom concept in the harbour of Zeebrugge and to support the full scale tests as described in 3.3.2, nevertheless some useful results were discovered.

3.2.2.2 Experimental setup

The experimental research was carried out in two stages. In a first stage some preliminary tests were performed in a small basin with a natural mud layer (15.5 x 2.25 x 0.28 m³) to realize the first point of the motivation of the research (3.2.2.1). A 1/70 scale model of a third generation container carrier was used to perform the tests. Undulations of the water-mud interface occurred and an analogous drop in the speed-rpm relationship as in Figure 3.3 was observed. However the results showed that natural mud was not suitable to perform model testing **[3.17]**.

In a second stage the basin was enlarged to 32 m **[3.16]**. Two ship models were tested above a solid bottom and an artificial mud layer, namely a mixture of 1-1-1 trichlorethane and petrol. The ship models were:

- A 1/70 scale model of an LNG carrier;
- A 1/40 scale model of a suction hopper dredger, Vlaanderen XVIII, see 3.3.2.

The ship models were equipped with propulsion and rudders and were forced to follow a guiding beam **[3.11]**, see Figure 3.6.

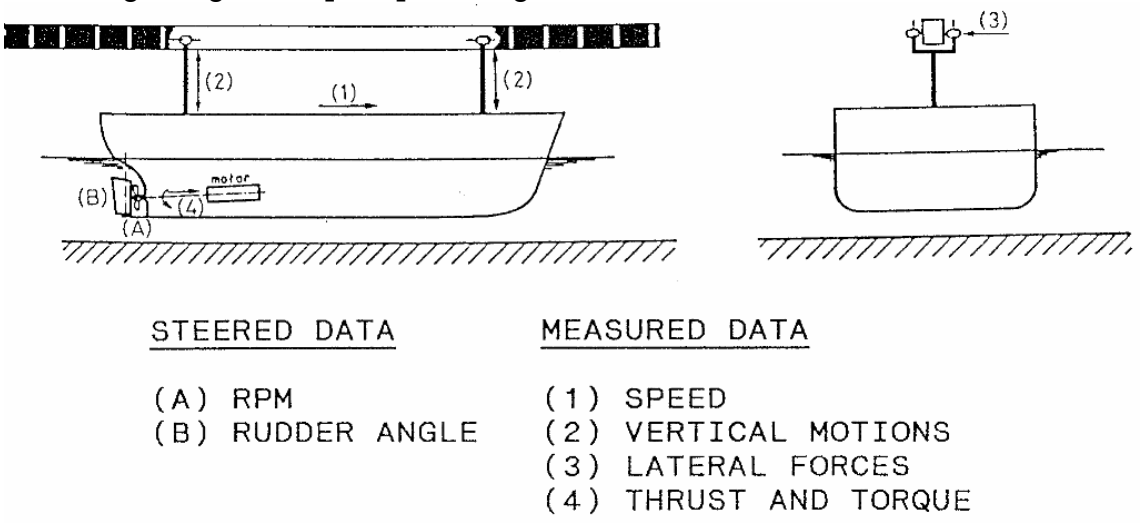

Figure 3.6. Model tests: experimental setup [3.11].

The following test runs were executed **[3.12,3.14,3.16]**:

- Steady state runs at a constant propeller rate;
- Deceleration runs;

- Steady state runs at a constant propeller rate and with different rudder angles.

The characteristics of the mud layer and the under keel clearances were different for each scale model:

- The LNG carrier was tested above a mud layer of 11 mm with a density of 1140 kg/m³. The under keel clearance was varied from 22% till -6% of draught referred to the water mud interface **[3.12]**;
- The suction hopper dredger was tested above three different mud layers **[3.14]**:
    - A density of 1220 kg/m³ and layer thickness of 35 mm;
    - A density of 1110 kg/m³ and layer thickness of 35 mm;
    - A density of 1110 kg/m³ and layer thickness of 16 mm.

  The under keel clearances were varied between 20% and -10% of draught referred to the water mud interface.

In all cases the mud layer had a viscosity of only 0.002 Pa.s. Additional runs with an artificial mud layer consisting of clay, carbon and quartz merely showed that this mixture was useless to perform model scale investigations **[3.13]**.

3.2.2.3 Observations

A summary of the observations is given based on **[3.11,3.12,3.14, 3.16]**.

The manoeuvring behaviour of the vessel is strongly related to the speed range, which can be linked to the occurrence of oscillations at the water mud interface. Three speed ranges can be detected:

- At low speed a small sinkage near the fore body is detected, which disappears amidships and turns into an elevation abaft;
- At a certain critical speed value the sinkage at the entrance changes suddenly into an elevation. The section at which the jump occurs moves abaft with increasing speed;
- If the speed increases more, the rising of the interface occurs behind the stern. The amplitude of the elevation can exceed the mud layer thickness several times.

A theoretical explanation of these speed ranges will be given in 5.1. The sinkage of the vessel is related to these speed ranges. At low speeds the mud layer causes a very slight increase of sinkage while at higher speed a sinkage decrease with mud layer is observed together with an increase of trim.

The propulsion behaviour of the ship is also closely related to the different speed ranges. In the second speed range a given propeller rate results in a significantly lower speed. This is in accordance with 3.2.1.3. An interface elevation in the second speed range implies a higher relative velocity between the ship's hull and the water, which causes an increase of viscous resistance, see Figure 3.7.

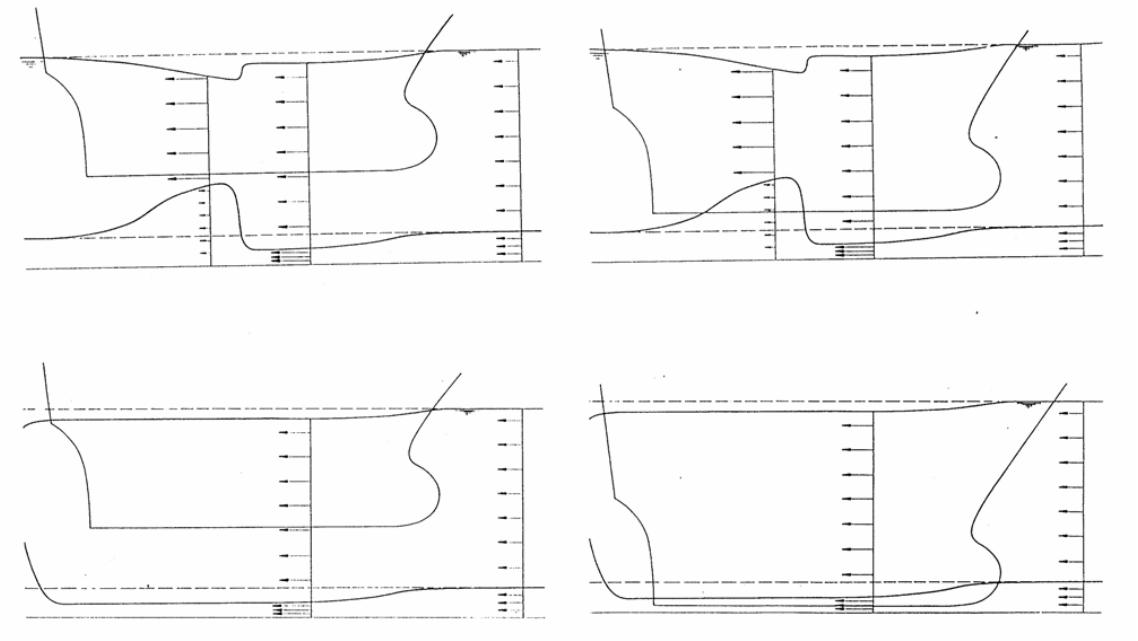

Figure 3.7. Flow around a ship navigating in a two-layer system [3.11].

There is also an effect on the performance of the propellers, as the thrust deduction factor seems to increase in the second speed range. Moreover when the rising takes place near the stern a further loss in propulsive forces has been observed. In addition an interfacial wave making resistance term should be added to the total ship's resistance.

The mud layer also affects the rudder forces. A significant increase of the lateral rudder force has been measured, without increase of the moment due to rudder action. Additionally the rudder action is unstable at small rudder angles and at under keel clearances from -4 to 10% of the draught. This is principally when the ship's keel is in contact with the two different fluids.

In the third speed range the usual shallow water effects are more dominant than mud effects.

3.2.2.4 Recommendations

Although some valuable observations had been made, the authors stated that a captive manoeuvring program was needed, especially to analyse the changed controllability of rudder and propeller.

[3.16] expects that in reality only the upper part of a mud layer is affected by the flow due to the ship's speed, so it is of importance to know the position of this active zone.

For the different types of artificial mud layers, undulations of the water-mud interface and a drop in the speed-rpm relationship were observed as was the case for the natural mud layer. The use of an artificial mud layer is consequently justified.

3.2.3 Research at SOGREAH

The research at SOGREAH has been summarized in **[3.2]**.

3.2.3.1 Motivation

The research study had two aims **[3.2]**:

- To allow ships to use port approach channels subject to siltation, taking full advantage of potential while at the same time ensuring excellent navigability conditions;
- To ensure that technical conditions and maintenance dredging programs are correctly adapted to the real requirements of port operations.

3.2.3.2 Experimental setup

Model scale tests were conducted in a looped wave flume, see Figure 3.8, with a trolley running on rails that pulled the ship model and took the measurements (squat and tractive force). A tanker model was tested at different scales (1/55, 1/75 and 1/100) to model different ships. Two different draughts were used. A large range of under keel clearances was covered.

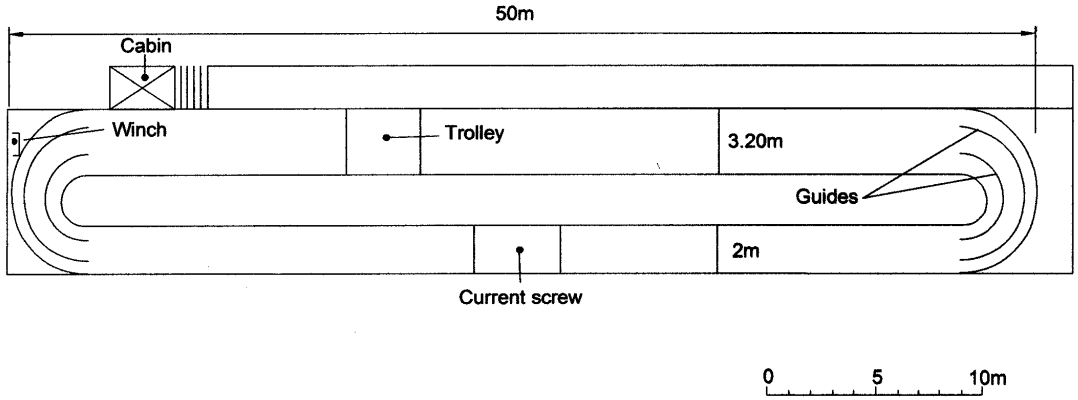

Figure 3.8. Plan of the looped flume [3.2].

The mud was modelled in such way that the rigidity was in proportion with the geometric scale. Unlike the previous described model tests a density gradient was included in function of depth: high, intermediate and low, see Figure 3.9. This was combined with mud of a high rigidity and mud of a low rigidity. Photographs were taken to observe the undulations of the water mud interface. Tests were carried out both above a solid and a muddy bottom and with or without currents.

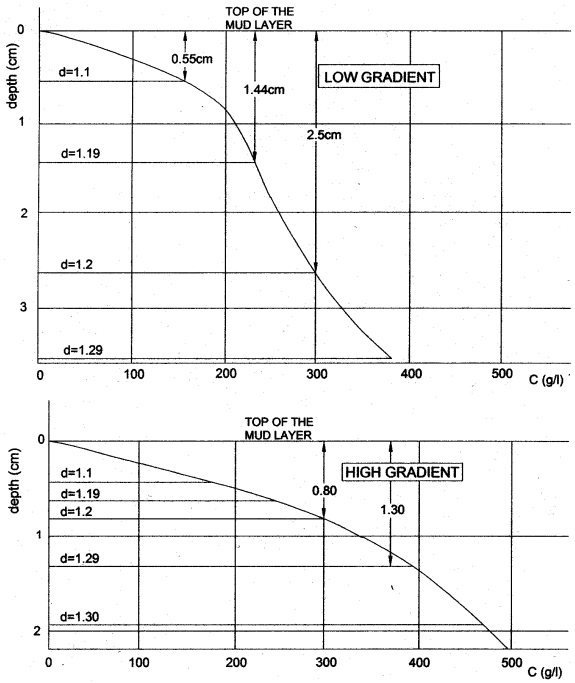

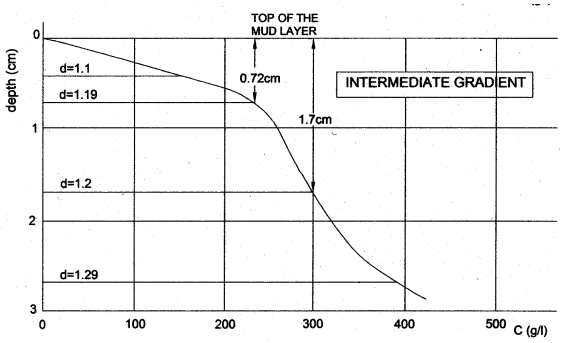

Figure 3.9. Density gradients on the model. Mud of high rigidity. Adapted from [3.2].

3.2.3.3 Observations

Solid bottom

The squat of the ship shows identical results as in **[3.8]**. If currents are included an increase of the sinkage up to 25% has been observed, while the trim does not vary.

The tractive force increases with decreasing under keel clearance and shows a linear relationship with the Froude number. Currents affect the tractive force depending on their direction referred to the direction of the ship's speed.

Muddy bottom

The sinkage is identical as in the solid bottom condition when the ship's keel does not penetrate the mud layer. An effect is observed at negative under keel clearances:

- The rigidity of the mud has only a small effect;
- The density gradient significantly affects the sinkage: the higher the gradient, the smaller the sinkage. It is assumed that the buoyancy is an important factor;
- Adding currents leads to further reduction of the sinkage.

The trim of the vessel is only significantly affected by rigid mud. In this case an increase of trim with increasing density gradient was observed. The sign of the trim changes when penetrating the mud.

Tractive forces are the same as above a solid bottom when the ship navigates above the mud layer. Once the ship penetrates the mud a rapid increase was

observed. Both rigidity and density gradient have their effect. In particular the tractive force could be approximated as:

$$F = F^0 + kV^2 \tag{3.1}$$

with:

- F^0 = 0 at positive under keel clearances and increasing with negative under keel clearance;
- k a coefficient that is higher in muddy areas.

The effect of the currents on tractive forces are equal as above a solid bottom. Undulations of the mud layer were observed with a similar behaviour as in **[3.8]**.

3.3 Full scale tests in muddy areas

3.3.1 Rotterdam

The full scale tests that were carried out in the harbour of Rotterdam are part of the research program described in 3.2.1. In 1975 full scale tests were carried out with a 318 000 deadweight tanker (SS Lepton). The tests consisted on entering the harbour, Figure 3.10, and monitoring the effect of the under keel clearance during a course change **[3.10]**. This was done by analysing the steering capacity, i.e. the maximal percentage of available rudder and propulsion and the speed of the vessel during the manoeuvre. The under keel clearance had no significant effect.

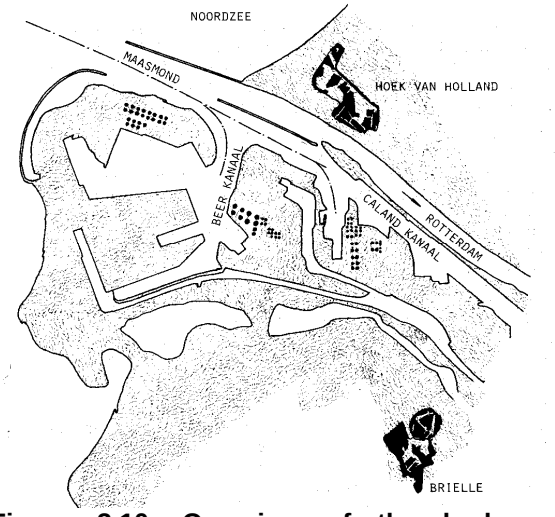

Figure 3.10. Overview of the harbour entrance to Europoort (Rotterdam) [3.10].

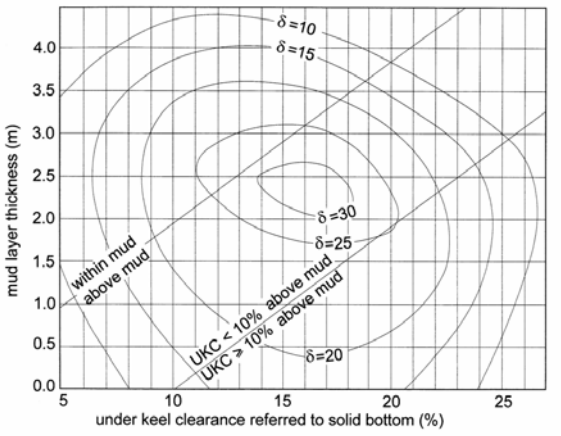

Figure 3.11. The necessary rudder deviation to carry out the course change (at a start speed of 5 knots) in function of the under keel clearance and the mud layer thickness. Adapted from [3.10].

On the other hand, calculations based on the model scale experiments, see Figure 3.11, showed that a small positive under keel clearance above the mud would be the most critical condition. The presence of undulations of the water-mud interface could be confirmed during the full scale tests.

3.3.2 Zeebrugge

Full scale tests were carried out with the double screw suction hopper dredger Vlaanderen XVIII (L_{OA} = 124 m) in 1986 and in 1988 **[3.5, 3.11,3.15]**. A suction hopper dredger was selected because of its availability and its ability to decrease draught rapidly, which is useful to increase the range of possible under keel clearances. The motivation for the full scale tests was:

- To assess the behaviour of the vessel in muddy areas in practical conditions;
- To have a basis for comparison and validation of the model tests.

Several test types were performed at under keel clearances varying between -0.35 m and +3 m referred to the water mud interface **[3.11]**:

- Type I: during a short lapse of time the propellers were put full ahead before the pitch was returned to zero. This is consequently an acceleration manoeuvre followed by a deceleration;
- Type II: constant manoeuvres, the propeller blades were put at a constant pitch;
- Type III: rotation of the ship at zero speed by means of the bow thruster.

The conclusions of the full scale tests were **[3.11,3.15]**:

- It is possible to navigate through top mud, with a tested under keel clearance up till -0.35 m, without any major difficulties. This was a general impression of the ship's crew;
- The under keel clearance, in the tested range of under keel clearances, has no influence on the manoeuvring behaviour of the vessel during slow speed (between -2.5 and 5 knots) trials;
- At higher speeds the resistance of the ship increases, without abrupt transition once the keel penetrates the mud layer, so that the speed and rate of turn of the vessel reduce with 50%.

An occasional full scale trial that deserves to be mentioned is when the ship navigated at slow speed in contact with the probable rheological transition level, situated at a density of 1.20 ton/m³. The crew of the ship thought the vessel would decelerate quickly due to contact with the highly viscous mud layer, but the opposite occurred. The ship kept navigating at slow speed and not even the reversed propellers or bow thrusters were able to stop the vessel. A disaster could be avoided in extremis by decreasing the draught of the vessel **[3.15]**.

A possible explanation for this behaviour is:

- At this level the ship's propeller makes contact with a dense mud layer, resulting in a larger propeller torque, see 6.4.2, so that possibly the normal propeller revolutions could not be reached;

- Propelling in dense mud may result in local recirculation of liquefied mud, so that less thrust is generated. This only happens when a large part of the propeller is immersed in the mud layer **[3.9]**.

These points indicate that the propulsion did not work at that point, so that the vessel could rely less on the braking effect of the reversed propeller.

In general the observations of the full scale test show agreement with the model tests, but the speed range at which the manoeuvring behaviour of the vessel is mostly affected was not included in the full scale trials **[3.15]**.

3.3.3 Nantes Saint-Nazaire

Full scale runs were carried out in the Loire estuary with the tanker “Alsace”. A good agreement was found with the results of the model scale tests at SOGREAH **[3.1]**.

3.4 Theoretical calculations

3.4.1 Introduction

The behaviour of mud has been studied empirically and theoretically by many authors, but mainly for hydraulic purposes. Worthwhile to mention are the investigations of Doctors, Miloh and Zilman **[3.3,3.6,3.19,3.20,3.21]** and Wu **[3.18]**. Furthermore in the literature some examples of rough calculations can be found to take the effect of the mud layer on a vessel rapidly into account.

3.4.2 Investigations of Doctors, Miloh and Zilman

[3.7] demonstrated that in muddy areas a sharp peak of the wave resistance occurs at the vicinity of the critical speed:

$$U_{crit} = \sqrt{\varepsilon g h} \tag{3.2}$$

in which:

$$\varepsilon = \frac{\rho_2 - \rho_1}{\rho_2} \tag{3.3}$$

$$h = \frac{\rho_2}{\frac{\rho_1}{h_1} + \frac{\rho_2}{h_2}} \tag{3.4}$$

U_{crit} increases thus with increasing mud density and increasing layer thickness. By using the potential theory **[3.19,3.20]** it was proved that for a ship moving over a shallow fluid mud layer with relatively low speed $U \sim U_{crit}$, the induced wave resistance is mainly affected by internal wave propagations on the mud-water-interface. On the other hand the viscosity is also of importance: for realistic values of the viscosity (0.1 – 0.001 m²/s) a considerable reduction in the wave resistance peak is attained.

Furthermore there is a clear indication that the shallow water approach can also serve as a quite reliable approximation for analyzing the case of a viscous lower layer, where the mud viscosity can be interpreted as an effective reduction in the total depth of the water **[3.3]**. This approach will be followed in Chapter 10. The mud properties seem to have a profound influence at subcritical speeds F_{nh}[1] < 1, while much less effect is found at supercritical speeds, which suggests that the mud has less chance to respond.

The calculations mainly focus on fast ships **[3.3]**, modelled by a Wigley[2] hull pattern or, on simplified bodies, but give some interesting results that can be compared with experimental data.

3.4.3 Rough calculations

An example of a rough calculation can be found in **[3.4]**. In order to know in which muddy conditions a fictitious ship of 100 000 ton deadweight can manoeuvre, the forces acting on this vessel at a speed of 5 knots are determined. The nautical bottom criterion is related to the strength of the mud: the critical shear stress.

This critical shear stress can be determined by taking the following steps:

- Define the thrust at a speed of 5 knots;
- The difference between the thrust and the resistance at 5 knots is a reserve that can be used to navigate in muddy areas;
- This difference is then a measure for the critical shear stress, leading to a nautical bottom criterion for this condition.

Results of such calculations are of course doubtful. For instance the changed propulsive behaviour above mud layers has not been taken into account, so that the method gives a too optimistic approximation of the nautical bottom criterion.

3.5 Conclusions

In this chapter the state of the art of the research on manoeuvring behaviour in muddy areas has been given. Some conclusions that follow from the different experimental research programs are quite similar:

- Undulations of the water mud interface occur, which are confirmed by full scale tests;
- The undulations have an effect on the manoeuvring behaviour of the ship.

Much emphasis was put on the determination of the resistance. A discussion on the scaling effects of the latter is provided in Appendix E. Nevertheless the programs were limited in time and possibilities, so that no general conclusions could be drawn. Additional experimental research is needed.

[1] F_{nh} is the Froude number based on the real depth.
[2] A Wigley hull form is a hull form that can be described by mathematical formulations.

3.6 References

[3.1] BROSSARD C., CAILLOT M., GALENNE M., GRANBOULAN J., MIGNIOT M., MONADIER P., ROUDIER J. *Sécurité de la navigation dans les chenaux envasés.* Proceedings 27th International Navigation Congress, PIANC, Osaka, Japan, Section II, Subject 1, 1990, pp. 23-28. (In French).

[3.2] BROSSARD C., DELOUIS A., GALICHON P., GRANBOULAN J., MONADIER P. *Navigability in channels subject to siltation.* Proceedings of the 22nd International Coastal Engineering Conference, Delft, The Netherlands, 1990, p. 3088-3101.

[3.3] DOCTORS L.J., ZILMAN G., MILOH T. *The influence of a bottom mud layer on the steady-state hydrodynamics of marine vehicles.* 21st Symposium on Naval Hydrodynamics, 1996, p. 727 – 742.

[3.4] INGENIEURSBUREAU HAVENWERKEN. *Nautische bodem van de voorhaven van IJmuiden*. Report, 1990. (In Dutch).

[3.5] KERCKAERT P., VANDENBOSSCHE D., MALHERBE B., DRUYTS M., VAN CRAENENBROECK K. *Maintenance dredging at the port of Zeebrugge: procedures to achieve an opertational determination of the nautical bottom*. KVIV Harbour Congress, 1988.

[3.6] MILOH T. *Ship motion in non-homogeneous media*. Ship Technology Research, Volume 42, no 3, 1995, pp. 17.

[3.7] MILOH T., TULIN M. P., ZILMAN G. *Dead water effects of a ship moving in stratified seas*, Trans. American society of Mechanical Engineers, Journal of Offshore Mechanics and Arctic Engineering, 115, 1992, p. 105-110.

[3.8] SELLMEIJER R., VAN OORTMERSSEN G. *The effect of mud on tanker manoeuvres.* The Royal Institution of Naval Architects, Spring Meetings 1983, paper no. 7, 1983.

[3.9] TOORMAN E. *Mud rheology: implications for navigability.* Workshop Nautical Bottom, Flanders Hydraulics Research, Antwerp, Belgium, April 29, 2005.

[3.10] VAN BOCHOVE G., NEDERLOF L. *Vaargedrag van diepstekende schepen in slibrijke gebieden.* De Ingenieur, volume 91, no 30/31, 1978, p 525-530. (In Dutch).

[3.11] VAN CRAENENBROECK K., VANTORRE M., DE WOLF P. *Navigation in muddy areas: establishing the navigable depth in the Port of Zeebrugge.* Proceedings of the CEDA PIANC conference, Accesible Harbours, Amsterdam, 1991.

[3.12] VANTORRE M. *Overeenkomst voor samenwerking in de studie van de scheepsgedragingen in verband met de vaargebieden en de zeehavens afgesloten met het Ministerie van Openbare Werken, Waterbouwkundig Laboratorium te Antwerpen-Borgerhout. 4de kwartaal: 16.10.1987-14.01.1988. Deel B. Pilootmodel nautische bodem (Mod. 428). Scheepsmodel METO. Proeven boven slibsimulatiemateriaal trichloorethaan/petroleum.* Gent, 1988. (In Dutch).

[3.13] VANTORRE M. *Overeenkomst voor samenwerking in de studie van de scheepsgedragingen in verband met de vaargebieden en de zeehavens afgesloten met het Ministerie van Openbare Werken, Waterbouwkundig Laboratorium te Antwerpen-Borgerhout. 6de en 7de kwartaal: 16.04.1988-30.09.1988. Deel B. Pilootmodel nautische bodem (Mod. 428). Scheepsmodel DRAGO. Proeven boven kunstmatig samengesteld slib.* Gent, 1988. (In Dutch).

[3.14] VANTORRE M. *Systematische proevenreeksen met het zelfaangedreven schaalmodel van een sleephopperzuiger boven een mengsel petroleum-trichloorethaan als slibsimulatiemateriaal: experimentele waarnemingen en theoretische interpretaties.* Report. Ghent University – Flanders Hydraulics Research, Ghent\Antwerp, 1990. (In Dutch).

[3.15] VANTORRE M. *Meetvaarten met sleephopperzuiger Vlaanderen XVIII te Zeebrugge (1986-1988): interpretatie der meetwaarden en vergelijking met modelproeven.* Report. Ghent University – Flanders Hydraulics Research, Ghent\Antwerp, 1990. (In Dutch).

[3.16] VANTORRE M., COEN I. *On sinkage and trim of vessels navigating above a mud layer.* The Royal Society of Flemish Engineers, Harbour Congress, 1988.

[3.17] WENS F., COEN I., VERBIST F., ROOVERS P. *Mod 428 – Nautische bodem in slibrijke gebieden. Syntheserapport.* Flanders Hydraulics Research, Antwerp, 1984. (In Dutch)

[3.18] WU G.X. *The representation of a body advancing in a stratified fluid by singularity distribution*, International Shipbuilding Progress, Vol. 40, No. 422, 1993, p. 127-135.

[3.19] ZILMAN G., MILOH T. *Hydrodynamics of a body moving over a mud layer – part 1: wave resistance.* Journal of Ship Research, Volume 39 no 3, 1995, p. 194-201.

[3.20] ZILMAN G., KAGAN L., MILOH T. *Hydrodynamics of a body moving over a mud layer – part 2: added mass and damping coefficients.* Journal of Ship Research, Volume 40 no 1, 1996, p. 39-45.

[3.21] ZILMAN G., MILOH T. *Hydrodynamics of a body moving over a mud layer*. 20th Symposium on Naval Hydrodynamics, 21-26 August 1994, Santa Barbara, California, USA. Proceedings: National Academy Press, Washington, D.C., USA, 1996, 18 pp.

No amount of experimentation can ever prove me right; a single experiment can prove me wrong.

A. Einstein

CHAPTER 4

EXPERIMENTAL PROGRAM

4.1 Need for additional research

Besides the general needs, as mentioned in Chapter 1, to carry out research on the manoeuvring behaviour in restricted navigation areas, specific observations at the end of the nineties showed that additional experimental research was acutely needed, not only to ensure the safety of the shipping traffic, but also to improve the maintenance dredging program of the harbour of Zeebrugge (see Appendix F for the port map):

- The registration of simultaneous rheology and density profiles in 1997 by T.V. Noordzee & Kust – N.V. Haecon showed that the actual situation was significantly different from the observations in 1985-88 **[4.2]**. In the central part of the new outer harbour (CDNB [1]) of Zeebrugge, the thickness of the mud layer increased up till 4 m. This layer is characterized by a low and quasi uniform density and a yield stress, which increases gradually and is considerably higher than in 1985-88. The rheological transition is no longer abrupt as observed in the eighties: at two different depths a transition can be noted, see Figure 4.1;

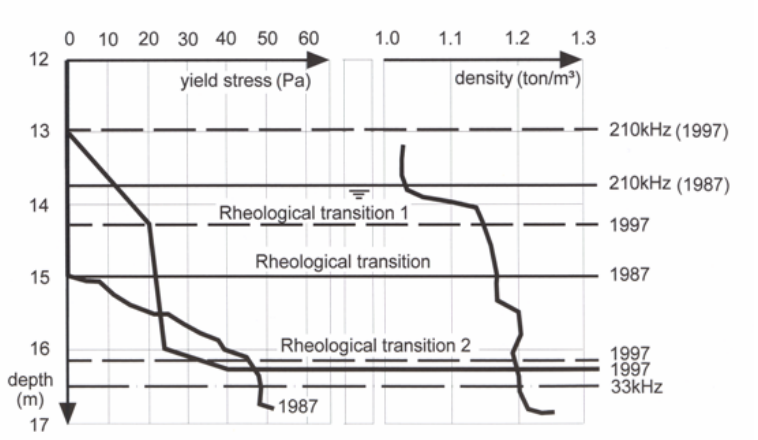

Figure 4.1. Rheology profile of the mud layer in the harbour of Zeebrugge. Comparison between the 1987 and the 1997 measurement campaign Adapted from [4.1]. The single curve for the density is illustrative.

- In the light of these events the question arose whether the 1150 kg/m³ density criterion was still significant. Perhaps the upper part of the mud layer, being loose and fluid, could be incorporated into the under keel clearance of the mud layer. Although, taking the nautical bottom definition into account, the manoeuvrability should be guaranteed;
- Another problem occurred at the swinging area 1 (ZP1), where a diminished manoeuvrability of deep drafted container vessels was observed. The nautical depth in this zone, characterized by a small mud layer, was based on the results of the low frequency echo (33 kHz);
- The results of a comprehensive series of model tests at Flanders Hydraulics (3.2.2), carried out in a provisory setup indicated that the presence of a fluid mud layer could have a negative influence on the controllability of the vessel. This diminished controllability seemed to be related to the deformation of the water-mud interface.

[1] In Dutch: Centraal Deel Nieuwe Buitenhaven

Consequently a redefinition of the nautical bottom was essential and should be based on an investigation of both the characteristics of the mud layer and the nautical implications:

a) *Investigation of the characteristics of the mud layer:* the resumption of the investigation of the relationship between density and rheology, especially the effect of time (the seasons) and space (location in the harbour). Both have their influence on the composition of the mud layer and thus its rheology. A first measurement campaign had been carried out in 1997.
b) Investigation of the nautical implications to establish the link between the manoeuvring behaviour of the ship, the bottom conditions (thickness, density profile and rheology profile of the mud layer) and the under keel clearance.

A research project *Determination of the nautical bottom in the harbour of Zeebrugge: Nautical implications* (April 2001 – July 2004) has been carried out co-operatively by Ghent University and Flanders Hydraulics Research, commissioned by T.V. Noordzee & Kust (Ostend, Belgium) in the frame of the optimisation of the maintenance dredging contract for the harbour of Zeebrugge, financed by the Maritime Access Section of the Flemish Government – Mobility and Public Works Department to investigate the nautical implications as mentioned in point b.

4.2 Selection of mud layers

4.2.1 Simplification and conditions of the mud layer characteristics

In order to assess the manoeuvring behaviour in muddy navigation areas, model captive testing is needed. A captive manoeuvring program has to be carried out above different bottom conditions and under keel clearances. Based on these captive test programs a mathematical model can be built.

It is extremely important that, once a bottom condition has been selected, it does not vary during the execution of a test program. In the ideal situation mud from the harbour of Zeebrugge should be transferred to the towing tank, but as explained in Chapter 2, the thixotropic behaviour of the mud layer leads to changed characteristics. Natural mud has to be replaced by an artificial mud layer, which does not show this time dependent behaviour.

The reader could point out that this simplification has too much effect on the scaling, but in real conditions the characteristics of the mud layer will have changed after the ship has passed. The newly formed mud will only affect the next ship and the first ship will not be affected by the thixotropy of the mud. In order to have a reproducible test program, the thixotropic behaviour of the material can consequently be omitted.

Another point is that the characteristics of the mud layer change with the depth. It is far more difficult to simulate a layered mud layer in a towing tank, so that only mud layers with constant characteristics will be used, see 4.3.2.

Moreover the artificial mud layer should satisfy the following conditions:

- not excessively toxic;
- minimal water-soluble;
- not miscible with water;
- restrictions concerning flash point and flammability;
- acceptable cost for removing the material and the contaminated water;
- acceptable aggression towards the ship models and the coating;
- does not influence the characteristics of water;
- possible to measure the undulations of the interface;
- density and viscosity can be varied between the in situ conditions;
- preferable Bingham-rheology.

The chosen artificial mud layer is characterized by its viscosity and density, but has no initial rigidity. As stated in Chapter 2 a mud layer is characterized by many more variables, but as the rheology is the main criterion, it is sufficient to take the viscosity and the density into account.

4.2.2 Selection of the mud layer material

It was found impossible to find a material that in its pure state would have the appropriate density. Therefore a base material was selected, which could be dissolved in another material to lower the density of the mixture. Of course the additional material has to satisfy the same conditions as the base material.

The material used to simulate the mud layer consists of:

- ***Cloparol52***, a chlorinated paraffin;
- a ***density regulating fluid*** (petrol);
- ***Cloparin50***, a highly viscous chlorinated paraffin, to regulate the viscosity.

With this mixture a wide range of viscosity and density values can be covered. Some disadvantages are:

- The lack of yield stress;
- The temperature dependence of the viscosity.

Moreover due to the corrosive action of the mixture measures had to be taken to protect the painting of the towing tank walls and the ship models.

4.2.3 Selection of density and viscosity values

The selection of the density and viscosity ranges that should be tested is mainly based on the in situ measurements in the harbour of Zeebrugge. Figure 4.2 gives such an example for the measurement campaign carried out in July 1997 at different positions (C1-C11) in the CDNB. As can be clearly seen the artificial mixture of Cloparol52 and petrol can be used to simulate the measured rheology profile.

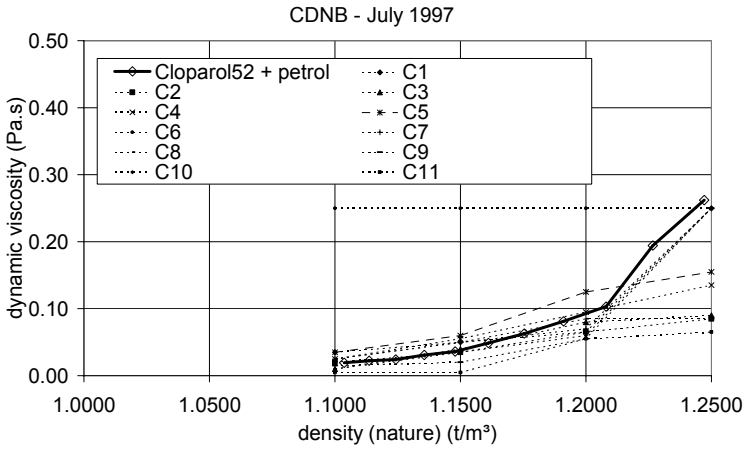

Figure 4.2. Mud samples from the central part of the new outer harbour in Zeebrugge. Density and viscosity of the samples, compared with the combination Cloparol52 and petrol.

Based on Figures like 4.2 the program as presented in Table 4.1 was proposed.

Table 4.1. Proposed characteristics of the mud layers

Mud type	density (nature) $\rho_2^{(N)}$ (kg/m³)	density (model) $\rho_2^{(M)}$ (kg/m³)	dynamic viscosity at 15°C η_2 (Pa.s)
E	1257	1226	0.29
F	1206	1177	0.11
G	1248	1218	0.33
H	1207	1178	0.19
B	1179	1150	0.10
C	1149	1121	0.06
D	1108	1081	0.03

The differences between nature and model densities need additional explanation. Model tests have been carried out in fresh water ($\rho_1^{(M)}$ = 1000 kg/m³), instead of sea water ($\rho_1^{(N)}$ = 1025 kg/m³). In order to have a correct ρ_2/ρ_1 ratio the density of the mud layer has been adapted. The viscosity values are equal on both model and full scale, see Appendix E for more information on scaling.

4.3 Selection of the experimental conditions

4.3.1 Selection of ship models

The initial idea was to use two ship models – available at Flanders Hydraulics Research – to carry out the tests (see Appendix B):

- Ship model D: a fourth generation container carrier (6000 TEU) on a scale 1/75;
- Ship model E of a tanker on a scale 1/85, that is representative for a fuller hull form (tankers, bulk carriers). At this scale the beam of the vessel is 53 m (nature), which is too large to cross the Pierre Vandamme lock (see Appendix F), therefore this model will be used on a scale 1/75.

By the end of the captive testing program (April 2004), it was obvious that soon larger container carriers than ship D would come to Zeebrugge harbour, therefore some runs were carried out with:

- Ship model U: an 8000 TEU container carrier on scale 1/80.

Following draughts were selected:

- model D: T = 13.5 m;
- model E: T = 15.5 m;
- model U: T = 14.5 m.

4.3.2 Selection of the mud layer thickness and under keel clearance

The thickness of the mud layer is also based on the measurements carried out in Zeebrugge harbour:

(1) $h_2^{(N)}$ = 0.75 m;
(2) $h_2^{(N)}$ = 1.50 m;
(3) $h_2^{(N)}$ = 3.00 m.

At the setup time of the experimental program the target depth in the harbour of Zeebrugge was 13.5 m. Consequently the depth above the nautical bottom varied between 14.85 and 18.0 m, taking the tide into account. For that reason the following depths had been selected:

(1) $h^{(N)} = h_1^{(N)} + h_2^{(N)}$ = 14.850 m;
(2) $h^{(N)} = h_1^{(N)} + h_2^{(N)}$ = 15.525 m;
(3) $h^{(N)} = h_1^{(N)} + h_2^{(N)}$ = 17.050 m;
(4) $h^{(N)} = h_1^{(N)} + h_2^{(N)}$ = 17.825 m.

which resulted in the following under keel clearances, referred to the solid bottom:

- model D at depth (1): 10% under keel clearance[2];
- model D at depth (2): 15% under keel clearance;
- model D at depth (3): 26% under keel clearance;
- model D at depth (4): 32% under keel clearance;
- model E at depth (3): 10% under keel clearance;
- model E at depth (4): 15% under keel clearance.

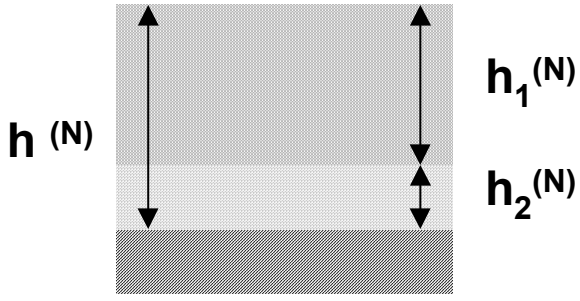

Figure 4.3. Definition of h_1 (height of the water layer), h_2 (mud layer thickness) and h (total depth).

[2] This is the minimal allowed under keel clearance within the harbour of Zeebrugge

For model U the same under keel clearances as for model D have been used, obviously resulting in different water depths. The depth h, further referred to as 'total depth', is the sum of h_1 (height between the water air and the water mud interface) and the thickness of the mud layer h_2, see Figure 4.3.

4.3.3 Environments: combinations of mud layer thickness, mud density and total depth

In the towing tank the term environment is used to define a combination of water depth and any obstacles (see also 1.2.1.2). Specifically in case of the research on manoeuvring behaviour in muddy areas the environment has been defined as a combination of:

- The letters "SLIB", i.e. "MUD" in Dutch;
- Mud type (B, C, D, E, F, G, H);
- Mud layer thickness (1, 2, 3);
- Total depth (1, 2, 3, 4).

Resulting in the following 68 combinations (mud layers E and F have only been tested with mud layer thickness (2)):

Table 4.2. Selected navigation conditions

$h^{(N)}$ (m) / $h_2^{(N)}$ (m)	14.85	15.525	17.05	17.825	x
0.75	SLIB**x**11	SLIB**x**12	SLIB**x**13	SLIB**x**14	G, H, B, C, D
1.50	SLIB**x**21	SLIB**x**22	SLIB**x**23	SLIB**x**24	E, F, G, H, B, C, D
3.0	SLIB**x**31	SLIB**x**32	SLIB**x**33	SLIB**x**34	G, H, B, C, D

In this work a combination of mud layer thickness and mud composition will be mentioned explicitly or referred to as a combination of a letter, defining the mud type, and a figure, defining the mud layer thickness, e.g. g3 stands for mud layer G with thickness 3, i.e. 3 m full scale.

4.3.4 Under keel clearances referred to the water mud interface

Based on the combinations of total depth, mud layer thickness and draught, the under keel clearances referred to the solid bottom and to the water-mud interface can be determined. Doing so for ship model D results in the following table:

- Referred to the solid bottom, in m / in % of draught:

Table 4.3. Tested under keel clearances referred to the solid bottom, ship D.

$h^{(N)}$ (m) / $h_2^{(N)}$ (m)	14.85	15.525	17.05[3]	17.825
0.75	1.35 / 10.0	2.025 / 15.0	~~3.55 / 26.3~~	~~4.325 / 32.0~~
1.50	1.35 / 10.0	2.025 / 15.0	3.55 / 26.3	4.325 / 32.0
3.0	1.35 / 10.0	2.025 / 15.0	3.55 / 26.3	4.325 / 32.0

[3] An under keel clearance of 26.3% or more above the solid bottom with a mud layer of 0.75 m was initially included in the program, but has been removed due to the negligible influence of the mud layer in this situation.

- Referred to the water-mud interface, in m / in % of draught:

Table 4.4. Tested under keel clearances referred to the water-mud interface, ship D.

$h_2^{(N)}$ (m) \ $h^{(N)}$ (m)	14.85	15.525	17.05	17.825
0.75	0.60 / 4.4	1.275 / 9.4	~~2.80/ 20.7~~	~~3.575/ 26.5~~
1.50	-0.15 / -1.1	0.525 / 3.9	2.05/ 15.2	2.825 / 20.9
3.0	-1.65 / -12.2	-0.975 / -7.2	0.55/ 4.1	1.325 / 9.8

Similar tables for ship model E are:

- Referred to the solid bottom, in m / in % of draught:

Table 4.5. Tested under keel clearances referred to the solid bottom, ship E.

$h_2^{(N)}$ (m) \ $h^{(N)}$ (m)	14.85	15.525	17.05	17.825
0.75	~~-0.65 / -4.2~~	~~0.025 / 0.2~~	1.55 / 10.0	2.325 / 15.0
1.50	~~-0.65 / -4.2~~	~~0.025 / 0.2~~	1.55 / 10.0	2.325 / 15.0
3.0	~~-0.65 / -4.2~~	~~0.025 / 0.2~~	1.55 / 10.0	2.325 / 15.0

- Referred to the water-mud interface, in m / in % of draught:

Table 4.6. Tested under keel clearances referred to the water-mud interface, ship E.

$h_2^{(N)}$ (m) \ $h^{(N)}$ (m)	14.85	15.525	17.05	17.825
0.75	~~-1.40 / -9.0~~	~~-0.725 / -4.7~~	0.80 / 5.2	1.575 / 10.2
1.50	~~-2.15 / -13.9~~	~~-1.475 / -9.5~~	0.05 / 0.0	0.825 / 5.3
3.0	~~-3.65 / -23.6~~	~~-2.975 / -19.2~~	-1.45 / -9.4	-0.675 / -4.4

The conditions that are crossed off had not been considered because they were not realistic (E) or not critical (D).

4.3.5 Tests above solid bottom

To be able to evaluate the manoeuvring behaviour above the different muddy bottoms, solid bottom conditions (h_2 = 0) were included as a reference. The following conditions – with exception of the ones that have been crossed off – were considered, with the under keel clearance in m / in % of the draught:

Table 4.7. Tests above solid bottom: ship models D/E

Environment	Water depth $h_1^{(N)}$ (m)	model D, $T^{(N)}$ = 13.5 m	model E, $T^{(N)}$ = 15.5 m
VAST000	14.445	0.945/7.0	~~-1.055/-7.3~~
VAST001	14.85	1.32/10.0	~~-0.65/-4.2~~
VAST002	15.525	2.025/15.0	~~0.025/0.2~~
VAST003	17.05	3.55/26.3	1.55/10.0
VAST004	17.825	4.325/32.0	2.325/15.0
VAST005	20.25	6.75/50.0	~~4.75/30.6~~
VAST006	27	13.5/100.0	~~11.5/74.2~~
VAST007	33.75	20.25/150.0	~~18.25/117.7~~

In the frame of another project **[4.3]**, a whole range of tests with ship model U above solid bottom conditions has been carried out. The different conditions are listed in Table 4.8:

Table 4.8. Tests above solid bottom: ship model U

Under keel clearance (% of draught)	h (m); $T^{(N)}$ = 12.0 m	h (m); $T^{(N)}$ = 13.5 m	h (m); $T^{(N)}$ = 14.544 m
10	13.200	14.850	15.998
35	16.200	18.225	19.634
100	24.000	27.000	29.088

4.3.6 Selection of speeds

A specific program of captive manoeuvring tests has been carried out in each of the proposed conditions (see Appendix A).

One of the most important parameters of the test program was the number and the magnitude of velocities. Not only the magnitudes had to be realistic, for instance between 10 knots (0.6 m/s on a scale 1/75) and -2 knots (-0.12 m/s on a scale 1/75), but also the scientific findings on velocity dependence (see Chapter 3) had to be taken into account. The critical speed at which the manoeuvring and propulsion behaviour significantly changes is a function of the density ratio and the water depth and varies between 3 and 6 knots for the proposed conditions.

The following velocities were selected for the test runs with ship model D:

- 1 velocity astern (2 knots);
- zero speed (bollard pull);
- 2 velocities under the critical speed (2 and 3 knots);
- 2 velocities above the critical speed (6 and 10 knots).

Test runs with ship model E did not include astern manoeuvres, as the emphasis was put on propulsion and steering.

4.4 Test types

4.4.1 Introduction

The development of an accurate mathematical model - able to simulate a wide range of harbour manoeuvres - starts with a well balanced test program, consisting of:

- Captive manoeuvring tests:
  - For model development;
  - For validation.
- Registration of the undulations of the water mud interface (see 5.3.1);
- Filming the undulations (see 5.3.2).

4.4.2 Bollard pull tests

Bollard pull tests have been executed with the combinations of propeller rate and rudder deflection as mentioned in Table 4.9.

Table 4.9. Bollard pull tests

Propeller rate	Rudder deflection
$0.7n_0$	-40°, -30°, -20°, -10°, 0°, 10°, 20°, 30°, 40°
n_0	-40°, -30°, -20°, -10°, 0°, 10°, 20°, 30°, 40°
$-0.7n_0$	0°
$-n_0$	0°

n_0 represents the nominal or maximal propeller rate, i.e. 100 rpm$^{(N)}$ for all tested ship models.

4.4.3 Stationary tests

During the regime of a sub trajectory in stationary tests all kinematical and control parameters are kept constant. The angle of the yawing table of the carriage is linked to the drift angle of the vessel by the following relationship:

- Navigating ahead: $\psi = \beta$;
- Navigating astern: $\psi = 180° + \beta$.

Table 4.10. Stationary tests

Velocity (kn - nature)	Propeller rate	Rudder deflection (°)	ahead (+) astern (-)	ψ (°)
2	$-n_0$	-30, 0, 30	-	0
	$-0.6n_0$	-30, 0, 30	-	0
	$0.75n_0$	-35, -25, -15, 0, 15, 25, 35	-	0
	n_0	-35, -25, -15, 0, 15, 25, 35	-	0
		-35, -15, 15, 35	-	2.5, 5
	$-n_0$	0	+	0, 2.5, 10, 25, 40, 55, 70
	$-0.75n_0$	0	+	0, 2.5
	0	0	+	90, 125, 155, 170
3	$-n_0$	-30°, 0, 30	+	0
		0	+	5
	$-0.75n_0$	0, -30°	+	0, 5
	$0.6n_0$	0	+	0
	n_0	0	+	0
6	$-n_0$	-30°, 0, 30°	+	0, 2.5
		0	+	5
	$-0.75n_0$	-30°, 0, 30°	+	0, 2.5
	$0.6n_0$	-2.5, 0, 2.5	+	0
	n_0	-2.5, 0, 2.5	+	0
10	$0.6n_0$	0	+	0
	n_0	0	+	0

4.4.4 Harmonic sway tests

All parameters are kept constant during regime, while the sway velocity varies harmonically:

$$y(t) = y_0 + y_{0A}\sin\left(\frac{2\pi}{T_y}t + \varphi_y\right) \tag{4.1}$$

The mean value y_0 and the phase φ_y are always zero. The other values are mentioned in Table 4.11.

Table 4.11. Harmonic sway tests

Velocity (kn - nature)	Propeller rate	Sway (model)		
		Amplitude y_{0A} (m)	Period T_y (s)	$\lvert\beta_{MAX}\rvert$ (°)
-2	0	0.2	70, 100	171, 174
	n_0	0.2	70, 100	171, 174
3	0	0.2	30, 40, 60, 80, 100	13, 10, 7, 5, 4
	n_0	0.2	30, 40, 60, 80, 100	13, 10, 7, 5, 4
6	0	0.2	27, 50, 60	7, 5, 4
	n_0	0.2	27, 50, 60	7, 5, 4

4.4.5 Harmonic yaw tests

In these tests all parameters, but the yaw velocity, are kept constant. The yaw velocity varies harmonically:

$$\psi(t) = \psi_0 + \psi_{0A}\sin\left(\frac{2\pi}{T_\psi}t + \varphi_\psi\right) \tag{4.2}$$

The phase φ_ψ is always zero. The other values have been listed in Table 4.12.

Table 4.12. Harmonic yaw tests

velocity (kn - nature)	Propeller rate	Rudder deflection (°)	ahead (+) astern (-)	Yaw (model)			
				average (°)	amplitude (°)	period (s)	$\lvert\gamma_{MAX}\rvert$ (°)
2	0	0	-	0	5, 15, 25	70	173, 160, 148
	0	0	-	+/-5, +/-2.5	15	70	160
	n_0	+/-40, +/-20, 0	-	0	15	70	160
	$-n_0$	0	-	0	15	70	160
	0	*0*	-	*0*	*35*	*70*	*139*
	0	*0*	-	*+/-5, +/-2.5*	*25*	*70*	*148*
	n_0	*+/-40, +/-20, 0*	-	*0*	*25*	*70*	*148*
	$-n_0$	*0*	-	*0*	*25*	*70*	*148*
	0	0	+	0	15, 25, 35	70	20, 32, 41
	0	0	+	+/-10, +/-5, +/-2.5	25	70	32
	n_0	+/-40, +/-20, 0	+	0	25	70	32
	$-n_0$	0	+	0	25	70	32
	$0.5n_0$	*0*	+	*0*	*25*	*70*	*32*
	0	*0*	+	*0*	*15, 25, 35*	*100*	15, 24, 32
	n_0	*0*	+	*0*	*25*	*100*	*24*
	0	*0*	+	*0*	*15, 25, 35*	*40*	33, 48, 57
	n_0	*0*	+	*0*	*25*	*40*	*48*

velocity (kn - nature)	Propeller rate	Rudder deflection (°)	ahead (+) astern (-)	Yaw (model)			
				average (°)	amplitude (°)	period (s)	$\|\gamma_{MAX}\|$ (°)
6	0	0	+	0	5, 12.5, 20	40	4, 10, 16
	0	0	+	+/-10, +/-5, +/-2.5	20	40	16
	n_0	+/-40, 0	+	5	20	40	16
	n_0	+/-40, +/-20, 0	+	0	20	40	16
	$-n_0$	0	+	0	20	40	16
	0	0	+	0	15, 25, 35	27	18, 28, 37
	0	0	+	+/-10, +/-5, +/-2.5	25	27	28
	n_0	+/-40, 0	+	5	25	27	28
	n_0	+/-40, +/-20, 0	+	0	25	27	28
	$-n_0$	0	+	0	25	27	28
	$0.5n_0$	*0*	+	*0*	*25*	*36*	*22*
	0	*0*	+	*0*	*15, 25, 35*	*36*	*14, 22, 30*
	n_0	*0*	+	*0*	*25*	*36*	*22*
	0	*0*	+	*0*	*15, 25, 35*	*22*	*22, 34, 43*
	n_0	*0*	+	*0*	*25*	*22*	*34*

The tests in italic have only been executed in conditions with 15% and 26% of under keel clearance referred to the solid bottom.

4.4.6 Multi-modal tests

The aim of these kinds of tests is to subject the ship model to a large combination of velocities, rudder deflections and propeller rates in one test run. In the current experimental program the following parameters have been varied harmonically:

- The propeller rate n;
- The rudder deflection δ;
- The longitudinal velocity u;
- A combination of kinematical and/or control parameters.

The latter has been used for validation tests. A parameter f follows a harmonic variation during the regime:

$$f(t) = f_m + f_A \sin\left(\frac{2\pi}{T_f} t + \varphi_f\right) \tag{4.3}$$

Where:

- f_m : mean value;
- f_A : amplitude;
- T_f : period;
- φ_f : phase.

4.4.6.1 Harmonic variation of the propeller rate

Variation of velocity, navigation direction, ψ and harmonic variation of the propeller rate:

Table 4.13. Multi-modal tests: harmonic variation of the propeller rate

velocity (kn) (nature)	ahead(+) astern(-)	ψ (°)	Propeller rate (model)			
			average	amplitude	period (s)	phase (°)
2	+	0, 2.5, 5, 10, 25, 40, 55, 70, 90	$0.5n_0$	$0.5n_0$	255	-90
3	+	0, 2.5, 5, 10, 25	$0.5n_0$	$0.5n_0$	170	-90
-2	-	0, 10, 25, 40, 55, 70, 90, 125, 155, 170	$0.5n_0$	$0.5n_0$	255	-90
-2	-	0, 10, 25, 40, 55, 70, 90	$-0.5n_0$	$0.5n_0$	255	90
-2	-	125, 155, 170	$-0.5n_0$	$0.5n_0$	255	-90

4.4.6.2 Harmonic variation of the rudder deflection

Variation of velocity, propeller rate, ψ and harmonic variation of the rudder deflection:

Table 4.14. Multi-modal tests: harmonic variation of the rudder deflection

velocity (kn) (nature)	Propeller rate	ψ (°)	Rudder deflection (model)			
			average (°)	amplitude (°)	period (s)	phase (°)
3	$0.55n_0$	0	0	40	60	0
	n_0	0, 2.5, 10, 25, 40	0	40	60	0
6	0	0, 5, 10	0	40	40	0
	$0.55n_0$	0	0	40	40	0
	n_0	0, 2.5, 5, 10	0	40	40	0
10	0	0, 2.5, 5	0	40	30	0
	$0.55n_0$	0	0	40	30	0
	n_0	0, 2.5, 5	0	40	30	0

4.4.6.3 Harmonic variation of the longitudinal velocity

In these tests only the longitudinal velocity varies harmonically. The other kinematical and control parameters are zero.

Table 4.15. Multi-modal tests: harmonic variation of the longitudinal velocity

Velocity			
average (kn - nature)	amplitude (kn)	period (s) (model)	phase (°)
-1.7	1.7	200	90
5	5	100	-90

4.4.6.4 Validation tests

In the standard experimental program 8 validation tests have been included. Those tests will not be used to build the mathematical model, but are intended as a validation of the mathematical model. The characteristics of the different validation tests are given in Table 4.16.

Table 4.16. Multi-modal tests: validation tests

	Validation 1 (4.4)				Validation 2 (4.5)				Validation 3 (4.6)			
	f_m	f_A	T_f	φ_f	f_m	f_A	T_f	φ_f	f_m	f_A	T_f	φ_f
n	$n_0/2$	$n_0/2$	30s	-90°	$n_0/2$	$n_0/2$	30s	-90°	$n_0/2$	$n_0/2$	30s	-90°
δ	0°	40°	40s	0°	0°	40°	40s	0°	0°	40°	40s	0°
u (m/s)	0.3	0.3	100s	-90°	0.18	0.18	100s	-90°	0.18	0.18	100s	-90°
ψ	-	-	-	-	10°	0°	-	-	-10°	0°	-	-
	Validation 4 (4.7)				**Validation 5 (4.8)**				**Validation 6 (4.9)**			
	f_m	f_A	T_f	φ_f	f_m	f_A	T_f	φ_f	f_m	f_A	T_f	φ_f
n	$n_0/2$	0	-	-	$n_0/2$	$n_0/2$	280s	180°	$n_0/2$	$n_0/2$	280s	180°
δ	-	-	-	-	0°	40°	45s	0°	0°	40°	45s	0°
u (m/s)	0.18	0.18	100s	-90°	0.12	0	-	-	0.12	0.12	140s	90°
ψ	0°	20°	100s	-90°	-	-	-	-	-	-	-	-
r (°/s)	-	-	-	-	0	2.25	70s	90°	0	2.25	70s	90°
	Validation 7 (4.10)				**Validation 8 (4.11)**							
	f_m	f_A	T_f	φ_f	f_m	f_A	T_f	φ_f				
u (m/s)	0	0.1	720s	90°	0	0.1	720s	-90°				
v (m/s)	0	0.1	720s	180°	0	0.1	720s	180°				
ψ	90°	0°	-	-	90°	0°	-	-				
r (°/s)	0.5	0	-	-	-0.5	0	-	-				

4.5 Set-up of the towing tank

The use of an artificial mud layer for captive manoeuvring testing in a towing tank has some consequences:

- The material cost, not only the purchasing cost, but also the cost to remove it ecologically, is proportional with the used volume;
- Water that has been in contact with the artificial mud layer is contaminated and has to be removed ecologically as well;
- As mud layers of different thickness, viscosity and density had to be tested, additional measures had to be taken for the storage and mixing operations.

To decrease the volume of material needed, the towing tank had been split into three parts, see Figure 4.4:

- A test section ($0 < x_0 < 44$ m);
- A reservoir for the storage of the artificial mud (44 m $< x_0 < 49$ m);

- A reservoir for the storage of the contaminated water (49 m < x_0 < 68 m).

Figure 4.4. Flanders Hydraulics Research shallow water tank: division into sections.

Figure 4.5. Flanders Hydraulics Research shallow water tank: mud reservoir with pump system.

The mixing of the artificial mud layer was outsourced. To perform tests with the thickest mud layer in the test section 14 m³ of artificial mud was needed. The mud was delivered by the outsourcer in barrels of 1 m³ each. The barrels were placed upon a platform next to the mud reservoir, see Figure 4.5, and then emptied into the mud reservoir. A pump system allowed the transportation of the fluids from one section to another.

Due to the corrosive action of the artificial mud layer, the bottom and the walls of the tank received a polyethylene coating. However the coating did not seem to be mud resistant over a longer span of time, as it absorbed the mud. As a result bulges appeared on the bottom of the towing tank. Test runs had to be adapted in order to avoid the bulges and in the end the coating had to be replaced. It is clear that better options for coating exist, such as polyvinylidene fluoride (PVDF), a product at least 10 times pricier than polyethylene.

4.6 References

[4.1] DE MEYER C.P., MALHERBE B. *Optimisation of maintenance dredging operations in maritime and estuarine areas.* Terra et Aqua 35, 1987, p 25-39.

[4.2] TV NOORDZEE EN KUST. *Bepaling van de nautische bodem. Opname van simultane rheologische en densiteitsprofielen. Deel 3: statistische analyse der meetresultaten.* Haecon, 1997. (In Dutch).

[4.3] VERZHBITSKAYA E., VAN KERKHOVE G., DELEFORTRIE G., VANTORRE M. *Leveren van wetenschappelijke bijstand voor het uitvoeren van proeven en het opstellen van wiskundige manoeuvreermodellen voor 8000 TEU containerschepen voor de toegang tot de Vlaamse havens – Deelopdracht 1 – Opmaken van een proevenprogramma voor gedwongen manoeuvreerproeven in de sleeptank voor manoeuvres in ondiep water.* Research project UGent-WL Mod. 749. Ghent / Antwerp, 2005. (In Dutch).

That great principle of undulation in nature, that shows itself in the inspiring and expiring of the breath; in desire and satiety; in the ebb and flow of the sea; in day and night; in heat and cold

R.W. Emerson

CHAPTER 5

UNDULATIONS OF THE WATER-MUD INTERFACE AND SINKAGE

5.1 Theory

5.1.1 Introduction

In all the model test programs that were carried out previously, see Chapter 3, undulations of the water mud interface had been observed. Moreover the undulations seemed to have a significant influence on the manoeuvring behaviour of the vessel. Consequently it is important to register the undulations that occur to assess their effect on the manoeuvring behaviour. This chapter will describe the measurement setup and provide a discussion of the observations. First of all an overview is given of theoretical calculations carried out in **[5.1,5.4,5.5,5.6]** that explain the existence of undulations of the interface and describe their behaviour.

5.1.2 Theory for ideal fluids

Consider a fixed vessel in a canal of width W in contact with two fluids that are moving with a velocity –U. The continuity equations are, see Figure 5.1:

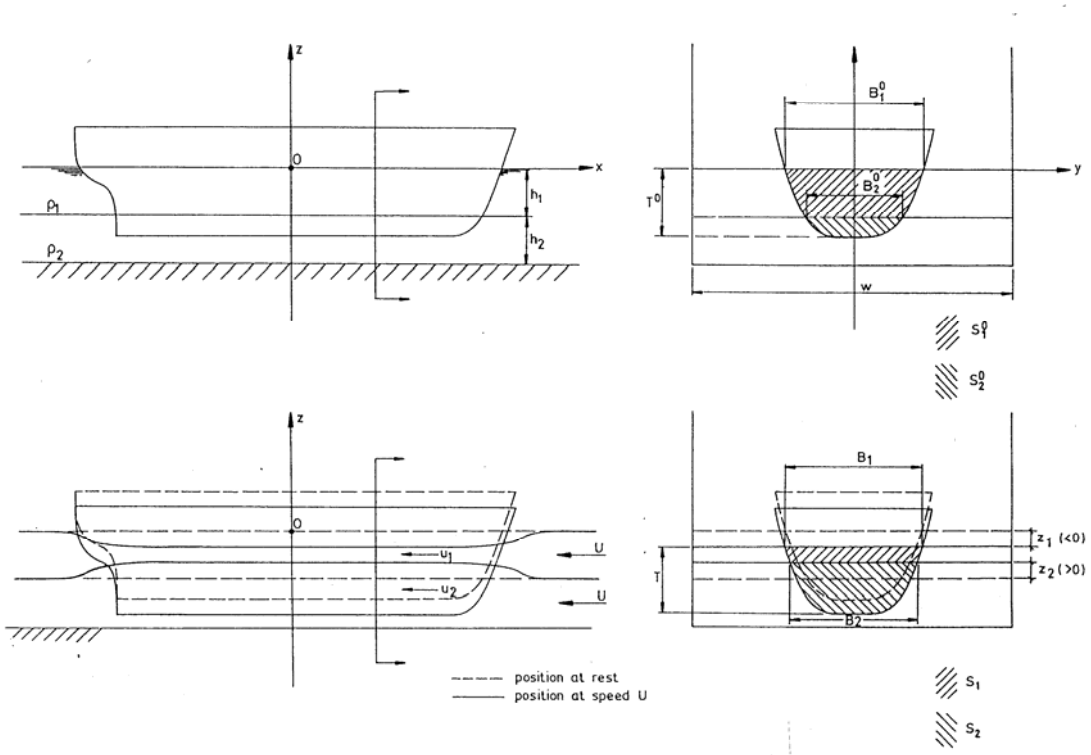

Figure 5.1. Symbols and conventions [5.5]

$$-UWh_1 = u_1(x)\left[W\left(h_1 + z_1(x) - z_2(x)\right) - S_1(x)\right] \quad (5.1)$$

$$-UWh_2 = u_2(x)\left[W\left(h_2 + z_2(x)\right) - S_2(x)\right] \quad (5.2)$$

In which S_i represents the wetted cross section of the vessel in contact with fluid i. As the fluid is considered ideal the Bernoulli equation applied to the free surface gives:

$$\frac{1}{2}U^2 = \frac{1}{2}u_1^2(x) + gz_1(x) \tag{5.3}$$

While on the interface between the two fluids the pressure has to be identical on both sides, leading to:

$$\rho_1\left[\frac{1}{2}u_1^2(x) + gz_2(x)\right] - \rho_2\left[\frac{1}{2}u_2^2(x) + gz_2(x)\right] = \frac{1}{2}[\rho_1 - \rho_2]U^2 \tag{5.4}$$

From the set of equations (5.1-5.4) the positions of the free surface z_1 and the position of the interface z_2 can be substituted, so that the following expressions are obtained:

$$f_1 = \frac{1}{2}F_1^2\frac{1}{1-\frac{\rho_1}{\rho_2}}\left[\frac{-u_1(x)}{U}\right]^3 - \left[1 - m_1(x) + \frac{1}{2}F_1^2\frac{1}{1-\frac{\rho_1}{\rho_2}}\left[\frac{-u_2(x)}{U}\right]^2\right]\left[\frac{-u_1(x)}{U}\right] + 1 = 0 \tag{5.5}$$

$$f_2 = \frac{1}{2}F_2^2\left[\frac{-u_2(x)}{U}\right]^3 - \left[1 - m_2(x) + \frac{1}{2}F_2^2\left[1 - \frac{\rho_1}{\rho_2} + \frac{\rho_1}{\rho_2}\left(\frac{-u_2(x)}{U}\right)^2\right]\right]\left[\frac{-u_2(x)}{U}\right] + 1 = 0 \tag{5.6}$$

In which F_1 and F_2 are depth related Froude numbers, given by:

$$F_1 = \sqrt{\frac{U^2}{gh_1}} \tag{5.7}$$

$$F_2 = \sqrt{\frac{U^2}{gh_2\left(1 - \rho_1/\rho_2\right)}} \tag{5.8}$$

m_1 and m_2 are local blockage factors of the upper and lower fluid layers:

$$m_i(x) = \frac{S_i(x)}{Wh_i} \tag{5.9}$$

Suppose the vessel has a positive under keel clearance referred to the water mud interface: $m_2 = 0$. Plots of equations (5.5-5.6) at different speeds U showed that, see Figure 5.2:

- At low speeds four solutions occur: two predict an interface sinkage, the two others predict an interface rising;
- The solutions, which predict an interface rising, converge with increasing speed;
- At a critical speed both solutions are equal, a further increase of speed can only result in an interface sinkage.

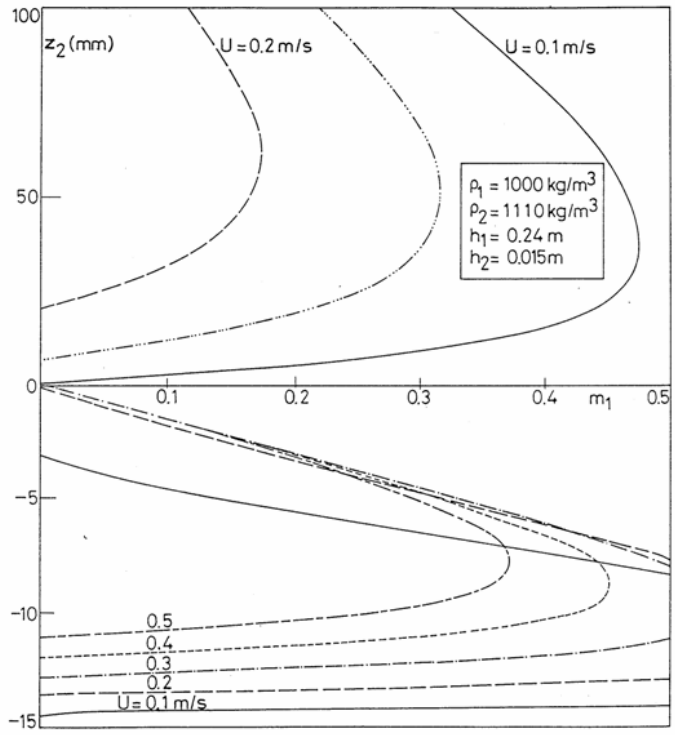

Figure 5.2. Vertical movements of the interface: possible equilibrium conditions

The effect of the speed on the undulations of the interface is in accordance with the observations in 3.2.2.3. The critical speed, at which a rising of the interface can no longer occur below the ship's hull, can also be approximated. **[5.5]** states that ($-u_2/U$) can be omitted in (5.5), so that:

$$f_1 \approx \frac{1}{2}F_1^2 \frac{1}{1-\frac{\rho_1}{\rho_2}}\left[\frac{-u_1(x)}{U}\right]^3 - \left[1-m_1(x)\right]\left[\frac{-u_1(x)}{U}\right] + 1 = 0 \qquad (5.10)$$

In order to have a single solution the derivative of (5.10) to ($-u_1/U$) should also equal zero:

$$\frac{\partial f_1}{\partial\left(-u_1/U\right)} \approx \frac{3}{2}F_1^2 \frac{1}{1-\frac{\rho_1}{\rho_2}}\left[\frac{-u_1(x)}{U}\right]^2 - \left[1-m_1(x)\right] = 0 \qquad (5.11)$$

From (5.10) and (5.11) an expression for the critical speed can be found:

$$U_{crit} = \sqrt{\frac{8}{27}gh_1\left[1-\frac{\rho_1}{\rho_2}\right](1-m_1)^3} \qquad (5.12)$$

(5.12) gives an expression for the critical speed at which a rising of the interface can only occur behind the stern of the ship. If m_2 does not equal zero (5.12) can also be used, but the blockage m_1 will be smaller and consequently the critical speed will increase.

[5.6] gives an approximation for the position x_J at which the jump of the interface occurs, based on the assumption that the volume of the lower fluid mud layer is constant:

$$\int_{-\frac{L}{2}}^{\frac{L}{2}} \left(Wz_2(x) - S_2(x)\right)dx = \int_{-\frac{L}{2}}^{x_J} \left(Wz_2^+(x) - S_2(x)\right)dx + \int_{x_J}^{\frac{L}{2}} \left(Wz_2^-(x) - S_2(x)\right)dx = 0 \qquad (5.13)$$

$z_2^+(x)$ and $z_2^-(x)$ represent the possible values for interface elevation (>0) and sinkage (<0) at section x.

5.1.3 Theory for viscous fluids

The application of the Bernoulli equation in 5.1.2 implies that the fluids are inviscid. Of course in case of a mud layer the viscosity should not be neglected. Starting from the Navier-Stokes equations **[5.1]** showed that the dynamic pressure matching along the interface (5.4) can be written as:

$$\rho_1\left[\frac{1}{2}u_1^2(x)\left(1+\left(\frac{\partial z_2}{\partial x}\right)^2\right)+gz_2(x)\right]-\rho_2\left[\frac{1}{2}u_2^2(x)\left(1+\left(\frac{\partial z_2}{\partial x}\right)^2\right)+gz_2(x)\right] \qquad (5.14)$$
$$-\left[\mu_1\frac{\partial u_1}{\partial x}-\mu_2\frac{\partial u_2}{\partial x}\right]=\frac{1}{2}[\rho_1-\rho_2]U^2$$

From the observations of the risings it can be concluded that the steepness of the undulations is small. Furthermore the viscosity of the upper water layer can be neglected, thus (5.4) becomes:

$$\rho_1\left[\frac{1}{2}u_1^2(x)+gz_2(x)\right]-\rho_2\left[\frac{1}{2}u_2^2(x)+gz_2(x)\right]+\mu_2\frac{\partial u_2}{\partial x}=\frac{1}{2}[\rho_1-\rho_2]U^2 \qquad (5.15)$$

while (5.3) remains identical. The set of equations (5.5) and (5.6) contain now a differential term. A solution for this problem has to be found numerically. Due to these complications (5.12) has been used which gives good results when the viscosity of the mud layer is small as was the case in the experimental research programs described in Chapter 3. Finally it is worthwhile to mention that equation (5.12) differs from the maximum velocity of propagation of internal waves, which is given by the formula:

$$C_{MAX}=\sqrt{gh_2\left(1-\frac{\rho_1}{\rho_2}\right)} \qquad (5.16)$$

As a consequence the undulation that occurs in the water-mud interface is rather a hydraulic jump than an internal wave **[5.1]**.

5.2 Experimental setup

The undulations of the interface have been registered in two ways:

- Using level followers, measuring the water air and the water mud interface 20 times per second;
- By video-recording or photographing the undulations.

5.2.1 Set-up

A mud level follower (mufo) and a water level follower (wafo) are assembled together on a platform supported by a tripod. The assembled system is referred to as wave meter, see Figure 5.3.

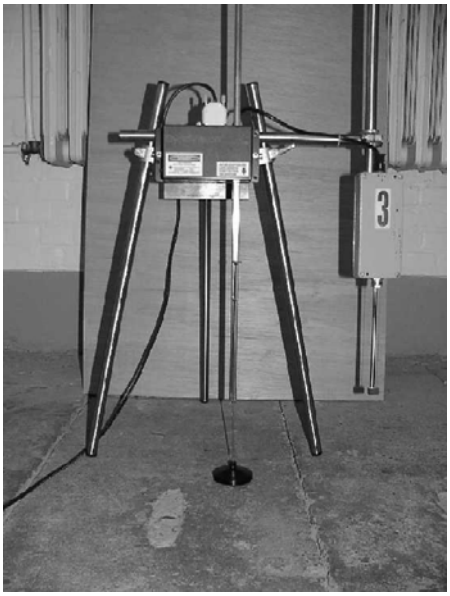

Figure 5.3. Front view of wave meter 3. The float of the mufo is resting on the ground. The black box emits a laser beam, which can be seen as a white glow. The box with number 3 on it is the equipment of the wafo.

5.2.1.1 Working principle of the mufo

The mufo consists of a chemical resistant floater with a density between water and mud. The floater rests upon the water-mud interface so that the undulations of the interface are linked to the vertical movement of the floater. The floater is connected to a disc which reflects a laser beam; consequently the variations of the reflected distance are a measure for the undulations.

5.2.1.2 Working principle of the wafo

The wafo has been designed for the use in a towing tank and is based on the principle of a potentiometer, see Figure 5.4. A constant current is sent through a homogeneous resistance wire. The voltage along the wire is thus constant. A tube in stainless steel is the second electrode. Within the tube two wires are connected to the end of the resistance wire. The tube will serve as a conductor - proportional with the immersion - for the potentiometer. The measured voltage is consequently a measure for the immersion of the wire or the undulation of the water-air interface.

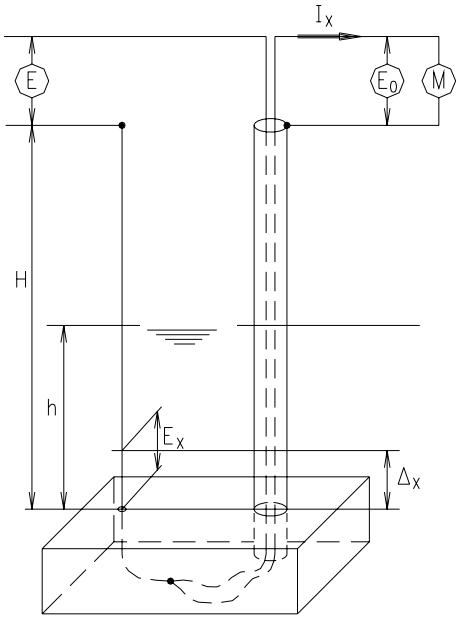

Figure 5.4. Working principle of the wafo

5.2.1.3 Positioning the wave meters

The measurements of the undulations have to be easily reproducible. Therefore the wave meters are always positioned at the same location. The location can effortlessly be determined using the positioning system of the towing carriage, see Figure 5.5 for the layout of positioning.

5.2.2 Visualisation

Videos of the undulations of the water mud interface have been recorded with a digital handy cam (Digital Video Camera Recorder-Sony DCR-TRV 520 E). In order to be able to film under water a box with front made out of Plexiglas has been built, see Figure 5.6.

Figure 5.6. Film set.

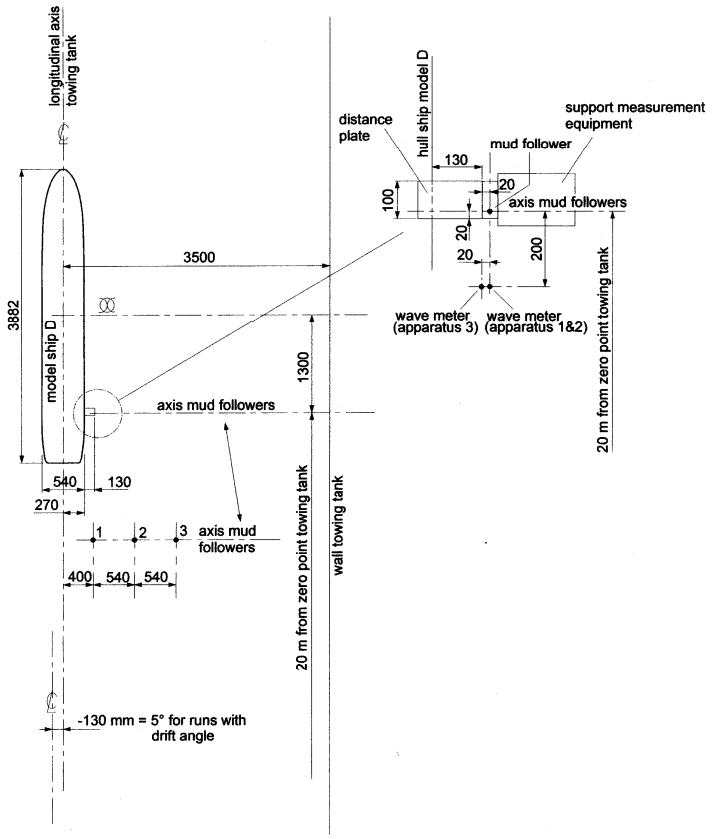

Figure 5.5. Positioning of the wave meters in the towing tank.

This waterproof box is placed longitudinally in the towing tank with its centre at x_0 = 20 m. The undulations can be recorded using a mirror, placed with a slope of 45°, within the box.

In two separate compartments bulbs were installed to provide the necessary illumination. A transparent measuring film was glued on the front of the box to allow the estimation of the magnitude of the undulations.

5.3 Test program

5.3.1 Wave meters

Three wave meters were used to measure the undulations of the interface, see Figure 5.5. The position of the wave meters has been based upon:

- The mufos were placed at x_0 = 20 m, which is the middle of the test section. In this way the accelerations or decelerations of the vessel have an insignificant influence on the registration;
- A first wave meter had to be placed as close as possible to the passing ship model. Due to the size of the wave meter and the equipment of the ship model, the closest possible was 130 mm from the ship's side. The lateral distance between each wave meter was equal to the ship's beam.
- The undulations of the interface are only registered with stationary tests. As they have a fixed straight trajectory the position of the ship referred to the wave meter can easily be determined. At zero drift angle the ship

navigates along the centre line of the tank. In this case the lateral positions of the wave meters are:

- y_1 = 0.5 B + 130 mm;
- $y_2 = y_1$ + B;
- $y_3 = y_2$ + B.

With the registrations of the undulations of the water mud interface the influence of the following parameters can be analysed:

- *Influence of the ship's velocity*.
  Tests have been carried out with increasing velocity in steps of 0.06 m/s (1 knot nature) to estimate the critical speed. With lower density mud layers even steps of 0.03 m/s have been used.
- *Influence of the propeller rate.*
  At one speed ahead and one speed astern tests have been conducted with 0%, 60% and 100% of the nominal propeller rate.
- *Influence of the drift angle and rudder deflection*
  At one speed ahead tests were conducted with a small drift angle up to 5° and rudder deflection up to 30°. Of course due to the drift angle the ship model cannot be towed along the centre line without collision with the wave meters, therefore the ship model is towed along a lateral position of y = -130 mm.

The test program has been resumed in Table 5.1.

Table 5.1. Test program for the registration of the undulations of the interface.

Velocity (kn - nature)	Propeller rate	ahead (+) astern (-)	y (mm-model)	ψ (°)	Rudder deflection (°)
2	$-0.6n_0$, 0, $0.6n_0$	-	0	0	0
	0	+	0	0	0
2.5[1]	0	+	0	0	0
3	0	+	0	0	0
		+	-130	+/-5, +/-2.5	0
	$0.6n_0$	+	*-130*[2]	*-5*	*0*
			0	0	0
			-130	*5*	*0*
	n_0	+	*-130*	*-5*	*-30, 0, 30*
			0	0	0
			-130	*5*	*-30, 0, 30*
3.5	0	+	0	0	0
4	0	+	0	0	0
4.5	0	+	0	0	0
5	0	+	0	0	0
5.5	0	+	0	0	0
6	$-0.6n_0$, 0, $0.6n_0$, n_0	+	0	0	0
6.5	0	+	0	0	0
7	0	+	0	0	0
7.5	0	+	0	0	0
8	0	+	0	0	0
8.5	0	+	0	0	0
9	0	+	0	0	0

[1] Speed steps of 0.5 kn were used for registration of mud D.
[2] Italic values have only been carried out for registration of mud layer E and F.

Velocity (kn - nature)	Propeller rate	ahead (+) astern (-)	y (mm-model)	ψ (°)	Rudder deflection (°)
9.5	0	+	0	0	0
10	0	+	0	0	0
10.5	0	+	0	0	0

5.3.2 Visualisation

The filming of the undulations has been carried out with the film set as described in 5.2.2. The lateral axis of the box was placed at x_0 = 20 m to avoid influences of the acceleration or deceleration of the vessel.

The box was placed along the wall of the towing tank, allowing its placement without entering the muddy test section. The ship model has been towed along a lateral position of y = +2000 mm to be able to film the undulations without colliding with the box.

The main purpose of the filming was illustrative and intended as a support for the interpretation of the results of the wave meters. The test program was thus the same, except for the y-values in Table 5.1 which had to be increased with 2000 mm.

5.4 Observations

5.4.1 General

In general the undulations of the interface depend on:

- The ship velocity;
- The propeller rate;
- The vessel type;
- The drift angle;
- The thickness of the mud layer;
- The under keel clearance;
- The composition of the mud layer.

Figure 5.7 shows that a variation of the rudder angle does not lead to a significantly different shape of the undulations. Consequently the rudder deflection has no significant influence on the undulations of the interface.

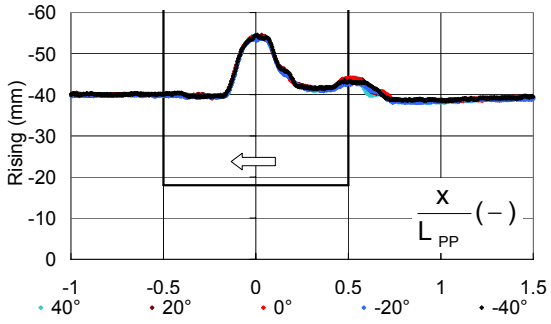

Figure 5.7. Ship model D: undulations of the interface at mufo 1 for different rudder angles. -12% under keel clearance referred to the water mud interface. U = 0.36 m/s, no propeller action.

5.4.2 Undulations of the interface for a 10 mm thick mud layer (0.75 m nature)

The undulations of a 10 mm thick mud layer are represented for different series and speeds in Figures 5.8a and 5.8b:

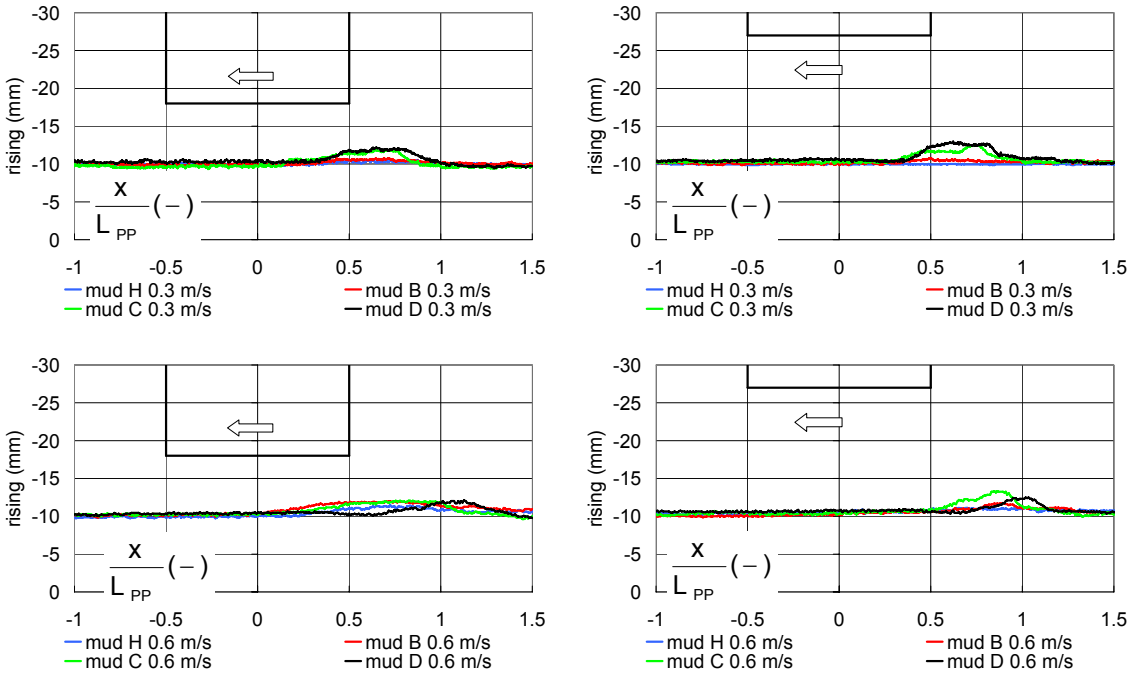

a. 4.4% under keel clearance referred to the water mud interface.

b. 9.4% under keel clearance referred to the water mud interface.

Figure 5.8. Ship model D: undulations of the interface at mufo 1 at different speeds, no propeller or rudder action. Thickness of the mud layer: 10 mm.

- The undulation increases with decreasing density and viscosity. The differences are larger at the largest under keel clearance;
- The maximal magnitude is reached at small velocities. The magnitude does not increase further with increasing speed, or will even decrease (mud D).

The maximum of the rising moves abaft with decreasing viscosity and density. Some characteristics of the rising are represented in Figures 5.9a-5.9c in function of the ship's velocity:

- The water mud interface of the higher density mud layer does not appear to undulate when a ship navigates above it. If the density and viscosity decrease the undulations increase with increasing speed, but for the lowest density mud layers a maximum is reached at a smaller velocity to further decrease with increasing velocity;
- At small speeds the magnitude is maximal near aft. This maximum occurs more abaft with increasing speed, especially with mud layers of small viscosity and density.
- The undulation starts near aft. At the highest speed, the undulation above mud layer D only starts after the ship has passed by, this can explain why in this case the magnitude decreases.

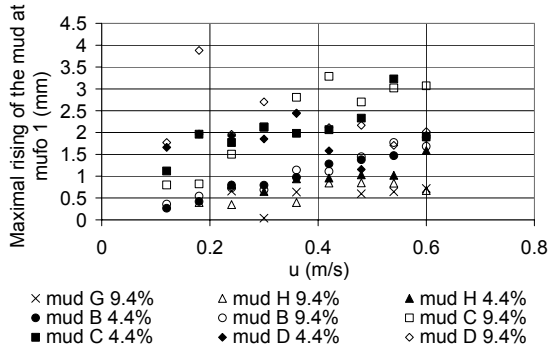

a. maximal rising in function of ship speed.

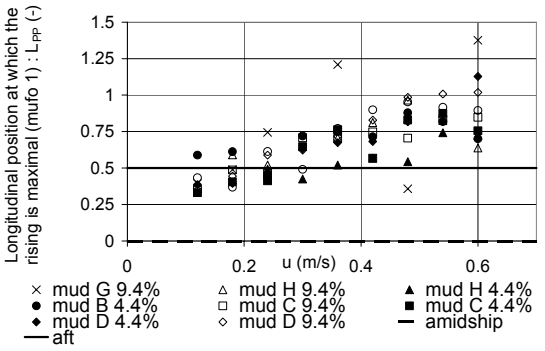

b. longitudinal position, at which the rising is maximal, in function of ship speed.

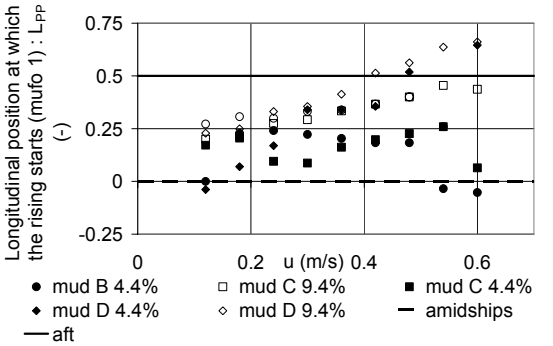

c. longitudinal position, at which the rising starts, in function of ship speed.

Figure 5.9. Ship model D. Thickness of the mud layer: 10 mm. No propeller or rudder action.

The influence of the propeller rate is shown on Figures 5.10a and 5.10b:

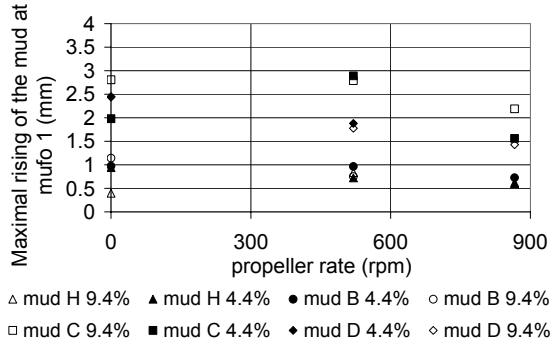

a. maximal rising in function of the propeller rate.

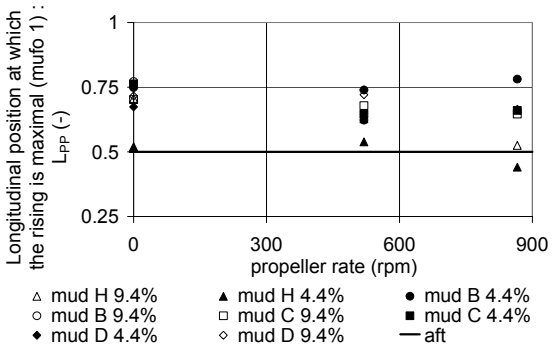

b. longitudinal position, at which the rising is maximal, in function of the propeller rate.

Figure 5.10. Ship model D. Thickness of the mud layer: 10 mm. Ship speed = 0.36 m/s. No rudder action.

- An increase of propeller rate results in a decrease of the magnitude of undulations [3]. The decrease is most significant for low density mud layers;
- The maximal rising moves abaft with increasing propeller rate.

[3] A detailed analysis shows that the top of the rising widens, while the magnitude decreases, the contained energy or perturbations do not diminish. An increased propeller rate consequently collapses the rising.

5.4.3 Undulations of the interface for a 20 mm thick mud layer (1.5 m nature)

Figures 5.11a and 5.11b represent the undulations of the interface when the ship model navigates above a 20 mm thick mud layer:

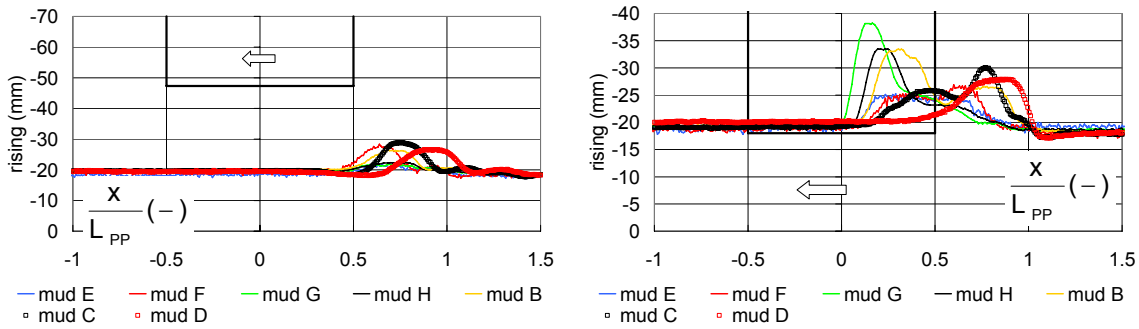

a. 3.9% under keel clearance referred to the water mud interface.

b. -1.1% under keel clearance referred to the water mud interface.

Figure 5.11. Ship model D: undulations of the interface at mufo 1, no propeller or rudder action. Ship speed = 0.6 m/s. Thickness of the mud layer: 20 mm.

- If the keel does not penetrate the mud layer, the rising will increase with decreasing density and viscosity until a certain density and viscosity. For even smaller densities and viscosities the rising will decrease again;
- If the keel penetrates the mud layer the rising occurs amidships for the highest densities and viscosities and aft for the smallest densities and viscosities. A double rising is observed for intermediate densities and viscosities.

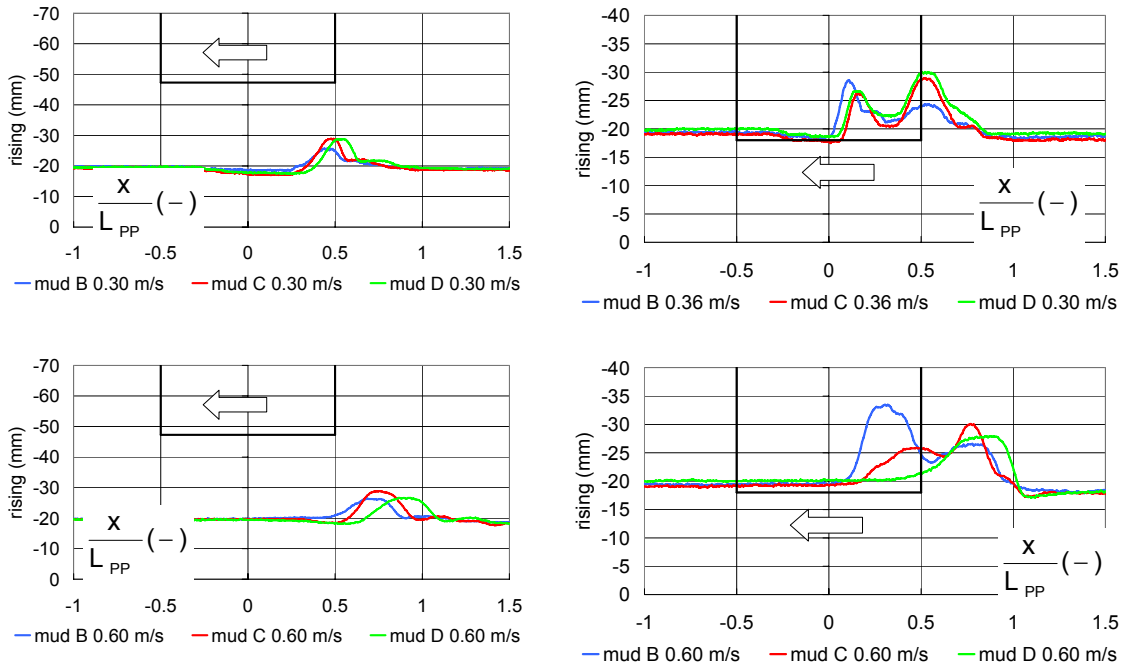

a. 3.9% under keel clearance referred to the water mud interface.

b. -1.1% under keel clearance referred to the water mud interface.

Figure 5.12. Ship model D: undulations of the interface at mufo 1 at different speeds, no propeller or rudder action. Thickness of the mud layer: 20 mm.

Figures 5.12a and 5.12b give an overview of the undulations at different speeds:

- With the lowest density mud layer the rising seems to decrease again;
- A double rising of the interface can be observed with the lowest density mud layers at low speeds and when the ship penetrates the mud layer.

Which can be confirmed by the results on Figures 5.13 - 5.15.

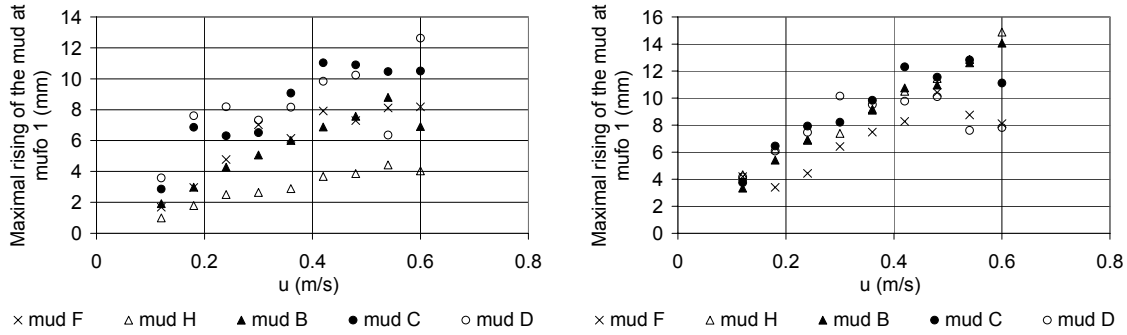

a. 3.9% under keel clearance referred to the water mud interface.

b. -1.1% under keel clearance referred to the water mud interface.

Figure 5.13. Ship model D: maximal rising in function of ship speed. Thickness of the mud layer: 20 mm. No propeller or rudder action.

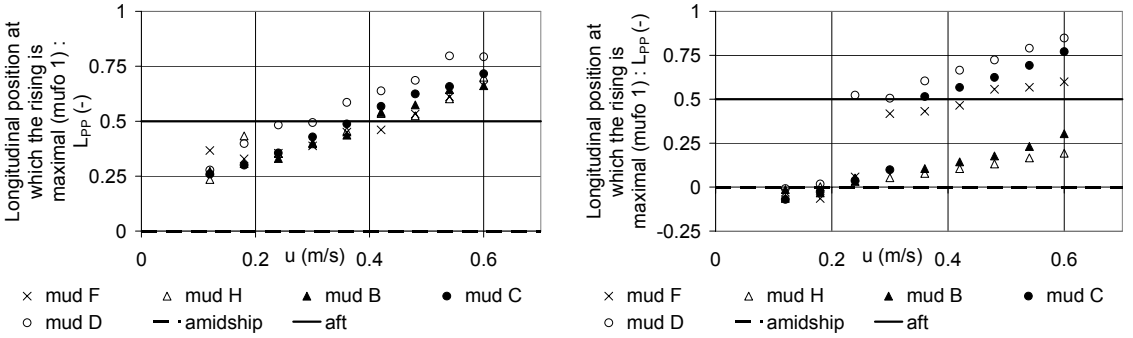

a. 3.9% under keel clearance referred to the water mud interface.

b. -1.1% under keel clearance referred to the water mud interface.

Figure 5.14. Ship model D: longitudinal position, at which the rising is maximal, in function of ship speed. Thickness of the mud layer: 20 mm. No propeller or rudder action.

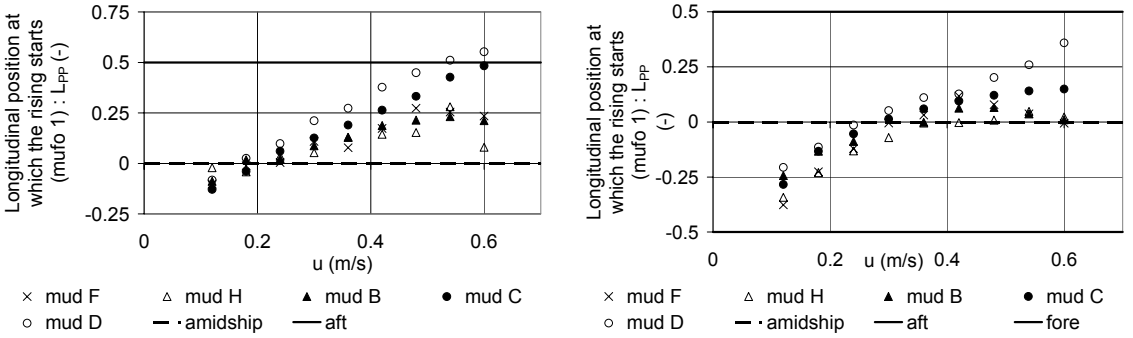

a. 3.9% under keel clearance referred to the water mud interface.

b. -1.1% under keel clearance referred to the water mud interface.

Figure 5.15. Ship model D: longitudinal position, at which the rising starts, in function of ship speed. Thickness of the mud layer: 20 mm. No propeller or rudder action.

The maximal risings in function of the propeller rate are given for the first quadrant in Figures 5.16a and 5.16b. A positive increase of propeller rate only results in a small increase of the magnitude. A further increase of propeller rate usually results in a magnitude decrease.

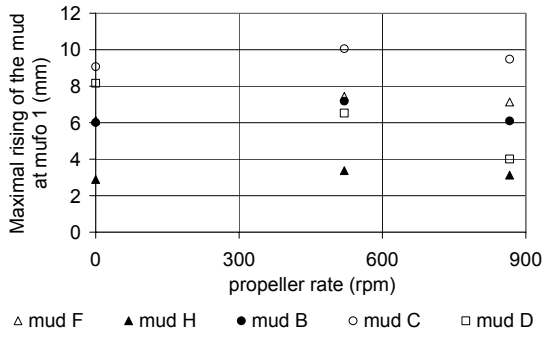

a. 3.9% under keel clearance referred to the water mud interface.

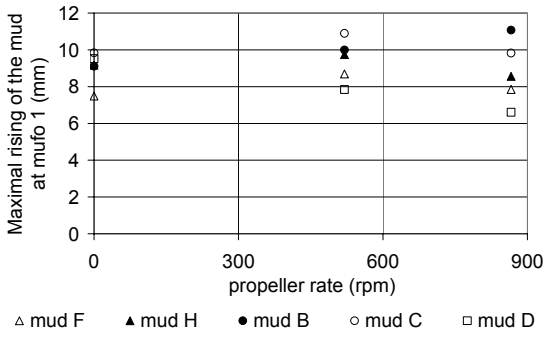

b. -1.1% under keel clearance referred to the water mud interface.

Figure 5.16. Ship model D: maximal rising in function of propeller rate. Thickness of the mud layer: 20 mm. No rudder action, ship speed = 0.36 m/s.

The longitudinal position at which the rising is maximal can be analysed with Figures 5.17a and 5.17b:

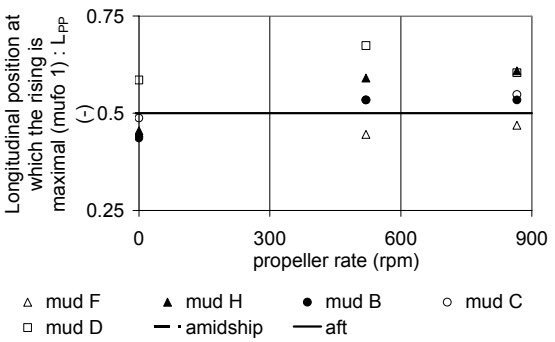

a. 3.9% under keel clearance referred to the water mud interface.

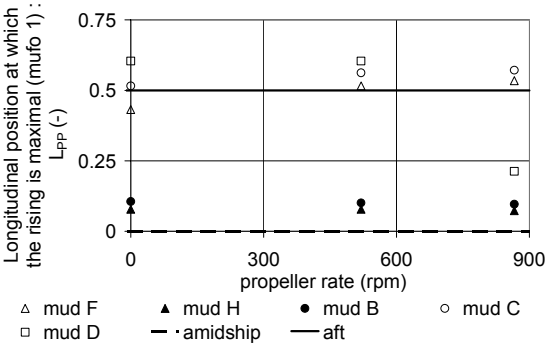

b. -1.1% under keel clearance referred to the water mud interface.

Figure 5.17. Ship model D: longitudinal position, at which the rising is maximal, in function of propeller rate. Thickness of the mud layer: 20 mm. No rudder action, ship speed = 0.36 m/s.

- Propeller action makes the rising move slightly abaft;
- Propeller action has no influence on the undulations when they are located amidships. The propeller is located too far from the undulations to have a significant influence;
- Propeller action is certainly significant from 0 to 60% n_{MAX}. A further increase does not lead to more variations.

The maximal risings in function of the propeller rate when the ship navigates astern are given in Figures 5.18a and 5.18b:

- An absolute increase of negative propeller action has no effect on the size of the undulations;

- A positive increase of propeller action results in an increase of the rising when the ship navigates above the mud layer. If the ship penetrates the mud layer, the opposite occurs.

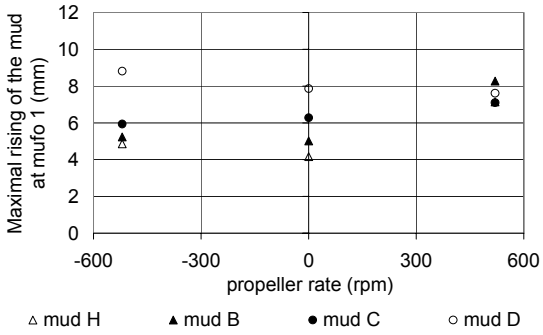

a. 3.9% under keel clearance referred to the water mud interface.

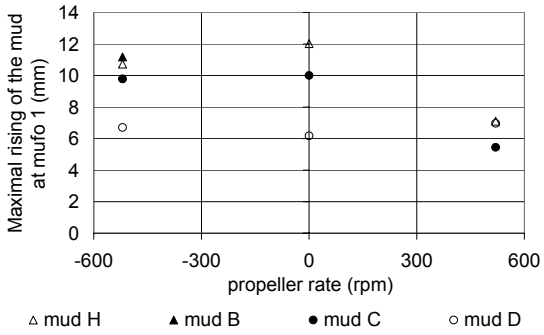

b. -1.1% under keel clearance referred to the water mud interface.

Figure 5.18. Ship model D: maximal rising in function of propeller rate. Thickness of the mud layer: 20 mm. No rudder action, ship speed = 0.36 m/s astern.

The longitudinal positions at which the rising is maximal are given in Figures 5.19a and 5.19b:

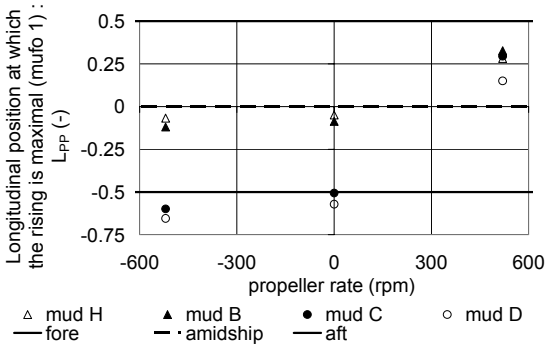

a. 3.9% under keel clearance referred to the water mud interface.

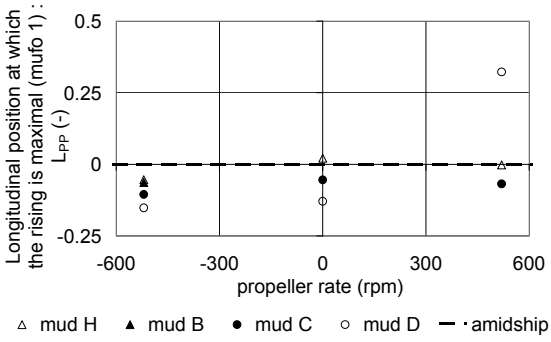

b. -1.1% under keel clearance referred to the water mud interface.

Figure 5.19. Ship model D: longitudinal position, at which the rising is maximal, in function of propeller rate. Thickness of the mud layer: 20 mm. No rudder action, ship speed = 0.36 m/s astern.

- If the ship navigates above the mud layer, the longitudinal position remains the same or will move abaft (in the fourth quadrant: $u < 0$, $n > 0$) with increasing propeller rate;
- If the keel penetrates the mud layer, the longitudinal position also remains equal, but will move forward (in the third quadrant: $u < 0$, $n < 0$) with increasing propeller rate.

5.4.4 Undulations of the interface for a 40 mm thick mud layer (3.0 m nature)

The rising of a 40 mm thick mud layer is given for different series and ship speeds on Figures 5.20:

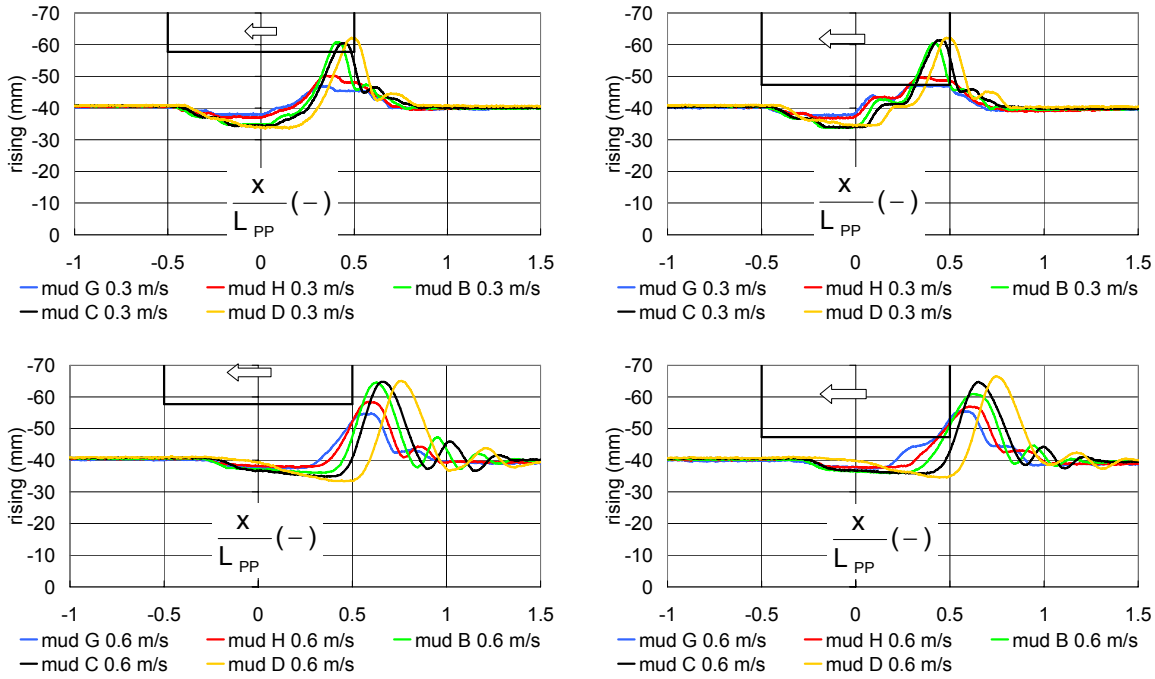

a. 9.8% under keel clearance referred to the water mud interface.

b. 4.1% under keel clearance referred to the water mud interface.

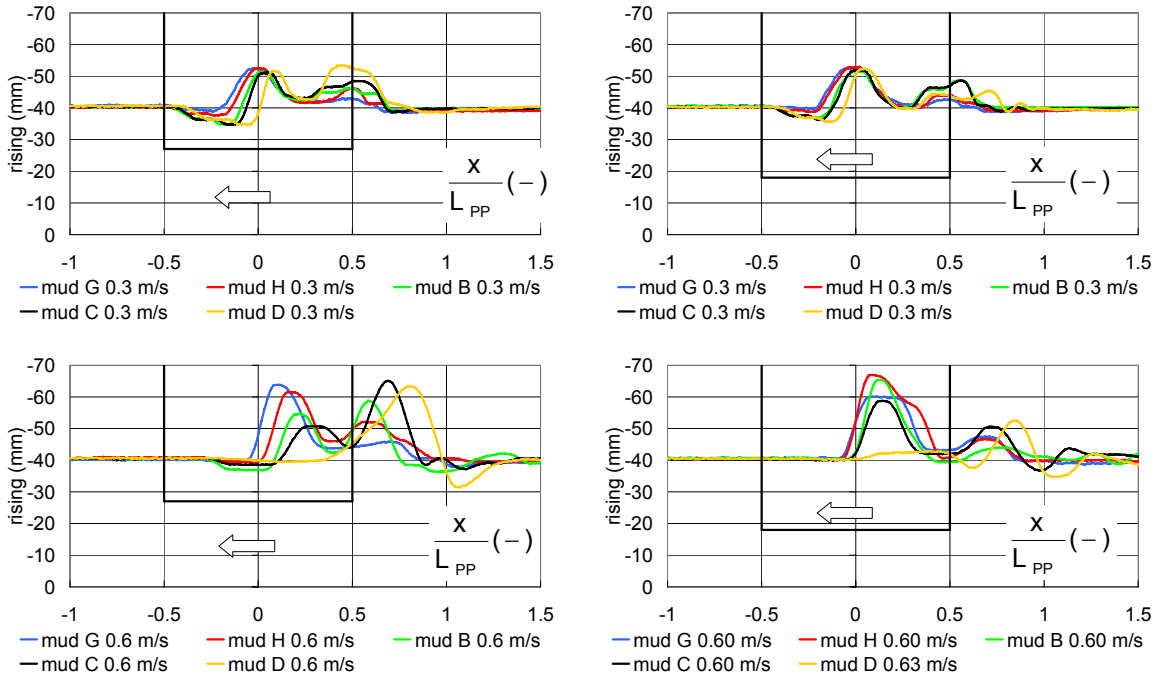

c. -7.2% under keel clearance referred to the water mud interface.

d. -12.2% under keel clearance referred to the water mud interface.

Figure 5.20. Ship model D: undulations of the interface at mufo 1 at different speeds, no propeller or rudder action. Thickness of the mud layer: 40 mm.

- The maximal rising moves abaft and increases with decreasing density and increasing velocity;
- The rising of the mud occurs in two phases when the ship navigates in contact with the mud layer. A first rising occurs amidships, a second one near the stern. An increased speed or a decreased viscosity and density

diminish the first rising in favour of the second one. For the mud layer with the lowest density the first phase has disappeared at high speeds.

Figures 5.21, 5.22 and 5.23 represent a couple of parameters of the risings. Figures 5.21a and 5.21b show the magnitude of the rising in function of the velocity for different under keel clearances.

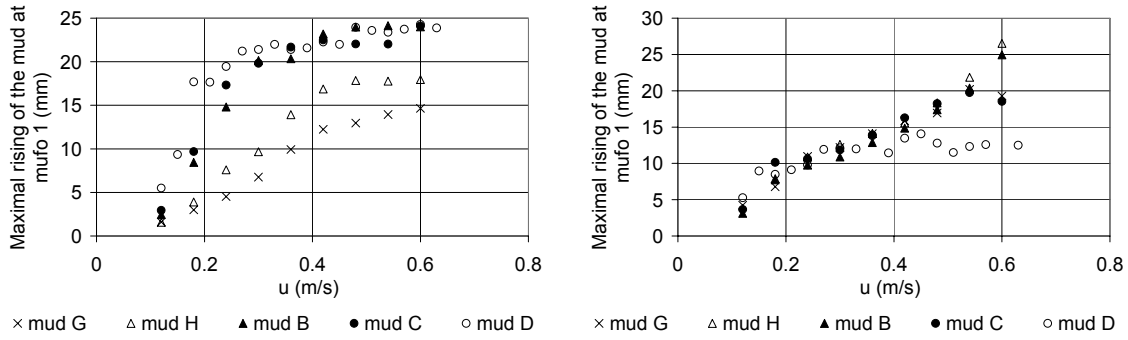

a. 9.8% under keel clearance referred to the water mud interface.

b. -12.2% under keel clearance referred to the water mud interface.

Figure 5.21. Ship model D: maximal rising in function of ship speed. Thickness of the mud layer: 40 mm. No propeller or rudder action.

- When the ship navigates above the mud layer the rising will increase faster with increasing velocity when the density and viscosity of the mud layer is lower. Although there is a limit to this increase. Once this limit has been reached the rising will not further increase with increasing speed;
- If the ship's keel penetrates most mud layers the rising of the interface will equally increase with increasing speed. For mud layer D an exception should be made. Around 0.4 m/s (6.5 knots nature) an abrupt transition occurs. In fact the importance of the first phase decreases in favour of the second one. Even the second phase will further decrease with increasing speed.

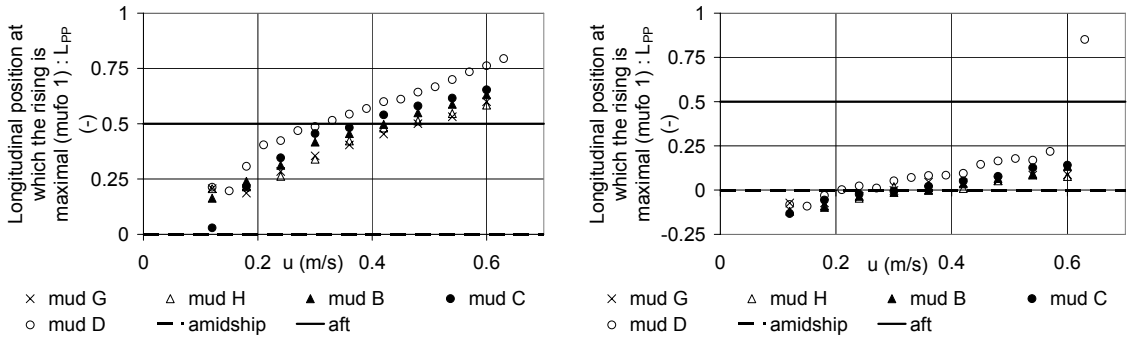

a. 9.8% under keel clearance referred to the water mud interface.

b. -12.2% under keel clearance referred to the water mud interface.

Figure 5.22. Ship model D: longitudinal position, at which the rising is maximal, in function of ship speed. Thickness of the mud layer: 40 mm. No propeller or rudder action.

The longitudinal position at which the rising becomes maximal is given for different under keel clearances in Figures 5.22a and 5.22b:

- If the keel does not penetrate the mud layer the undulations move abaft with increasing speed and decreasing density and viscosity;
- Again it can be clearly observed how the second phase of the undulations becomes more prominent with increasing speed and decreasing density and viscosity.

Figures 5.23a and 5.23b show the starting position of the risings. In all cases the starting position moves abaft with increasing speed and decreasing density and viscosity.

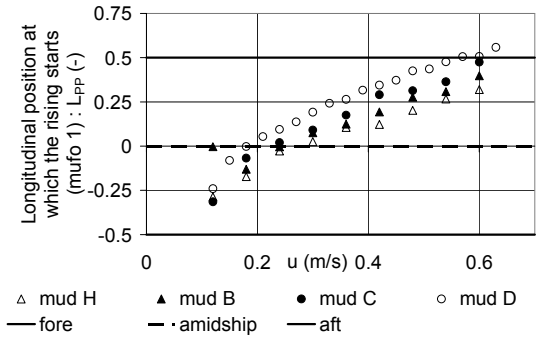

a. 9.8% under keel clearance referred to the water mud interface.

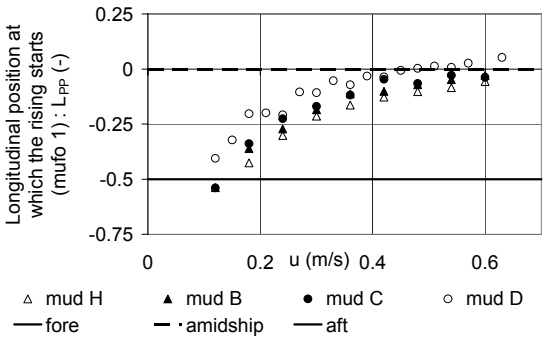

b. -12.2% under keel clearance referred to the water mud interface.

Figure 5.23. Ship model D: longitudinal position, at which the rising starts, in function of ship speed. Thickness of the mud layer: 40 mm. No propeller or rudder action.

Figures 5.24a and 5.24b give an overview of the influence of the propeller rate. A positive propeller rate has no significant influence on the undulations.

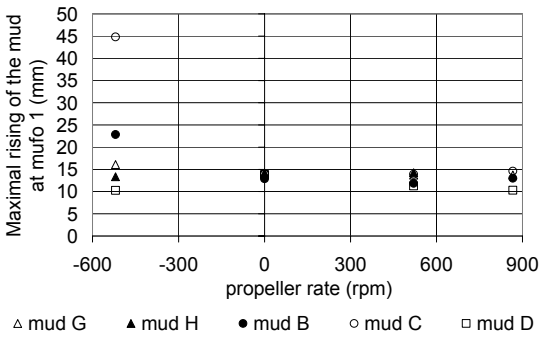

a. maximal rising

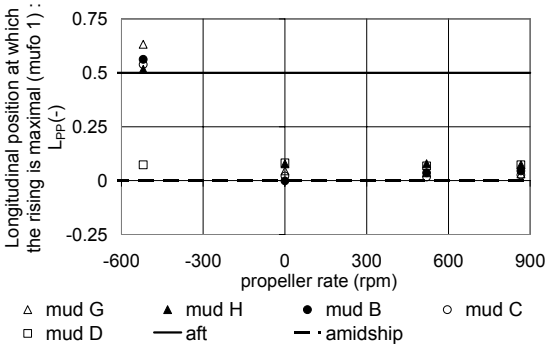

b. corresponding longitudinal position

Figure 5.24. Ship model D: influence of the propeller rate. Thickness of the mud layer: 40 mm. No rudder action. Ship speed = 0.36 m/s.

5.4.5 Conclusions

- The rising increases with increasing speed;
- The increase is limited. Once the limit has been reached the rising can decrease again as it is the case with low density mud layers. The latter occurs when the undulations are behind the ship;
- When the vessel navigates above the mud layer the rising will increase faster when the density and viscosity of the mud layer are small. With thinner mud layers the rising becomes significant once the viscosity

drops below a certain value, which is located between 0.12 and 0.18 Pa.s;

- A significant undulation is always observed when the ship navigates in contact with the mud layer. The rising is mostly located amidships for higher density mud layers. For lower density and viscosity the rising is located abaft. The transitory situation is a rising occurring in two phases;
- When navigating ahead a positive propeller rate only influences the rising when it is located near the stern. Full influence is already observed at a small propeller rate, resulting in a small increase of the rising and a small shift abaft. This effect is even smaller with increasing propeller rate;
- Reversed propeller action in case of navigating ahead yields a relatively large rising near the propeller. The pattern of the undulations is rather random;
- Navigating astern with reversed propeller has little to zero influence on the rising, only in case of an extreme negative under keel clearance a decrease of the rising can be observed;
- The effect of navigating astern with positive propeller rate depends on whether the ship penetrates the mud layer or not. In the first case an increase of the rising is observed, while in the second case a decrease occurs.

From a manoeuvring point of behaviour the rising of the mud layer can be especially annoying when the ship navigates with an extreme positive under keel clearance above the mud layer and when the rising occurs near the stern, which is the case for the lower density mud layers. This disturbs the propeller action, see 6.4.2. With high density mud layers the problem is rather the increased resistance of the ship due to the contact with the mud layer.

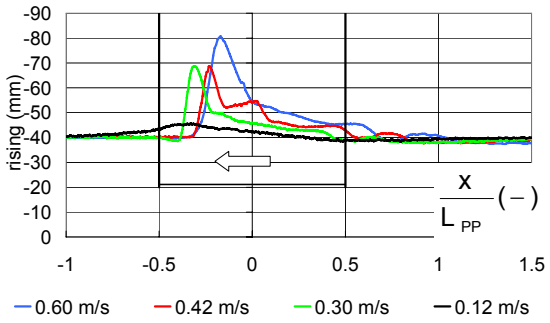

Figure 5.25. Ship model E, undulations of the interface at mufo 1, -9.4% under keel clearance referred to the top of mud g3.

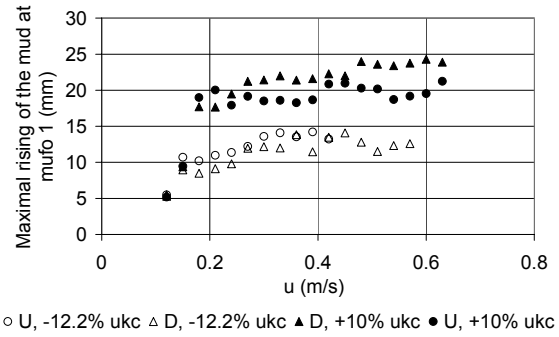

Figure 5.26. Mud d3, comparison between the risings of ships U and D.

The influence of the drift angle and the vessel type have not been thoroughly analysed, but in general the following can be stated:

- An increase of the drift angle will increase the magnitude of the rising, especially when the rising occurs fore or amidships;
- The influence of speed and propeller rate is not so pronounced with fuller vessel types. The rising will usually occur fore, see Figure 5.25;
- The tested container carriers have similar risings, see Figure 5.26.

5.5 Modelling the undulations

5.5.1 The critical under keel clearance

The modelling of the undulations does not belong to the scope of this work. However a better understanding of the undulations allows relating their effect to the mathematical manoeuvring models.

An example of a time series of undulations at different lateral distances is represented on Figure 5.27. The propagation and the magnitude ζ of the undulations can be considered as linear and are similar to the Kelvin pattern observed at the water-air interface. An elevation of the interface is preceded by a rather small sinkage, which increases with decreasing ukc.

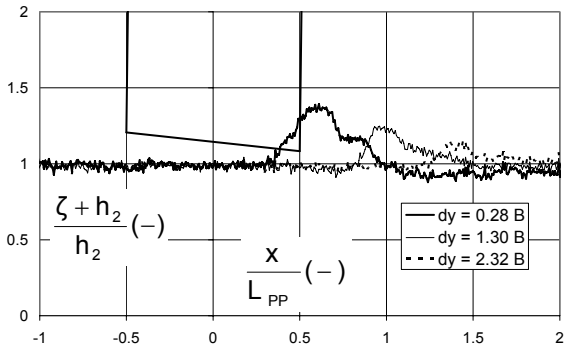

Figure 5.27. Undulations of the interface at various lateral distances of the ship. Mud f2, +3.9% ukc, F_n = 0.088, 0 rpm. The ship is represented taking squat into account.

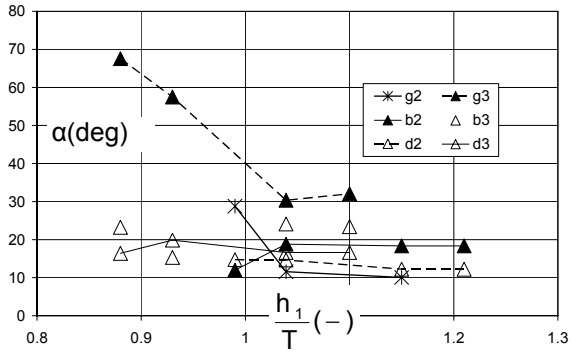

Figure 5.28. Propagation angle of the rising of the mud water interface. Effect of bottom conditions at self propulsion at harbour full (572 rpm, model scale).

Vander Donckt **[5.3]** has modelled the under keel clearance at which contact between the vessel and the mud layer is likely when the ship is navigating above the mud layer. To do so, some assumptions were made. The rising of the interface had to be known closer to the ship than what the measurement of the mufo's provided, so a (linear) extrapolation of the measurements had to be made.

In order to perform the extrapolations, two angles α and β are introduced, Figure 5.29:

- α is the angle between the longitudinal plane (x,z) of the ship and the straight line through the measured longitudinal positions (x,y) where the maximal rising has been registered by the three mufo's;
- β is the angle between the (x,y) plane and the straight line through the maximal risings (x,z).

The angle of propagation α is represented for self propelled conditions in Figure 5.28. The propagation angle takes values from 15 to 20 deg. Navigating in contact with high density mud layers will significantly increase the propagation angle. This is nevertheless in relationship with the lower speed the ship reaches due to the increased resistance.

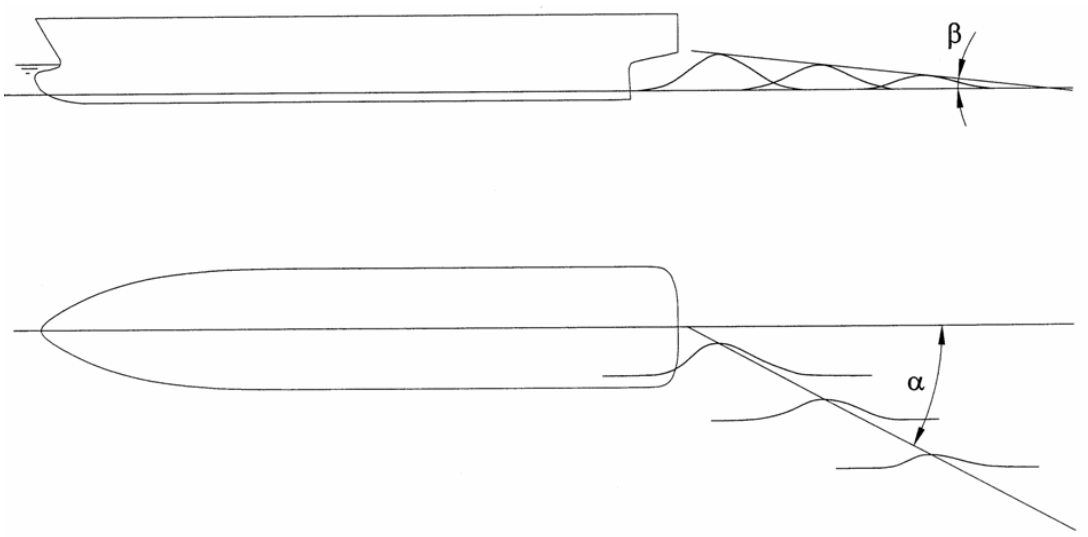

Figure 5.29. Definition of the angles α and β.

For each test run the maximal rising and its longitudinal position near the ship can be determined with the angles α and β. An important result is that the undulations are only behind the ship in a limited number of conditions, i.e. with mud layers of low density and at high speeds. Contrary to the previous model test programs described in Chapter 3, the velocities of the experimental program belong to the same speed range, consequently no major influence of the velocity on the manoeuvring behaviour is expected.

Now that the maximal rising near the ship is known, the so-called critical under keel clearance ukc_{crit} can be determined, being the minimal under keel clearance at which contact between the mud layer and the ship is likely to occur. This critical under keel clearance depends on:

- The ship's speed, expressed by its Froude number;
- The composition of the mud layer, expressed as $\frac{\rho_1}{\rho_2}$;
- The thickness of the mud layer, expressed as $\frac{h_2}{T}$;
- The propeller thrust, expressed as: $C_T = \frac{T_P}{\frac{1}{2}\rho_1 A_0 V^2}$;
- The ship's squat in those conditions.

In **[5.3]** a polynomial expression has been built in function of these parameters to predict the value for ukc_{crit}. Some examples are represented in Figure 5.30. The critical under keel clearance increases with increasing speed, and decreasing mud density. However, as seen before, once the rising occurs behind the ship, the critical under keel clearance will drop again.

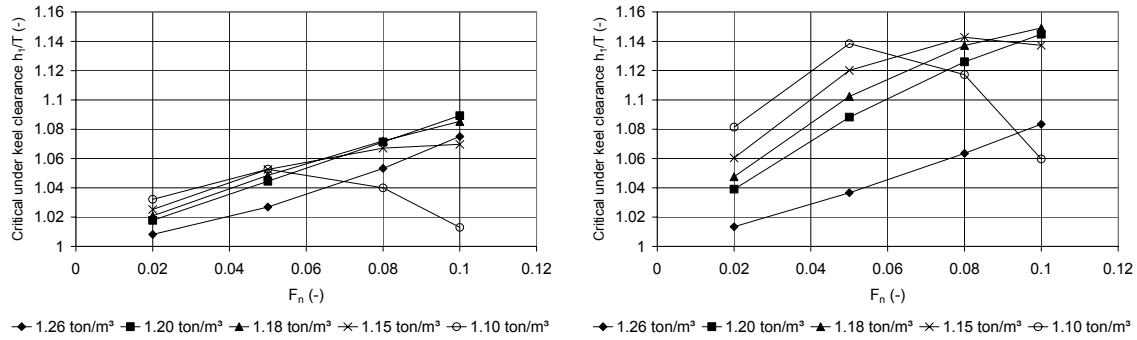

a. $h_2/T = 0.11$ b. $h_2/T = 0.22$

Figure 5.30. Critical under keel clearance $h_{1,\ crit}/T$ for different mud layers, stopped propeller, model ship D.

With the present measurements the transition from the second to the third speed range takes however place at a higher speed than calculated with (5.12). The explanation can be found in the large viscosity differences between present and prior results and the lack of viscosity dependency in (5.12). The effect of the viscosity on the speed ranges has also been observed in **[5.4]**.

5.5.2 Conclusions

The introduction of the propagation angles of the rising of the water-mud interface gave an idea on the behaviour of the undulations closer to the ship hull:

- The undulations occur behind the ship hull only in a limited number of conditions, consequently all experimental velocities belong to the same speed range and no major velocity influence on the manoeuvring behaviour is expected;
- In the previous research programs artificial mud layers of a low viscosity were used. The use of the theory for inviscid fluids to predict the rising of the water-mud interface gave good results. In the current research project artificial mud of a higher viscosity has been used. Although the behaviour of the risings is quite similar, the occurrence of the speed ranges is different.

5.6 Squat

5.6.1 Sinkage

Figure 5.31 gives an overview of the ship's sinkage in function of the speed for different bottom conditions. The following can be observed:

- When the ship navigates above the mud layer the rising of the interface is significantly larger for mud layers with a viscosity below a critical viscosity (see 5.4.5). When the under keel clearance is small, this can eventually result in contact between the vessel and the mud layer. The mud will yield an increase of buoyancy, which results in a decrease of the sinkage;

- If the ship's keel penetrates the mud layer, the large rising amidships, which occurs for higher density mud layers, will cause an increase of buoyancy. The sinkage will consequently be smaller.

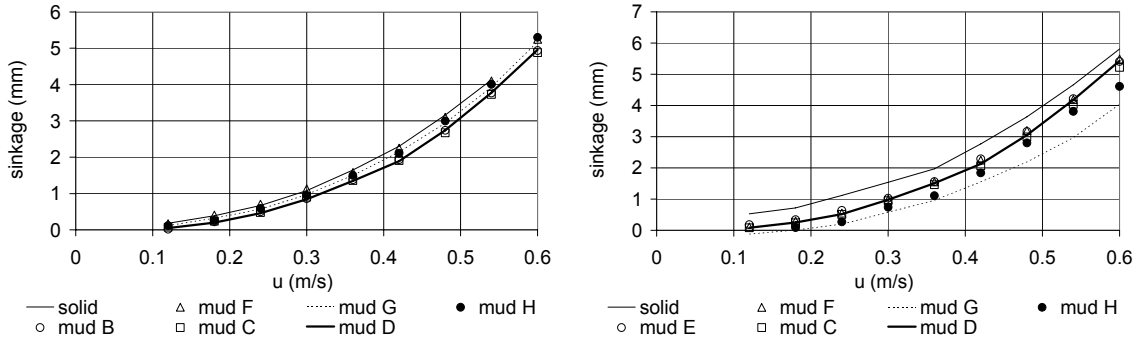

a. 3.9% under keel clearance referred to the water mud interface.

b. -1.1% under keel clearance referred to the water mud interface.

Figure 5.31. Ship model D: sinkage in function of the ship speed. Thickness of the mud layer: 20 mm. No propeller or rudder action.

The sinkage, for the same under keel clearance referred to the solid bottom, is always larger above a solid bottom than above a muddy bottom. The same observations were made in **[5.7]**, nevertheless the latter mentioned a slight increase of sinkage at low speeds.

5.6.2 Trim

As the sinkage is not constant along the ship's hull, the ship will be dynamically trimmed. For slender hulls this results in a larger sinkage at the stern, while full bodies have a larger sinkage at the bow. When the ship navigates in a muddy area, the trim will be influenced as well and will usually increase, due to the extra asymmetry in the buoyancy caused by the rising of the interface. The trim is represented for different navigation conditions in Figure 5.32, where a negative trim means a larger draught abaft. It can be stated that, in combination with the observations of the undulations of the interface:

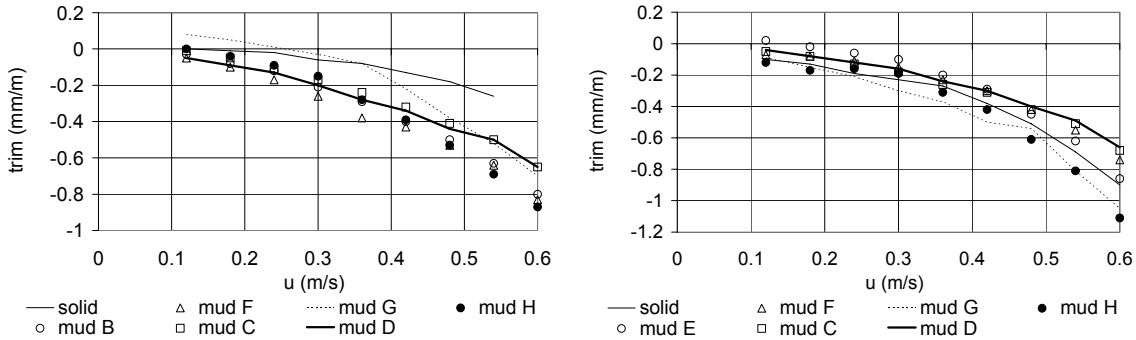

a. 3.9% under keel clearance referred to the water mud interface; 15% under keel clearance referred to the solid bottom.

b. -1.1% under keel clearance referred to the water mud interface; 10% under keel clearance referred to the solid bottom.

Figure 5.32. Ship model D: trim in function of the ship speed. Thickness of the mud layer: 20 mm. No propeller or rudder action.

- A rising will have the largest influence on the trim when it takes place amidships. The influence will decrease when the rising moves abaft;

- The trim will be smaller when the top of the rising is wider;
- In all cases a larger rising causes a larger asymmetry and thus a larger trim. This is in accordance with the observations in **[5.7]**.

5.6.3 Modelling

As with the undulations, the modelling of squat in muddy areas will not be tackled thoroughly in this work. Based on the captive manoeuvring series in muddy areas at Flanders Hydraulics, some models have been developed to predict squat in muddy navigation areas. More information can be found in **[5.2,5.3]**.

5.7 References

[5.1] FERDINANDE V., VANTORRE M. *The behaviour of a mud-water interface underneath a slowly advancing ship at small keel clearance*, Proceedings of International Symposium on Hydro- and Aerodynamics in Marine Engineering (HADMAR '91), Volume 1, Paper No. 4, Varna, Bulgaria, 1991, 10 pp.

[5.2] QUINTELIER R. *Squat bij scheepvaart in slibrijke vaarwateren.* M. Sc. Thesis, Faculty of Engineering, Ghent University, Ghent, 2006. (In Dutch).

[5.3] VANDER DONCKT S. *Scheepvaart in slibrijke gebieden: interne golfvorming en squat.* M. Sc. Thesis, Faculty of Engineering, Ghent University, Ghent, 2005. (In Dutch).

[5.4] VANTORRE M. *Verslag van de werkzaamheden in het kader van de "Overeenkomst voor samenwerking in de studie van de scheepsgedragingen in verband met de vaargebieden en de zeehavens" afgesloten met het Ministerie van Openbare Werken, Waterbouwkundig Laboratorium te Antwerpen-Borgerhout. 6de en 7de kwartaal: 16.04.1988-30.09.1988. Deel C.* Gent, 1988. (In Dutch).

[5.5] VANTORRE M. *Systematische proevenreeksen met het zelfaangedreven schaalmodel van een sleephopperzuiger boven een mengsel petroleum-trichloorethaan als slibsimulatiemateriaal: experimentele waarnemingen en theoretische interpretaties.* Report. Ghent University – Flanders Hydraulics Research, Ghent\Antwerp, 1990. (In Dutch).

[5.6] VANTORRE M. *Ship behaviour and control at low speeds in layered fluids*, Proceedings of International Symposium on Hydro- and Aerodynamics in Marine Engineering (HADMAR '91), Volume 1, Paper No. 5, Varna, Bulgaria, 1991, 9 pp.

[5.7] VANTORRE M., COEN I. *On sinkage and trim of vessels navigating above a mud layer.* The Royal Society of Flemish Engineers, Harbour Congress, 1988.

Now that we have all this useful information, it would be nice to do something with it. (Actually, it can be emotionally fulfilling just to get the information. This is usually only true, however, if you have the social life of a kumquat.)

UNIX Programmer's Manual

CHAPTER 6

MATHEMATICAL MODELLING

6.1 General

6.1.1 Equations of motion

A ship has six degrees of freedom:

- Three translations along the x, y and z-axis (surge, sway and heave);
- Three rotations around the x, y and z-axis (roll, pitch and yaw).

For manoeuvring purposes the forces in the horizontal XY-plane are important: surge, sway and yaw. The roll has been neglected. The ship moves relative to a space fixed coordinate system, as represented on Figure 6.1.

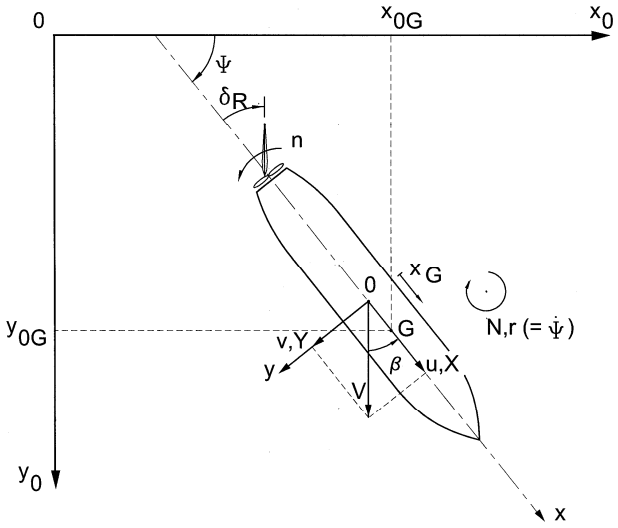

Figure 6.1. Space fixed coordinate system: definitions.

The equations of motion in this system are:

$$\begin{aligned} m\left(\dot{u} - vr - x_G r^2\right) &= X \\ m\left(\dot{v} + ur + x_G \dot{r}\right) &= Y \\ I_{zz}\dot{r} + mx_G\left(\dot{v} + ur\right) &= N \end{aligned} \qquad (6.1)$$

6.1.2 Classification of mathematical models

A mathematical model gives an expression for X, Y and N in (6.1) as a function of the control (n, δ) and kinematical parameters (u,v,r). This can be achieved in two ways:

- Purely mathematically by building up polynomial expressions as a function of the control and kinematical parameters:

$$\text{force} = \sum_{i,j,k,\ldots} u^i n^j \delta^k \ldots \tag{6.2}$$

  Examples of these kinds of models can be found in **[6.1]** and **[6.8]**. The advantage is that with these models a quick result can be achieved; however there is no clear relationship between the model and the physical background.
- This physical background is used as a starting point to build up modular mathematical models, in which a distinction is made between the hull, propeller and rudder forces:

$$F = F_H + F_P + F_R \tag{6.3}$$

  Examples of these models can be found in **[6.9]** and **[6.10]**.

In this chapter modular mathematical models will be used. More information on the selection, determination and evaluation of mathematical models can be found in **[6.5]**. Information on the regression analysis used to determine the coefficients can be found in Appendix D. The mathematical model presented in 6.3-6.5 has previously been published in **[6.3]**.

6.2 Linear manoeuvring model

Before proceeding with the comprehensive four quadrants manoeuvring model, an estimation of the manoeuvrability will be given when the ship has only small deviations from a straight course. In this case a linear set of equations of motions can be used:

$$\begin{aligned} \left(Y_{\dot{v}} - m\right)\dot{v} + \left(Y_{\dot{r}} - mx_G\right)\dot{r} + Y_{uv}uv + \left(Y_{ur} - m\right)ur + Y_{\delta uu}\delta u^2 &= 0 \\ N_{\dot{v}}\dot{v} + \left(N_{\dot{r}} - I_{zz}\right)\dot{r} + N_{uv}uv + \left(N_{ur} - mx_G\right)ur + N_{\delta uu}\delta u^2 &= 0 \end{aligned} \tag{6.4}$$

The values for the hull derivatives displayed in the following paragraphs are based on harmonic ("PMM") sway and yaw tests carried out at speeds of 2 to 6 knots (full scale). The control derivatives resulted from multimodal test carried out with constant speed and rpm, but varying rudder angle, and are valid in self-propulsion conditions.

Results based on the linear manoeuvring model have already been published, see **[6.4]** and **[6.13]**.

6.2.1 Inertia derivatives

The inertia derivatives are considered to be a measure for the extra inertia a vessel has when accelerating. This is because the surrounding fluid has to be accelerated as well. Figure 6.2 shows a selection of results of harmonic sway

tests. The added mass for sway motion increases significantly with decreasing water depth and increasing density and viscosity of the mud layer, and takes very large values, (even seven times the ship's mass for the D-model) in case the ship's keel penetrates deep into the mud.

The mud characteristics and the layer thickness appear to be important parameters, even if no contact occurs with the mud layer: the shallow water effect is smoothed with increasing layer thickness and decreasing mud density and viscosity. Indeed, an abrupt transition cannot be observed at $h_1/T = 1$. It should be noted that the results of tests carried out with layers of rather high viscosity and density can be considered as an extrapolation of results above a solid bottom. Similar conclusions can be drawn for the yaw inertia.

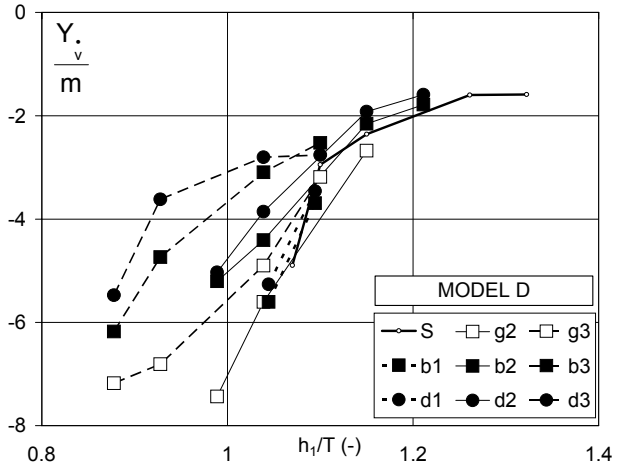

Figure 6.2: Sway added mass: influence of bottom characteristics and under keel clearance.

6.2.2 Velocity derivatives

The magnitude of lateral force and yawing moment due to drift increases significantly with decreasing water depth. This is illustrated in Figure 6.3, displaying the sway velocity derivative Y_{uv} as a function of water depth to draft ratio for several bottom conditions. However, Y_{uv} appears to reach a maximum for zero under keel clearance relative to the mud-water interface. The presence of a mud layer results in an increase of the lateral force due to drift. This is not the case for the drift induced yawing moment, as is shown in Figure 6.4: the presence of a mud layer results in a decrease of N_{uv}. The latter reaches a maximum if the keel touches the mud layer.

The evolution of the yaw velocity induced lateral force and yawing moment derivatives is of particular interest. The magnitude of the yaw damping moment derivative N_{ur} gradually increases with decreasing under keel clearance and stagnates once the ship's keel touches the mud layer, see Figure 6.5. The hydrodynamic lateral force due to the yaw rate ($Y_{ur}ur$), which in deep water is practically negligible compared with the centrifugal inertia force (-mur), is of increasing importance and counteracts the centrifugal inertia force completely at extremely small positive under keel clearances, as shown in Figure 6.6. For smaller and negative under keel clearances, the resulting lateral force due to yaw is even centripetal. The transition from centrifugal to centripetal action takes place at larger values of the under keel clearance when the density and

viscosity of the mud layer increase and the thickness of the layer decreases. Therefore, this effect is not to be considered as a typical characteristic for ship behaviour in muddy areas, but rather as a (very) shallow water effect.

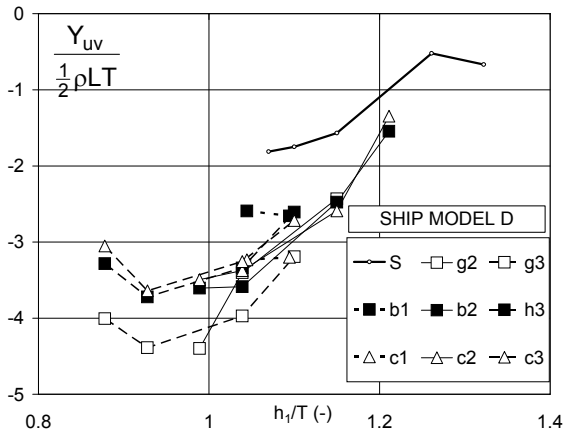

Figure 6.3: Linear sway velocity derivative for lateral force: influence of bottom characteristics and under keel clearance.

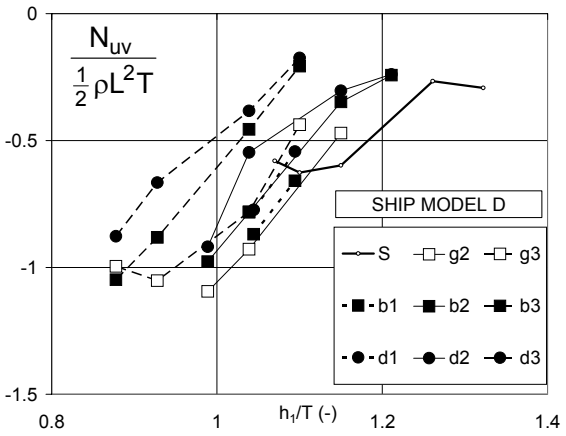

Figure 6.4: Linear sway velocity derivative for yawing moment: influence of bottom characteristics and under keel clearance.

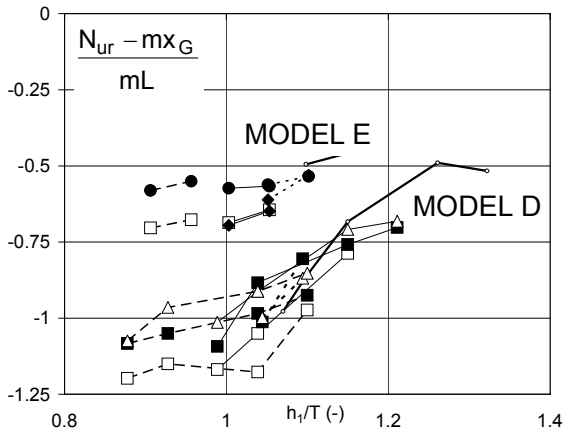

Figure 6.5: Linear yaw velocity derivative for yawing moment: influence of bottom characteristics and under keel clearance (see Figure 6.7 for legends).

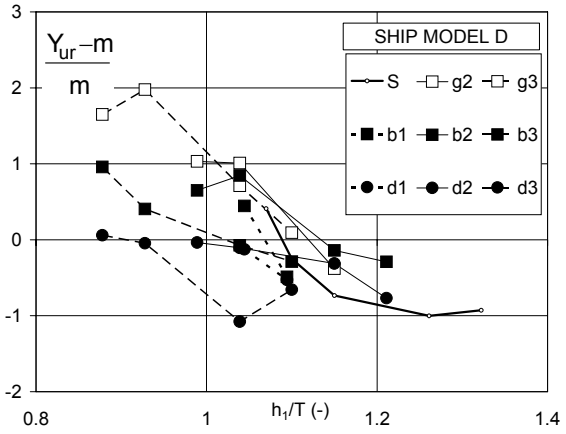

Figure 6.6: Linear yaw velocity derivative for lateral force: influence of bottom characteristics and under keel clearance.

6.2.3 Control derivatives

The linear coefficients for the sway force induced by rudder action at self propulsion conditions for the models are given in Figure 6.7. These characteristics are greatly affected by the resistance and propulsion performance; for this reason, the propeller rate required to reach a forward speed of 6 knots is displayed in Figure 6.8.

For mud layers with a higher density, the control derivatives increase considerably in case of contact between the ship's keel and the mud layer, due to the higher propeller loading required to overcome the increased resistance.

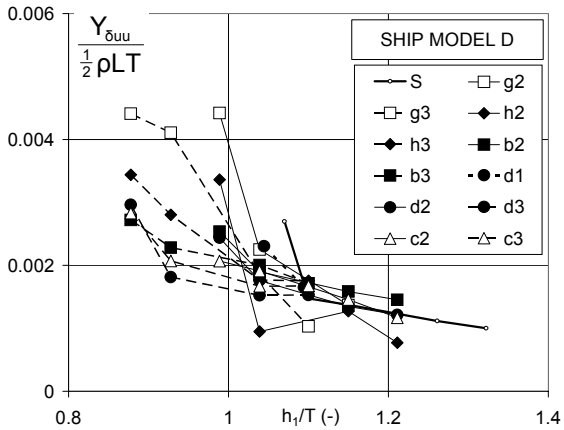

Figure 6.7: Linear control derivative for lateral force: influence of bottom characteristics and under keel clearance.

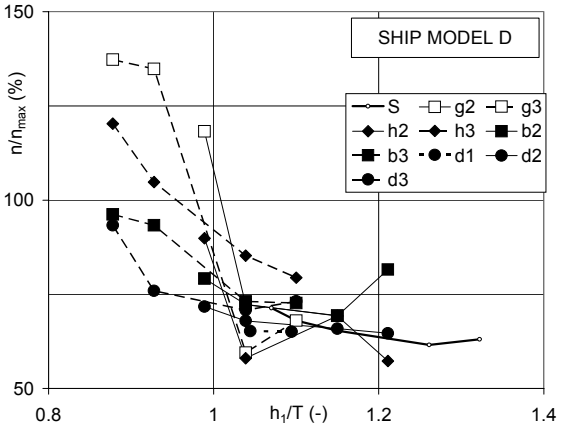

Figure 6.8: Propeller rpm required to reach a forward speed of 6 knots.

Tests carried out with lower density mud layers resulted into a more gradual transition between positive and negative under keel clearance. Near $h_1/T = 1$, fluctuations can occur, due to the effect of the internal wave patterns.

6.2.4 Straight-line stability

The linear equations of motion (6.4) lead to following values for the straight line stability indices **[6.11]**:

$$\sigma_{1,2} = -\frac{B \pm \sqrt{B^2 - 4AC}}{2A} \tag{6.5}$$

using following notations:

$$A = \left(Y_{\dot{v}} - m\right)\left(N_{\dot{r}} - I_{zz}\right) - \left(Y_{\dot{r}} - mx_G\right)N_{\dot{v}} \tag{6.6}$$

$$B = Y_{uv}\left(N_{\dot{r}} - I_{zz}\right) + \left(Y_{\dot{v}} - m\right)\left(N_{ur} - mx_G\right) - \left(Y_{ur} - m\right)N_{\dot{v}} - \left(Y_{\dot{r}} - mx_G\right)N_{uv} \tag{6.7}$$

$$C = Y_{uv}\left(N_{ur} - mx_G\right) - \left(Y_{ur} - m\right)N_{uv} \tag{6.8}$$

A ship is characterised by straight line stability if the real part of the stability indices is negative. A and B being positive, this is the case if C>0. As can be observed in Figure 6.9, a decrease of under keel clearance results in a significant increase of C. Ship model D, which is slightly unstable and marginally stable at under keel clearance values of 32% and 26% of draft, respectively, appears to be extremely stable if the under keel clearance reaches very small and negative values. If the ship penetrates into the mud, the straight line stability criterion C takes the largest values for the mud layers with high density and viscosity. Fluctuations occur near $h_1/T = 1$.

Another particularity concerns the sign of the discriminant d: Figure 6.10 shows that $d \equiv B^2 - 4AC$ takes negative values, leading to complex stability indices and, therefore, sub-critical, oscillating damping with decreasing under keel clearance.

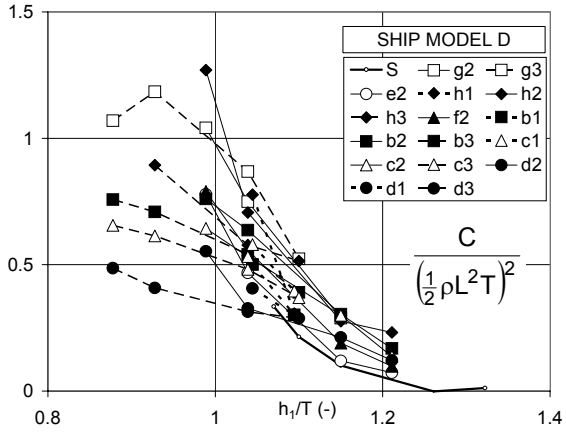

Figure 6.9: Straight-line stability criterion "C": influence of bottom characteristics and under keel clearance.

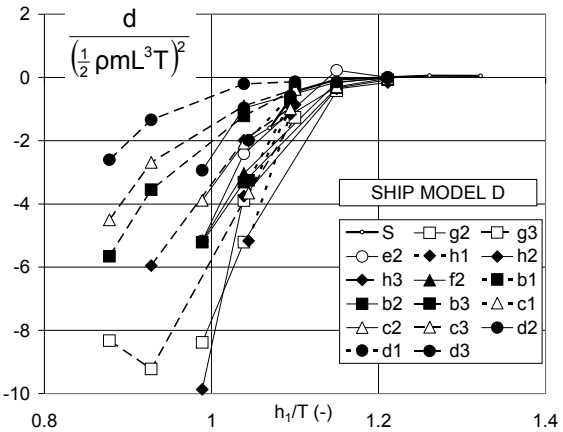

Figure 6.10: Discriminant of quadratic equation for stability indices: influence of bottom characteristics and under keel clearance.

An alternative formulation for the straight-line stability criterion is based on the relative longitudinal position of the application points of the forces due to sway and yaw, the so-called stability levers:

$$x_v \equiv \frac{N_{uv}}{Y_{uv}} \quad ; \quad x_r \equiv \frac{N_{ur} - m x_G}{Y_{ur} - m} \tag{6.9}$$

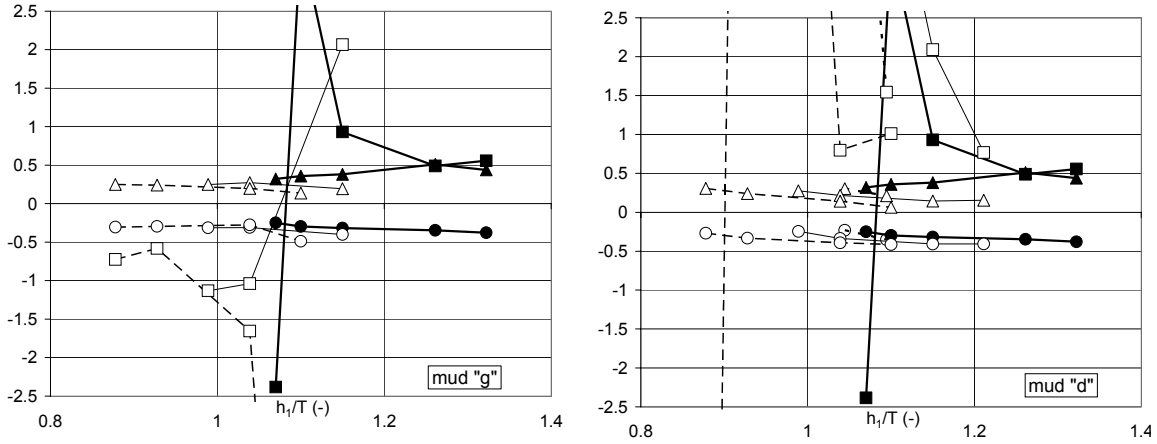

Figure 6.11: Model D. Application point of lateral force due to sway (x_v/L: Δ), yaw (x_r/L: □), rudder action (x_δ/L: O) Open symbols: mud; full symbols: solid; Mud layer thickness: 0.75 m (- - -), 1.50 m (——), 3.00 m (– – –).

For a selection of tested conditions, these stability levers are displayed in Figure 6.11. The test results indicate that the application point of the resulting force due to sway is always located fore of amidships. This is not the case for the force due to yaw: with decreasing water depth, the denominator in the expression for the yaw stability lever will change sign, while the moment due to yaw has always the opposite sense of the yaw motion. As a result, x_r increases with decreasing water depth, becomes infinite at a particular under keel clearance and takes a negative value at still lower water depth. This transition takes place at lower under keel clearances when the density of the mud layer decreases. The criterion for straight-line stability can therefore be formulated as follows: $x_r > x_v$ if $Y_{ur} - m < 0$; $x_r < x_v$ if $Y_{ur} - m > 0$. In deep water, the centrifugal inertia force is dominating, so that C>0 is fulfilled if $x_r > x_v$. This is not

the case, however, in very shallow water, including negative under keel clearances.

6.2.5 Response to rudder action: steady state

A steady-state solution for the system (6.4) of the equations of motion can be obtained if $\dot{v} = \dot{r} = 0$, so that following values for v and r can be calculated:

$$\frac{v}{u} = \delta \frac{-Y_{\delta uu}\left(N_{ur} - mx_G\right) + N_{\delta uu}\left(Y_{ur} - m\right)}{Y_{uv}\left(N_{ur} - mx_G\right) - N_{uv}\left(Y_{ur} - m\right)} = -\delta \frac{Y_{\delta uu}}{Y_{uv}} \frac{x_r - x_\delta}{x_r - x_v} \tag{6.10}$$

$$\frac{rL}{u} = \delta \frac{-Y_{uv}N_{\delta uu} + N_{uv}Y_{\delta uu}}{Y_{uv}\left(N_{ur} - mx_G\right) - N_{uv}\left(Y_{ur} - m\right)} = \delta \frac{Y_{\delta uu}L}{Y_{ur} - m} \frac{x_v - x_\delta}{x_r - x_v} \tag{6.11}$$

In (6.10-6.11), $x_\delta \equiv N_{\delta uu} \div Y_{\delta uu}$ denotes the longitudinal coordinate of the application point of the rudder induced lateral force, which is located aft of amidships for all tested conditions, see Figure 6.11. Indeed, $Y_{\delta uu} > 0$ and $N_{\delta uu} < 0$, so that $x_\delta < 0$.

The results of (6.10-6.11) are displayed in Figure 6.12. For the yaw rate, it can be concluded that for a ship with straight-line stability, which is the case in all, except one, tested conditions, the resulting steady-state value always has the expected sense, i.e. opposite to the rudder angle. Indeed, $(Y_{ur}–m)\ (x_r–x_v) < 0$, while x_v-x_δ and $Y_{\delta uu}$ are always positive. At small positive under keel clearance, the yaw rate appears to reach a minimum.

The sway velocity ($v/u = – \tan \beta$) takes the sign of the rudder angle, implying that the ship's bow is located within the turning circle – which can be considered as a normal situation – in following cases: $x_\delta < x_v < x_r$ and $x_r < x_\delta < x_v$. At extremely low water depth, however, the application point of the yaw induced lateral force moves fore which leads to a very small, but still positive drift angle. However if the asymmetry of the propeller is taken into account the resulting drift angle can have a sign change in some situations, which means that the ship's bow is located outside the turning circle.

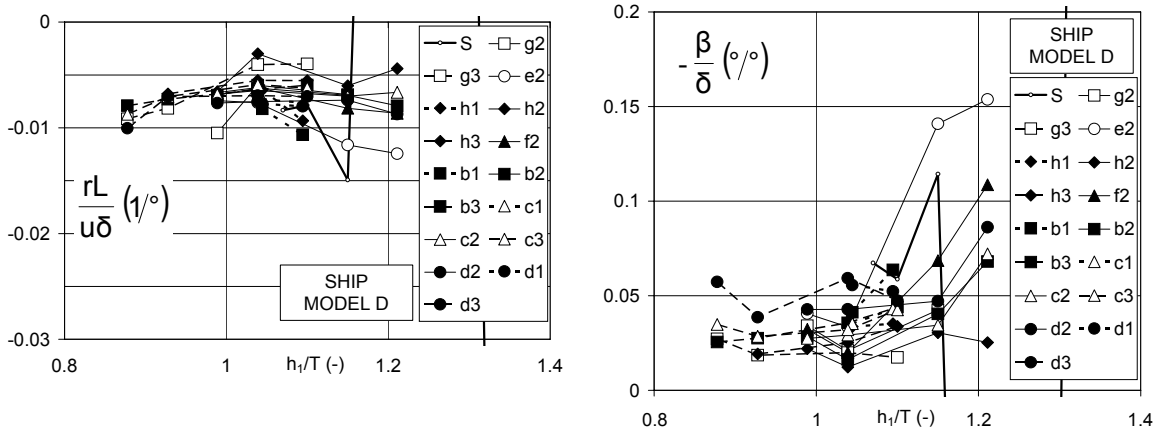

Figure 6.12: Steady-state response to rudder action: yaw rate, drift angle. Influence of bottom characteristics and under keel clearance.

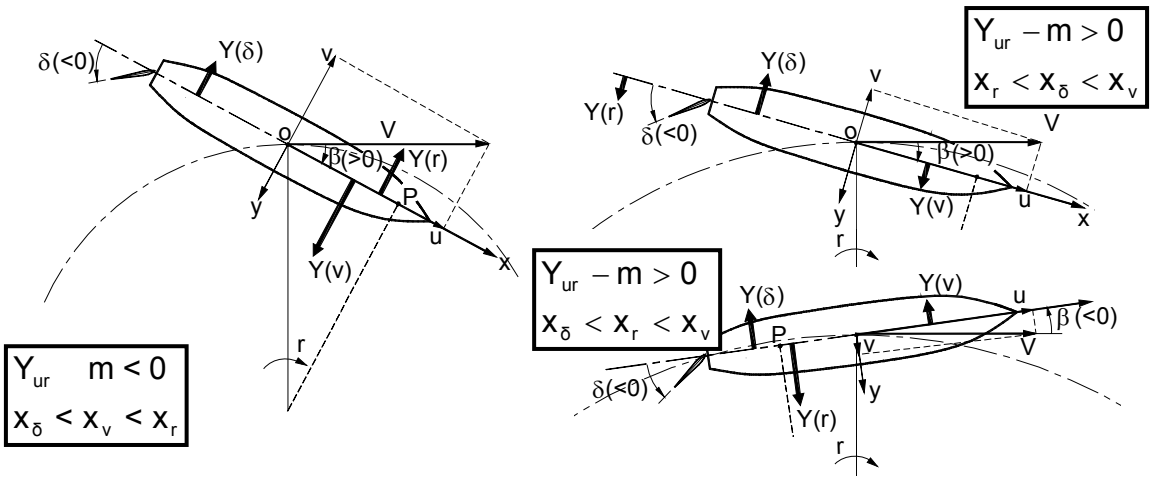

Figure 6.13: Steady-state response to rudder action: force balance.

Figure 6.13 illustrates the force balance in the different situations. Due to the evolution of yaw rate and drift angle, the pivoting point moves aft with decreasing water depth, as shown in Figure 6.14.

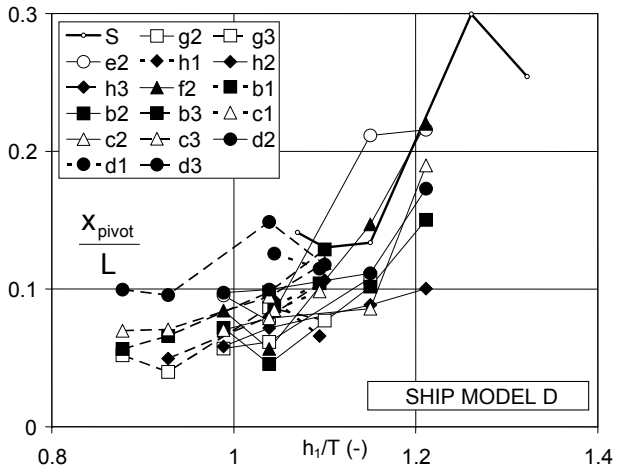

Figure 6.14: Steady-state response to rudder: position of pivoting point. Influence of bottom characteristics and under keel clearance.

6.3 Hull forces

6.3.1 Longitudinal force

The longitudinal hull force is as given by:

$$X_H = \left(X_{\dot{u}}(u) - m \right)\dot{u} + mvr + mx_G r^2 \left[X_{\dot{v}\dot{v}}(u)\dot{v}^2 + X_{\dot{v}}(u)\dot{v} + X_{\dot{r}\dot{r}}(u)\dot{r}^2 + X_{\dot{r}}(u)\dot{r} \right] + \tfrac{1}{2}\rho LT\left\{ \left(u^2 + v^2\right)\left(X'(\beta)\right) + \left(u^2 + \left(\tfrac{1}{2}rL\right)^2\right)X'(\gamma) + \left(v^2 + \left(\tfrac{1}{2}rL\right)^2\right)X'(\chi) \right\} \quad (6.12)$$

The effect of the velocities is modelled with tabular non-dimensional functions of the drift angle β, the yaw rate angle γ and a drift-yaw correlation angle χ, defined as:

$$\beta = \arctan\left(-\frac{v}{u} \right) \quad (6.13)$$

$$\gamma = \arctan\left(\frac{r}{u}\frac{L}{2}\right) \tag{6.14}$$

$$\chi = \arctan\left(\frac{r}{v}\frac{L}{2}\right) \tag{6.15}$$

The arctan-function normally results in an angle located in the range [-π/2, π/2]. In this dissertation a four quadrants, see 6.4.1, harbour manoeuvring model will be developed which covers the range [-π, π]. To do so the arctan-function will always include the following correction:

- arctan(y/x) = arctan1(y/x) for x > 0;
- arctan(y/x) = arctan1(y/x)+π for x < 0 and y > 0;
- arctan(y/x) = arctan1(y/x)-π for x < 0 and y < 0;
- arctan(y/x) = π/2 for x = 0 and y > 0;
- arctan(y/x) = -π/2 for x = 0 and y < 0.

where arctan1(y/x) gives the angle located in the range[-π/2, π/2].

A point of interest is the dependence on the accelerations ($\dot{u},\dot{v},\dot{r}$) in (6.12). Usually the longitudinal force will only be affected by longitudinal accelerations. However, when the ship's keel gets in contact with a higher density mud layer (>1200 kg/m³), sway and yaw acceleration also appear to have a significant influence. Moreover, the speed-force relationship appears to be no longer quadratic, so that for each speed a separate tabular function must be introduced. In case no contact occurs or when the mud layer has a low density (<1200 kg/m³) these influences are unimportant.

The non-dimensional resistance of the ship is shown as a function of under keel clearance for several bottom conditions in Figure 6.15. Contact with high density mud layers leads to a dramatic, very sharp increase of resistance, while the interface does not appear to be a strict boundary in case of lower density mud.

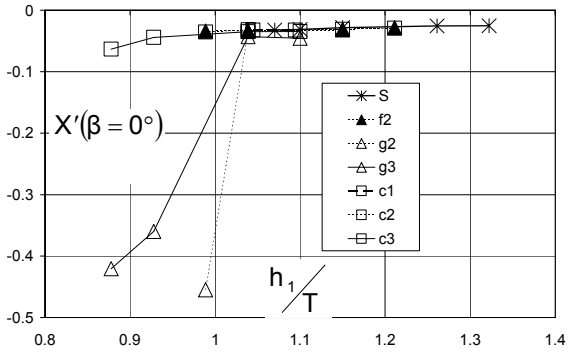

Figure 6.15. Ship D: resistance: influence of bottom characteristics and under keel clearance at slow speed (2 knots full scale)

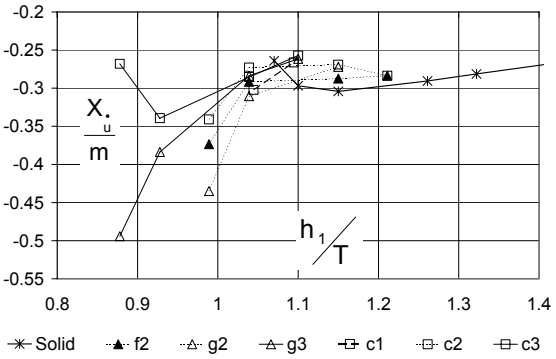

Figure 6.16. Ship D: influence of bottom condition on $X_{\dot{u}}$ at speed ahead.

This increase of resistance results in a significant decrease of speed, as can be observed from the results of the fast- and real-time simulations, see Chapters 7 and 8.

Figure 6.16 shows the influence of the bottom condition on $X_{u}^{\cdot}$:

- For the largest under keel clearances the bottom condition has only a small influence on $X_{u}^{\cdot}$;
- For under keel clearances below 10% $X_{u}^{\cdot}$ becomes more negative to reach a maximum when the keel is near the water-mud interface;
- If the ship penetrates the mud layer, $X_{u}^{\cdot}$ seems to return to its initial value.

  This occurs at smaller penetration depths in mud layers of a smaller density and viscosity.

Figure 6.17 shows $X_{vv}^{\cdot\cdot}$ as an example of the effect of the additional hydrodynamic inertia when the keel penetrates high density and viscosity mud layers. One can observe that the effect of $X_{vv}^{\cdot\cdot}$ diminishes with decreasing density and viscosity.

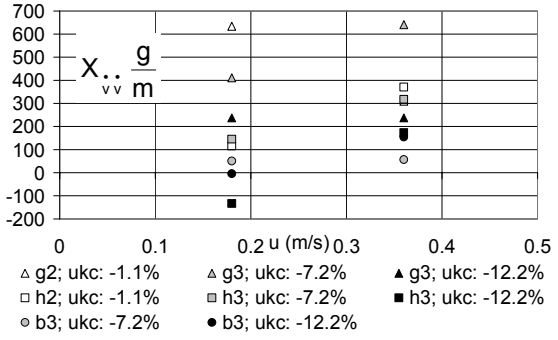

Figure 6.17. Ship D: influence of bottom condition on $X_{vv}^{\cdot\cdot}$ at speed ahead.

6.3.2 Sway force

The sway force is modelled as follows:

$$Y_H = \left(Y_{\dot{v}}^{\cdot} - m\right)\dot{v} + \left(Y_{\dot{r}}^{\cdot}(\beta) - mx_G\right)\dot{r} - mur + \tfrac{1}{2}\rho LT\left\{\begin{array}{c}\left(u^2+v^2\right)Y'(\beta)+\\ \left(u^2+\left(\tfrac{1}{2}rL\right)^2\right)Y'(\gamma)+\\ \left(v^2+\left(\tfrac{1}{2}rL\right)^2\right)Y'(\chi)\end{array}\right\} \quad (6.16)$$

The non-dimensional lateral force, due to drift, increases with decreasing under keel clearance, as shown on Figure 6.18. The thickness of the mud layer appears to have only a small effect on the force magnitude; this is illustrated by comparing conditions (g2; -1.1% under keel clearance) and (g3; -12.2% under keel clearance), both carried out with 10% under keel clearance above the solid bottom.

Figure 6.19 shows that the drift induced sway force increases when navigating in muddy areas of high density and viscosity, even when no contact occurs between ship and mud.

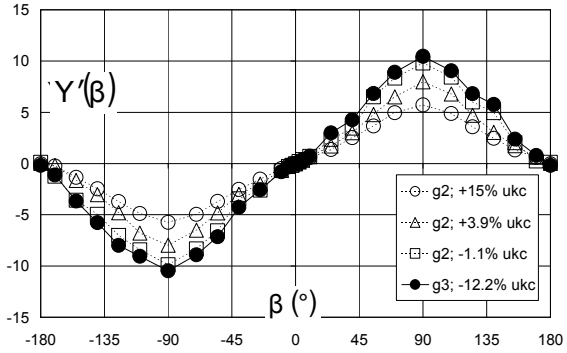

Figure 6.18. Ship D: drift induced lateral force: influence of under keel clearance.

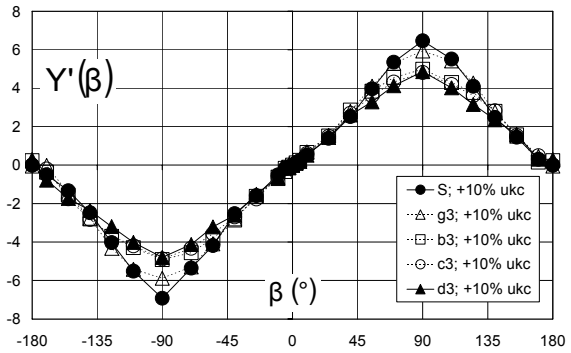

a. positive under keel clearance

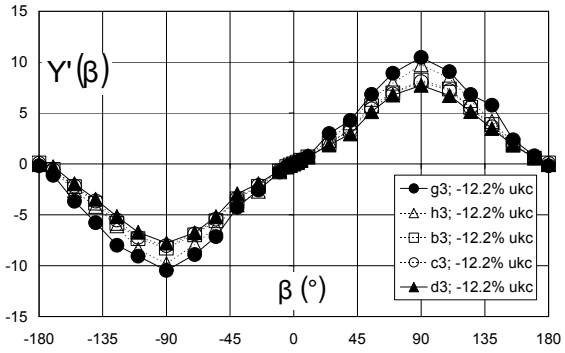

b. negative under keel clearance

Figure 6.19. Ship D: drift induced lateral force: influence of bottom characteristics.

Figures 6.20 and 6.21 show Y'(γ)[1] for different conditions:

- When navigating ahead (-90°< γ <90°) Y'(γ) increases with increasing density and viscosity of the mud layer. Observe that for small values of γ above a solid bottom γ and Y'(γ) have the opposite sign, while they have the same sign for a muddy bottom, see also Figure 6.6;
- The influence of the bottom is less clear when navigating astern.

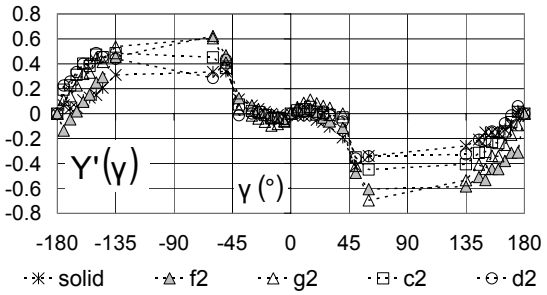

a. 3.9% under keel clearance to the water-mud interface, 15% to the solid bottom

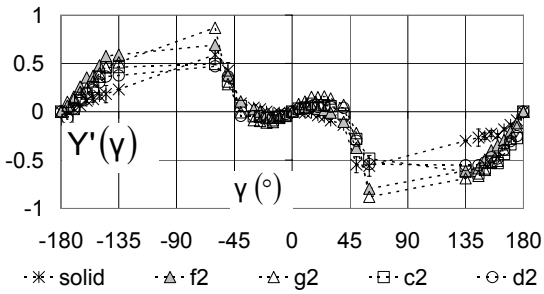

b. -1.1% under keel clearance to the water-mud interface, 10% to the solid bottom

Figure 6.20. Ship D: yaw induced lateral force: influence of bottom characteristics. Thickness of the mud layer: 1.5 m.

[1] Results are missing in the range +/-[60°-135°] because of the lack of experimental data. The mentioned range corresponds with a large yaw rate combined with a small longitudinal velocity. Harmonic yaw tests in these conditions are difficult, because in no time the ship is moving in its own wake. A linear interpolation is proposed to cover the range, although it is also possible to use other types of interpolation.

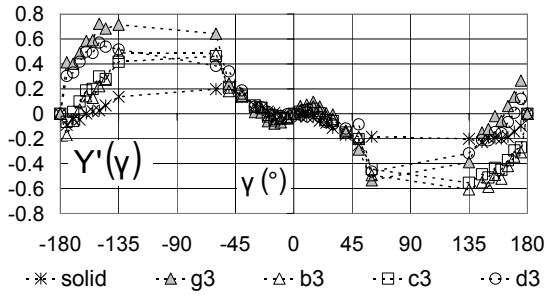

a. 4.1% under keel clearance to the water-mud interface, 26% to the solid bottom

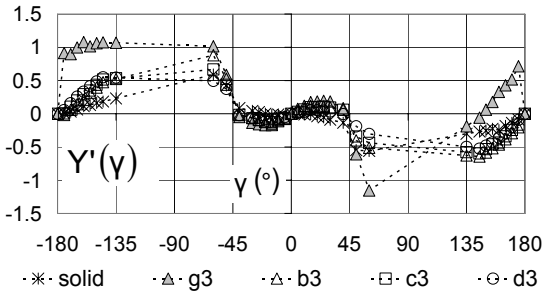

b. -12.2% under keel clearance to the water-mud interface, 10% to the solid bottom

Figure 6.21. Ship D: yaw induced lateral force: influence of bottom characteristics. Thickness of the mud layer: 3 m.

6.3.3 Yaw moment

The yaw moment is modelled in a similar way to the lateral force:

$$N_H = \left(N_{\dot{v}} - mx_G\right)\dot{v} + \left(N_{\dot{r}}(\beta) - I_{zz}\right)\dot{r} - mx_G ur + \tfrac{1}{2}\rho L^2 T\left\{\begin{array}{c}\left(u^2+v^2\right)N'(\beta)+\\ \left(u^2+\left(\tfrac{1}{2}rL\right)^2\right)N'(\gamma)+\\ \left(v^2+\left(\tfrac{1}{2}rL\right)^2\right)N'(\chi)\end{array}\right\} \qquad (6.17)$$

Figure 6.22 shows N'(β) for different series. The moments above a muddy bottom are mostly similar to the ones above a solid bottom, although the slope at small drift angles is smaller above a solid bottom, see also Figure 6.4.

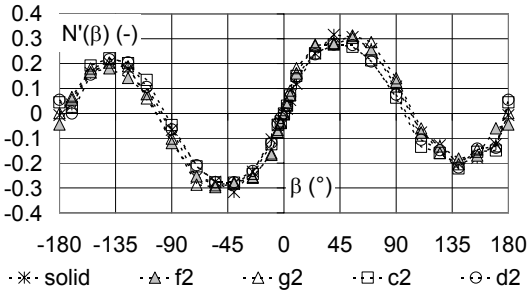

a. 3.9% under keel clearance to the water-mud interface, 15% to the solid bottom. Thickness of the mud layer: 1.5 m.

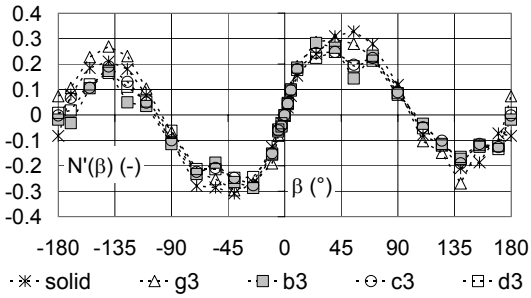

b. -12.2% under keel clearance to the water-mud interface, 10% to the solid bottom. Thickness of the mud layer: 3 m.

Figure 6.22. Ship D: drift induced yawing moment: influence of bottom characteristics.

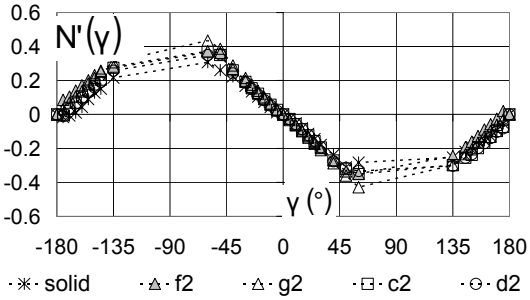

a. 3.9% under keel clearance to the water-mud interface, 15% to the solid bottom. Thickness of the mud layer: 1.5 m.

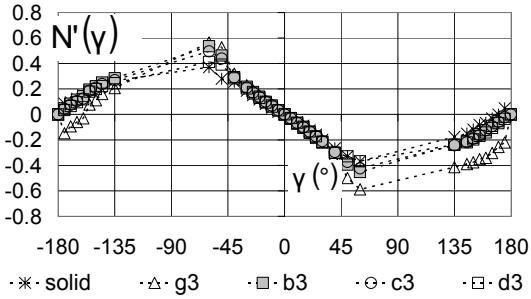

b. -12.2% under keel clearance to the water-mud interface, 10% to the solid bottom. Thickness of the mud layer: 3 m.

Figure 6.23. Ship D: drift induced yawing moment: influence of bottom characteristics.

N'(γ) is represented on Figure 6.23:

- N'(γ) increases with increasing mud density and viscosity when navigating ahead;
- The evolution is variable and less symmetric when navigating astern.

6.4 Propeller induced forces

6.4.1 Propeller thrust and torque

All ship models were equipped with a single propeller, see Appendix B. For each propeller open water data $C_T(\varepsilon)$ and $C_Q(\varepsilon)$ for the four quadrants is available, or could be derived from the Wageningen B-series **[6.7]**. The hydrodynamic advance angle ε is given by:

$$\varepsilon = \arctan\left(\frac{u_P}{0.7\pi\, nD_P}\right) = \arctan\left(\frac{u(1-w)}{0.7\pi\, nD_P}\right) \tag{6.18}$$

With:

- u_P the longitudinal inflow velocity near the propeller. In open water conditions this is the velocity the propeller is driven at;
- w the wake factor;
- $0.7\pi nD_P$ a measure for the peripheral velocity near the propeller.

The four quadrants are defined as:

- 1st quadrant (Q1): 0 deg < ε < 90 deg; u > 0 ; n > 0;
- 2nd quadrant (Q2): 90 deg < ε < 180 deg; u > 0 ; n < 0;
- 3rd quadrant (Q3): 180 deg < ε < 270 deg; u < 0 ; n < 0;
- 4th quadrant (Q4): 270 deg < ε < 360 deg; u < 0 ; n > 0.

The thrust and torque coefficients are defined as:

$$C_T(\varepsilon) = \frac{T_P}{\frac{1}{2}\rho A_0\left[u^2 + (0.7\pi\, nD_P)^2\right]} \tag{6.19}$$

$$C_Q(\varepsilon) = \frac{Q_P}{\frac{1}{2}\rho A_0 D_P\left[u^2 + (0.7\pi\, nD_P)^2\right]} \tag{6.20}$$

A value for the wake factor can be found by means of the thrust or the torque identity. The thrust identity is based on a comparison between the thrust coefficient in open water as a function of the advance ratio, $K_T(J)$, and the

measured thrust coefficient behind the hull as a function of the apparent advance ratio, $K_T(J')$, with

$$J' = \frac{u}{nD_P} = \frac{J}{1-w} \tag{6.21}$$

w(J') can be calculated by comparing J and J' at constant K_T. Unlike a propeller in open water, the wake behind the hull varies over the propeller disk, which results in a different wake factor when derived using the torque identity. Moreover the measured thrust and the torque during the experiments cannot be predicted correctly when the same wake factor is used. For these reasons two different wake factors, $w_T(J')$ and $w_Q(J')$, are determined. The wake factor is therefore more a modelling concept to predict the thrust force and propeller torque.

Although there are indications that the propeller thrust is affected by drift **[6.6]**, this influence has not been taken into account and will be incorporated in the thrust deduction factor.

Using equations (6.19) to (6.21) a model for the thrust and the torque can be developed:

$$T_P = \frac{0.7^2}{8}\pi^3 \rho n^2 D_P^4 C_T(\varepsilon)\left(1+\tan^2\varepsilon\right) \tag{6.22}$$

$$Q_P = \frac{0.7^2}{8}\pi^3 \rho n^2 D_P^5 C_T(\varepsilon)\left(1+\tan^2\varepsilon\right) \tag{6.23}$$

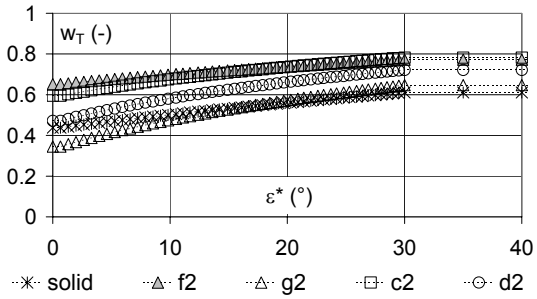

a. 3.9% under keel clearance to the water-mud interface, 15% to the solid bottom.

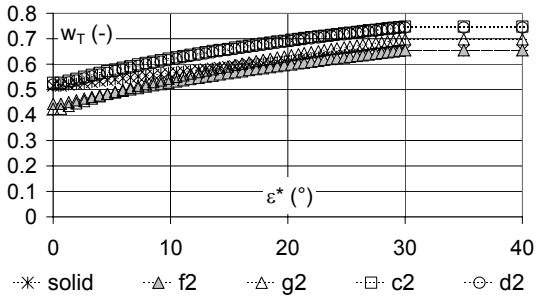

b. -1.1% under keel clearance to the water-mud interface, 10% to the solid bottom.

Figure 6.24. Ship D: $w_T(\varepsilon^*)$: influence of bottom characteristics. Thickness of the mud layer: 1.5 m.

The wake factor determined with the thrust identity is represented on Figures 6.24 and 6.25 as a function of the apparent hydrodynamic advance angle ε^*:

$$\varepsilon^* = \arctan\left(\frac{u}{0.7\pi\, nD_P}\right) = \arctan\left(\frac{J'}{0.7\pi}\right) \tag{6.24}$$

- The wake factor increases with decreasing mud density;
- The evolution as a function of ε^* is steeper in a muddy area;

- Small wake factors are obtained when navigating in contact with a high density mud layer;
- In the other quadrants the wake factor equals zero.

A larger wake factor implies a reduced inflow of the propeller. With low density mud layers this reduction can be ascribed to the undulations of the water mud interface that occur near the propeller (see 6.4.2), disturbing the water flow.

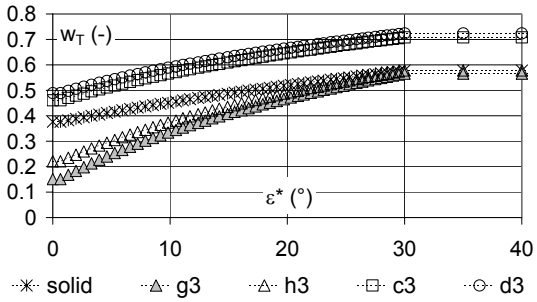

a. 4.1% under keel clearance to the water-mud interface, 26% to the solid bottom.

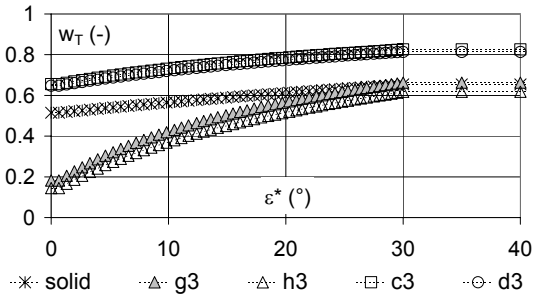

b. -12.2% under keel clearance to the water-mud interface, 10% to the solid bottom.

Figure 6.25. Ship D: $w_T(\varepsilon^*)$: influence of bottom characteristics. Thickness of the mud layer: 3 m.

The small wake factors when navigating in contact with high density mud layers can be ascribed to the larger impulse caused by the mud inflow of the propeller. However, this does not lead to an overall better efficiency, see also 6.4.2 and **[6.12]**. Indeed, small wake factors also indicate that the difference between a propeller working in open water and a propeller behind the hull is smaller. In the bollard pull condition, a condition that approaches the open water condition the most, a significant lost of thrust is observed when navigating in contact with high density mud layers, see 10.4.1.1.

The wake factor determined with the torque identity can be found on Figures 6.26 and 6.27:

- In muddy areas the wake does not vary much with ε*;
- When penetrating thick mud layers the wake factor approaches 1;
- In the other quadrants the wake factor equals zero.

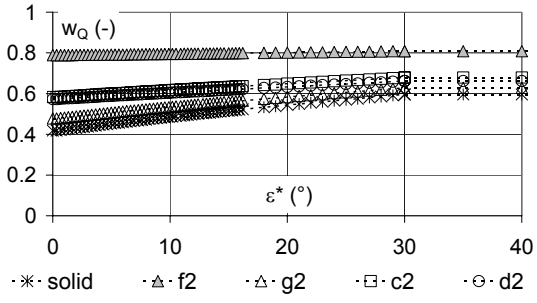

a. 3.9% under keel clearance to the water-mud interface, 15% to the solid bottom.

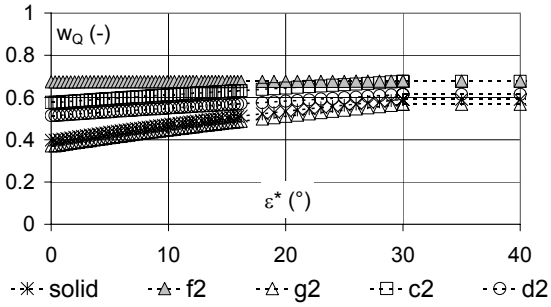

b. -1.1% under keel clearance to the water-mud interface, 10% to the solid bottom.

Figure 6.26. Ship D: $w_Q(\varepsilon^*)$: influence of bottom characteristics. Thickness of the mud layer: 1.5 m.

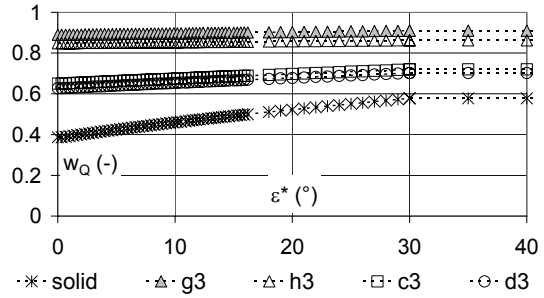

a. 4.1% under keel clearance to the water-mud interface, 26% to the solid bottom.

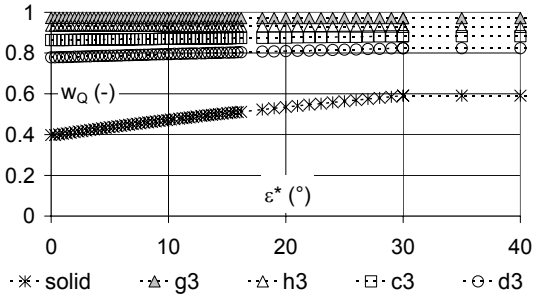

b. -12.2% under keel clearance to the water-mud interface, 10% to the solid bottom.

Figure 6.27. Ship D: $w_Q(\varepsilon^*)$: influence of bottom characteristics. Thickness of the mud layer: 3 m.

The torque increases significantly when the propeller operates behind the ship's hull. Moreover this increase is almost independent of the working condition of the propeller.

6.4.2 Propeller efficiency

Figure 6.28 represents the thrust and the torque when navigating at harbour full (572 rpm, model scale). Thrust increases slightly with decreasing under keel clearance. A stronger increase is observed with the torque.

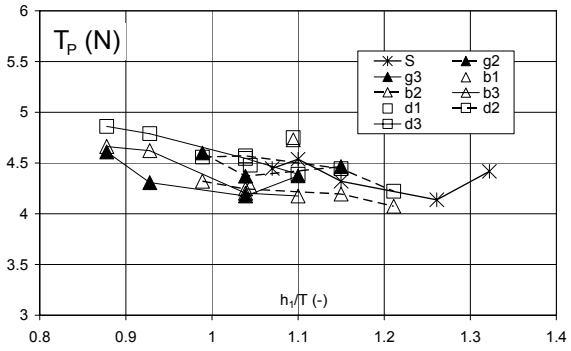

a. Thrust

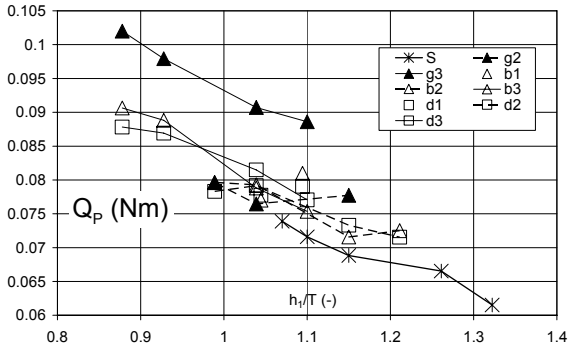

b. Torque

Figure 6.28. Thrust and torque: Influence of bottom conditions and ukc at harbour full (572 rpm, model scale)

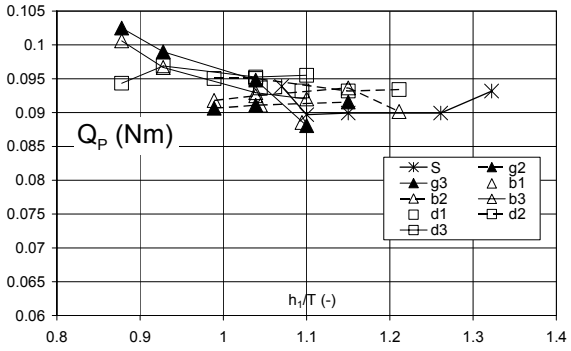

Figure 6.29. Torque: influence of bottom conditions and under keel clearance at harbour full (572 rpm, model scale), bollard pull condition.

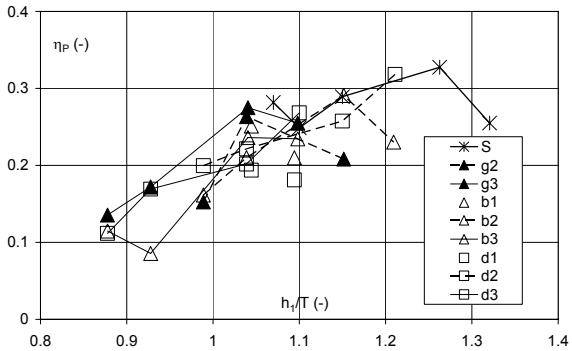

Figure 6.30. Overall propeller efficiency: influence of bottom characteristics and under keel clearance.

The increase of the torque is mainly due to the increased resistance and the slower speed at small under keel clearances. The influence of the mud layer can be seen on Figure 6.29, representing the torque in bollard pull condition. In this condition the only movement of the interface is due to propeller disturbance.

At positive under keel clearance a more or less constant torque can be observed, nevertheless if the ship penetrates the mud layer the torque increases, especially with high density mud layers, as the propeller tip, which touches the mud layer, is subjected to a higher resistance.

The propeller power P_D is defined as:

$$P_D = 2\pi n Q_P \tag{6.25}$$

Figure 6.28b in combination with (6.25) shows that to navigate at harbour full in contact with high density mud layers up to 60% more propeller power is needed. The thrust power is given by

$$P_T = T_P(1 - w_T)V \tag{6.26}$$

With (6.25) and (6.26) the propeller efficiency behind the ship can be calculated:

$$\eta_P = \frac{P_T}{P_D} \tag{6.27}$$

and is represented in Figure 6.30. The overall efficiency, which is already low above a solid bottom, compared to deep water conditions, decreases significantly with decreasing under keel clearance. To have a better insight the overall efficiency can be written as:

$$\eta_P = \eta_0 \eta_R \tag{6.28}$$

In which η_0 is the propeller open water efficiency and η_R the relative rotative efficiency, i.e. the change of efficiency due to placing the propeller behind the ship's hull.

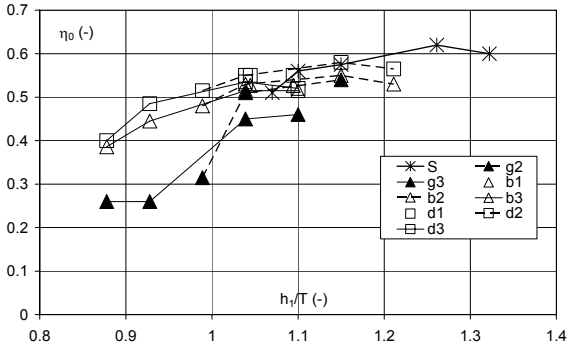

Figure 6.31. Propeller open water efficiency: influence of bottom characteristics and under keel clearance.

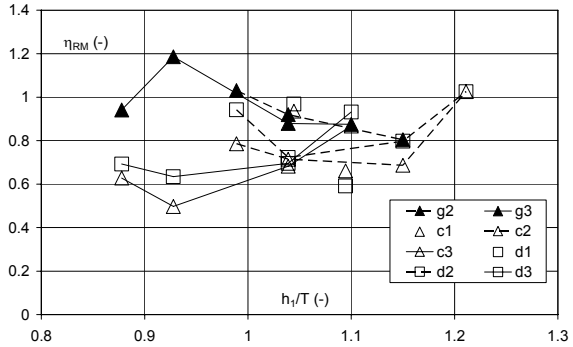

Figure 6.32. Propeller relative rotative efficiency due to undulations: influence of bottom characteristics and under keel clearance.

The propeller open water efficiency is shown on Figure 6.31. η_0 decreases with decreasing under water keel clearance. This is mainly due to the increased resistance and the increased torque when penetrating the mud layer.

A propeller behind the hull will be operating in another flow environment, not only because of the presence of the hull, but also due to the undulations of the interface caused by the ship's hull.

To take those two effects separately into account, the relative rotative efficiency can be written as:

$$\eta_R = \eta_{RS}\eta_{RM} \tag{6.29}$$

η_{RS} is the relative rotative efficiency above solid bottoms, due to the wake of the hull, which varies with the under keel clearance. η_{RM} is an additional rotative efficiency above mud layers, taking the undulations of the interface into account, and is represented on Figure 6.32.

η_{RM} reaches a minimum when the ship's keel is located close to the water-mud interface, especially when the mud density is small. When penetrating the mud layer, the loss of efficiency is high with low density mud layers, while high density mud layers have no, or even an opposite, effect on the efficiency. Moreover the effect of the mud layer seems nil once the ship has an under keel clearance of 20% above the water mud interface.

A smaller value of η_{RM} corresponds with an undulation that is closer to the ship and which has a larger magnitude. The presence of undulations near the propeller seems therefore to disturb the inflow of water to the propeller. This mechanism results in an apparent larger wake factor, as observed on Figures 6.24 and 6.25.

Those results are valid in any self propelled conditions. If the propeller rate is increased, the speed will also increase. Eventually the elevation with low density mud layers will completely take place behind the ship, resulting in a better η_{RM}-value. This occurs at ship speeds of 10 knots or more, which is higher than normal harbour conditions, so that this condition is less relevant. With high density mud layers more speed is difficult to achieve due to the significant resistance and torque and a limited available engine power.

A decrease of propeller rate will decrease the ship's speed, nevertheless, with low density mud layers a significant rise of the interface is already observed at low speed. A decrease of speed will thus only have a small effect on the η_{RM}-value.

The cause for the loss of efficiency in muddy navigation areas depends thus on the density of the mud layer:

- With high density mud layers a significant increased resistance leads to bad propeller working conditions. Moreover the torque increases when the propeller tip touches the mud layer;

- Significant undulations of the interface occur at the aft perpendicular of the ship when navigating above or through lower density mud layers. Those undulations disturb the water inflow to the propeller, resulting in a higher apparent wake value.

6.4.3 Longitudinal force

The thrust yields a longitudinal force given as:

$$X_P = \left[1 - t\left(\varepsilon^*, \varphi^*, \gamma^*\right)\right] T_P \tag{6.30}$$

t being the thrust deduction factor, formulated as a function of the apparent hydrodynamic angles ε*, φ* and γ*, given in expressions (6.24), (6.31) and (6.32).

$$\varphi^* = \arctan\left(\frac{|v|}{0.7\pi\, n D_P}\right) \tag{6.31}$$

$$\gamma^* = \arctan\left(\frac{|0.5 r L|}{0.7\pi\, n D_P}\right) \tag{6.32}$$

A larger value for t – which implies a smaller longitudinal force for a given thrust – is obtained at positive under keel clearances with high density mud layers; if the ship's keel touches the mud, on the other hand, t is larger for the lightest mud layers (Figure 6.33a).

φ* only appears to have a significant effect in the first quadrant when navigating above light mud layers (Figure 6.33b). γ*, on the other hand, is only significant in the fourth quadrant, especially when navigating in contact with high density mud layers.

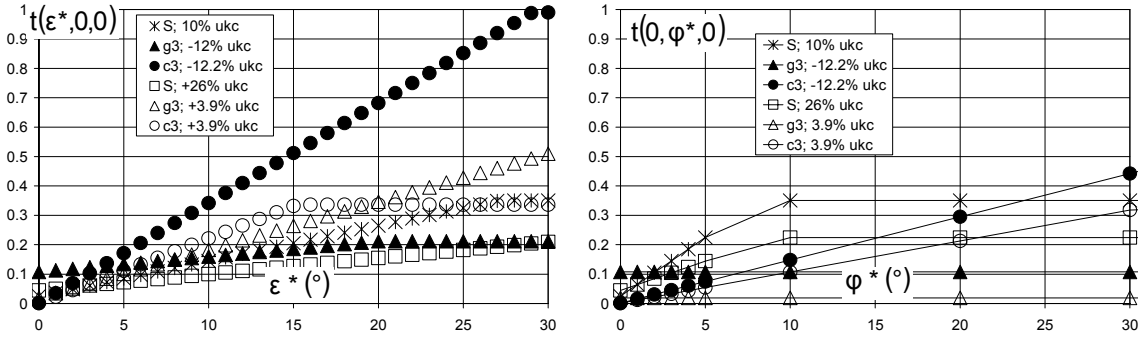

a. Influence of ε* b. Influence of φ*

Figure 6.33. Ship D: thrust deduction factor: influence of bottom characteristics and under keel clearance.

6.4.4 Lateral force and yaw moment

6.4.4.1 Formulation

Besides a longitudinal force, propeller action also causes a lateral force and a yawing moment due to asymmetry of the flow. This phenomenon is especially

important in the second and fourth quadrants. In shallow water, it is observed that these actions are not constant with time **[6.14]**, but contain an important slowly oscillating component with an amplitude whose order of magnitude is that of the propeller thrust, Figure 6.34.

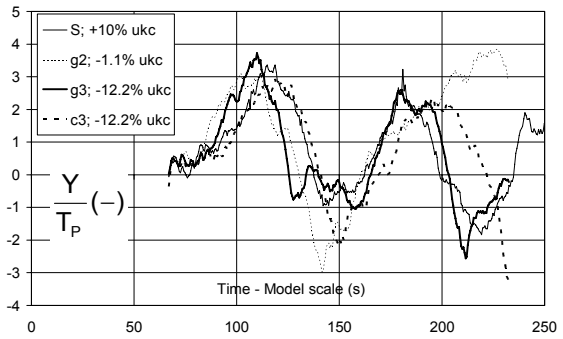

Figure 6.34. Ship D: fluctuations of the lateral force due to combinations of forward speed and propeller action astern.

This effect is also included in the mathematical models:

$$Y_P = \left|\frac{n}{n_0}\right|\left(Y'^{n}_{v}\dot{v} + Y'^{n}_{r}\dot{r}\right) + \begin{bmatrix} K_1\left[Y_{PT}(\beta,\varepsilon^*) + Y_{PT}(\gamma,\varepsilon^*)\right] \\ + K_2\left[Y_{PTA}(\beta,\varepsilon^*)\right]\left[\cos\left(\omega(\beta,\varepsilon^*)t + \varphi(\beta,\varepsilon^*)\right)\right] \end{bmatrix} T_P(\varepsilon^*) \quad (6.33)$$

$$N_P = \left|\frac{n}{n_0}\right|\left(N'^{n}_{v}\dot{v} + N'^{n}_{r}\dot{r}\right) + \begin{bmatrix} \left[N_{PT}(\beta,\varepsilon^*) + N_{PT}(\gamma,\varepsilon^*)\right] + \\ \left[N_{PTA}(\beta,\varepsilon^*,K_2)\right]\left[\cos\left(\omega(\beta,\varepsilon^*)t + \varphi(\beta,\varepsilon^*)\right)\right] \end{bmatrix} L_{PP} T_P(\varepsilon^*) \quad (6.34)$$

The K_1 and K_2 parameters depend on the quadrant. $K_1 = F_n$ in quadrant 1 and equals 1 in other quadrants; $K_2 = 1$ in quadrants 1, 2, 3 and takes a value between 0 and 1 in quadrant 4, depending on the yaw rate and yaw acceleration (see 6.4.4.6).

6.4.4.2 Effect on hydrodynamic inertia

Figure 6.35 shows the additional sway added mass due to a propeller action full ahead. As a result, the total sway added mass will decrease in muddy navigation areas, but increase when navigating above a solid bottom, although the effect is rather small, compare Figures 6.2 and 6.35.

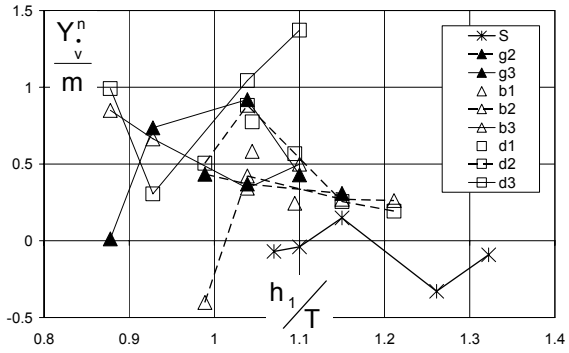

Figure 6.35. Ship D: sway added mass, component due to propeller action full ahead: influence of bottom characteristics and under keel clearance.

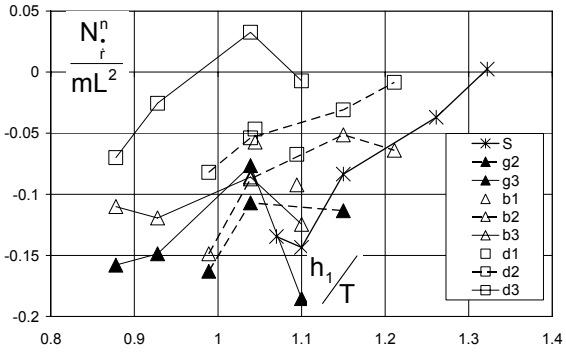

Figure 6.36. Ship D: yaw added moment of inertia, component due to propeller action full astern in Q3: influence of bottom characteristics and under keel clearance.

With astern propeller action a significant influence on the added mass terms is observed (Figure 6.36). In the yaw equation, additional added moment of inertia terms at full propeller loading have the same magnitude as the corresponding inertia terms at 0 rpm. In the fourth quadrant even higher values are reached.

In the following paragraphs only the results for the sway force will be discussed. Analogous conclusions can be drawn for the yawing moment.

6.4.4.3 Results in the 1st quadrant

There are no oscillations in the first quadrant, consequently the amplitude Y_{PTA} equals zero and the harmonic term disappears. The contribution of β and γ to Y_{PT} is equal in the first quadrant. The working condition of the propeller does not affect Y_{PT}. On the other hand a correlation with the ship's speed exists, which has been modelled with the Froude number, whereas this speed correlation does not exist in the other quadrants. Figures 6.37 and 6.38 show the average value Y_{PT}:

- The asymmetry force due to propeller action increases with increasing drift and/or yaw angle;
- The sway force due to propeller action will usually be larger above a muddy bottom, on the other hand the asymmetry will decrease with increasing thickness of the mud layer;
- The remarkable difference between starboard and port drift can be explained by the fact that the ship has been equipped with a single right handed propeller.

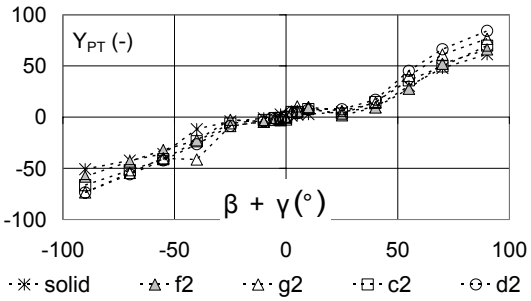

a. 3.9% under keel clearance to the water-mud interface, 15% to the solid bottom.

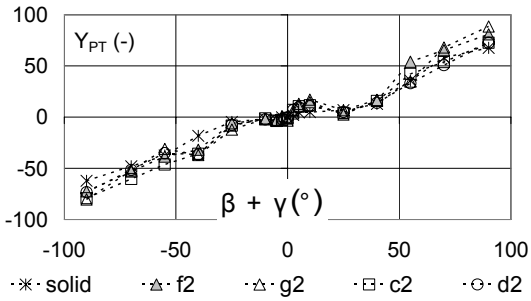

b. -1.1% under keel clearance to the water-mud interface, 10% to the solid bottom.

Figure 6.37. Ship D: $Y_{PT}(\beta)$ in Q1: influence of bottom characteristics and under keel clearance. Mud layer thickness: 1.5 m.

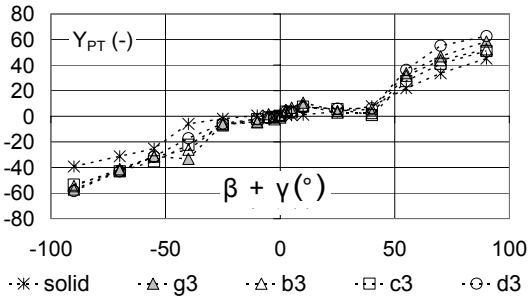

a. 4.1% under keel clearance to the water-mud interface, 26% to the solid bottom.

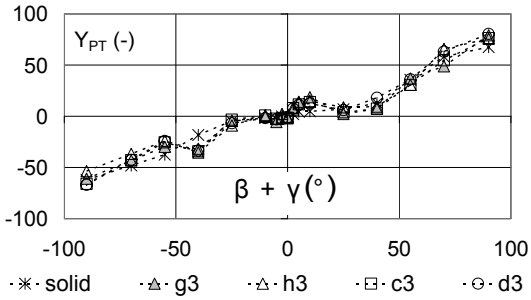

b. -12.2% under keel clearance to the water-mud interface, 10% to the solid bottom.

Figure 6.38. Ship D: $Y_{PT}(\beta)$ in Q1: influence of bottom characteristics and under keel clearance. Mud layer thickness: 3 m.

6.4.4.4 Results in the 2nd quadrant

Unlike in the first quadrant oscillations occur, so that the harmonic term has to be modelled as well.

The average value in the second quadrant is only a function of ε*, which already takes the drift angle into account. The yawing does not affect the average value. Figures 6.39 and 6.40 represent Y_{PT} in different conditions:

- Starting at bollard pull with reversed propeller action (ε* = 180°) Y_{PT} increases to a maximum that is reached around ε* = 170°. From this point on results are linearly interpolated until the first quadrant (ε* = 90°);
- Y_{PT} is usually larger with high density and viscous mud layers;
- A local maximum can be observed near 178°. The data points between 178 and 180° represent conditions with large drift angles. In the same interval conditions without drift angle have not been carried out. As a result it was very difficult to model the effect of the drift angle. Therefore it is assumed that any condition between 178° and 180° will follow the shown tendency and that the effect of the drift angle is taken into account by the definition of ε*.

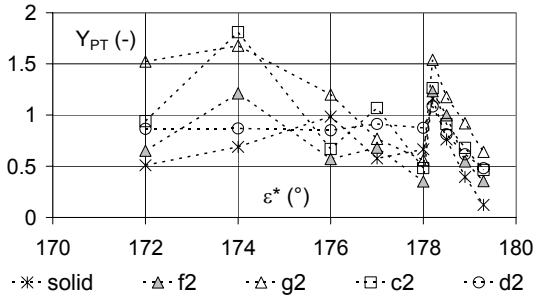

a. 3.9% under keel clearance to the water-mud interface, 15% to the solid bottom.

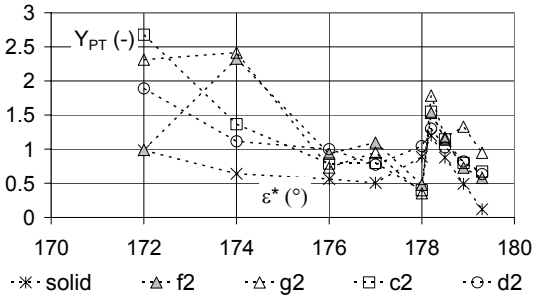

b. -1.1% under keel clearance to the water-mud interface, 10% to the solid bottom.

Figure 6.39. Ship D: $Y_{PT}(\varepsilon^*)$ in Q2: influence of bottom characteristics and under keel clearance. Mud layer thickness: 1.5 m.

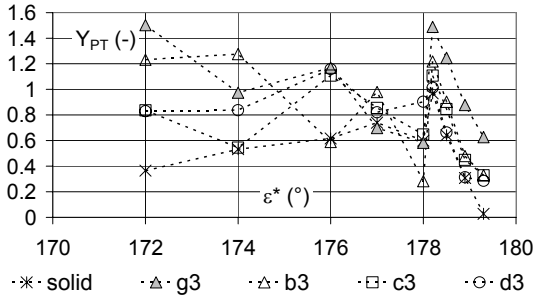

a. 4.1% under keel clearance to the water-mud interface, 26% to the solid bottom.

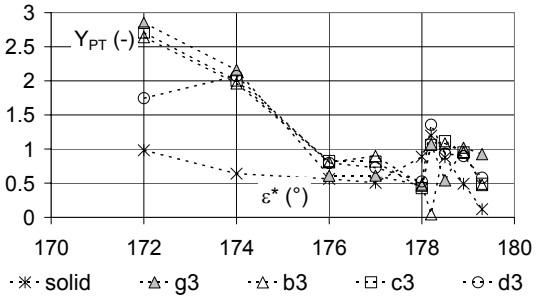

b. -12.2% under keel clearance to the water-mud interface, 10% to the solid bottom.

Figure 6.40. Ship D: $Y_{PT}(\varepsilon^*)$ in Q2: influence of bottom characteristics and under keel clearance. Mud layer thickness: 3 m.

For a given ship speed u, Y_{PT} increases with decreasing propeller rate, while the thrust itself decreases. The average sway force due to propeller action remains thus more or less constant with decreasing propeller rate and will only diminish at small propeller rates.

Y_{PTA}, the amplitude of the oscillations, is in the 2nd quadrant also a function of the angle ε*, see Figures 6.41 and 6.42.

- Y_{PTA} becomes more negative with decreasing ε* to reach a minimum around 172°. Y_{PTA} turns zero at 90°, i.e. the border with the first quadrant;
- The amplitudes of the oscillations are larger in muddy areas.

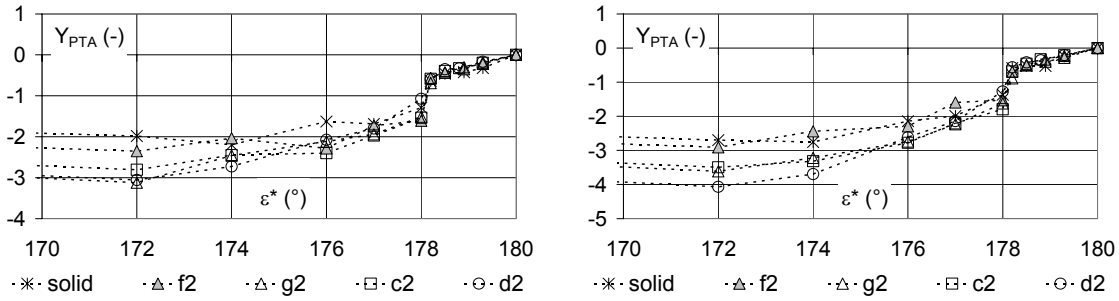

a. 3.9% under keel clearance to the water-mud interface, 15% to the solid bottom.

b. -1.1% under keel clearance to the water-mud interface, 10% to the solid bottom.

Figure 6.41. Ship D: $Y_{PTA}(\varepsilon^*)$ in Q2: influence of bottom characteristics and under keel clearance. Mud layer thickness: 1.5 m.

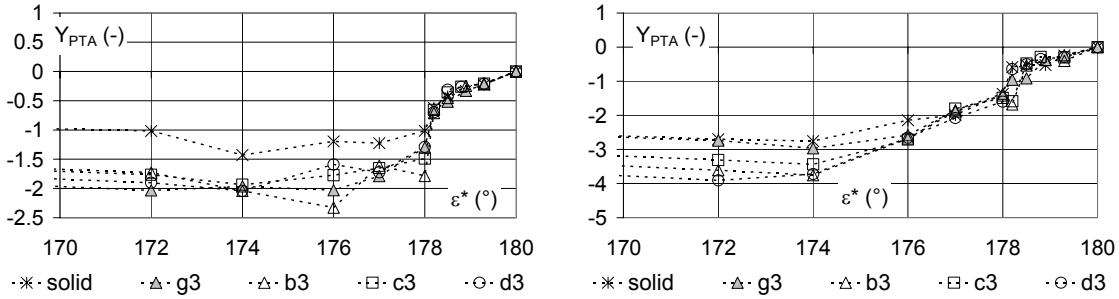

a. 4.1% under keel clearance to the water-mud interface, 26% to the solid bottom.

b. -12.2% under keel clearance to the water-mud interface, 10% to the solid bottom.

Figure 6.42. Ship D: $Y_{PTA}(\varepsilon^*)$ in Q2: influence of bottom characteristics and under keel clearance. Mud layer thickness: 3 m.

The amplitudes of the oscillation reach their maximum at large propeller rates and at small speed. Once the propeller rate drops or the speed increases, the amplitude will diminish until zero. If on the other hand the speed drops to zero – bollard pull – the amplitude will turn zero as well.

The full scale period of the oscillations has an order of magnitude of minutes. The frequency is represented on Figures 6.43 and 6.44 in a non-dimensional way:

$$\omega' = \omega\sqrt{\frac{L}{g}} \tag{6.35}$$

The frequencies are equal for Y and N. The frequency increases with decreasing propeller rate to reach a maximum and decrease again. The maximum frequency is larger in the 2nd quadrant than in the 4th quadrant. The frequencies do not seem to be affected significantly by the bottom condition, only the maximal value seems to depend on the bottom condition.

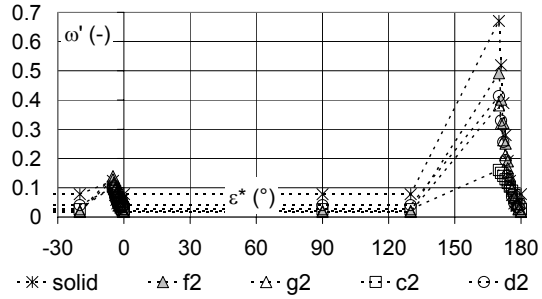

a. 3.9% under keel clearance to the water-mud interface, 15% to the solid bottom.

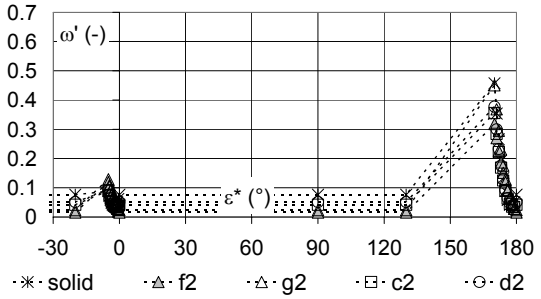

b. -1.1% under keel clearance to the water-mud interface, 10% to the solid bottom.

Figure 6.43. Ship D: frequency of oscillations: influence of bottom characteristics and under keel clearance. Mud layer thickness: 1.5 m.

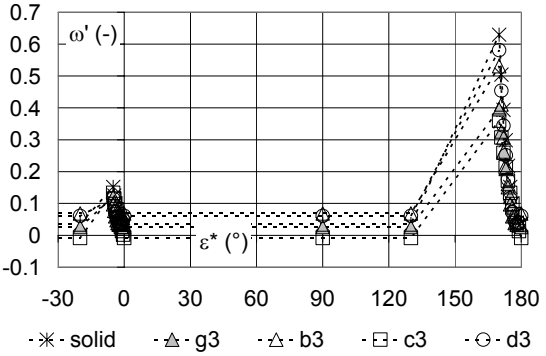

a. 4.1% under keel clearance to the water-mud interface, 26% to the solid bottom.

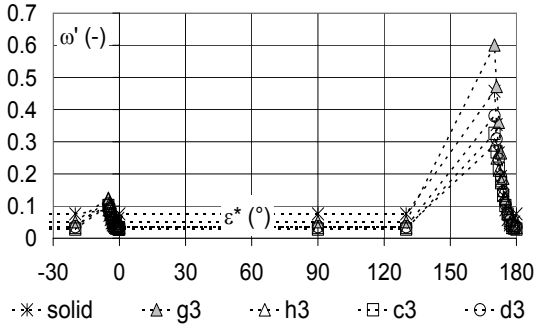

b. -12.2% under keel clearance to the water-mud interface, 10% to the solid bottom.

Figure 6.44. Ship D: frequency of oscillations: influence of bottom characteristics and under keel clearance. Mud layer thickness: 3 m.

A last parameter of the oscillations is the phase shift φ, which seems to be only randomly dependent on the bottom condition. During simulation runs the time step t in equations (6.33-6.34) starts from zero once the quadrant turns even.

6.4.4.5 Results in the 3rd quadrant

As in the first quadrant there are no oscillations. β and γ have, contrary to the first quadrant, a different influence on the average term Y_{PT}. The influence of the drift angle is shown on Figures 6.45 and 6.46:

- $Y_{PT}(\beta)$ is larger above a solid bottom and reinforces the hull force, due to the sign of the thrust;
- Above muddy areas $Y_{PT}(\beta)$ will counteract the hull force for drift angles close to -90°. The resistance to sway consequently decreases with increasing propeller thrust.

The figures only show negative drift angles, for positive drift angles, anti-symmetry is proposed, due to the lack of measurements. Unlike $Y_{PT}(\beta)$, $Y_{PT}(\gamma)$ will always reinforce the hull force.

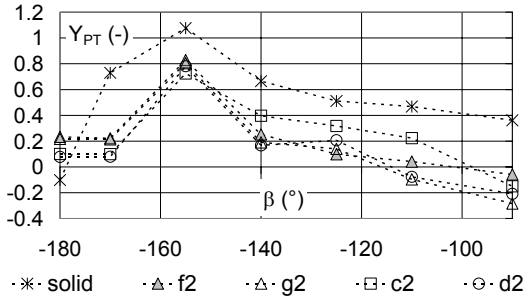

a. 3.9% under keel clearance to the water-mud interface, 15% to the solid bottom.

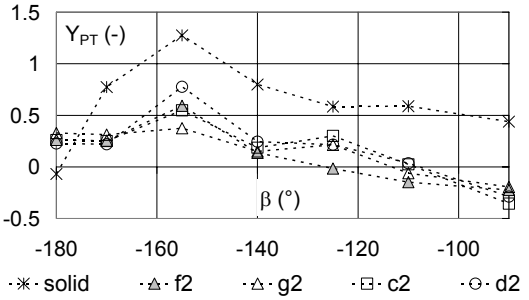

b. -1.1% under keel clearance to the water-mud interface, 10% to the solid bottom.

Figure 6.45 Ship D: $Y_{PT}(\beta)$ in Q3 influence of bottom characteristics and under keel clearance. Mud layer thickness: 1.5 m.

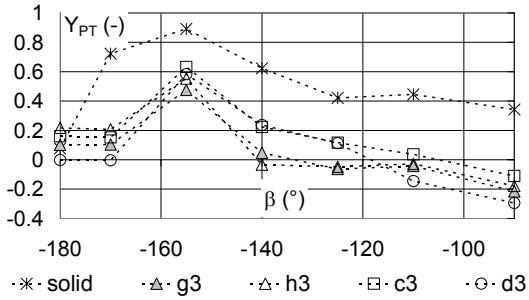

a. 4.1% under keel clearance to the water-mud interface, 26% to the solid bottom.

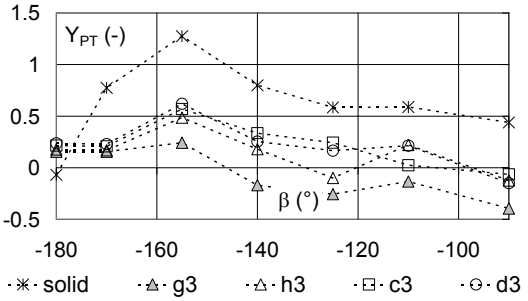

b. -12.2% under keel clearance to the water-mud interface, 10% to the solid bottom.

Figure 6.46 Ship D: $Y_{PT}(\beta)$ in Q3 influence of bottom characteristics and under keel clearance. Mud layer thickness: 3 m.

6.4.4.6 Results in the 4th quadrant

As in the third quadrant β and γ have a different influence on the average values Y_{PT}. Also a harmonic term has to be modelled to predict the oscillations. $Y_{PT}(\beta)$ is modelled by means of ε* as the influence of the propeller loading is larger than the influence of the drift angle.

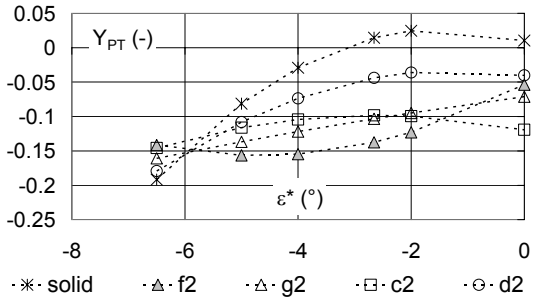

a. 3.9% under keel clearance to the water-mud interface, 15% to the solid bottom.

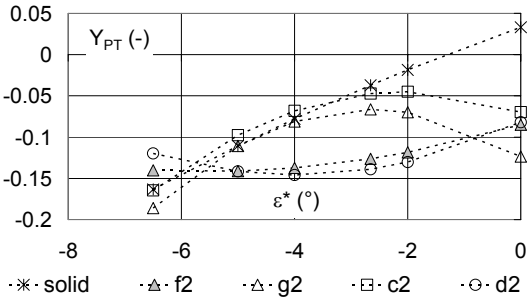

b. -1.1% under keel clearance to the water-mud interface, 10% to the solid bottom.

Figure 6.47. Ship D: $Y_{PT}(\varepsilon^*)$ in Q4: influence of bottom characteristics and under keel clearance. Mud layer thickness: 1.5 m.

$Y_{PT}(\varepsilon^*)$ is shown for different conditions on Figures 6.47 and 6.48:

- $Y_{PT}(\varepsilon^*)$ is usually more negative above muddy bottoms;
- $Y_{PT}(\varepsilon^*)$ is significantly smaller in comparison with the second quadrant.

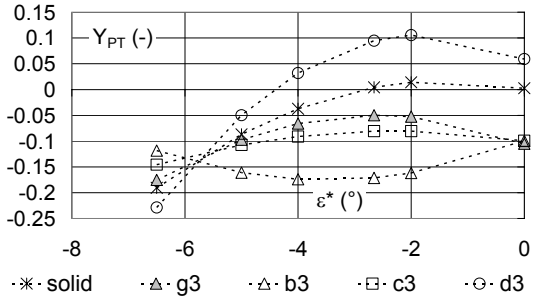

a. 4.1% under keel clearance to the water-mud interface, 26% to the solid bottom.

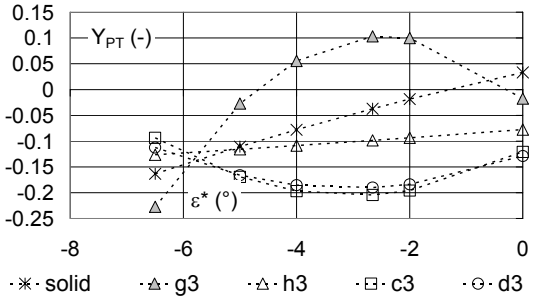

b. -12.2% under keel clearance to the water-mud interface, 10% to the solid bottom.

Figure 6.48. Ship D: $Y_{PT}(\varepsilon^*)$ in Q4: influence of bottom characteristics and under keel clearance. Mud layer thickness: 3 m.

In the second quadrant yawing did not generate any significant extra force. In the fourth quadrant this is not the case, as can be seen on Figures 6.49 and 6.50:

- $Y_{PT}(\gamma)$ is larger above a muddy bottom and increases with increasing density and viscosity and with decreasing under keel clearance;
- $Y_{PT}(\gamma)$ has the same sign as in the third quadrant, but in this case the hull force will be counteracted as the sign of the thrust is opposite.

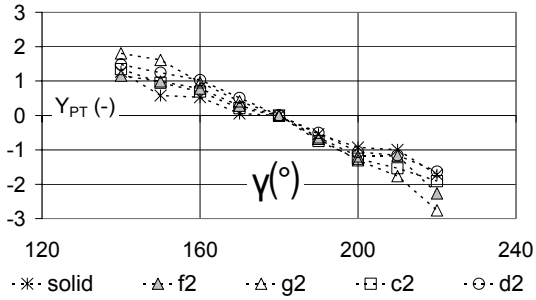

a. 3.9% under keel clearance to the water-mud interface, 15% to the solid bottom.

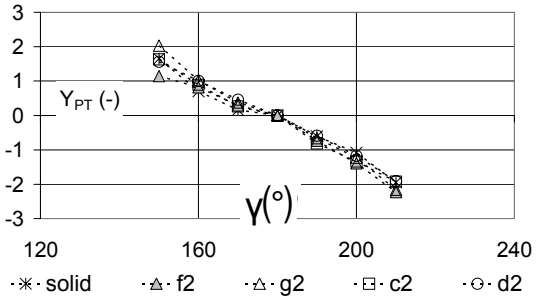

b. -1.1% under keel clearance to the water-mud interface, 10% to the solid bottom.

Figure 6.49. Ship D: $Y_{PT}(\gamma)$ in Q4: influence of bottom characteristics and under keel clearance. Mud layer thickness: 1.5 m.

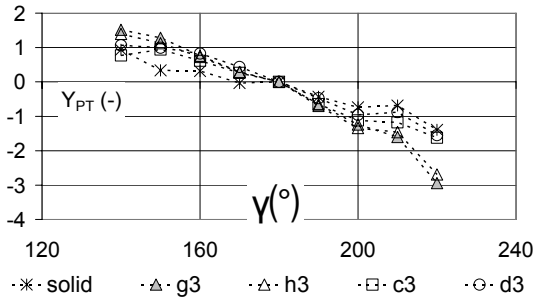

a. 4.1% under keel clearance to the water-mud interface, 26% to the solid bottom.

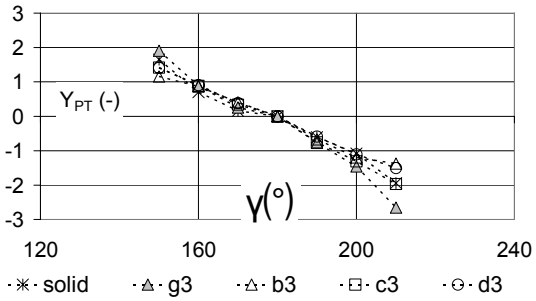

b. -12.2% under keel clearance to the water-mud interface, 10% to the solid bottom.

Figure 6.50. Ship D: $Y_{PT}(\gamma)$ in Q4: influence of bottom characteristics and under keel clearance. Mud layer thickness: 3 m.

The amplitude of oscillations in the 4th quadrant is smaller in comparison with the 2nd quadrant. Oscillations do not always occur, see for example Figure 6.51. When the vessel yaws with sufficiently large amplitude, the amplitude of the oscillations seems to drop to zero:

- When the ship yaws with an amplitude of 10° or more there are no oscillations;
- For small yaw movements, like 2.5° or less, oscillations occur;
- For intermediate yaw movements, a fraction of the oscillations can be observed.

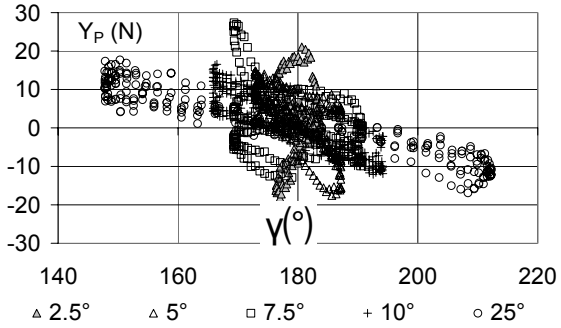

Figure 6.51. Ship model D: Y_P (in N model scale) as a function of γ. Result of tests at different yaw amplitudes, 26% of under keel clearance above a solid bottom, ship model velocity: -0.12 m/s.

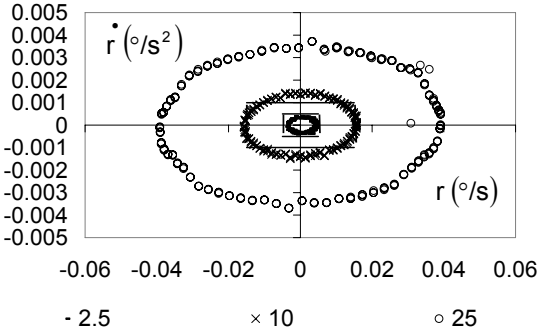

Figure 6.52. Oscillation check in Q4.

Figure 6.52 allows expressing the above observations mathematically. Two squares are drawn:

- Outside the outer square 'os' no oscillations occur or when:

$$\left|\dot{r}\right| \geq \dot{r}_{os,max} \text{ or } \left|r\right| \geq r_{os,max} \tag{6.36}$$

  In this case K_2 in (6.33) equals zero.
- Inside the inner square 'is' oscillations occur, this is when:

$$\left|\dot{r}\right| \leq \dot{r}_{is,max} \text{ or } \left|r\right| \leq r_{is,max} \tag{6.37}$$

  In this case K_2 in (6.33) equals one.
- Between the two squares K_2 is interpolated between 0 and 1. The step of the interpolations is determined with r or $\dot{r}$, depending on which parameter is located the closest to the non-oscillation area 'os'.

6.5 Rudder induced forces

6.5.1 Rudder dynamics

All ship models were equipped with a single rudder. Open water tests have been carried out for each rudder, measuring lift and drag in a 360 deg range of angles of attack α_R. The non-dimensional drag and lift coefficient are defined as follows:

$$C_D(\alpha_R) = \frac{D_R}{\frac{1}{2}\rho A_R U^2} \tag{6.38}$$

$$C_L(\alpha_R) = \frac{L_R}{\frac{1}{2}\rho A_R U^2} \tag{6.39}$$

D_R being the drag, L_R the lift force, A_R the movable fraction of the rudder area and U the flow velocity. The rudder angle δ_R differs from the angle of attack α_R:

$$\alpha_R = \delta_R + \delta_0 + \beta_R \tag{6.40}$$

δ_0, the rudder angle where the normal force F_N vanishes, is a correction for flow asymmetry:

$$\delta_0 = -\delta_R(F_N = 0) \tag{6.41}$$

The asymmetry correction is approximately -2 deg for the D-ship above a solid bottom or low density mud layers. The correction turns positive for high density mud layers. The influence of slip ratio on δ_0 is neglected. β_R in (6.40) is the local drift angle at the rudder:

$$\beta_R = \arctan\left(\frac{-v_R}{u_R}\right) \tag{6.42}$$

u_R, v_R being the longitudinal and transverse component of the flow velocity near the rudder:

$$V_R = \sqrt{u_R^2 + v_R^2} \tag{6.43}$$

Using expressions (6.38-6.43) the forces on the rudder can be determined:

$$F_X = \frac{1}{2}\rho A_R V_R^2 [C_L(\alpha_R)\sin\beta_R + C_D(\alpha_R)\cos\beta_R] \tag{6.44}$$

$$F_Y = \frac{1}{2}\rho A_R V_R^2 [C_L(\alpha_R)\cos\beta_R - C_D(\alpha_R)\sin\beta_R] \tag{6.45}$$

The flow velocity on the rudder depends on the hull form, which provokes wake (in the longitudinal direction) and change of flow direction (in transverse direction), and on the propeller which accelerates the longitudinal flow, depending on the rudder-propeller distance and the rudder area affected by the propeller flow. The wake at the rudder is not necessarily the same as at the propeller: a new wake factor has to be introduced. Different wake factors for F_X and F_Y will be derived from test results as the wake factor depends on the rudder angle. The water velocity aft of the propeller can be approximated by expressions based on momentum theory (see Appendix C):

- for the first quadrant:

$$u_R = \frac{1-w_R}{1-w_P} \sqrt{\left[\eta\left[(1-k)\sin\varepsilon + k\sqrt{C_T+\sin^2\varepsilon}\right]^2 + (1-\eta)\sin^2\varepsilon\right]\left[[(1-w_P)u]^2 + [0.7\pi n D_P]^2\right]} \quad (6.46)$$

- for the fourth quadrant:

$$u_R = (1-w_R) \sqrt{\left[\eta\left[(1-k)|\sin\varepsilon| - k\sqrt{C_T+\sin^2\varepsilon}\right]^2 - (1-\eta)\sin^2\varepsilon\right]\left[u^2 + [0.7\pi n D_P]^2\right]} \quad (6.47a)$$

or

$$u_R = (1-w_R)\left\{\begin{array}{l}\sqrt{\left[\eta\left[(1-k)\sin\varepsilon + k\sqrt{(C_T+\sin^2\varepsilon)}\right]^2 - (1-\eta)\sin^2\varepsilon\right]\left[u^2 + (0.7\pi n D_P)^2\right]} - \\ |u|\sqrt{\left[\eta\left[(k-1) + k\sqrt{(C_T+1)}\right]^2 - (1-\eta)\right]} + \\ u\end{array}\right\} \quad (6.47b)$$

In (6.46-6.47), η is the propeller diameter to rudder height ratio; k is a factor taking account of the distance rudder-propeller. The different values for k can be found in Table 6.1 as a function of x_{RP}/D_P, with x_{RP} the distance between the rudder stock and the tip of the propeller blades. For the D-model this proportion is 0.75 m so that k = 0.94.

Table 6.1. Relationship between the parameter k and the distance between the rudder stock and the propeller tips.[6.2]

x_{RP}/D_P	0.00	0.25	0.50	0.75	1.00
k	0.50	0.79	0.88	0.94	0.96

Rudder forces appear to be less important in the second and third quadrants. The following simplified expression may be used there to calculate the flow velocity u_R:

$$u_R = \xi n + (1-w_R)u \quad (6.48)$$

ξ being a coefficient that takes account of the propeller effect. For the second quadrant, the wake factor for the first quadrant can be taken; in the third quadrant, w_R equals the wake factor of the fourth quadrant.

One should be aware that some alternative formulations for (6.46-6.47) are physically more correct, see Appendix C, **[6.5]**; nevertheless, acceptable models are obtained.

A model for the lateral flow velocity, valid in each quadrant is:

$$v_R = k_{HR}\left(v + rx_R\right) \tag{6.49}$$

k_{HR} being the straightening coefficient and x_R the longitudinal position of the rudder axis. k_{HR} takes the change of flow direction into account. In the literature, k_{HR} values varying between zero and values greater than 1 are found, depending on the propeller loading; moreover, it is often reported that the k_{HR} value for yaw is twice the value for drift. However, during modelling it seemed more appropriate to set the value of k_{HR} to 1. The change of flow direction is then covered by using a wake factor, which is dependent of the drift and yaw rate angle.

Drift and yaw rate angle seem to influence the wake factor in the same way. The sum of both angles is therefore considered. This assumption is acceptable for small drift or yaw rate angles:

$$\frac{v + x_R r}{u} = \frac{v - \frac{1}{2}Lr}{u} = -\tan\beta - \tan\gamma \approx -\left(\beta + \gamma\right) \tag{6.50}$$

In this dissertation, however, β+γ is used for the whole range, although one could use Arctan (tan β + tan γ) instead of β+γ.

Figure 6.53 shows the evolution of the wake factor for F_X when β=γ= 0. For large rudder angles the wake is smaller for high density mud layers. With low density mud layers the wake increases in comparison to the wake factors obtained with a solid bottom.

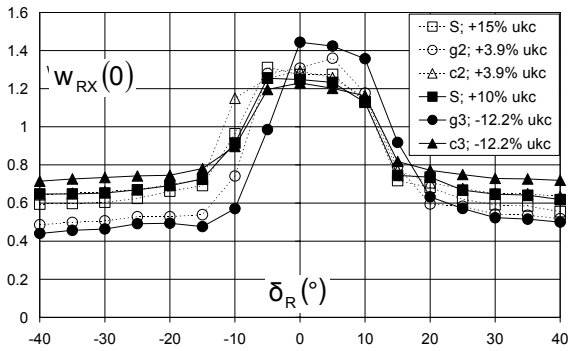

Figure 6.53. Ship D: wake factor for the longitudinal rudder force: Q1.

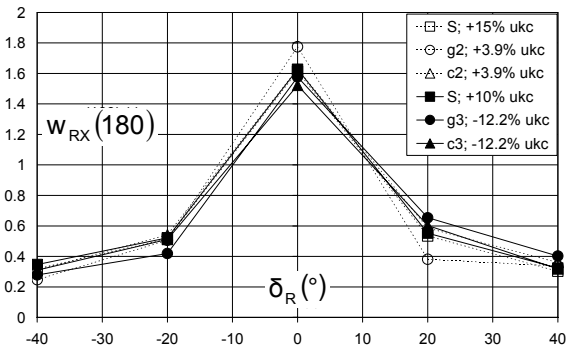

Figure 6.54. Ship D: wake factor for the longitudinal rudder force: Q4.

It is remarkable that the wake is greater than the unity at small rudder angles, indicating a reversed flow. A possible explanation can be found in the pressure distribution, although this is still to be confirmed. When β or γ differ from zero, a significant increase of w_{RX} is observed if the sign of β+γ is opposite to the sign of the rudder angle, which is for instance the case for a ship in a turning circle. Similar conclusions can be drawn for the fourth quadrant (Figure 6.54). The wake factor for larger rudder angles is smaller and varies less with the navigation area.

The longitudinal velocity of the flow near the rudder with reversed propeller depends on the ξ-coefficient in (6.48), which is shown for some conditions on Figure 6.55. The influence of propeller action increases with decreasing under keel clearance.

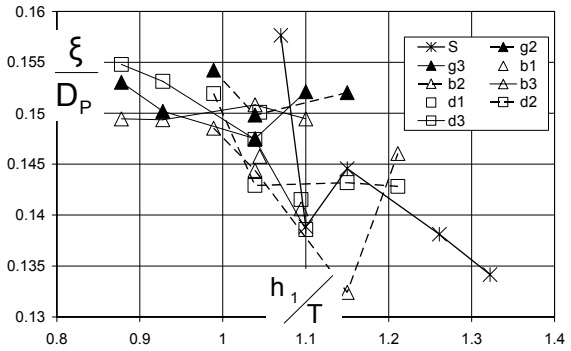

Figure 6.55. Ship D: ξ-coefficient of propeller action in Q2 and Q3. Influence of bottom characteristics and under keel clearance.

Figures 6.56 and 6.57 show the wake factor for F_Y if β=γ=0; similar conclusions as for F_X are valid. In the fourth quadrant, values larger than 1 are obtained in some cases.

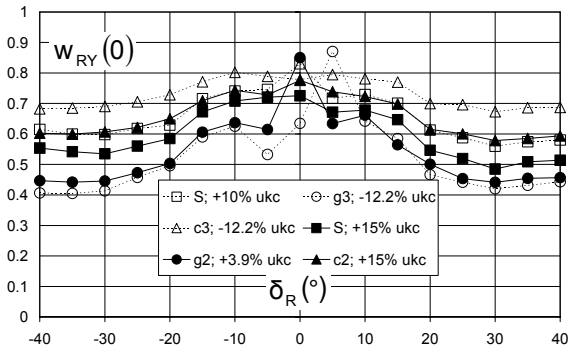

Figure 6.56. Ship D: wake factor for the lateral rudder force: Q1.

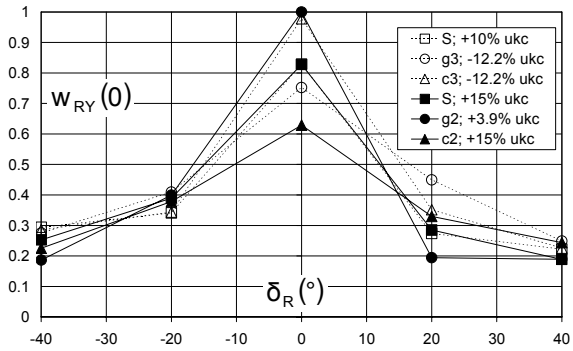

Figure 6.57. Ship D: wake factor for the lateral rudder force: Q4.

6.5.2 Rudder induced longitudinal force

The longitudinal rudder force F_X yields an increase of resistance X_R. Usually the increase will be smaller than F_X, which is modelled as follows:

$$X_R = (1 - t_R) F_X \tag{6.51}$$

with t_R>0. However, the difference between X_R and F_X seemed insignificant; setting t_R to zero was therefore acceptable.

6.5.3 Rudder induced lateral force

The asymmetric flow induced by the rudder not only results in a lateral force F_Y on the rudder (with application point x_R), but also in an extra lateral force $a_H F_Y$ (with application point x_H) due to an asymmetric flow around the hull. This leads to:

$$Y_R = (1 + a_H) F_Y \tag{6.52}$$

The coefficient a_H is a function of ε* and β+γ in the first quadrant. Some examples for β+γ=0 are shown in Figure 6.58. a_H reaches a maximum[2] at a certain propeller loading, which is noticeably lower above solid bottoms. In self-propelled conditions a_H increases with decreasing under keel clearance and decreasing layer thickness. Navigating with a yaw or drift angle also increases a_H to a maximum. The coefficient will drop to zero when the advance angle reaches 90 deg.

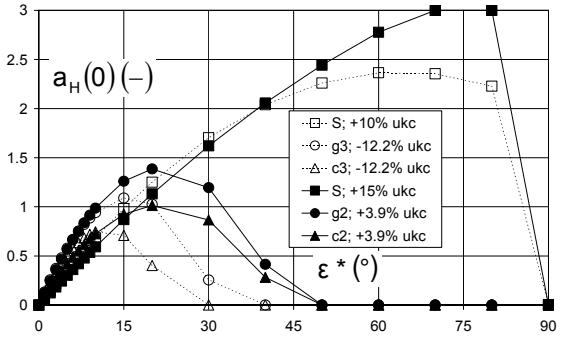

Figure 6.58. Ship D: coefficient a_H for the rudder induced lateral force, Q1.

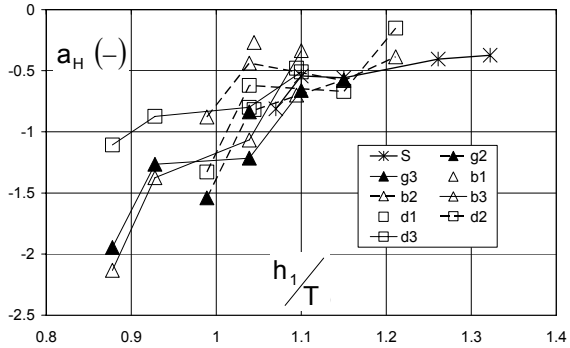

Figure 6.59. Ship D: coefficient a_H for the rudder induced lateral force, Q4.

In the second quadrant the rudder does not seem to have a significant influence on the hull. Satisfactory results are obtained with a_H=0. Rudder angle variations do not affect the oscillations that are typical in this quadrant.

Also in the third quadrant rudder forces are small, but still a difference is observed between F_Y and Y_R. A constant a_H is used. Most remarkable is the sign reversal of a_H between solid and muddy bottoms.

As for the fourth quadrant some results are presented in Figure 6.59. Again a constant value for a_H seemed satisfactory. For positive under keel clearances a_H lies between 0 and -1, but when the ship's keel is near the interface, a_H is more or less -1. In this case the rudder has no effect upon the hull. With even smaller under keel clearances the rudder induces an opposite effect.

6.5.4 Rudder induced yawing moment

The lateral force (6.52) yields a yawing moment which can be written as:

$$N_R = (x_R + a_H x_H) F_Y \tag{6.53}$$

The application point x_H can be written as a function of β+γ in the first quadrant. x_H takes a constant value in the third and fourth quadrants, and has no relevance in the second quadrant (a_H = 0). Figure 6.60 shows some values of x_H in the first and fourth quadrants for β+γ=0: x_H moves amidships with decreasing under keel clearance.

[2] The coefficient a_H reaches larger values compared to deep water conditions. However, the values larger than 2 are obtained for apparent hydrodynamic angles in a range where the propeller loading is small. As a consequence the rudder forces will also be small, which reduces the significance of a_H.

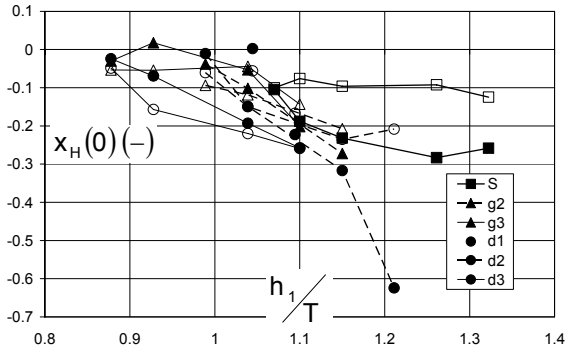

Figure 6.60. Ship D: coefficient x_H for the rudder induced yawing moment. Q1 and Q4 (full symbols), influence of under keel clearance and bottom conditions.

The asymmetric force $a_H F_Y$ due to an asymmetric flow around the hull, increases with decreasing under keel clearance, and even counteracts the rudder force F_Y in the fourth quadrant. The application point of this force also moves amidships, resulting in only a small effect for the moment N_R. x_H moves aft with small positive drift and yaw rate angles, but moves fore when drift or yaw is negative.

6.6 References

[6.1] ABKOWITZ M.A. *Lectures on ship hydrodynamics – Steering and manoeuvrability.* Hydro- of Aerdynamisk Laboratorium, Report No. Hy-5. Lyngby, 1964.

[6.2] BRIX J. (Editor). *Manoeuvring Technical Manual*. Seehafen Verlag GmbH, Hamburg, 1993.

[6.3] DELEFORTRIE G., VANTORRE M., ELOOT K. *Modelling navigation in muddy areas through captive model tests.* Journal of Marine Science and Technology, **10**, 4, 2005, p 188-202.

[6.4] DELEFORTRIE G., VANTORRE M., ELOOT K. *Linear manoeuvring derivatives in muddy navigation areas.* International Journal of Maritime Engineering, Part 4:13, 2005.

[6.5] ELOOT K. *Selection, Experimental Determination and Evaluation of a Mathematical Model for Ship Manoeuvring in Shallow water.* Doctoral thesis, Ghent University, Faculty of Engineering, 2006, 414 pp.

[6.6] ELOOT K., VANTORRE M. *Prediction of low speed manoeuvring based on captive model tests: opportunities and limitations.* 31st Annual General Meeting of IMSF, Antwerp Maritime Academy & Flanders Hydraulics Research, Antwerp, 2004.

[6.7] KUIPER G. *The Wageningen Propeller Series*. MARIN Publication 92-001, 1992.

[6.8] NORRBIN, N.H. *Theory and observations on the use of a mathematical model for ship manoeuvring in deep and confined waters.* Swedish State Shipbuilding Experimental Tank, Publication No. 68, Göteborg, 1971.

[6.9] OGAWA A., KASAI H. *On the mathematical model of manoeuvring motion of ships.* International Shipbuilding Progress, Volume 25, No. 292, 1978, p. 306-319.

[6.10] OLTMANN P., SHARMA S.D. *Simulation of combined engine and rudder maneuvers using an improved model of hull-propeller-rudder interactions.* 15th Symposium on Naval Hydrodynamics, 1984.

[6.11] THE MANOEUVRING COMMITTEE *Final Report and Recommendations to the 23rd ITTC.* Proceedings of the 23rd International Towing Tank Conference, Venice, 2002.

[6.12] TOORMAN E. *Mud rheology: implications for navigability.* Workshop Nautical Bottom, Flanders Hydraulics Research, Antwerp, Belgium, April 29, 2005.

[6.13] VANTORRE M., DELEFORTRIE G., LAFORCE E., DE VLIEGER H., CLAEYS S. *Ship manoeuvring at very small and negative under keel clearance*. 6th IFAC Conference on Manoeuvring and Control of Marine Craft (MCMC 2003), Girona, 2003.

[6.14] VANTORRE M., ELOOT K. *Hydrodynamic phenomena affecting manoeuvres at low speed in shallow navigation areas.* In: Proceedings of the 11th International Harbour Congress (ed. Smitz H. & Thues G.), pp. 535-546. The Royal Flemish Society of Engineers, Antwerp, 1996.

The computer programmer is a creator of universes for which he alone is responsible. Universes of virtually unlimited complexity can be created in the form of computer programs.

Joseph Weizenbaum

CHAPTER 7

FAST-TIME SIMULATIONS

7.1 Overview

During fast-time simulations the position of the ship is determined using the mathematical model. All simulations have been carried out with the model from Chapter 6. Simulations with the model from Chapter 10 are planned for the near future. Following fast-time runs were executed using the 6000 TEU container carrier:

- Acceleration tests;
- Turning circles;
- Zigzag tests;
- Crash-stops;
- Tug assistance;
- Course change;
- Course keeping in current;
- Back & fill.

Course change and course keeping simulations are performed using an autopilot. Following input is necessary:

- The course to be followed;
- The speed along the trajectory;
- The interval Δt_δ needed to change the rudder angle, expressed in time cycles (1 cycle being 0.2 s);
- The interval Δt_n at which the propeller rpm can be changed, expressed in time cycles;
- The time to anticipate t_a, in seconds. Depending on the ship's speed the distance to anticipate can be calculated.

At each time interval the autopilot determines the difference between the course to be followed and the course that will be followed, both at $t + t_a$, with several rudder angles or propeller rates. The rudder angle or propeller rate that leads to a minimum for the cost function:

$$\text{COST} = \alpha.dy_{\text{fore}}^2 + \beta.dy_{\text{mid}}^2 + \gamma.dy_{\text{aft}}^2 \qquad (7.1)$$

is chosen. The autopilot will always try to correct the course only using a different rudder angle. Rudder angles are changed in steps of 5 deg. If the rudder angle cannot be changed an increase of propeller rate is considered, as long as the desired speed is not affected. Propeller rate is changed according the position of the telegraph, see Table 7.1.

Table 7.1. Engine orders and propeller rate for the D-ship (6000 TEU container carrier)

Order	rpm
Full astern	-66
Half astern	-54
Slow astern	-42
Dead slow astern	-30

Order	rpm
Stop	0
Dead slow ahead	30
Slow ahead	42
Half ahead	54
Full ahead	66 (harbour), 88 (sea)

7.2 Modelling the engine torque

The engine orders presented in Table 7.1 cannot be executed immediately. In case of a crash stop for instance, the propeller will have to slow down until its minimal rate n_{min}, to allow an engine reversal. The acceleration rate of the propeller is closely related to the engine type of the vessel and is modelled using:

$$2\pi I_{PP} \dot{n} = Q_E - Q_P \tag{7.2}$$

In which:

- I_{PP}: the polar moment of inertia about the propeller shaft;
- $\dot{n}$: acceleration rate of the propeller;
- Q_E: engine torque;
- Q_P: propeller torque.

The propeller torque has been modelled in 6.4.1. The engine torque has been determined using the tendency of maximal engine torque of similar container vessels. The engine torque is then calibrated so that its relationship with the propeller rate is realistic. Engine reversal times have not been taken into account.

The engine torque model changes in accordance with the telegraph position:

- Order ahead:
  - Acceleration of the propeller (e.g. from *slow astern* to *half ahead):*

IF ($n < -n_{min}$) THEN

$$Q_E = \alpha B^- |n| \tag{7.3}$$

IF [($n > -n_{min}$) AND ($n < n_{min}$)] THEN

$$Q_E = \beta\left(A^+ + B^+ |n|\right) \tag{7.4}$$

IF ($n > n_{min}$) THEN

$$Q_E = \gamma\left(A^+ + B^+ |n|\right) \tag{7.5}$$

- Deceleration of the propeller (e.g. from *full ahead* to *slow ahead*)

$$Q_E = -\lambda \left| B^+ n \right| \tag{7.6}$$

- Order stop:
  - With negative propeller rate:

$$Q_E = \lambda \left| B^- n \right| \tag{7.7}$$

  - With positive propeller rate:

$$Q_E = -\lambda \left| B^+ n \right| \tag{7.8}$$

- Order astern:
  - Deceleration of the propeller (e.g. from *full astern* to *slow astern*):

$$Q_E = \lambda \left| B^- n \right| \tag{7.9}$$

  - Acceleration of the propeller (e.g. from *slow ahead* to *half astern):*

IF $(n > n_{min})$ THEN

$$Q_E = \alpha B^+ \left| n \right| \tag{7.10}$$

IF $[(n > -n_{min})$ AND $(n < n_{min})]$ THEN

$$Q_E = \beta \left(A^- + B^- \left| n \right| \right) \tag{7.11}$$

IF $(n < -n_{min})$ THEN

$$Q_E = \gamma \left(A^- + B^- \left| n \right| \right) \tag{7.12}$$

The coefficients A^+, B^+, A^-, B^-, α, β, γ, and λ are determined so that the trend of the engine torque is as realistic as possible.

7.3 Acceleration tests

Acceleration tests are performed at harbour full ahead. The acceleration test stops when acceleration drops below 0.0005 m/s². The speed the vessel finally reaches reduces with smaller under keel clearance as represented in Figure 7.1. A significant effect of the composition of the mud layer can be noticed when the keel touches the mud. The higher the mud density the lower the speed will be. Figure 7.2 shows that with smaller under keel clearance the final speed is already reached after navigating $0.5L_{PP}$ or less.

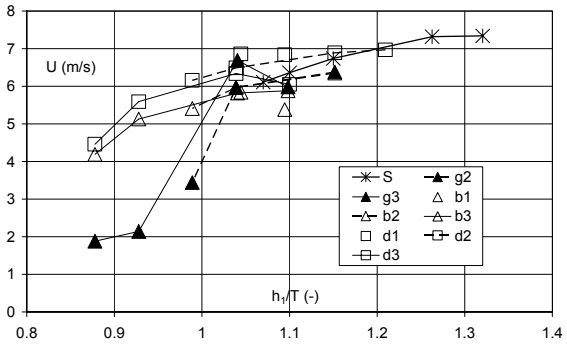

Figure 7.1. Acceleration test – model D – reached speed at harbour full ahead. Influence of bottom characteristics and under keel clearance.

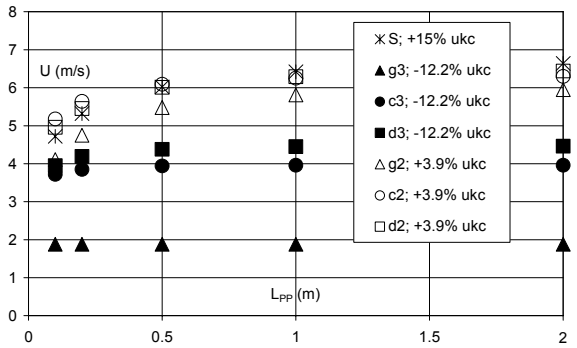

Figure 7.2. Acceleration test – model D – reached speed at harbour full ahead as a function of the covered distance. Influence of bottom characteristics and under keel clearance.

The speed reached with a departure at half astern is represented in Figure 7.3. At positive under keel clearance the final speed is more or less constant, although a local maximum can be noted at extremely small under keel clearance above a high density mud layer. Once the ship penetrates into the mud, the same evolution can be observed as when navigating ahead. In all cases the final speed at full astern is reached when navigating $0.5L_{PP}$ or less astern, as can be seen in Figure 7.4.[1]

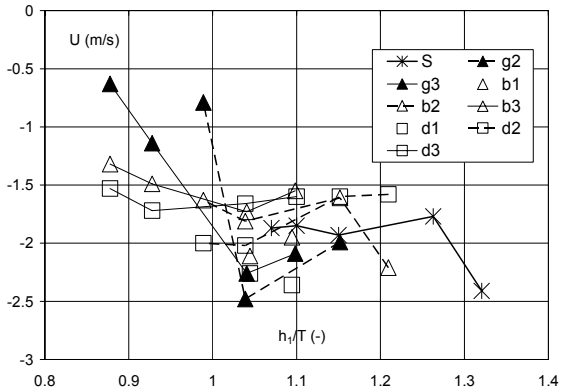

Figure 7.3. Acceleration test – model D – reached speed at half astern. Influence of bottom characteristics and under keel clearance.

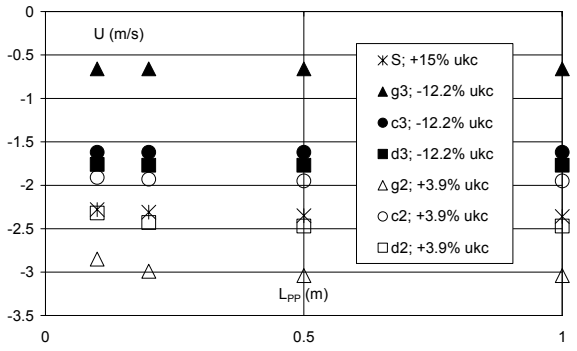

Figure 7.4. Acceleration test – model D – reached speed at harbour full astern as a function of the covered distance. Influence of bottom characteristics and under keel clearance.

7.4 Turning circles

As can be observed on Figures 7.5 and 7.6, the turning ability of the vessel, which is already small at 30% under keel clearance above a solid bottom, compared to deep water conditions, will further decrease when navigating above a mud layer. The tactical diameter appears to reach a maximum at extremely small positive under keel clearance. In those conditions the wake

[1] In most cases the speed the vessel reaches at half astern is already beyond the scope of the values of the experimental program. The largest speed astern of the experimental program was -1.03 m/s on full scale. The figures are merely illustrative for the effect of the mud layer when the vessel is navigating at a reversed propeller rate.

factor also reaches a maximum. This less effective propulsion is probably due to the rising of the mud water interface near the propeller, which disturbs the propeller flow. Once the ship penetrates the mud layer the tactical diameter decreases, and, in high density mud layers, becomes even smaller than above a solid bottom. Comparable effects have been observed at MARIN, see 3.2.1.4.

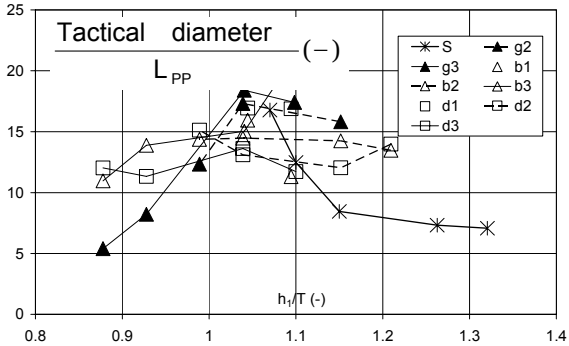

Figure 7.5. Turning circle at harbour full ahead – model D – tactical diameter. Influence of bottom characteristics and under keel clearance. δ_R = 35 deg port.

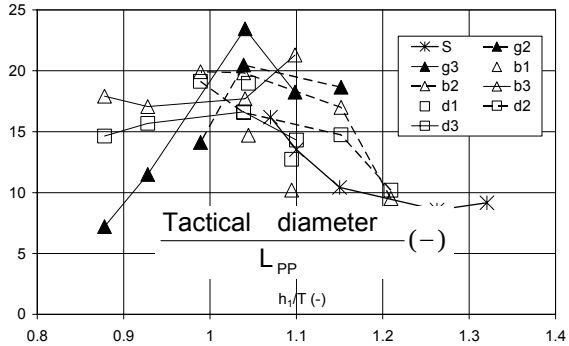

Figure 7.6. Turning circle at harbour full ahead – model D – tactical diameter. Influence of bottom characteristics and under keel clearance. δ_R = 35 deg starboard.

Another point of interest is the difference between turning to port and turning to starboard, the latter resulting in larger diameters. A possible explanation therefore can be found in the asymmetry caused by the single right handed propeller, which is remarkably larger in muddy navigation areas, see 6.4.4.3.

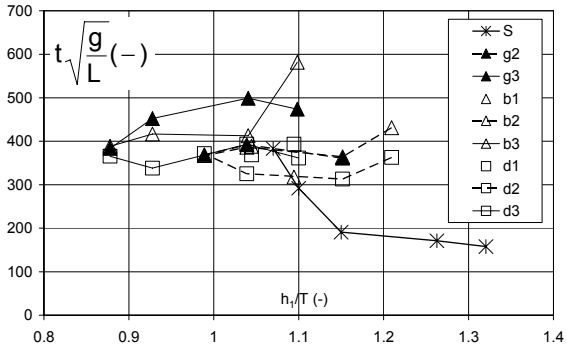

Figure 7.7. Turning circle at harbour full ahead – model D – time to turn 270 deg. Influence of bottom characteristics and under keel clearance. δ_R = 35 deg port.

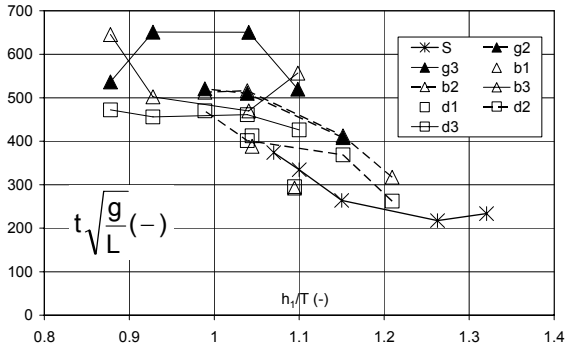

Figure 7.8. Turning circle at harbour full ahead – model D – time to turn 270 deg. Influence of bottom characteristics and under keel clearance. δ_R = 35 deg starboard.

The same observations can be made for the advance, the transfer and the final diameter of the turning circle. The turning time is shown in Figures 7.7 and 7.8. The time to turn 270 deg increases with decreasing under keel clearance, although stagnation can be noted once the keel penetrates the mud layer. The turning circle in high density mud layers is of similar dimension as above a solid bottom, but takes twice the time to carry out.

The ship carries out the turning circle with a drift angle which has the opposite sign to the rudder angle, implying that the ship's bow is located within the

turning circle. In muddy navigation areas this is still the case, but the drift angle is smaller, Figure 7.9, and even takes the opposite sign if e.g. the ship, in contact with a high density mud layer, turns to starboard at sea full ahead. The resulting drift angle is however very small. The same effect was already noticed analyzing the linear manoeuvring derivatives, see Figure 6.13.

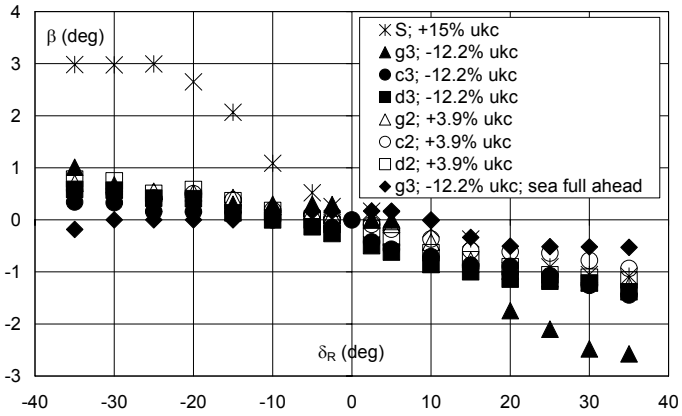

Figure 7.9. Drift angle in turning circle at harbour full ahead – model D. Influence of bottom characteristics and under keel clearance.

7.5 Zigzag tests

10/10 and 20/20 zigzag tests have been carried out. The observations for both types are the same. The covered distance and the period of the zigzag manoeuvre are similar to the parameters of the turning circle and will not need further discussion. Typical for zigzag tests however is the overshoot which occurs at every change of heading. The parameters of the first overshoot are represented on Figures 7.10-7.12.

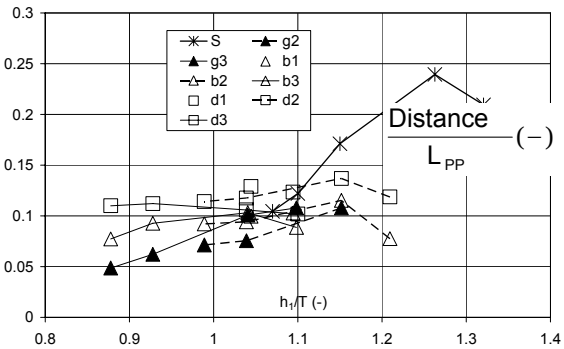

Figure 7.10. 20/20 zigzag test at harbour full ahead – model D – distance covered between first change of heading and maximum heading. Influence of bottom characteristics and under keel clearance.

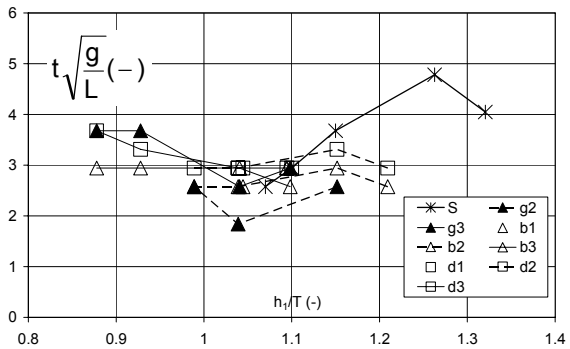

Figure 7.11. 20/20 zigzag test at harbour full ahead – model D – time between first change of heading and maximum heading. Influence of bottom characteristics and under keel clearance.

The overshoot is larger above a solid bottom, due to the higher speed the ship possesses, and decreases significantly in muddy navigation areas. A local minimum of overshoot time and angle can be observed at extremely small positive under keel clearance.

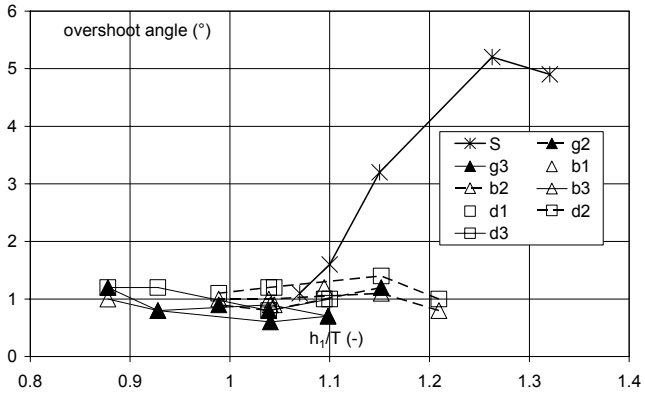

Figure 7.12. 20/20 zigzag test at harbour full ahead – model D – first overshoot angle. Influence of bottom characteristics and under keel clearance.

The relationship between yaw velocity and rudder angle can be expressed, according to Nomoto **[7.4]**:

$$T'\dot{r}' + r' = K'\delta \tag{7.13}$$

T being the time constant and K the amplification:

$$K = \frac{\text{rudder action}}{\text{damping}}$$
$$T = \frac{\text{inertia}}{\text{damping}} \tag{7.14}$$

The overshoot angles are in proportion with the product KT. When the ship navigates at extremely small positive under keel clearance the damping forces appear to be maximal. Once the ship penetrates the mud layer the manoeuvrability will increase. The same can be observed from the results at MARIN, see Figure 3.4. On the other hand the resistance will also increase leading to lower speeds at the same engine order. Eventually manoeuvres will take longer.

7.6 Crash stops

Crash stops were carried out departing from half ahead and half astern. As stopping time and stopping distance depend on the initial speed, the following parameter is introduced:

$$\varsigma = \frac{U_{half}}{gt_{stop}} \tag{7.15}$$

and is represented on Figures 7.13 and 7.14.

A larger nominal value of ς implies a better ability to stop, which is the case at small positive under keel clearance, where damping is more important. When the ship navigates in contact with a high density mud layer, the time to stop is relatively large, but still acceptable.

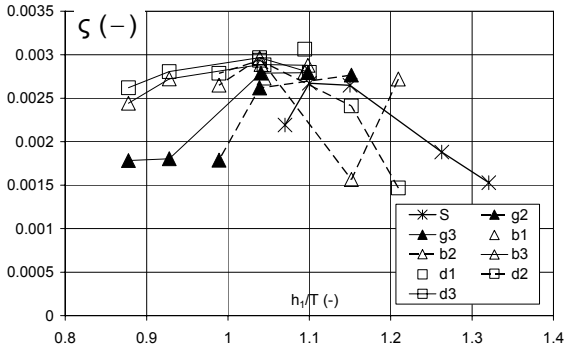

Figure 7.13. Crash stop departing at half ahead – model D – stopping parameter. Influence of bottom characteristics and under keel clearance.

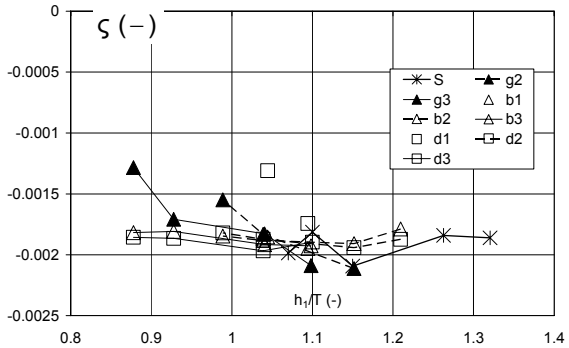

Figure 7.14. Crash stop departing at half astern – model D – stopping parameter. Influence of bottom characteristics and under keel clearance.

During the stopping manoeuvre the ship will be subjected to yaw and sway accelerations due to the oscillations and the asymmetry induced by the propeller action. The followed trajectory will therefore not be a straight one. The lateral deviation and change of heading is represented on Figures 7.15-7.18.

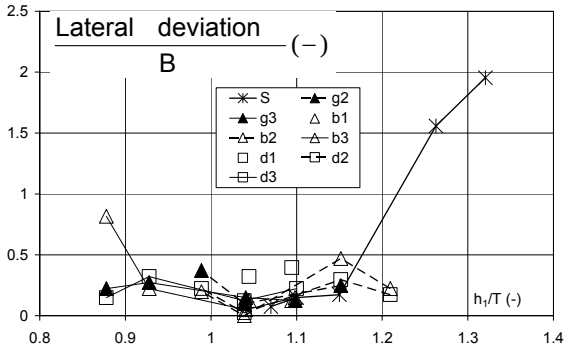

Figure 7.15. Crash stop departing at half ahead – model D – lateral deviation. Influence of bottom characteristics and under keel clearance.

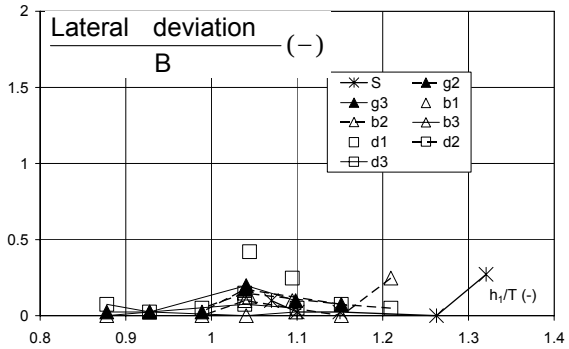

Figure 7.16. Crash stop departing at half astern – model D – lateral deviation. Influence of bottom characteristics and under keel clearance.

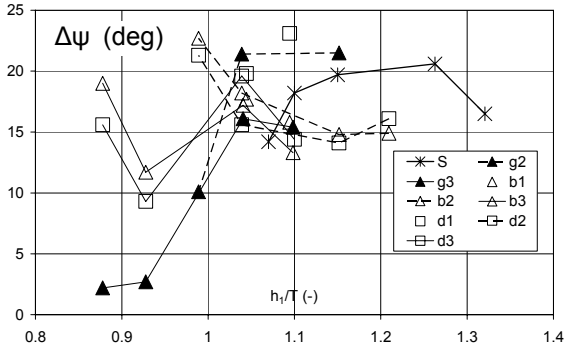

Figure 7.17. Crash stop departing at half ahead – model D – change of heading. Influence of bottom characteristics and under keel clearance.

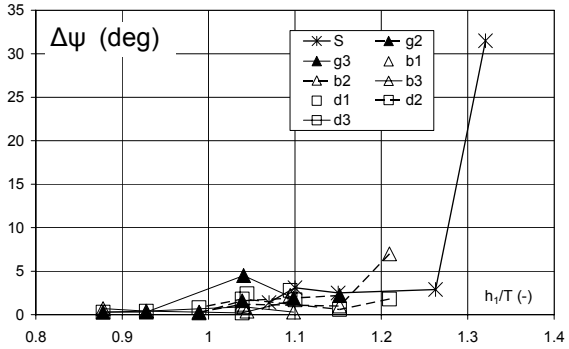

Figure 7.18. Crash stop departing at half astern – model D – change of heading. Influence of bottom characteristics and under keel clearance.

The lateral deviation reaches a minimum at extremely small positive under keel clearance during a crash stop departing from half ahead, while a small maximum is reached when departing half astern. The change of heading is far

more important when departing ahead and reaches a maximum at extremely small positive under keel clearance.

7.7 Tug assistance

Tug assistance is needed to simplify manoeuvres in harbours and access channels. Yaw and sway manoeuvres of model D, without propeller or rudder action, have been assessed with assistance of one or two tugs of 45 ton bollard pull. During the fast-time manoeuvres no corrections on the position of the ship have been taken into account. Figure 7.19 represents the time to yaw to 90 deg starboard with assistance of one tug. Time will increase with decreasing under keel clearance, but a maximum seems to occur for series where the keel is situated close to the water-mud interface. In those conditions the benefit of two tugs will be more pronounced, as can be seen on Figure 7.20. Another point of interest is the superfluous longitudinal movement of the vessel during the yaw manoeuvre. At extremely small positive or negative under keel clearance this movement can be $0.5L_{PP}$ or more, Figure 7.21. This distance is relatively important in harbours and access channels and can represent a possible insecurity. Two tugs will decrease the longitudinal movement to a maximum of $0.2L_{PP}$.

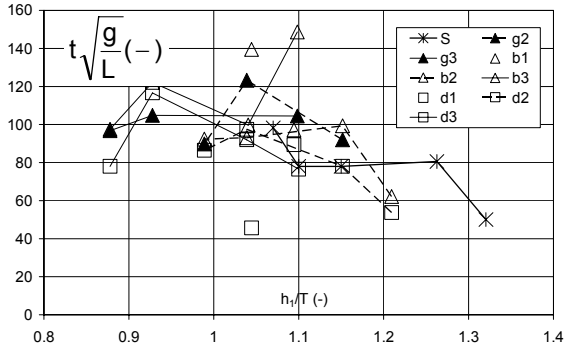

Figure 7.19. Tug assistance – model D – time to yaw 90 deg to starboard with one tug of 45 ton bollard pull at starboard aft. Influence of bottom characteristics and under keel clearance.

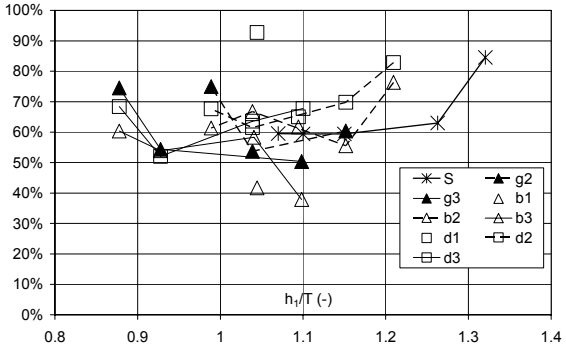

Figure 7.20. Tug assistance – model D – time to yaw 90 deg to starboard with one tug at starboard aft and one at port fore, both of 45 ton bollard pull, in comparison with one tug at starboard aft. Influence of bottom and under keel clearance.

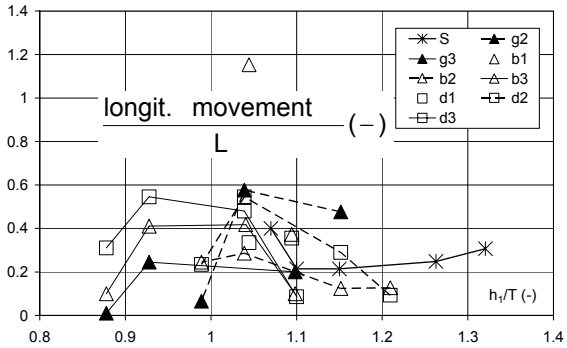

Figure 7.21. Tug assistance – model D – longitudinal movement of the ship during yaw 90 deg to starboard with one tug of 45 ton bollard pull at starboard aft. Influence of bottom characteristics and under keel clearance.

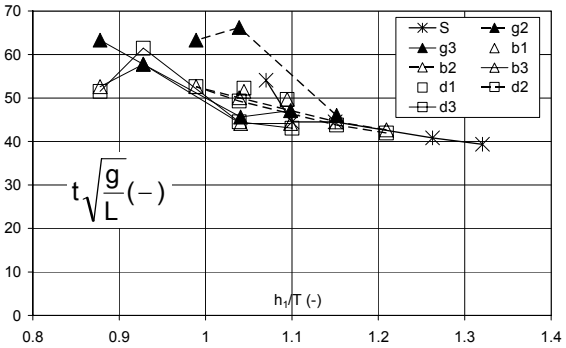

Figure 7.22. Tug assistance – model D – time to sway 1 B to port with one tug of 45 ton bollard pull at starboard amidships. Influence of bottom characteristics and under keel clearance.

The time to execute a sway manoeuvre with assistance of one tug, Figure 7.22, increases with decreasing under keel clearance. Two tugs will perform the same manoeuvre at 70% of the time[2], Figure 7.23. An important aspect during this manoeuvre is the unnecessary change of heading, Figure 7.24, which reaches maximal values when the keel is near the water-mud interface. Two tugs will not reduce this change of heading significantly, so human correction during the manoeuvre will be needed.

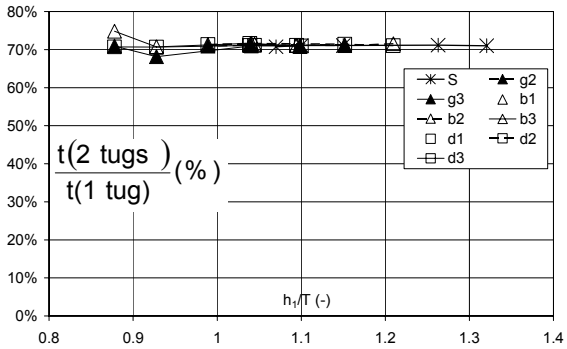

Figure 7.23. Tug assistance – model D – time to sway 1 B to port with one tug at starboard aft and one at starboard fore, both of 45 ton bollard pull, in comparison with one tug at starboard amidships. Influence of bottom characteristics and under keel clearance.

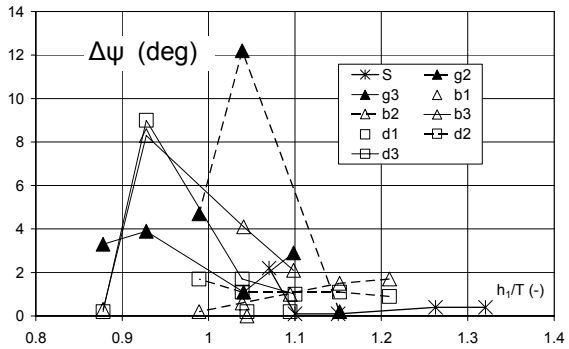

Figure 7.24. Tug assistance – model D – change of heading of the ship during sway 1 B to port with one tug of 45 ton bollard pull at starboard amidships. Influence of bottom characteristics and under keel clearance.

7.8 Course change

The ability to change the course is important when e.g. the ship has to follow the bend of an access channel. The course is calculated with the autopilot (see 7.1) and the ship has no assistance of tugs. Furthermore there is neither wind nor current. The only parameter that has been changed was the condition of the bottom. The characteristics of the bend are represented in Figure 7.25.

Fast-time simulations were carried out using following curves:

- R = 500 m, 1000 m and 1500 m;
- ψ_A = 15, 30, 45, 60, and 75 deg, to port and to starboard.

Analysis of the runs was performed using the maximal lateral deviation of the course. Bends of 15 deg never led to any problems, as the maximal deviation was 0.75B. The difficulty increases however when taking a bend of 30 deg, as shown in Figures 7.26 and 7.27. The largest deviations occur at extremely small positive under keel clearance. As with turning circles, a significant difference between bends to port and bends to starboard can be noticed. Another important parameter is the engine order. At sea full or harbour full ahead, the rudder effectiveness is better, but the speed of the ship and the asymmetry caused by the propeller are larger. It will be easier to follow the course when navigating slow ahead.

[2] In fact the forces are proportional with V². Doubling the forces will increase the speed with $\sqrt{2}$ and decrease time with $\sqrt{2}$ or 70%.

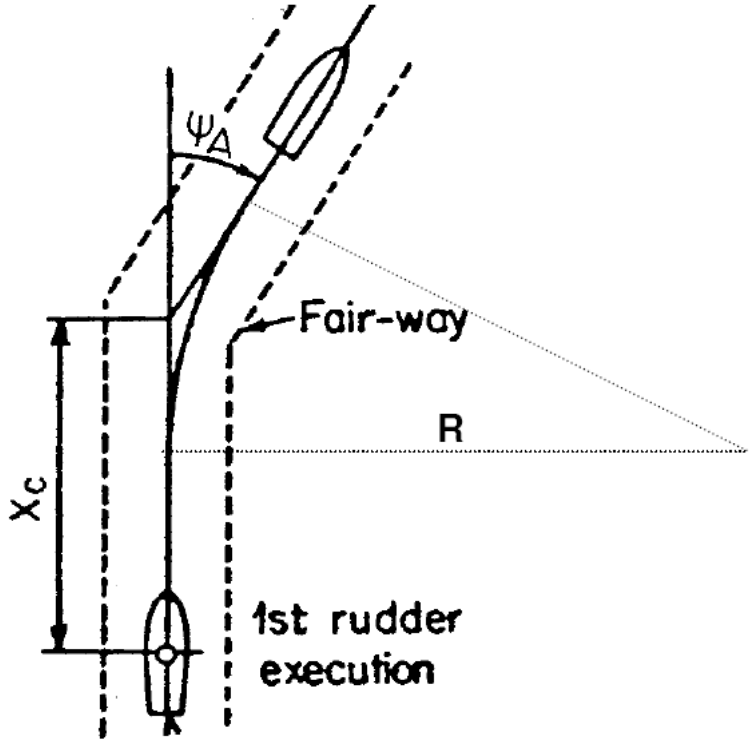

Figure 7.25. Characteristics of a curve.

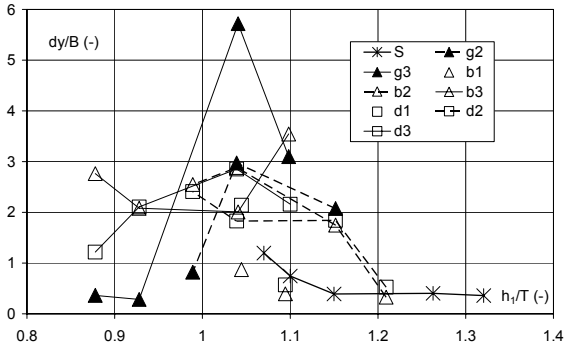

Figure 7.26. Course change of 30 deg to starboard at harbour full ahead, R = 1500 m – model D – maximal lateral deviation. Influence of bottom characteristics and under keel clearance.

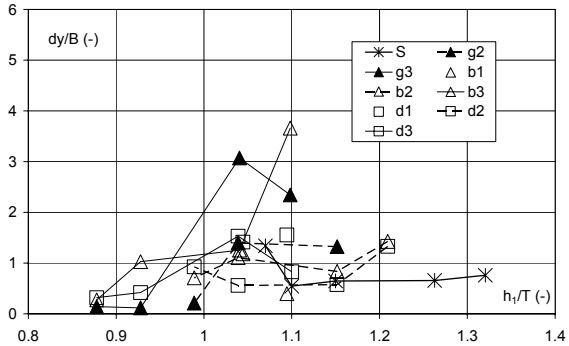

Figure 7.27. Course change of 30 deg to port at harbour full ahead, R = 1500 m – model D – maximal lateral deviation. Influence of bottom characteristics and under keel clearance.

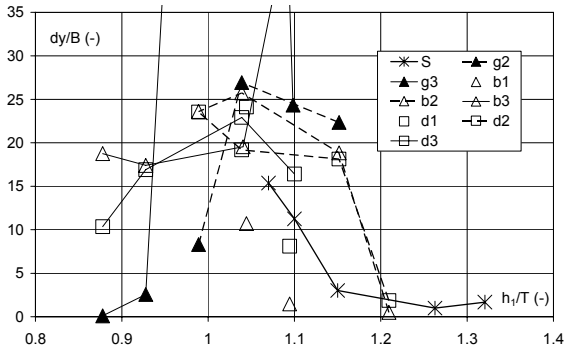

Figure 7.28. Course change of 75 deg to starboard at harbour full ahead, R = 1500 m – model D – maximal lateral deviation. Influence of bottom characteristics and under keel clearance.

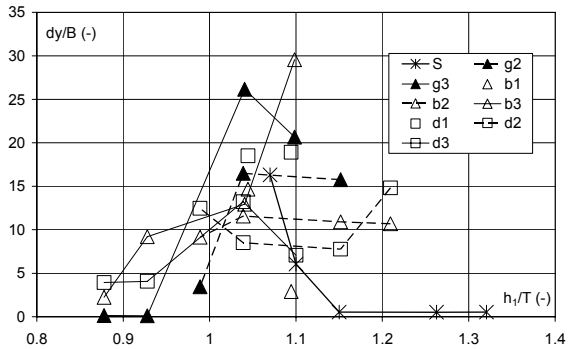

Figure 7.29. Course change of 75 deg to port at harbour full ahead, R = 1500 m – model D – maximal lateral deviation. Influence of bottom characteristics and under keel clearance.

A bend of 75 deg cannot be taken by the ship if navigating at extremely positive under keel clearance, unless serious lateral deviations are acceptable, see Figures 7.28 and 7.29. It is clear that in those cases tug assistance is needed.

7.9 Course keeping in current

In the access channel to the harbour of Zeebrugge the ship is subjected to currents, varying with the tide. The container carrier D calling the harbour at 10 to 15% under keel clearance will be subjected to currents as shown in Figure 7.30.

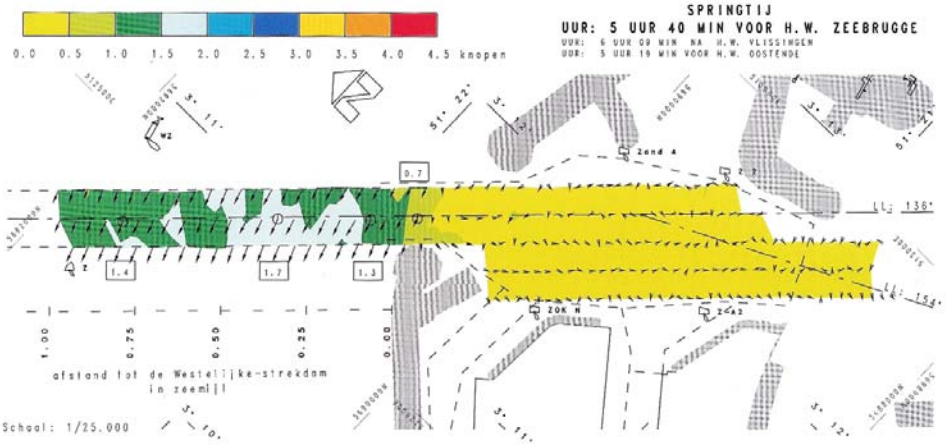

Figure 7.30. Current in the access channel of the harbour of Zeebrugge, 5h40min before spring-tide [7.3].

Fast-time simulations have been carried out in conditions with an under keel clearance of 10 to 15%, referred to the solid bottom. The start position of the ship was 2 km outside the harbour borders. The test stopped when the ship reached the central part of the new harbour, i.e. after 3.2 km.

Figure 7.31 shows the variation of the rudder angle during the test. The rudder angle reaches a maximal value to starboard after 1800 m. At this position the ship is entering the area protected by the breakwaters. The current has no longer effect on the bow of the ship, while amidships and abaft the current is still acting on the ship, causing a yaw moment to port, which is counteracted by a rudder angle to starboard.

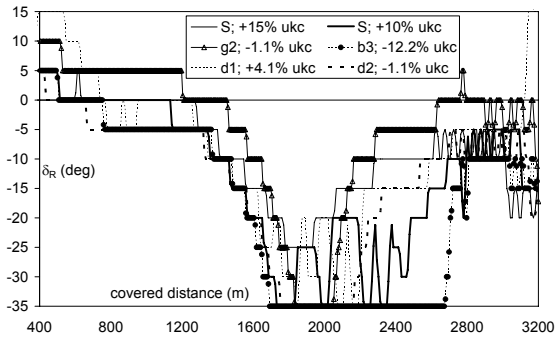

Figure 7.31. Entering the harbour of Zeebrugge – model D – evolution of the rudder angle. Influence of bottom characteristics and under keel clearance.

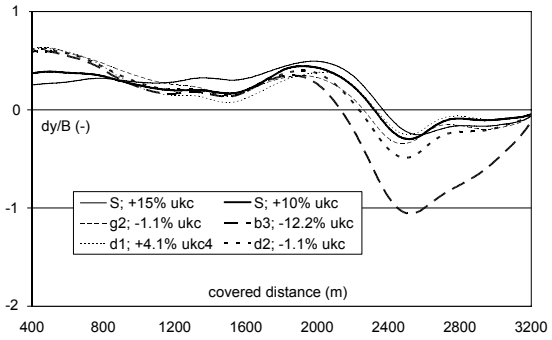

Figure 7.32. Entering the harbour of Zeebrugge – model D – evolution of the lateral deviation. Influence of bottom characteristics and under keel clearance.

When navigating above a solid bottom the counteracting rudder force is still sufficient. A decrease of course stability can however be noted at 10% under keel clearance due to oscillations in the variations of the rudder angle. The same can be concluded when navigating above the mud layer. If the keel penetrates the mud, the rudder angle stays a longer time at its maximal value of 35 deg to starboard, the rudder force is no longer sufficient.

The decrease of rudder effectiveness leads to larger deviations of the course, see Figure 7.32. Nonetheless the deviations are relatively small and the safety of the ship is guaranteed.

On the other hand one should be aware the fast-time simulations have been carried out with an ideal autopilot, knowing the magnitude of the current at each position. The lack of availability of rudder force is therefore more relevant, and a human pilot, will have a hard time manoeuvring the ship through the access channel of the harbour.

7.10 Back & Fill

These rather new manoeuvres can be classified into “Fill First” and “Back First”. An extensive description of the manoeuvre can be found in **[7.2]**. The aim is assessing a fourth quadrant manoeuvring model at slow speeds.

7.10.1 Fill First

The ship leaves from standstill at slow ahead. The following actions are taken:

- Give a maximal rudder deviation (35°) to starboard (or port);
- When the ship’s heading has changed with 45°, change the telegraph position to half astern;
- At zero velocity, change the rudder deviation to 35° port (or starboard);
- The test finishes once the change of heading reaches 90°.

7.10.2 Back First

The ship leaves from standstill at half astern. The following actions are taken:

- Give a maximal rudder deviation (35°) to port (or starboard);
- When the ship’s heading has changed with 45°, change the telegraph position to slow ahead;
- At zero velocity, change the rudder deviation to 35° starboard (or port);
- The test finishes once the change of heading reaches 90°.

7.10.3 Discussion

The interesting output of back and fill tests is:

- The time needed to reach:
  - A change of heading of 45°;
  - Zero velocity;
  - A change of heading of 90°.
- The advance and transfer at zero velocity and at a change of heading of 90°;
- The forces acting on the vessel at a change of heading of 90°.

A lot of parameters have their effect on the course the ship follows during a back & fill manoeuvre. It resulted difficult to compare the results of the manoeuvres above the different bottom conditions. One very important reason was that in some conditions, due to the presence of the mud layer, the ship would yaw in the opposite way of what could be expected. Of course the times to reach the different change of headings are then seriously affected. Similar problems with back & fill manoeuvres have been described in **[7.1]**.

To avoid these problems only the duration of the manoeuvre was analysed by dividing the manoeuvre into three parts:

- The time needed to reach a change of heading of 45°;
- The additional time to reach zero velocity;
- The additional time to reach a change of heading of 90°.

The first time is a measure for the execution time of a turning circle, both ahead (fill first) and astern (back first). The second time gives an idea of the execution time of a crash stop, both from ahead (fill first) and from astern (back first). Finally the third time gives again a measure for the execution time of a turning circle, both astern (fill first) and ahead (back first).

The main conclusion is that execution times can be very large, especially when the ship has a small positive under keel clearance referred to the water mud interface, which confirms the results of the turning circles.

7.11 Conclusions

A series of fast-time simulations has been carried out to assess navigation in muddy areas. It is clear that the presence of a mud layer has its effect on the controllability of the ship. When navigating at small positive under keel clearance above a mud layer the turning circle enlarges and changing course is more difficult combined with a decrease of propeller efficiency. Once the keel penetrates the mud layer the controllability seems to increase again, but a significantly increased resistance leads to large execution times, which from an economic viewpoint can be unacceptable.

Fast-time simulations offer an insight of the manoeuvrability of the ship in muddy navigation areas, but the lack of a decisive human factor makes it unreliable to redefine the nautical bottom.

7.12 References

[7.1] ABRAMOWICZ-GERIGK T. *Practical aspects of application of ship slow speed manoeuvring standards.* Joint 16th International Conference on Hydrodynamics in Ship Design, 3rd International Symposium on Ship Manoeuvring (HYDMAN05), Ostroda, Poland, 2005.

[7.2] HWANG W. Y., JAKOBSEN B.K., BARR R.A., ANKUDINOV V.K., FULLER N.R., VEST L.C., MORRIS M.A., MCGOVERN A.W., LANDSBURG A.C. *An exploratory study to characterize ship maneuvering performance at slow speed.* International Conference on Marine Simulation and Ship Maneuverability (Marsim 2003), Kanazawa, Japan, 2003.

[7.3] *Stroomatlas, haven van Zeebrugge*, Flemish Authorities, LIN, AWZ, WWK, Hydrography , 1998. (In Dutch).

[7.4] THE MANOEUVRING COMMITTEE. *Final Report and Recommendations to the 23rd ITTC.* Proceedings of the 23rd International Towing Tank Conference, Venice, 2002.

Disinterested intellectual curiosity is the life blood of real civilisation

George Macaulay Trevelyan

CHAPTER 8

REAL-TIME SIMULATIONS

8.1 Introduction

The final purpose of the research program, described in Chapter 4, consisted in determining revised operational limits for the navigation in the muddy areas of the harbour of Zeebrugge. Taking account of the central role the pilots play in the shipping traffic, their experience and assessment was required and highly appreciated. Moreover, in the previous chapter it was clear that carrying out fast-time simulations was not sufficient enough to redefine the nautical bottom in the harbour of Zeebrugge due to the lack of a decisive human factor. For this reason a real-time simulation program had been setup. All runs were carried out with the 6000 TEU container carrier, the standard ship for Zeebrugge at that time.

A first simulation program was carried out at Flanders Hydraulics Research during spring 2004. The program had several objectives:

1. *Validation of the mathematical model*, which can be done with simulations above existing bottoms, such as a solid bottom or with a positive under keel clearance above a mud layer.
2. *Defining the limit of controllability*: a selection of conditions with small negative under keel clearance to define the nautical bottom.
3. *Assessing the navigability in contact with mud layers*. Adopting a larger critical limit will lead to contact between the ship's keel and mud layers of a lower density. A selection of those conditions had to be made as well.

During this program 15 Zeebrugge pilots, all qualified for handling the largest class of container carriers, carried out 63 runs during 8 days. This simulation program was followed by a second one at Flanders Hydraulics Research during spring 2006 (10 Zeebrugge pilots carried out 69 runs during 7 days) to fulfil several additional needs:

1. In the first program an identical bottom condition was set throughout the harbour, thus a mud layer was even present in the access channel to the harbour, which had its effect on the initial manoeuvrability
2. During the first program each condition was carried out only once due to the short span of time. For a thorough statistical analysis the critical runs should be repeated by several pilots.
3. A more methodical use of the tug power was needed to classify navigability as a function of tug power.

Summarized, the second program would give a confirmation of the results of the first one. In this chapter both simulation programmes will be discussed, focussing on the first one, which covered the most bottom conditions.

8.2 First simulation program

The results of the first simulation program have already been published in **[8.1]**, **[8.2]**, **[8.3]**, **[8.4]**, **[8.5]** and **[8.8]**.

8.2.1 Setup

The selection of bottom conditions that would meet the objectives of the simulation program are represented in Figure 8.1.

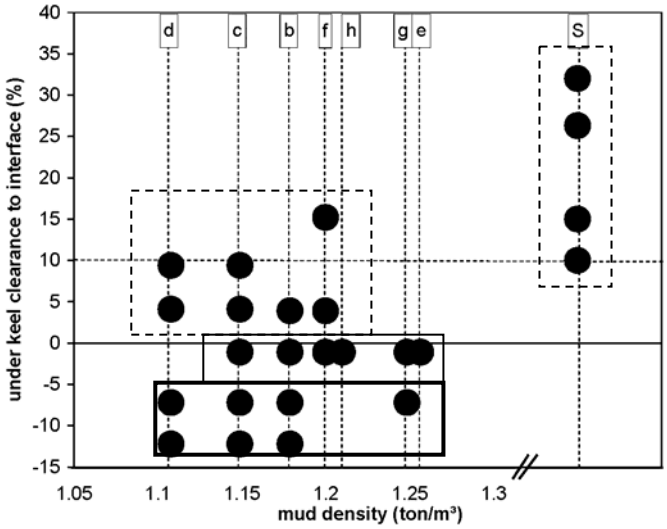

Figure 8.1. Selected conditions for real-time simulation runs with ship D. The conditions to validate the mathematical model are within the dotted square. The other squares give the conditions where the ship's keel is in contact with the mud layer to define the nautical bottom (thin line) or to assess the navigability in contact with mud layers (thick line).

For each condition up to four trajectories, see Figure 8.2, were carried out. The trajectories had to be realistic and had to cover a wide range of hydrodynamic conditions, such as velocities, rudder angles, etc. Moreover they had to be typical for large deep-drafted container vessels calling at Zeebrugge, so that the link with common practice was guaranteed and the pilots could compare the simulated ship behaviour with the real life behaviour. A description of the trajectories can be found in Table 8.1.

Table 8.1. Selected trajectories and division into sub-trajectories.

Trajectory	Sub-trajectory	Tugs	# runs
1. Arrival, berthing on starboard side at quay 205	1.1. Entering breakwaters	no	10
	1.2. Deceleration	yes	
	1.3. Rounding old mole	yes	
	1.4. Berthing	yes	
2. Arrival, berthing on port side at quay 205	2.1. Entering breakwaters	no	23
	2.2. Deceleration	yes	
	2.3. Rounding old mole	yes	
	2.4. Swinging	yes	
	2.5. Berthing	yes	
3. Departure from quay 205, moored on port side	3.1. Unberthing	yes	26
	3.2. Proceeding	yes	
	3.3. Rounding old mole	yes	
	3.4. Acceleration	no	
4. Arrival at Flanders Container Terminal.	4.1. Entering breakwaters	no	4
	4.2. Berthing	yes	

During the real-time simulation runs, pilots could rely on the assistance of two tugs of 45 ton bollard pull, while two more tugs of 45 ton bollard pull were placed on standby, however pilots never had to make use of them. In some conditions the power of the tugs was increased to 60 ton bollard pull. Forces exerted by the tugs depend on the tug characteristics (tug type, bollard pull); the force in the 50 m long tow line is limited as a function of the assisted ship's

motion (forward speed, lateral speed, rate of turn) and of the application point, the direction of the towing line and the tug power requested by the pilot.

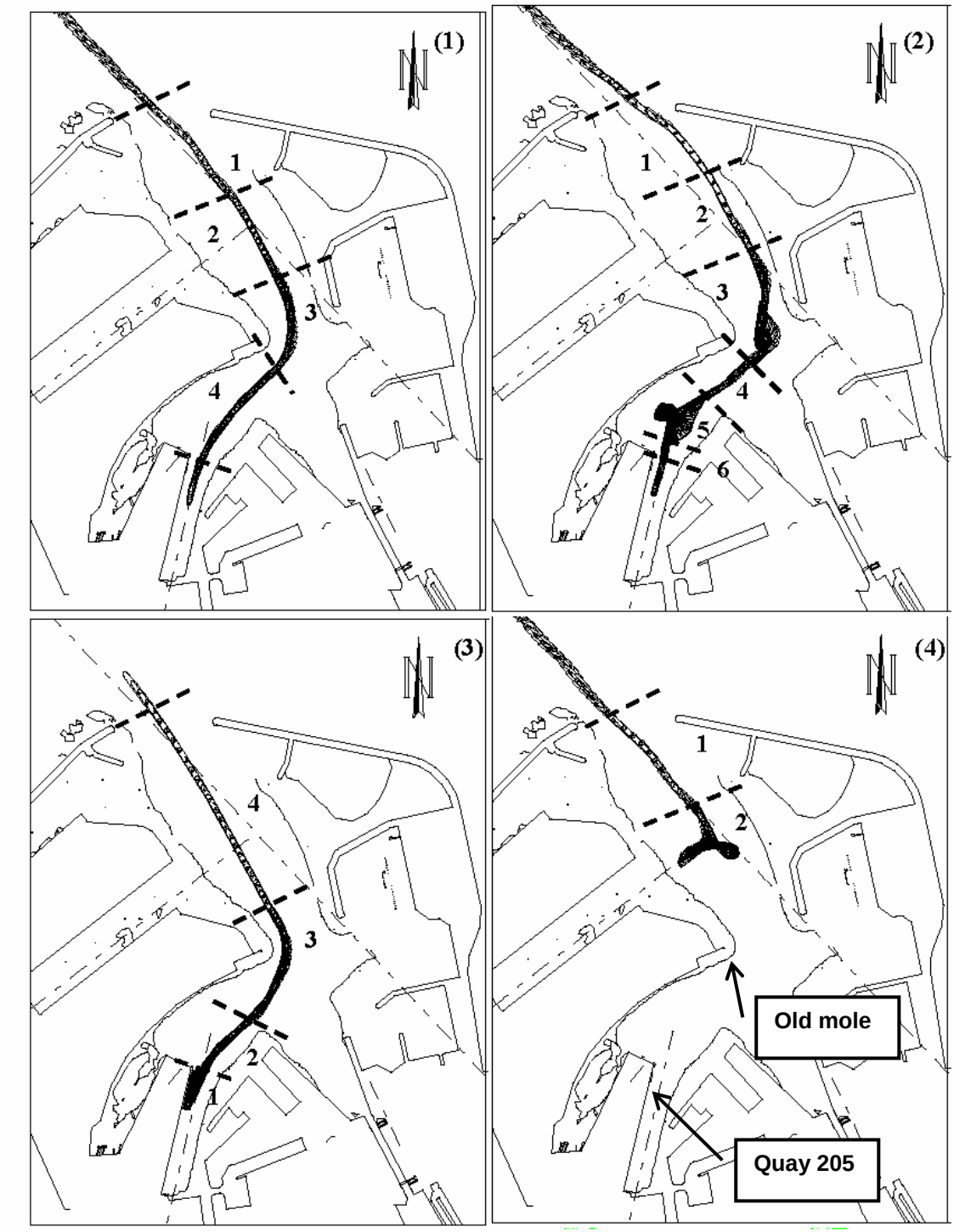

Figure 8.2. Harbour of Zeebrugge. Real time simulations: trajectories and sub-trajectories.

A moderate, frequently occurring wind condition (SW 4BF) was selected, so that the evaluation of the manoeuvres would not be disturbed by extreme wind conditions. In some runs, the ship was subjected to stronger wind. This is the case for the runs where the ship's keel touches a mud layer of 1.20 ton/m³:

- W 7BF was carried out with 3 tugs of 45 ton bollard pull;

- E 6BF was carried out with 2 tugs of 45 ton bollard pull.

In the access channel to the harbour of Zeebrugge, located outside the area protected by the breakwaters, ship control is affected by tidal currents, which at low tide take values of 2 to 2.5 knots. As these currents greatly affect the shipping traffic, realistic current patterns were introduced into the simulation environment, see also 7.9.

During each simulation run one single bottom condition was available. It was assumed that during the whole trajectory the bottom conditions did not vary.

8.2.2 Qualitative evaluation by the pilots

8.2.2.1 Global evaluation

After each run pilots were asked to fill in a questionnaire, enquiring the realism of the simulations and the difficulty of the manoeuvre. Pilots could denote a manoeuvre as acceptable, difficult or unacceptable. As can be seen in Table 8.2 the pilots qualified the simulations as satisfactory. Feedback was also given by additional comments. In order of frequency pilots mentioned their interest to simulate the effect of a bow thruster, the effect of tugs with different power and the effect of varying weather conditions.

Table 8.2. Enquiry among pilots after real-time simulations about the realism of the simulations

Topic	excellent	good	sufficient	insufficient	bad	total
Visual system	4	28	17	0	0	49
Ship behaviour	12	27	8	1	0	48
Tug assistance	19	24	8	1	0	52
Radar	15	34	0	0	0	49
Total	25.2%	57.1%	16.7%	1.0%	0	198

The possibility of using a bow thruster was disabled, as no experimental manoeuvring tests have been carried out with bow thrusters in muddy areas. Runs with different tug capacity and varying wind conditions were therefore added to the simulation program.

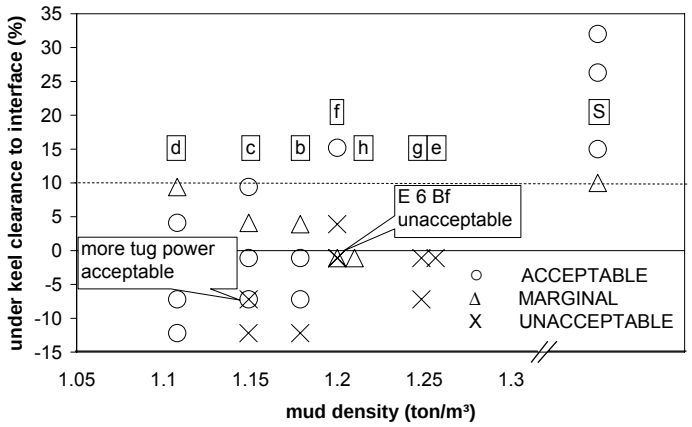

Figure 8.3. Ship D, real time simulations.
Qualitative evaluation of all manoeuvres.

Figure 8.3 gives the pilot's opinions on the difficulty of the manoeuvres:

- Contact with a mud layer having a density of 1.20 ton/m³ or more leads always to dramatic conditions;
- Contact with mud layers of a lower density is problematic once the under keel clearance is -7% or less;
- When the ship navigates above the mud layer with a small under keel clearance the difficulty of the manoeuvre increases, without affecting the feasibility. The same degree of difficulty is also found when navigating with an under keel clearance of 10% of draught above a solid bottom.

In accordance with the definition of the nautical bottom, 1.20 ton/m³ seems to be the critical limit from a ship's manoeuvring behaviour point of view. The observed difficulties at extremely small positive under keel clearances above the mud layer can be ascribed to the disturbances of the undulations of the interface.

An additional problem is the penetrability of the mud layer. An under keel clearance of 7% within a mud layer of 1.15 ton/m³, which corresponds with a keel penetration of 1 m within the mud, can lead to a hazardous situation. Consequently not only the top of the mud layer should be monitored, but also the nautical bottom level and an intermediate level to assess the penetrability.

8.2.2.2 Evaluation per manoeuvre

Figure 8.4 represents the degree of difficulty when entering the harbour. The apparent nautical bottom level remains at 1.20 ton/m³. Entering the harbour in contact with mud layers of a lower density does not seem to cause any difficulties. Some runs are unacceptable:

- At a small under keel clearance above a mud layer of 1.20 ton/m³ the behaviour of the vessel is unstable, as the pilot had to change the rudder deviation continuously;
- The tugs have not enough power to assist the manoeuvre when penetrating high density mud layers, especially the berthing manoeuvre could use assistance of four tugs instead of two.

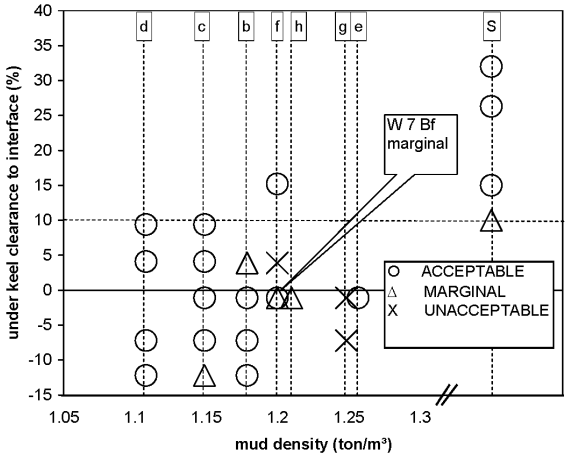

Figure 8.4. Ship D, real time simulations. Qualitative evaluation of the manoeuvres entering the harbour.

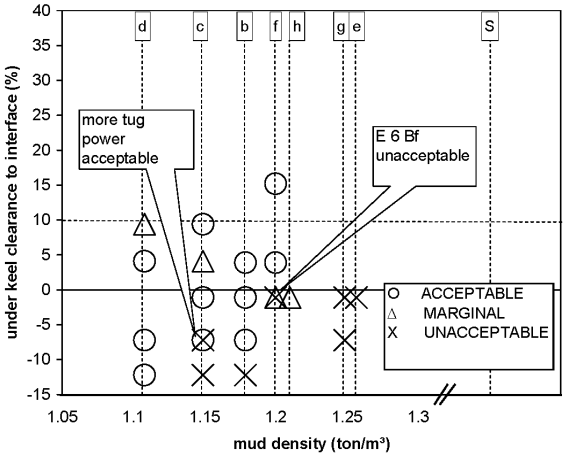

Figure 8.5. Ship D, real time simulations. Qualitative evaluation of the manoeuvres leaving the harbour.

Additional problems occur when analysing the departures, Figure 8.5. The restriction for the penetrability of the mud layer is mainly due to the lack of speed that is reached in those conditions. After all to counteract the tidal currents outside the harbour the ship needs sufficient velocity.

The main reasons to denominate the conditions as marginal, for both entering and leaving the harbour, are:

- The available tug power is certainly needed. It would be risky to carry out the manoeuvre with less tug power;
- The controllability is sometimes different, especially when navigating astern. This occurs mainly at small positive under keel clearances referred to the water mud interface and can be ascribed to the undulations of this interface;
- The ship's speed when leaving the harbour is just sufficient.

Trajectory 4 (Figure 8.2) has only been carried out occasionally. This manoeuvre is strongly affected by the currents outside the breakwaters, which, in combination with an unrealistic mud layer in the access channel, led to a too difficult manoeuvre. The use of a more realistic bottom condition in the access channel during the second simulation programme allowed the execution of more runs with trajectory 4, see 8.3.

8.2.3 Quantitative analysis of the simulation runs

8.2.3.1 Criteria

The evaluation of the pilots gives a good insight in the mud conditions where controllability problems can occur, but is not free of subjectivity. A quantitative analysis can be made based on the following criteria:

- *Speed*: is the speed the departing vessel reaches sufficient to counteract the tidal currents outside the harbour breakwaters? A speed of 10 knots was considered to be safe; leaving the harbour at 8 knots is still possible, but difficult.
- *Course stability*: has the ship sufficient stability when navigating by her own means, i.e. without tug assistance? A suitable criterion appears to be the standard deviation of the yaw rate. An unstable ship will have a high standard deviation; values of 6°/min or more were assessed as unacceptable.
- *Controllability*: with the ship's own means and the provided tug assistance, is the ship still manoeuvrable? This criterion can be evaluated by introducing the so-called control power concept.

The manoeuvres have been divided in significant sub-trajectories (Figure 8.2). In every relevant sub-trajectory the criteria have been checked.

8.2.3.2 Speed criterion

The speed criterion only applies in sub-trajectory 3.4. Figure 8.6 shows the speed of the vessel when reaching the breakwaters while leaving the harbour. To counteract the tidal current safely, pilots pointed out a speed of 10 knots was required. A speed of 8 knots or less was insufficient, as the ship drifted away to the sand banks outside the harbour. A speed between 8 and 10 knots was marginal. The evaluation of the speed criterion is represented in Figure 8.7.

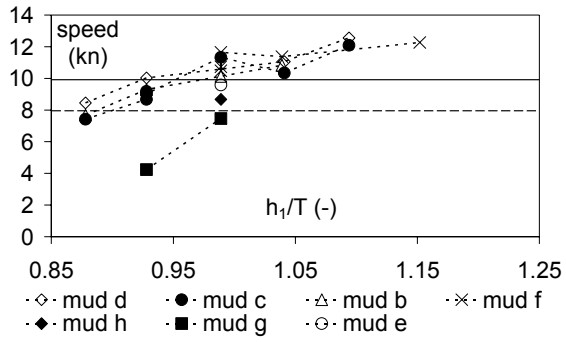

Figure 8.6. Ship D, real time simulations. Ship speed at the breakwaters when leaving the harbour (sub-trajectory 3.4).

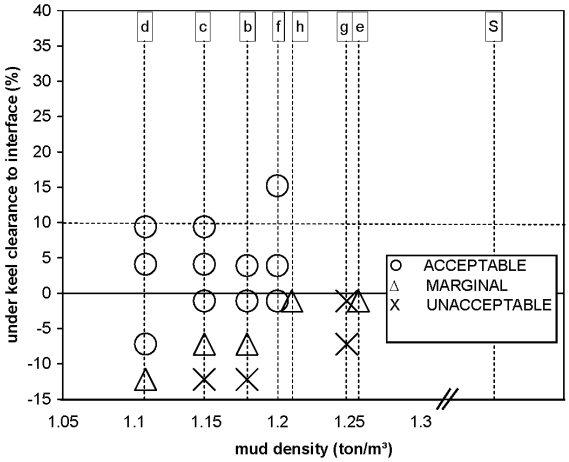

Figure 8.7. Ship D, real time simulations. Quantitative evaluation of the speed criterion.

The speed criterion is decisive when navigating in contact with high density mud layers, as the ship resistance significantly increases. It should be noted that the speed criterion is only valid in harbours subjected to tidal currents outside the breakwaters as Zeebrugge. If no damage or uncontrollability are caused, speed reduction as such is no reason for rejecting a specific situation. On the other hand, speed reduction may lead to unacceptable transfer times and cause economic damage – not only for the ship, but also for the harbour when the fairway is blocked for a longer time – and may therefore be considered as a decisive factor.

8.2.3.3 Course stability criterion

The course stability criterion is only applicable in sub-trajectory 3.4 when the ship is navigating without tug assistance. A representative indicator for the course stability of the ship is the standard deviation of the yaw velocity: a large value means the ship has difficulty to maintain a constant heading. The standard deviation of the yaw rate when leaving the harbour is represented in Figure 8.8.

Runs with a standard deviation exceeding 6 deg/min were explicitly rejected by the pilots due to lack of course stability. The use of the standard deviation of the yaw is therefore a relevant decision factor. Runs with standard deviation between 5 and 6 deg/min were labelled as marginally acceptable, which is the case e.g. under strong west wind conditions. The evaluation of the conditions based on the course stability criterion is represented in Figure 8.9.

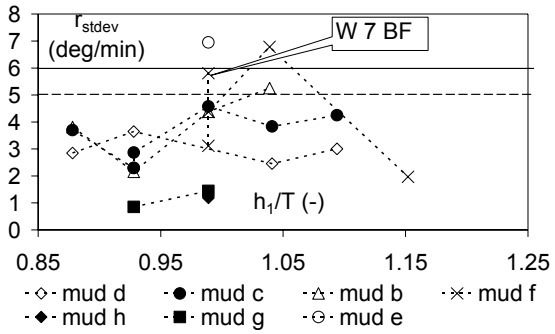

Figure 8.8. Ship D, real time simulations. Standard deviation of the yaw velocity of the ship's when leaving the harbour (sub-trajectory 3.4).

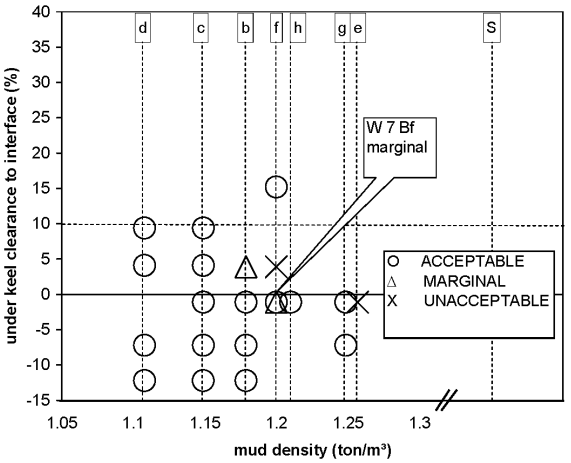

Figure 8.9. Ship D, real time simulations. Quantitative evaluation of the course stability criterion.

8.2.3.4 Controllability criterion

Introduction

To control the ship the pilot can rely on the propeller and the rudder, and also on the two (or more) tugs available. The rudder angle as such cannot be considered as a relevant parameter for analysing the ship's own controls, as a rudder command is only effective in combination with sufficient propeller rate. Moreover it is advisable to take the total control power into consideration for estimating the effort to carry out a manoeuvre, as some pilots prefer to rely on tug assistance, while others make more use of the ship's own controls. A steering force is therefore introduced, expressed as the sum of the absolute lateral force on the ship induced by the rudder force and the lateral force produced by the tugs:

$$Y_{RS} = \sum_i |S_i| + |Y_R| \tag{8.1}$$

Similarly, a steering moment can be defined:

$$N_{RS} = \sum_i |S_i x_i| + |N_R| \tag{8.2}$$

S_i is the force exerted by tug number i and applies at a longitudinal position x_i on the ship. Y_R and N_R are given by (6.52) and (6.53).

Another important aspect is the time needed to carry out a manoeuvre. If only the force were analysed, an excessive force yielding a fast manoeuvre would result in a rejection, while the pilot was only in a hurry to finish his work. Therefore steering forces and moments should be integrated with respect to time, yielding an impulse of steering force and steering moment:

$$I_Y = I_{YT} + I_{YR} = \sum_i \int S_i dt + \int |Y_R| dt = \int Y_{RS} dt \tag{8.3}$$

$$I_N = I_{NT} + I_{NR} = \sum_i \int S_i x_i dt + \int |N_R| dt = \int N_{RS} dt \tag{8.4}$$

Formulae (8.3) and (8.4) take into account which force has to be applied for how long in order to carry out the manoeuvre. The smaller the value of the impulse functions the higher the controllability of the ship is. Expression (8.5) also allows assessing the controllability of the ship with different tug assistance (x ton bollard pull) than the provided one (45 ton bollard pull):

$$I_{Y,max}^{(x\ ton)} = I_{Y,max}^{(45\ ton)} \left(\frac{I_{YR}}{I_Y} + \frac{x}{45} \frac{I_{YT}}{I_Y} \right) \tag{8.5}$$

This expression is correct if the own control force is equal in all simulated conditions, which is normally not the case. However (8.5) can be used because the contribution of own controls to the impulse functions I_Y and I_N does not vary significantly for the different simulation runs. General conclusions will thus only be marginally affected.

Expressions (8.3) and (8.4) offer the advantage that both the force and the span of time required to carry out the manoeuvre are taken into account. The value of the integral of the steering force or steering moment is in proportion with the difficulty of the manoeuvre and can therefore be considered as an objective decision parameter. On the other hand some dynamic effects are not taken into account by (8.3) and (8.4). A large force during a short time will have more effect than a small one during a longer time. As the execution time of the manoeuvres is within the same ranges for the different bottom conditions, the dynamic effect will not be significant.

For the different sub-trajectories carried out with tug assistance, the control power above different bottom conditions will be compared. Sub-trajectories in which the lateral movement is dominating, as (un)berthing, are assessed using the impulse I_Y. On the other hand, if the ship carries out a yaw manoeuvre, as with rounding the old mole, the control power is examined with the impulse I_N. The emphasis is put on the (un)berthing manoeuvre and rounding the old mole as those proved to be the most critical manoeuvres.

Analysis of departure

Sub-trajectory 3.1: unberthing

Unberthing is a typical tug assisted manoeuvre. The impulse of steering force during the departure is shown in Figure 8.10. Some simulation runs, in which pilots mentioned the lack of tug power, have been marked. Based on the comment that for one series two tugs of 45 ton bollard pull are just sufficient a limit of impulse can be defined. With expression (8.5) this limit can be extrapolated to limits for different tug assistance. Note that two tugs of 60 ton bollard pull will be sufficient in all tested conditions, unless there is strong east wind. The influence of the available tug power is very important. Two tugs of 30 ton bollard pull are insufficient once the under keel clearance referred to the water mud interface is 5% or lower.

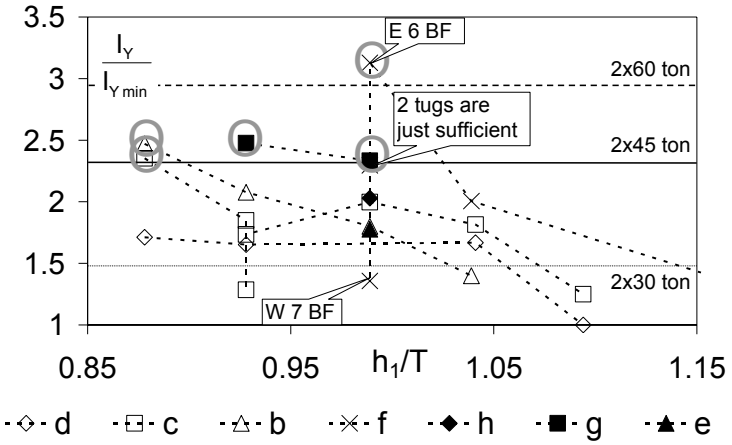

Figure 8.10. Ship D, real time simulations. Impulse of steering force when leaving quay 205 (sub-trajectory 3.1)

Encircled symbols denote unacceptable conditions.

Of particular interest is the effect of the wind condition. It can be noted that the wind has a far more important influence on the manoeuvre than the bottom condition. Due to the location of quay 205, see Figure 8.2, a SW wind will facilitate the departure, while an arrival will be more difficult. Due to lack of time the arrival manoeuvres were not fully executed, but the limits at arrival will be somewhat more severe as the SW wind counteracts the manoeuvre. Also the role of the E and W wind will be inversed.

Sub-trajectory 3.3: rounding old mole

During this turning manoeuvre the integral of the steering moment will be more important, see Figure 8.11. Manoeuvres that pilots found difficult are marked and are characterised by a high value for the integral of the steering moment. Some differences between the pilots' evaluation and the steering impulse can be observed:

- *The run with 10% under keel clearance above mud c.* The available tug assistance was assessed as insufficient, but the manoeuvre was completed in a record time, which resulted into a smaller impulse. The manoeuvre can therefore be categorised as acceptable.
- *The run with -1% under keel clearance in mud c.* A large integral of steering is needed to complete the manoeuvre in this condition, although the pilots found the tug capacity sufficient.

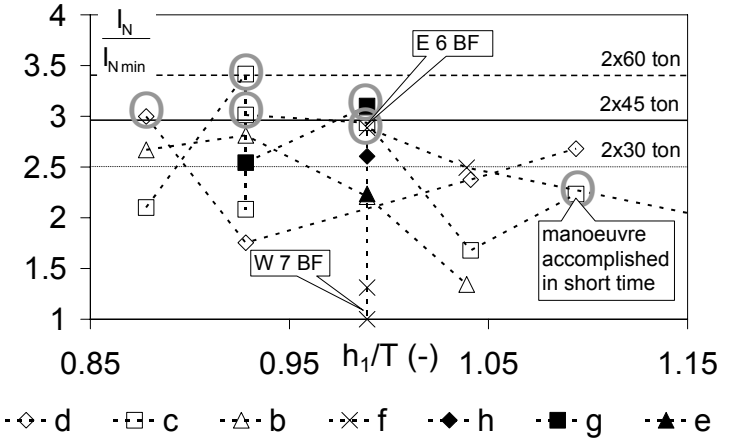

Figure 8.11. Harbour of Zeebrugge: impulse of steering moment of the ship's when turning around the old port entrance (trajectory 3, sub-trajectory 3) during real-time simulation with ship D.

Encircled symbols denote unacceptable conditions.

Limits for different tug power can be determined. The influence of tug capacity is smaller than when leaving the quay, as the own controls of the ship have now a larger share in the total control power. Two tugs of 60 ton bollard pull are sufficient to carry out the manoeuvre above any bottom condition, while it is not advisable to touch the mud layer when only two tugs of 30 ton bollard pull are available.

General analysis of departure

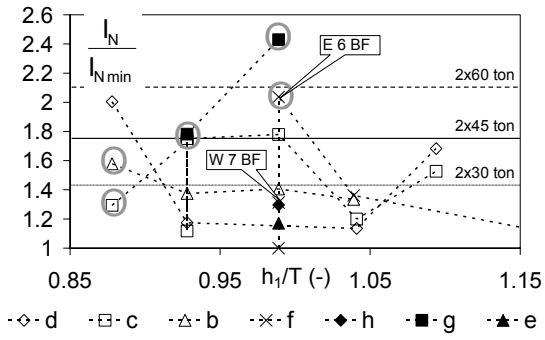

Figure 8.12. Ship D, real time simulations. Impulse of steering moment of the ship's during departure (trajectory 3, all sub-trajectories). Encircled symbols denote unacceptable conditions.

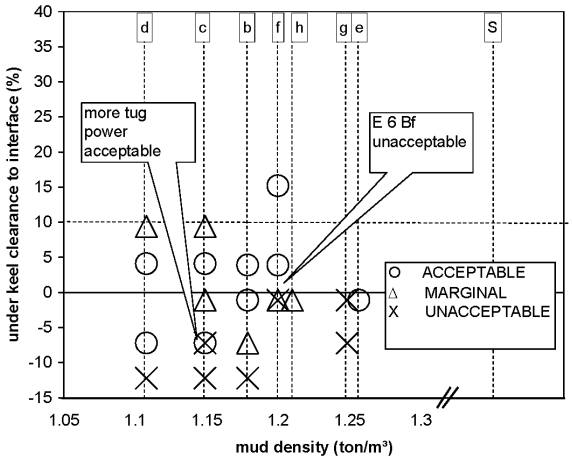

Figure 8.13. Ship D, real time simulations. Quantitative evaluation of the control power criterion when leaving the harbour.

Departure at quay 205 and rounding the old mole were considered the most critical sub-trajectories. A general assessment of the control power during departure can be carried out as well. Figure 8.12 represents the integral of the steering moment from the berth till tugs were disconnected.

Two series were carried out with a rather high value of the steering moment integral, but pilots did not mention tug insufficiency. The evaluation based on the control power above the different bottom conditions when leaving the harbour is resumed in Figure 8.13.

Analysis of arrival

Sub-trajectories 1.4 and 2.5: berthing at quay 205

Due to lack of time, berthing manoeuvres at arrival (trajectory 1 or 2) have not been fully executed. On the other hand as wind plays an important role, and as the dominant SW wind hinders the berthing more than the departure, the limit of steering impulse will be more severe. If two tugs were just sufficient for departure, the available power will be too small for a normal berthing manoeuvre.

Sub-trajectories 1.3 and 2.3: Rounding old mole

The limit of the integral of the steering moment, Figure 8.14, with assistance of two tugs of 45 ton bollard pull is basically the same as with departure. However,

rounding the old mole will be different during arrival compared with departure, as in the first case the ship, which needed sufficient speed to counteract the tidal current when entering the harbour, has to slow down. The speed at the beginning of the manoeuvre will therefore be higher, and the ship will be still relying more on its own controls. The limits of two tugs of 60 or 30 ton bollard pull will be consequently different, see Figures 8.12 and 8.15, where both I_{Nmin} are of the same magnitude.

Pilots mentioned insufficient tug assistance for five runs, which are encircled on the graph. The ship had nevertheless sufficient control power in two of the mentioned runs.

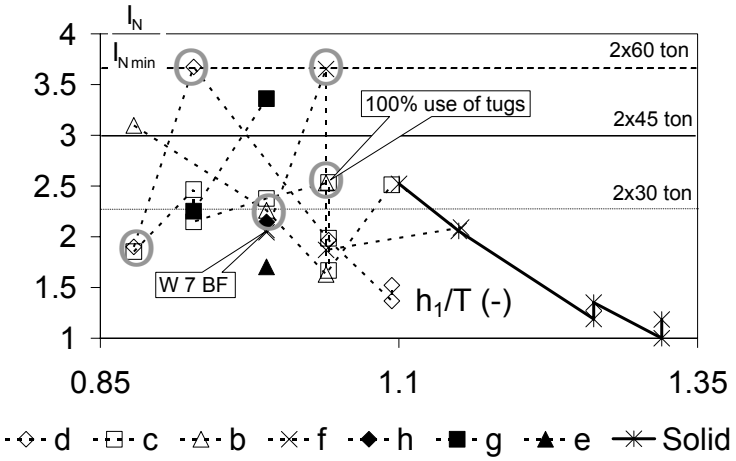

Figure 8.14. Harbour of Zeebrugge: impulse of steering moment of the ship's when turning around the old port entrance (trajectories 1 and 2, sub-trajectory 3) during real-time simulation with ship D.

Encircled symbols denote unacceptable conditions.

The manoeuvre can always be carried out with two tugs of 60 ton bollard pull; although in some cases the limit is reached. With two tugs of 30 ton bollard pull the manoeuvre is already risky at 10% under keel clearance above a solid bottom. Moreover touching the mud layer always results in dangerous situations, so that the nautical bottom with this tug assistance should at least be located near the water-mud interface.

Of special interest is the run at an under keel clearance of -7% in mud d. The impulse of the steering moment is significantly larger compared to the manoeuvre when leaving the harbour. This phenomenon can be explained due to the high speed the ship possessed when entering the harbour. The pilot switched the propeller to astern in order to decrease the speed, but due to the asymmetry induced by the propeller the steering moment was counteracted and more steering power was needed.

Sub-trajectory 2.5: swinging manoeuvre

The pilots did not mention the swinging manoeuvre as critical. As can be seen on Figure 8.15 a yaw manoeuvre of 120 deg can be carried out in an average time of 12 minutes. The availability of two tugs of 60 ton bollard pull resulted even in a calmer and longer execution of the manoeuvre. Using two tugs of 30 ton bollard pull is probably harder, because more time will be needed, but it is difficult to define a critical limit, which will principally depend of external factors, such as shipping traffic or weather conditions.

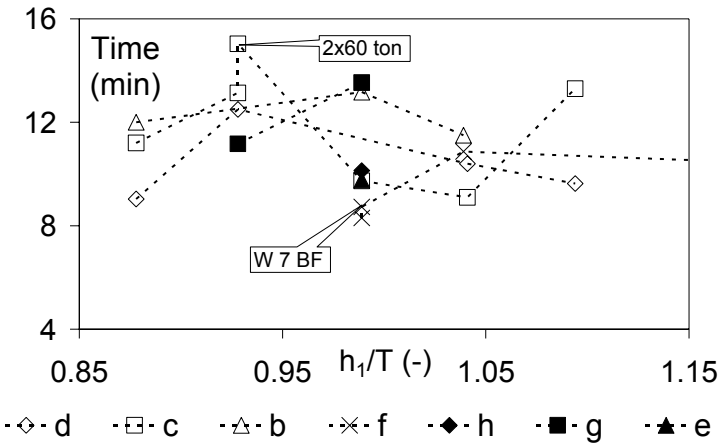

Figure 8.15. Ship D, real time simulations. Time to yaw 120 deg (sub-trajectory 2.5).

General analysis of arrival

Rounding the old mole is the most critical manoeuvre. Berthing at quay 205 is quite similar to the departure manoeuvre, but SW wind conditions are less favourable when berthing. Based on the analysis of the control power the evaluation as shown in Figure 8.16 can be made.

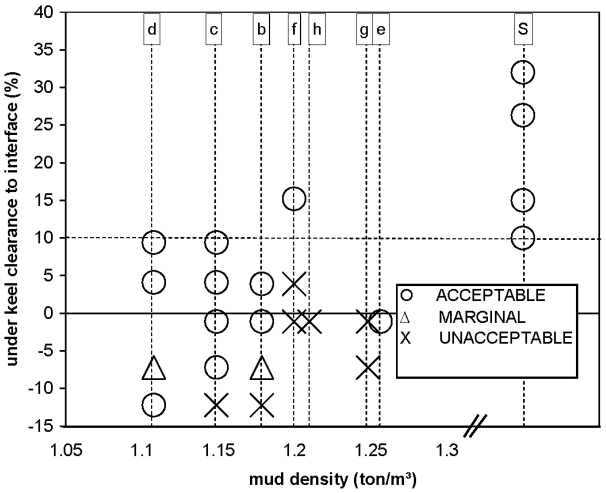

Figure 8.16. Ship D, real time simulations. Quantitative evaluation of the control power criterion when arriving at the harbour.

8.2.3.5 General analysis based on all criteria

Taking all criteria into consideration, a classification of the runs above different bottom conditions has been made when the ship is assisted by two tugs of 45 ton bollard pull, see Figure 8.17a. The manoeuvring behaviour is unacceptable when the keel touches a mud layer of a density of 1.20 ton/m³ or more. According to the definition of the nautical bottom, the nautical bottom can be defined at 1.20 ton/m³. Use of tugs of 60 ton bollard pull will not change the definition of the nautical bottom, see Figure 8.17b.

On the other hand, in comparison with the pilots' evaluation the restriction of keel penetration into the mud layer is more severe:

- With two tugs of 45 ton bollard pull the penetration depth is limited to -5% for mud layers of 1.15 ton/m³ and to -7% for mud layers of a lower density;

- This constraint is less severe when two tugs of 60 ton bollard pull are provided. In this case navigating at - 7% in mud of 1.15 ton/m³ is still acceptable - and in fact this restriction can be totally ascribed to the speed criterion - and in less dense mud layers an under keel clearance of even -12% is still possible.

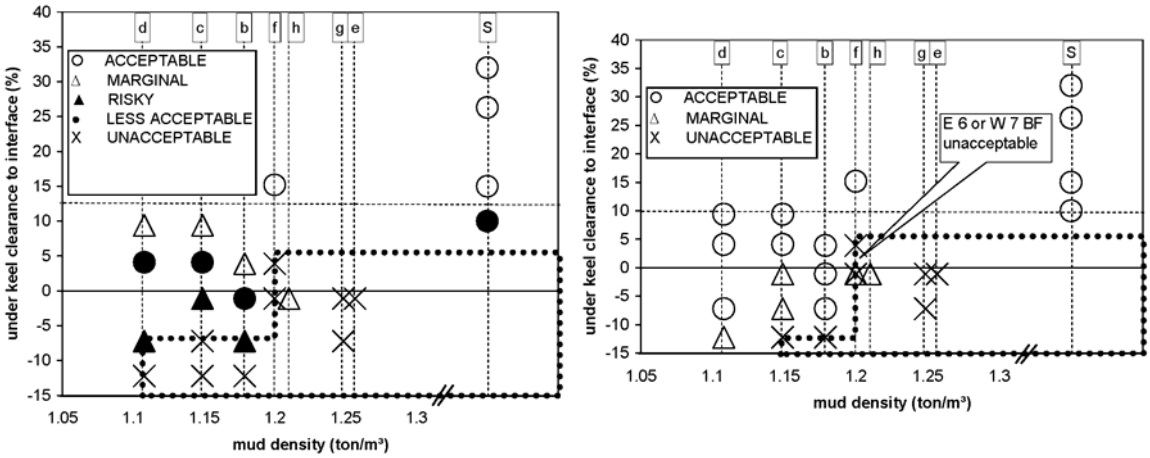

a. assistance by two tugs of 45 ton bollard pull b. assistance by two tugs of 60 ton bollard pull

Figure 8.17. Ship D, real time simulations. Quantitative evaluation of all criteria for the harbour of Zeebrugge, dotted area = "unacceptable".

As pointed out in paragraph 8.2.2.2 the speed criterion is mainly dependent of the specific situation of Zeebrugge. A classification is therefore also made excluding this speed criterion, see Figure 8.18. Excluding the speed criterion has no effect on the definition of the nautical bottom, but increases the navigability through lower density mud layers when assisted by two tugs of 60 ton bollard pull. With assistance of two tugs of 45 ton bollard pull, the classification is only affected marginally, as the control power is the decisive factor.

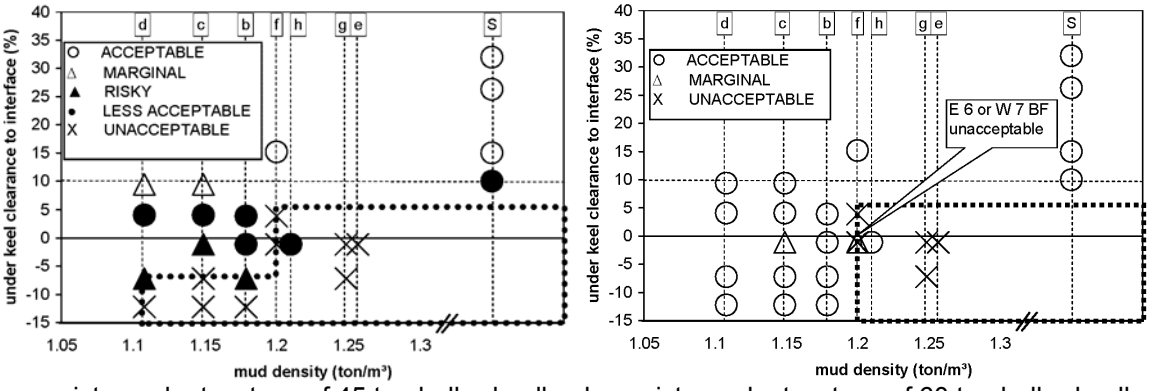

a. assistance by two tugs of 45 ton bollard pull b. assistance by two tugs of 60 ton bollard pull

Figure 8.18. Ship D, real time simulations. Quantitative evaluation of all criteria, except the speed criterion, for the harbour of Zeebrugge, dotted area = "unacceptable".

Finally, it is also worthwhile to mention that manoeuvring in muddy areas is completely different compared to hard bottom conditions, and that pilots should be informed about the modified ship behaviour and trained accordingly. Especially with a small positive under keel clearance relative to the water-mud interface, difficulties in ship handling are observed. Therefore, pilots should not

only have full knowledge of the position of the nautical bottom, but also of the position of the interface.

8.2.4 Conclusions of the first simulation program

A series of real-time simulations has been carried out by the Zeebrugge pilots in order to define the nautical bottom of the harbour of Zeebrugge. Runs have been analysed both on a qualitative base as on a numerical base. The use of an impulse of steering has proven to be effective to evaluate the control power in simulation runs.

As a result, the nautical bottom can be defined at a critical density of 1200 kg/m³. This definition is not without limitations:

- At least two tugs of 45 ton bollard pull have to assist manoeuvres of deep drafted container vessels;
- Navigability through lower density mud layers is constrained to -7% of under keel clearance;
- More tug power reduces this constraint, but does not affect the definition of the nautical bottom;
- If less tug power is available the water-mud interface should be considered as the nautical bottom;
- The present situation in the access channel outside the breakwaters should not be changed.

It should be emphasized that these specific conclusions are only valid for deep-drafted container carriers arriving at or departing from Zeebrugge harbour, as the mud characteristics, the environmental conditions (e.g. current) and harbour layout are typical for this area.

On the other hand, a similar methodology can be applied for assessing the limits for navigation in other harbours and waterways suffering from fluid mud deposits, provided that the local conditions (bottom, ship type, …) are covered by the experimental database and, therefore, the mathematical model. The present approach offers an important advantage: the new criterion for the nautical bottom is not merely based on one single physical property of the mud layer, but has been determined taking into account all significant factors such as harbour layout, bottom characteristics, ship behaviour, environmental conditions (current, wind), available tug assistance and human control.

8.3 Second simulation program

8.3.1 Setup

The second simulation program focussed on the validation of the nautical bottom criterion and the penetrability of the mud layers of a smaller density. The selection of conditions is represented in Figure 8.19.

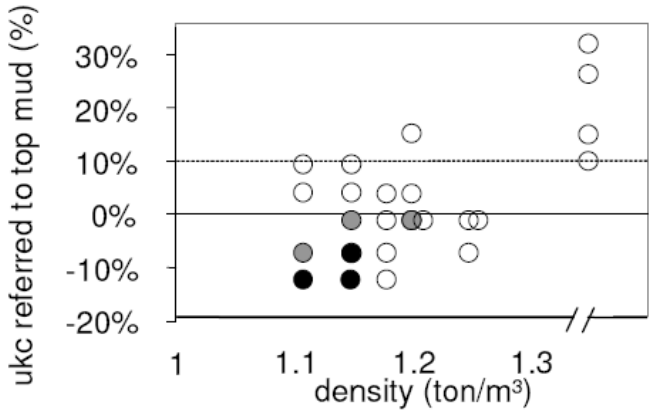

Figure 8.19. Conditions for real-time simulation runs with ship D. Only the grey (assistance of 45 bollard pull tugs) and the black (both 45 ton and 60 ton bollard pull tugs) conditions have been carried out.

The trajectories were the same as in the first simulation program, but swinging was no longer included as this manoeuvre was not critical. Also more runs were carried out with trajectory 4. The same tidal conditions and moderate wind conditions were applied. Each bottom condition has been carried out several times by different pilots.

The major difference between the two simulation programs is that in the second one transitions between a solid bottom and a mud layer or between different mud layers were included. The algorithm to model those transitions has been described in **[8.6]**.

8.3.2 Results

The simulation runs were analysed in the same way as during the first simulation runs. Both a qualitative and a quantitative analysis have been carried out, based on the same criteria. The analyses can be found in **[8.7]**. The conclusions of the first simulation program, see 8.2.4, can be confirmed and even simplified. The critical density in the harbour of Zeebrugge is thus determined at 1.20 ton/m³, while the penetration of the vessel into lower density (up to 1150 kg/m^3) is constrained, depending on the available tug assistance:

- 12% of draft if two tugs of 60 ton bollard pull are available;
- 7% for two tugs of 45 ton bollard pull;
- 0% for 2 * 30 ton bollard pull and less.

8.4 References

[8.1] DELEFORTRIE G., LAFORCE E., VANTORRE, M. *Bepaling van de nautische bodem in de haven van Zeebrugge: onderzoek nautische implicaties. Fase B: eigenlijke onderzoeksfase.* Final report. Research project UGent 51H01200, WL Mod. 582B. Ghent / Antwerp, 2004. (In Dutch).

[8.2] DELEFORTRIE G., VANTORRE M. *The nautical bottom concept in the harbour of Zeebrugge*. Proceedings PIANC congress 2006, Estoril, Portugal, 2006, 10 pp.

[8.3] DELEFORTRIE G., VANTORRE, M., LAFORCE, E. *Revision of the nautical bottom concept of Zeebrugge based on the manoeuvrability of deep-drafted container ships.* Proceedings of the CEDA Dredging Days 2005, 2005.

[8.4] DELEFORTRIE G., VANTORRE M., LAFORCE E., DE BRAUWER D., *A new approach for defining the nautical bottom in the harbour of Zeebrugge.* IHMA Congress Malta 2006 Proceedings 2006, 2006, 8 pp.

[8.5] DELEFORTRIE G., VANTORRE M., VERZHBITSKAYA E., SEYNAEVE K. *Evaluation of safety of navigation in muddy areas through real time manoeuvring simulation*. Journal of Waterway, Port, Coastal and Ocean Engineering, Vol. 133, 2, 2007, p 125-135.

[8.6] VANDER DONCKT S., VANTORRE M. *Bepaling van de nautische bodem in de haven van Zeebrugge. Onderzoek nautische implicaties. Fase C: validatie concept nautische bodem.* Third preliminary report. Research project UGent 174F5605, WL Mod. 582C. Ghent / Antwerp, 2006. (In Dutch).

[8.7] VANDER DONCKT S., VANTORRE M. *Bepaling van de nautische bodem in de haven van Zeebrugge. Onderzoek nautische implicaties. Fase C: validatie concept nautische bodem. Deelopdracht 4: aanvullen en verifiëren beslissingsschema: real-time simulaties mei-juni 2006.* Research project UGent 174F5605, WL Mod. 582C. Ghent / Antwerp, 2006. (In Dutch).

[8.8] VANTORRE M., LAFORCE E., DELEFORTRIE G. *A novel methodology for revision of the nautical bottom.* Seminar: Flanders, a maritime region of knowledge (MAREDFlow). Editors PEETERS Y., FOCKEDEY N., SEYS J., MEES J. Oostende, Belgium : Flanders Marine Institute (VLIZ), 2006, p 15-35.

If there be light, then there is darkness; if cold, heat; if height, depth; if solid, fluid; if hard, soft; if rough, smooth; if calm, tempest; if prosperity, adversity; if life, death.

Pythagoras

CHAPTER 9

MODELLING THE UNDER KEEL CLEARANCE EFFECT

9.1 Introduction

In Chapter 6 a mathematical model for each single bottom condition and under keel clearance has been developed. However this kind of model has two main shortcomings:

- The effect of the bottom and under keel clearance can only be estimated - and not calculated - due to the non bottom related sets of coefficients;
- The use in simulation runs is restricted to a constant bottom condition throughout the environment.

Both disadvantages show the necessity of developing mathematical models taking under keel clearance and bottom conditions into account. In this chapter an under keel clearance dependent model above solid bottom conditions will be developed. The description of this mathematical model has been accepted for publication **[9.6]**.

9.2 Effect of the under keel clearance

9.2.1 Overview

The best known effect of the under keel clearance on ship manoeuvring behaviour is an increase of the dimensions of the turning circle of the vessel with decreasing under keel clearance. At the same time a reduction of the drift angle is observed. Ships also tend to have a larger straight-line stability with decreasing under keel clearance, see 6.2.4 and **[9.5]**.

The state of the art of the effect of water depth restrictions on the ship manoeuvring behaviour has been summarized by the Manoeuvring Committee **[9.18]** of the 23rd International Towing Tank Conference. This chapter will specifically focus on formulations expressing the effect of under keel clearance on hydrodynamic forces.

Sheng **[9.17]** determined expressions for the effect of shallow water on hydrodynamic forces acting on elliptical sections. Extensions by Clarke **[9.2,9.3,9.4]** and Ankudinov **[9.1]** increased the range of water depths and ship parameters that could be covered by these formulae.

When a modular mathematical model is used, a clear distinction between the effect on hull, propeller and rudder forces can be made. In **[9.8]** the effect of a decreasing under keel clearance appears only of importance for the hull forces, as a significant increase of the hydrodynamic derivatives is observed.

On the other hand Yasukawa **[9.22]** has observed an increase of the wake factor with decreasing under keel clearance. The forces acting on the rudder do not seem to be affected by the under keel clearance, but the rudder induced forces on the hull are affected, as an increase of the factor a_H was reported.

The effect of the under keel clearance is mostly taken into account by adding under keel clearance related terms to an initial set of coefficients, valid for deep water conditions. Starting from the deep water case of the MMG-model **[9.10]**, Kijima **[9.11]** used the following expression to take the effect of the under keel clearance into account:

$$D_{shallow} = f\left(\frac{h}{T}\right) D_{deep} \tag{9.1}$$

with D a hydrodynamic derivative and f a correction factor:

$$f\left(\frac{h}{T}\right) = \frac{1}{\left[1-\frac{T}{h}\right]^{n}} \frac{T}{h} \tag{9.2}$$

where the exponent n can be written as a function of ship geometry parameters.

Li **[9.14]** formulated the following water depth dependency for the added inertia coefficients:

$$\frac{m_{22}}{m_{22\infty}} = 1 + \frac{f\left(\frac{B}{T}\right)}{\left(\frac{h}{T}-1\right)^{0.82}} \tag{9.3}$$

Hirano **[9.9]**, Kobayashi **[9.13]**, Millward **[9.15]** and Sadakane **[9.16]** also proposed expressions to take account of the shallow water effect. A validation of different proposed models was carried out by Vantorre **[9.19]**.

As a final example of published methods to account for shallow water effects on ship manoeuvring, Gronarz **[9.7]** expresses the shallow water influence on the hydrodynamic coefficients f as follows:

$$f = c_0 + c_n\left(\frac{T}{h}\right)^{n} \tag{9.4}$$

where c_0, c_n and n have to be determined experimentally.

9.2.2 Selection of the under keel clearance parameter

The above expressions and other examples mostly take the under keel clearance into account with the parameter:

$$\frac{h}{T} \tag{9.5}$$

or its reciprocal

$$\frac{T}{h} \tag{9.6}$$

having the advantage of turning zero in infinite water depth. (9.5) and (9.6) are possible candidates to model the water depth; nonetheless they seem to have difficulties to predict the forces in cases where very shallow water conditions lead to sharp increases, as is the case for the sway added mass, represented in Figure 9.1.

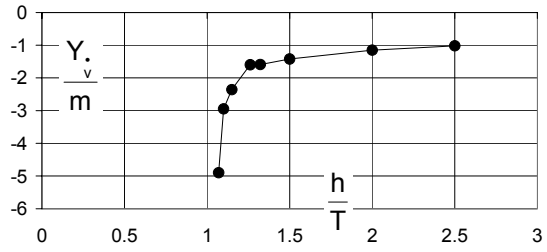

Figure 9.1. Ship model D: sway added mass, navigating ahead, stopped propeller. Influence of under keel clearance above a solid bottom.

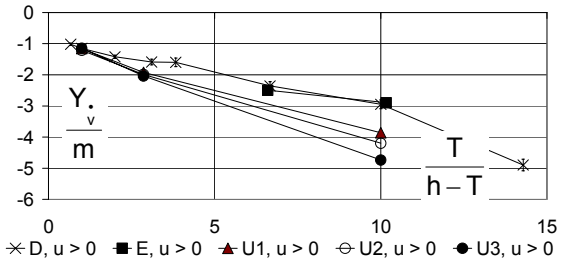

Figure 9.2. Ship models D, E, U: Sway added mass, forward motion ahead, stopped propeller. Influence of under keel clearance above a solid bottom.

An exponential relationship can be observed as in expression (9.4). However another parameter representing the under keel clearance can be derived from equations (9.2) and (9.3). If the exponent equals 1, the following parameter is found:

$$\frac{T}{h-T} \tag{9.7}$$

and is used in the abscissa of Figure 9.2. This parameter offers the advantage to reach large values for small under keel clearances. Moreover the parameter turns zero in infinitely deep water. The suitability of this parameter is illustrated in Figure 9.2, where an almost linear relationship of the sway added mass is shown as a function of parameter (9.7).

Another example is shown in Figure 9.3, based on Gronarz **[9.8]**. Whereas the use of (9.6) requires an exponential model as proposed in (9.4), with (9.7) a linear model fits the data fairly well.

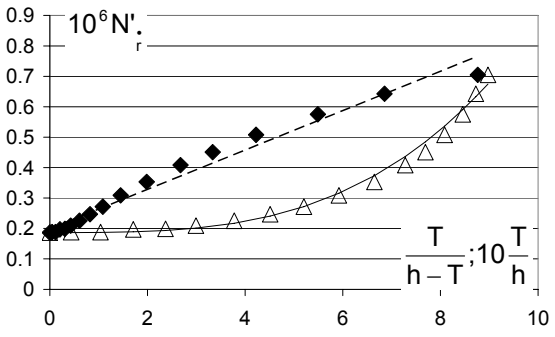

Figure 9.3. Yaw added moment of inertia, calculated with WAMIT ([9.8] – Fig 2). Comparison between the parameter (9.7) (full symbols) and (9.6) (transparent symbols) in the abscissa.

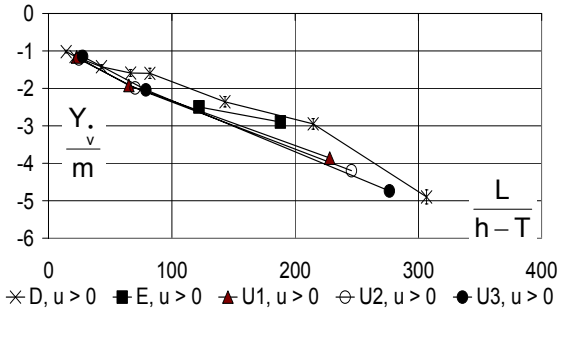

Figure 9.4. Ship models D, E, U: sway added mass, forward motion ahead, stopped propeller. Influence of under keel clearance above a solid bottom.

In spite of the linear correlation some discrepancies can be observed in Figure 9.2 when analyzing the smallest under keel clearance at different drafts for ship U. The non-dimensional sway added mass increases with decreasing draft, which can be ascribed to following effects:

- The sway force is made non-dimensional by means of the ship's mass, which decreases with decreasing draft;
- The absolute under keel clearance, i.e. the distance in m between the ship's keel and the bottom, decreases with decreasing draft for equal depth to draft ratio.

In general the water flow under the ship's keel needs to take place in a gap with a length equal to the ship's length L and a height equal to the absolute under keel clearance (h-T). An increase of L or a decrease of h-T narrows the passage in a vertical sense, while enlarging it in a longitudinal sense, resulting in larger hydrodynamic (reaction) forces. Consequently the following parameter, which can be interpreted as an inverse aspect ratio of the clearance gap, is proposed:

$$\frac{L}{h-T} \tag{9.8}$$

An increase of this parameter will result in a more three-dimensional flow around the ship's hull. The sway added mass is represented as a function of (9.8) in Figure 9.4. Obviously, a linear correlation valid for all considered draft values for ship model U is possible.

The mathematical model will use (9.5), (9.7) and (9.8) as under keel clearance parameters.

9.3 Mathematical model

The under keel clearance related mathematical model will be built up by analysing the coefficients of the mathematical model as described in Chapter 6. With the relationship between the observed coefficient and the under keel clearance parameter a new mathematical model can be built. The new coefficients are then determined with regression analysis from the initial set of measured data, which now comprises all under keel clearances.

9.3.1 Hull forces

For each under keel clearance the hull forces were modelled using (6.12), (6.16) and (6.17). However in case of a solid bottom, the $(\dot{v},\dot{r})$-dependence can be omitted, in this case the longitudinal force is:

$$X_H = \left(X_{\dot{u}}(u) - m\right)\dot{u} + mvr + mx_G r^2 + \tfrac{1}{2}\rho LT\left\{\begin{array}{l}\left(u^2+v^2\right)X'(\beta)+\\ \left(u^2+\left(\tfrac{1}{2}rL\right)^2\right)X'(\gamma)+\\ \left(v^2+\left(\tfrac{1}{2}rL\right)^2\right)X'(\chi)\end{array}\right\} \tag{9.9}$$

where the functions of β, γ and χ (6.13-6.15) are tabulated for a discrete number of values.

9.3.1.1 Longitudinal force

Added mass

The added mass has been represented in Figure 9.5 for different under keel clearances. Although the standard deviation for this term is quite high and consequently an under keel clearance independent value of the added mass would be acceptable, a linear correlation with the under keel clearance (9.7) will be modelled:

$$X_{\dot{u}} = X_{\dot{u},deep} + \frac{T}{h-T}\xi \tag{9.10}$$

This offers the advantage of:

- All hydrodynamic inertia will be modelled in a similar way;
- The model can be fine tuned if a significant under keel clearance is observed above muddy bottoms (see 10.3.1.1).

The first point could use some more information: for most of the hydrodynamic derivatives and functions in equations (6.16), (6.17) and (9.9), in the following denoted by F, a linear relationship with the non-dimensional under keel clearance parameters T / (h-T) and L / (h-T) appears to result in adequate approximations:

$$F = F_{deep} + \frac{P}{h-T}\xi_1 \tag{9.11}$$

In (9.11) P denotes either the ship's length or its draft; ξ_1 represents a constant or a function taking the under keel clearance effect into account.

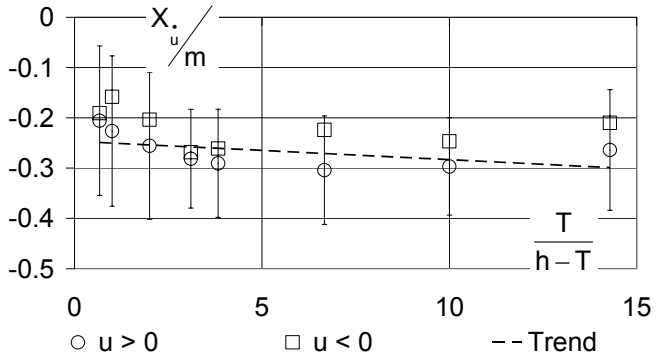

Figure 9.5. Ship D. Longitudinal force added mass, solid bottom conditions, stopped propeller.

Drift function for the longitudinal force

Figure 9.6 shows the drift function for each under keel clearance modelled separately. Some major preliminary conclusions can be drawn:

- X'(β) has an important asymmetry between the port and the starboard side. This is due to the differences in the experimental program between the starboard and the port drift angles[1]. To avoid these asymmetries X'(β) will be determined as a function of |β|;
- X'(β) has a non-linear influence of the under keel clearance, due to the different drift angles at which the sign changes. A quadratic model seems appropriate (see also the yaw function for the sway force), so that the following model is proposed:

$$X'(\beta) = X'(|\beta|)_{deep} + \frac{T}{h-T}\xi_1(|\beta|) + \left(\frac{T}{h-T}\right)^2 \xi_2(|\beta|) \tag{9.12}$$

This model gives good results, although for the smallest under keel clearance (7%) the correlation is less.

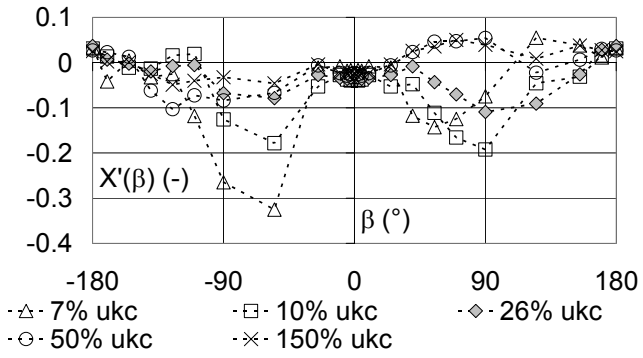

Figure 9.6. Ship D: longitudinal force, non-symmetrical drift function, solid bottom conditions, stopped propeller.

Yaw and chi function for the longitudinal force

The yaw function is shown for some yaw angles in Figure 9.7. Again a linear correlation with the under keel parameter seems acceptable. Moreover the trends are similar for the three ship models. The proposed model is thus:

$$X'(\gamma) = X'(\gamma)_{deep} + \frac{T}{h-T}\xi(\gamma) \tag{9.13}$$

An analogous model can be used for the chi-function:

$$X'(\chi) = X'(\chi)_{deep} + \frac{T}{h-T}\xi(\chi) \tag{9.14}$$

[1] E.g. drift angles to port have been executed in combination with positive and negative propeller rates, while drift angles to starboard have only been executed in combination with positive propeller rates.

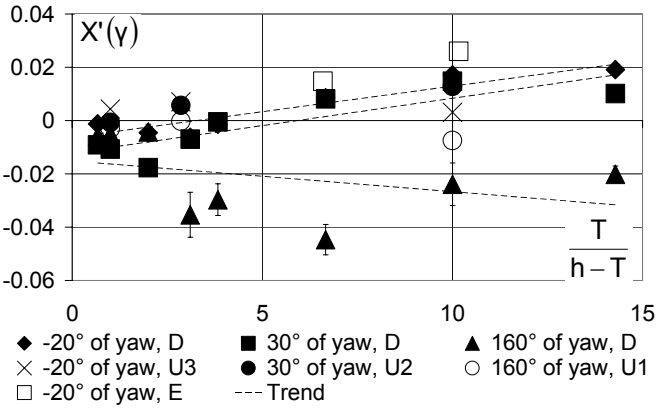

Figure 9.7. Ship models D, E and U: yaw function for longitudinal force. Stopped propeller, γ = -20, 30 and 160°. Trends for γ = -20, 30 and 160°, ship model D.

9.3.1.2 Sway force

Sway added mass

The sway added mass has already been used as an example to define the under keel clearance parameters. The sway added mass has been represented in Figure 9.8 for all ship models, both at positive and negative navigation speed.

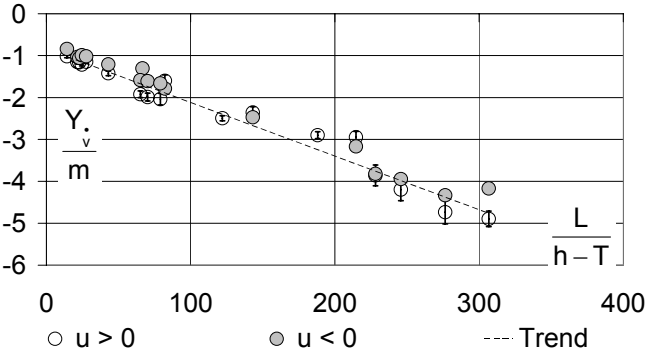

Figure 9.8. Ship models D, E, U: sway added mass, solid bottom conditions, stopped propeller.

It is clear that a same and linear formulation will do for both speeds and for all considered ship models:

$$Y'_v = Y'_{v,deep} + \frac{L}{h-T}\xi \tag{9.15}$$

Yaw acceleration derivative for the sway force

As with the sway added mass the yaw acceleration derivative shows a linear trend with L/(h-T), see Figure 9.9. The yaw acceleration derivative depends however on the drift angle, but the trends seem to converge in deep water conditions, meaning the drift angle only affects the yaw acceleration derivative in shallow water conditions. Unlike the sway added mass a distinction between forward and backward navigation speeds is still needed. The following model is proposed:

$$Y'_r = Y'_{r,deep}[\mathrm{sgn}(u)] + \frac{L}{h-T}\xi(\beta) \tag{9.16}$$

The reader will have noted that a discontinuity occurs when the ship's speed drops to zero. Model tests have been carried out at a minimal Froude number of 0.0195, while the available astern speed was F_n = -0.0195. Between those velocities a clear distinction was observed in the sign of the yaw acceleration derivative. To avoid discontinuities a weighted average is proposed once the magnitude of the Froude number drops below 0.0195.

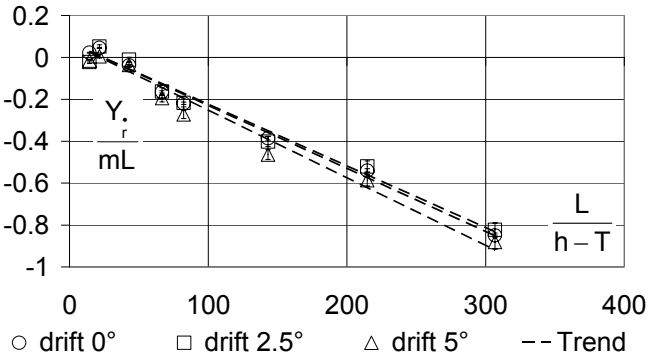

Figure 9.9. Ship D: yaw acceleration derivative, solid bottom conditions, stopped propeller, β = 0, 2.5 and 5°.

Drift function for the sway force

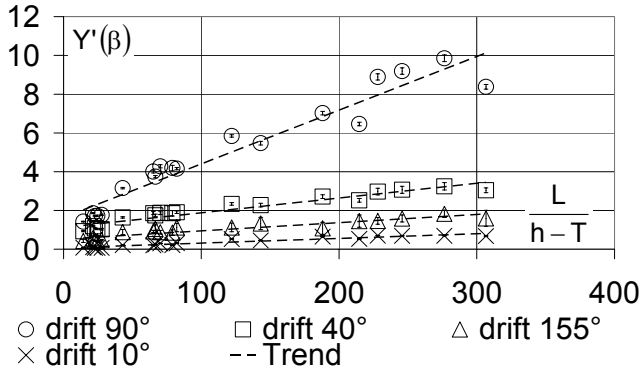

Figure 9.10. Ship models D, E, U: drift function for sway, solid bottom conditions, stopped propeller, β = 40, 90 and 155°.

The trends for the yaw acceleration derivative can also be applied to the drift function, as shown in Figure 9.10, accordingly model (9.17) will be used.

$$Y'(\beta) = Y'(\beta)_{deep} + \frac{L}{h-T}\xi(\beta) \qquad (9.17)$$

Yaw function for the sway force

The effect of the under keel clearance on the yaw velocity derivative is more complicated, see Figure 9.11:

- The values of the yaw function increase from deep to shallow water;
- From shallow to extreme shallow the absolute values of the yaw function further increase, but the sign is opposite.

Such effects cannot longer be modelled using a linear model; a quadratic model seemed to fit well:

$$Y'(\gamma) = Y'(\gamma)_{deep} + \frac{T}{h-T}\xi_1(\gamma) + \left(\frac{T}{h-T}\right)^2 \xi_2(\gamma) \tag{9.18}$$

Note also that the use of parameter T/(h-T) resulted more appropriate than L/(h-T), as no significant difference was measured for the different draughts of ship U.

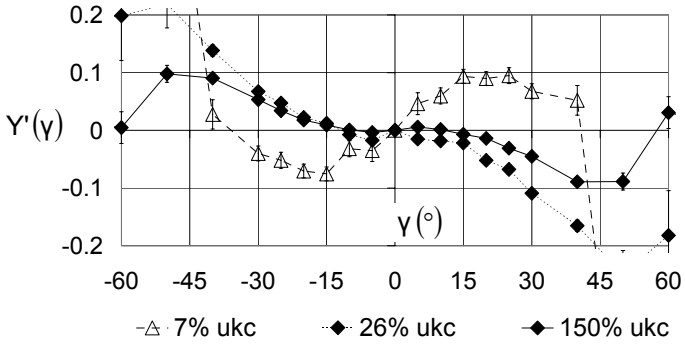

Figure 9.11. Ship D: yaw function for the sway force, stopped propeller, navigating ahead. Influence of the under keel clearance, solid bottom.

Chi function for the sway force

The chi function models the correlation between yaw and drift movements. The effect of the under keel clearance can be modelled using:

$$Y'(\chi) = Y'(\chi)_{deep} + \frac{T}{h-T}\xi(\chi) \tag{9.19}$$

Some trends are shown in Figure 9.12. The chi-function has the same trend for the other ship models, but the values differ.

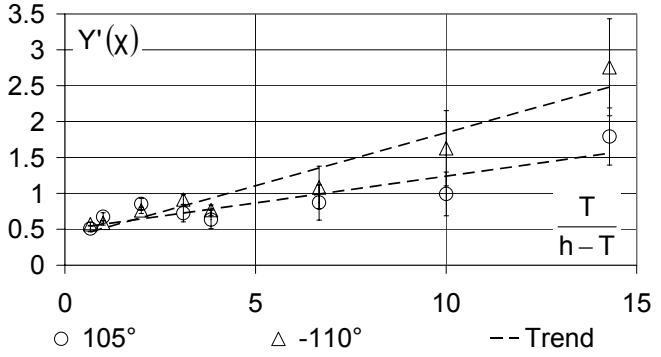

Figure 9.12. Ship D: chi function for sway, solid bottom conditions, stopped propeller, χ = -110 and 105°.

9.3.1.3 Yaw moment

Sway acceleration derivative for the yaw moment

For the yaw moment, a similar expression as (9.15) can be used:

$$N'_{\dot{v}} = \mathrm{sgn}(u)\left[N'_{\dot{v},deep} + \frac{L}{h-T}\xi\right] \tag{9.20}$$

Somehow there are differences:

- From Figure 9.13 can be seen that the derivative for the E-model (tanker/bulk carrier) has the same slope ξ, but a significantly different value for $N'_{v,deep}$ in comparison with the container carriers;
- The sign of the derivative depends of the sign of the ship's speed.
- The same remarks as for (9.16) are valid to avoid discontinuities.

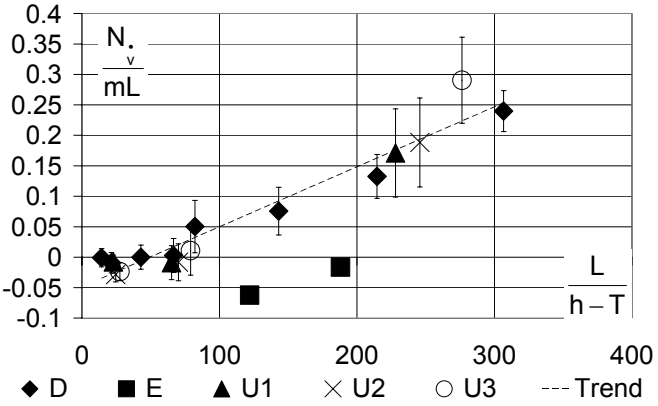

Figure 9.13. Ships D, E and U: Sway acceleration derivative for the yaw moment, stopped propeller, ahead. Trend for ship D.

Yaw added moment of inertia

The model for the yaw added moment of inertia is similar to (9.16), but the convergence point is the same for forward and backward navigation speeds.

$$N'_r = N'_{r,deep} + \frac{L}{h-T}\xi(\beta) \tag{9.21}$$

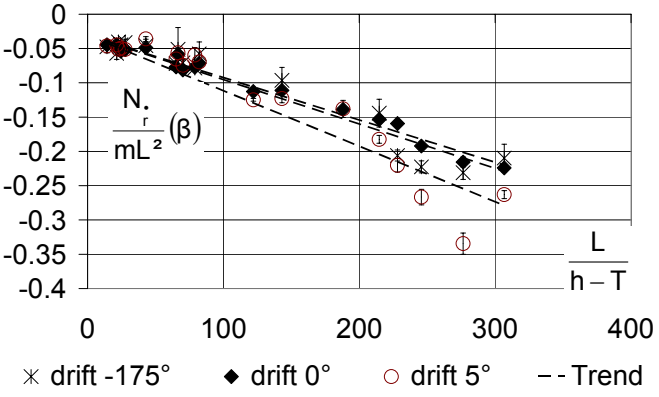

Figure 9.14. Ships D, E, U: yaw added moment of inertia, solid bottom conditions, stopped propeller, β = -175, 0 and 5°.

Drift function for the yaw moment

Rather than modelling N'(β) it seemed more convenient to model $x'_Y(\beta)$, being the application point of the sway force Y'(β). This application point is represented in Figure 9.15 for some drift angles. A small linear trend with the under keel clearance parameter can be observed, so that the proposed model is:

$$x'_Y(\beta) = x'_Y(\beta)_{deep} + \frac{T}{h-T}\xi(\beta) \tag{9.22}$$

Note that the application point in deep water is slightly different for the tanker or bulk carrier in comparison with the container carriers. N'(β) can now easily be determined using (9.17) and (9.22):

$$N'(\beta) = x'_Y(\beta)_{deep}\, Y'(\beta)_{deep} + \frac{T}{h-T}\xi_{x_Y}(\beta) + \frac{L}{h-T}\xi_Y(\beta) + \frac{LT}{(h-T)^2}\xi_{x_Y}(\beta)\xi_Y(\beta) \qquad (9.23)$$

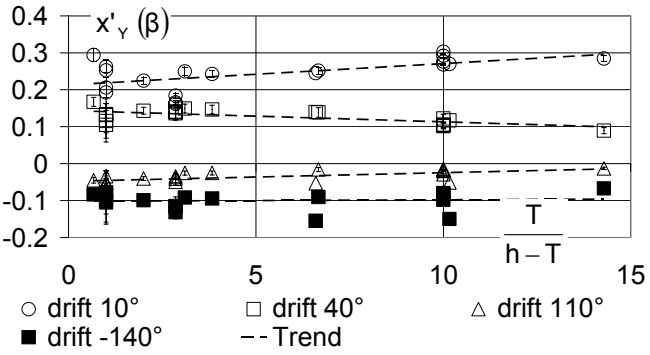

Figure 9.15. Ships D and U: application point of Y'(β), solid bottom conditions, stopped propeller, β = -140, 10, 40 and 110°.

Yaw and chi function for the yaw moment

Figure 9.16 shows the effect of the under keel clearance on the yaw function. A linear fitting is acceptable, so that the following model will be used:

$$N'(\gamma) = N'(\gamma)_{deep} + \frac{T}{h-T}\xi(\gamma) \qquad (9.24)$$

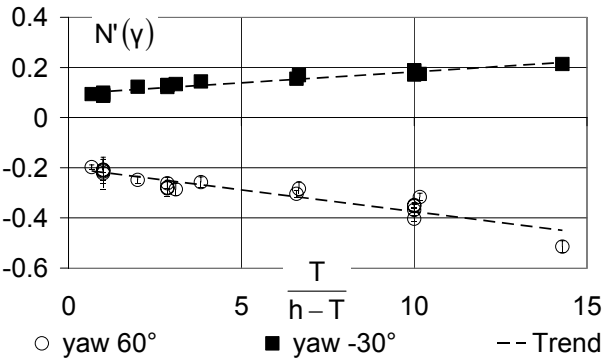

Figure 9.16. Ship models D, E, U: yaw function, solid bottom conditions, stopped propeller, γ = -30 and 60°.

For the chi function a similar model as (9.19) is proposed:

$$N'(\chi) = N'(\chi)_{deep} + \frac{T}{h-T}\xi(\chi) \qquad (9.25)$$

9.3.1.4 Conclusions

For the three ship models the same mathematical formulation may be used. The non-dimensional deep water values have the same magnitude. An exception has to be made for the effect of sway velocity on the yawing moment. Although the same slope (ξ) can be used for the three ship models, the tanker type has a different value in deep water conditions.

A linear relationship with the under keel clearance parameters can be used in almost all cases. As already seen in 6.2.2 the hydrodynamic lateral force due to yaw rate has an opposite sign at extreme shallow under keel clearances; such an effect can only be modelled using a non-linear (e.g. quadratic) relationship of the under keel clearance parameter:

$$F = F_{deep} + \frac{P}{h-T}\xi_1 + \left(\frac{P}{h-T}\right)^2 \xi_2 \tag{9.26}$$

The different models have been summarized in Table 9.1.

Table 9.1. Under keel clearance models for the hull forces F ("c" means constant)

F	P	order	ξ	Remarks
X'_u	T	1	c	
$X'(\beta)$	T	2	f(|β|)	
$X'(\gamma)$	T	1	f(γ)	
$X'(\chi)$	T	1	f(χ)	
Y'_v	L	1	c	
$Y'_r(\beta)$	L	1	f(β)	$Y'_{r,deep}$ depends of sign(u), but not of β
$Y'(\beta)$	L	1	f(β)	
$Y'(\gamma)$	T	2	f(γ)	
$Y'(\chi)$	T	1	f(χ)	
N'_v	L	1	c	$N'_{v,deep}$ and ξ depend of sign(u)
$N'_r(\beta)$	L	1	f(β)	$N'_{r,deep}$ does not depend of β
$x'_Y(\beta)$	T	1	f(β)	
$N'(\gamma)$	T	1	f(γ)	
$N'(\chi)$	T	1	f(χ)	

9.3.2 Propeller forces

9.3.2.1 Wake factors

The wake factors in the first quadrant are determined by means of the thrust or torque identity. The open water data of each propeller are known, but corrected so that for J = 0 the measured bollard pull values for thrust and torque are obtained. Figure 9.17 shows the $K_T(J')$ characteristic for the propeller behind the hull of ship D. This characteristic is significantly linear at each under keel clearance, however the slope of the characteristic increases with increasing under keel clearance. Moreover the bollard pull thrust and torque decrease with increasing under keel clearance. The evolution with the keel clearance is best described using h/T.

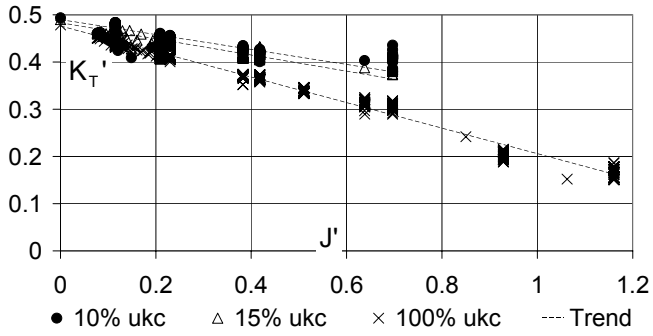

Figure 9.17. $K_T(J')$ characteristic for different under keel clearances, ship model D, first quadrant.

The bollard pull thrust and torque can be modelled as:

$$K_{(J=0)} = K_{(J=0,h=T)} + \left(\frac{T-h}{T}\right)y \tag{9.27}$$

so that the $K_T(J')$ characteristic can be written as:

$$K = K_{(J=0)} + \left[x_{2(h=T)} + \left(\frac{T-h}{T}\right)x_1\right]J' \tag{9.28}$$

in which x_1, x_2 and y need to be determined by regression. The open water characteristic for the first quadrant of the propeller can be estimated as follows, with z_i a set of yet unknown coefficients:

$$K = K_{(J=0)} + z_1 J + z_2 J^2 \tag{9.29}$$

Using the thrust or torque identity expression (9.28) equals (9.29) so that the wake factor can be calculated:

$$w = \frac{J'-J}{J'} \tag{9.30}$$

This can be rewritten as:

$$w(\varepsilon^*) = w(\varepsilon^*)_{(h=T)} + \left(\frac{T-h}{T}\right)\xi(\varepsilon^*) \tag{9.31}$$

In quadrants II, III and IV, the influence of the wake can be neglected, so that:

$$w(\varepsilon^*) = 0 \tag{9.32}$$

9.3.2.2 Thrust and torque

Obviously (9.31) is only valid for the range of under keel clearances that has been tested. The above model has only been analysed for ship D, but ship U follows the same trends. Once K, J and w are known the thrust and torque can be calculated using (6.22) and (6.23).

9.3.2.3 Thrust deduction

The thrust yields a longitudinal force expressed as:

$$X_P = [1 - t(\varepsilon^*, \varphi^*, \gamma^*)]T_P \tag{9.33}$$

t being the thrust deduction factor, formulated as a function of the apparent hydrodynamic angles ε*, φ* and γ*.

Bollard pull

Figure 9.18 represents the thrust deduction factor in bollard pull conditions.

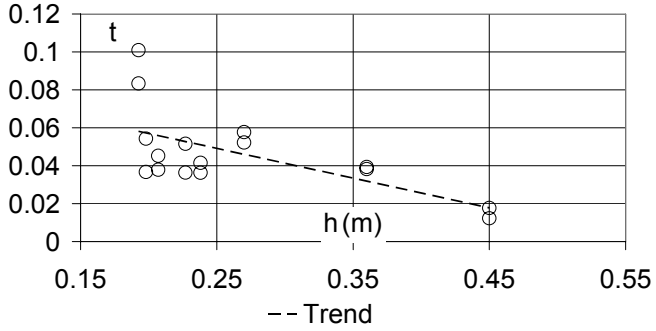

Figure 9.18 Thrust deduction factor in bollard pull conditions, positive rpm, ship model D.

A linear relationship can be observed with the under keel clearance parameter h/T. For negative propeller rate the thrust factor can be set to zero, so that the following model is proposed:

$$\begin{aligned} t_{BP} &= x_1 - \frac{h}{T}x_2; \text{rpm} > 0 \\ &= 0; \text{rpm} < 0 \end{aligned} \tag{9.34}$$

First quadrant

The thrust deduction factor has been modelled for each solid bottom condition with a linear correlation with both ε* and φ*.

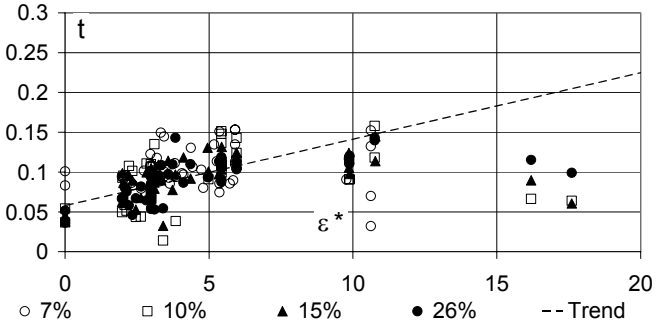

Figure 9.19. Thrust deduction factor in the first quadrant (shallow), ship model D.

As can be observed from Figure 9.19, the thrust deduction factor increases with decreasing propeller loading. From ε* = 10° the trend is a decreasing one, but this is merely due to a smaller thrust and consequently a larger error on the measured thrust deduction factor. A linear relationship between t and ε* is therefore sufficient. The slope of the relationship seems to increase with decreasing under keel clearance h/T. Analogous conclusions are valid for φ*. Therefore the proposed model for the first quadrant is:

$$t = t_{BP} + \left[x_1 - y_1 \frac{h}{T} \right] \varepsilon^* + \left[x_2 + y_2 \frac{h}{T} \right] \varphi^* \qquad (9.35)$$
$$t_{BP} \le t < 1$$

Other quadrants

For the other quadrants models have been built in a similar way as in the first quadrant. Unlike in the first quadrant the under keel clearance is modelled using $\frac{T}{h-T}$.

Following models will be used:

- Quadrant 2:

$$t = (\varepsilon^* - 180°)\left(x + y \frac{T}{h-T} \right) \qquad (9.36)$$
$$\text{with } -1 < t \le 0$$

- Quadrant 3:

$$t = (\varepsilon^{*2} - 180°^2)\left(x_1 - y_1 \frac{T}{h-T} \right) + (\varepsilon^* + 180°)\left(x_2 - y_2 \frac{T}{h-T} \right) \qquad (9.37)$$
$$\text{with } 0 \le t < 1$$

- Quadrant 4:

$$t = t_{BP} + \left[-x_1 + y_1 \frac{T}{h-T} \right] \varepsilon^* + \left[x_2 + y_2 \frac{T}{h-T} \right] \gamma^* \qquad (9.38)$$
$$\text{with } t_{BP} \le t < 1$$

ε*, φ* and γ* are formulated in degrees in expressions (9.35) – (9.38). In (9.38) the dependency of γ* disappears once ε* is larger than -1°. This is done by a linear interpolation and to avoid discontinuities with the first quadrant. All coefficients x_i and y_i have positive values:

- In bollard pull conditions the thrust deduction increases with decreasing under keel clearance. More thrust is lost with decreasing under keel clearance, as the bollard pull thrust increases with decreasing under keel clearance; consequently the net X_P-force is rather insensitive to the under keel clearance.
- In both the first and the third quadrant the thrust deduction increases with decreasing propeller loading, an increase that is certainly significant in areas where the under keel clearance is small, meaning a loss of propeller efficiency;
- In the even quadrants where the ship slows down, a larger brake force is obtained with decreasing under keel clearance. An increase of yawing in the fourth quadrant has the opposite effect.

9.3.2.4 Propeller induced sway force and yawing moment

Hydrodynamic inertia

The lateral force and the yawing moment induced by propeller action are given in (6.33) and (6.34). The hydrodynamic inertia due to propeller action can be modelled using similar expressions as in Table 9.1:

$$D = D_{deep}(\text{quadrant}) + \frac{L}{h-T}\xi(\text{quadrant}) \tag{9.39}$$

with D representing a hydrodynamic inertia in (6.33) or (6.34). Figure 9.20 shows as an example the evolution of Y'^{n}_{v} and Y'^{n}_{r} with the under keel clearance.

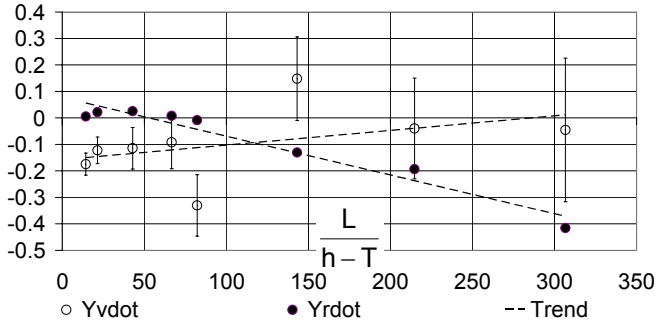

Figure 9.20. Y'^{n}_{v} **and** Y'^{n}_{r} **in the first quadrant, ship model D, maximal propeller rate.**

Stationary force and moment

The average values Y_{PT}, N_{PT} and the amplitudes of oscillations Y_{PTA}, N_{PTA} seem to depend on water depth in the following way:

$$F_{PT(A)} = \xi_1(\beta, \gamma, \varepsilon^*) + \sqrt{\frac{T}{h-T}}\xi_2(\beta, \gamma, \varepsilon^*) \tag{9.40}$$

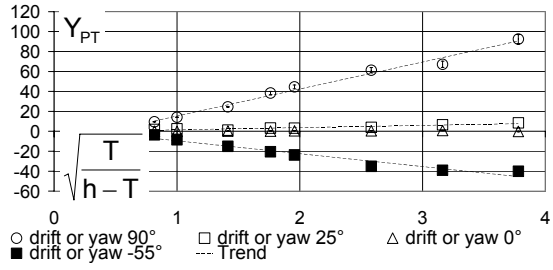

Figure 9.21. Effect of the propeller action on the sway force $Y_{PT}(\beta,\gamma)$ in the first quadrant, ship model D.

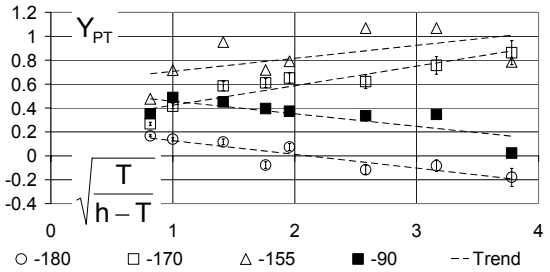

Figure 9.22. $Y_{PT}(\beta)$ in the third quadrant, ship model D, β = -90, -155, -170 and -180°.

Figures 9.21 to 9.24 show different examples. The fact that the square root can be used in (9.40) shows that the effect of the under keel clearance is less stringent in comparison with the hull forces; anyhow the effect cannot be neglected. Unlike the previous models the coefficient which does not depend on the under keel clearance cannot be denominated “deep”, in Figure 9.21 it is clear that in most cases Y_{PT} will reach zero somewhere between deep and

medium deep water; an extrapolation is not physically acceptable. Hence the under keel clearance reliant term in (9.40) will be truncated once a critical under keel clearance has been reached.

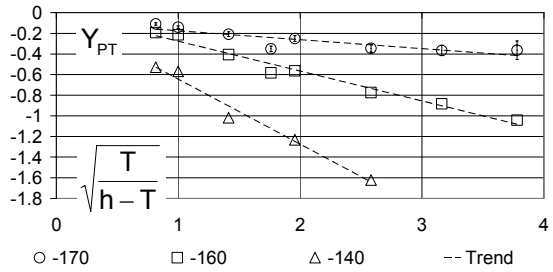

Figure 9.23. $Y_{PT}(\gamma)$ in the fourth quadrant, ship model D, γ = -140, -160 and -170°.

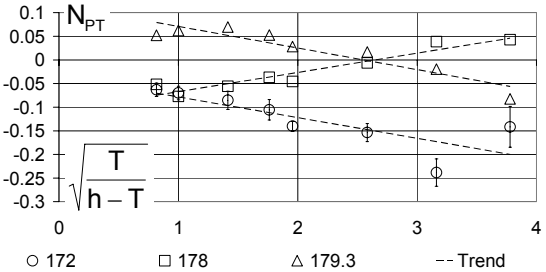

Figure 9.24. $N_{PT}(\varepsilon^*)$ in the second quadrant, ship model D, ε* = 172, 178 and 179.3°.

Non stationary force and moment

The amplitude of the oscillations can be modelled using (9.40) as well. The oscillation frequency for both the yaw moment and the sway force are represented in Figure 9.25. The slope of the frequency, having a linear correlation with J^2, decreases with decreasing under keel clearance. The decrease of the slope is of magnitude $\frac{T}{h-T}$ - the frequencies decrease sharply in very shallow water - so that following expression can be used:

$$\omega' = J^2\left[\frac{T}{h-T}x_1 + x_2\right] \tag{9.41}$$

Leading to

$$\omega'(\varepsilon^*) = \omega'_{deep}(\varepsilon^*) + \frac{T}{h-T}\xi(\varepsilon^*) \tag{9.42}$$

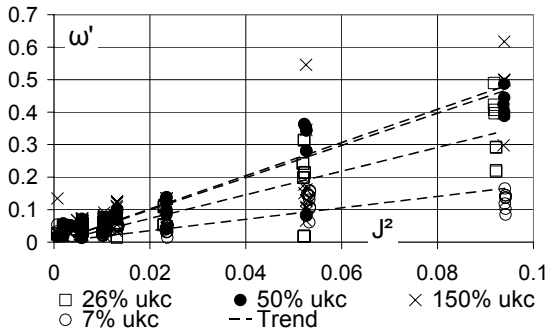

Figure 9.25. Oscillation frequencies in the even quadrants, ship model D.

The phase angles φ appear to be randomly distributed. The best fit is therefore an average over all under keel clearances.

9.3.3 Rudder forces

Wake factors

The forces acting on the rudder are given by expressions (6.44) and (6.45). All angles and V_R are affected by the wake induced by the presence of the hull and the propeller. Figure 9.26 shows that the wake factors follow:

$$w(\delta,\beta+\gamma)=\xi_1(\delta,\beta+\gamma)+\left(\frac{h}{T}\right)\xi_2(\delta,\beta+\gamma) \tag{9.43}$$

In the fourth quadrant (6.47b) has been used to determine the flow velocity near the rudder. Although equation (9.43) suggests a clear relationship between the rudder forces and the under keel clearance, the rudder forces do not vary significantly with the under keel clearance. The increasing wake factor in (9.43) mainly counteracts the increasing thrust. This confirms the observations of **[9.22]**, but cannot be generalized as **[9.12]** reports a significant shallow water effect on the rudder forces.[2]

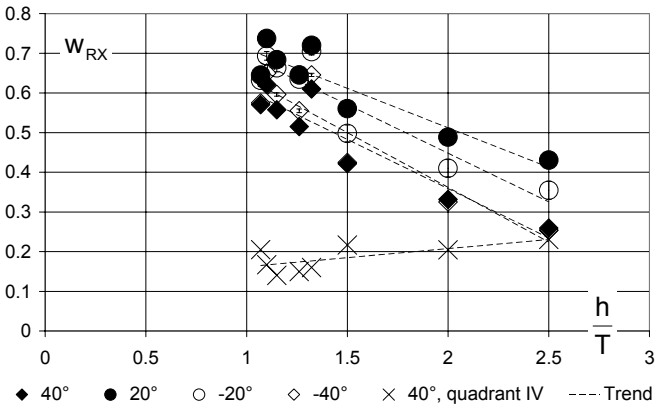

Figure 9.26. Wake factor for the longitudinal rudder force F_X, ship model D, quadrants I and IV.

To take the effect of the under keel clearance into account, model (6.48) can be written as:

$$u_R=\left[\xi_1+\xi_2\frac{h}{T}\right]n+(1-w_R)u \tag{9.44}$$

with w_R as in (9.43).

Rudder induced forces

The mathematical models for the rudder induced forces are given in (6.51) – (6.53). In the first quadrant a_H, which is zero for bollard pull, increases with decreasing propeller loading until a maximum is reached and then decreases

[2] From the results of the open water tests, carried out at Flanders Hydraulics Research **[9.20]**, with a rudder at different under keel clearances, it could be concluded that a small shallow water effect occurs, which nevertheless is not significant once the rudder is located behind the ship's hull.

with further decreasing propeller loading **[9.21]**. The trend is a parabolic one, so that a_H can be written as:

$$a_H = x_1 \varepsilon^* + x_2 \varepsilon^{*2} \tag{9.45}$$

The coefficients x_1 and x_2 are shown in Figure 9.27.

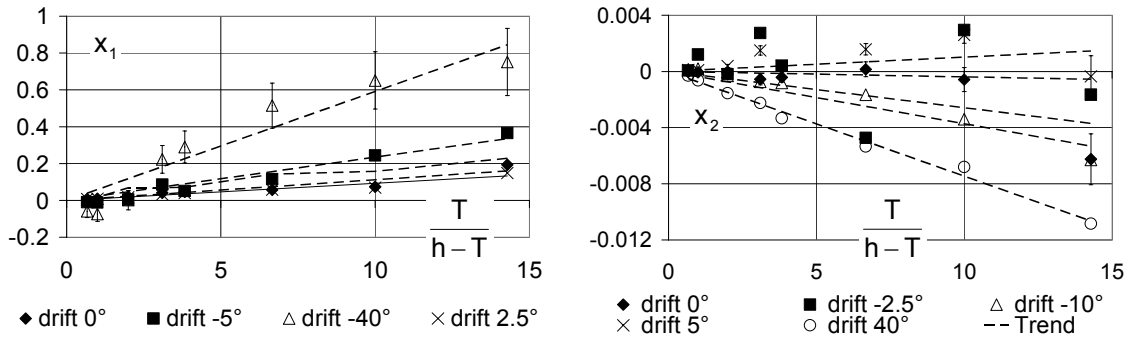

a. coefficient x_1 from (9.45) b. coefficient x_2 from (9.45)

Figure 9.27. a_H, ship model D, quadrant I, influence of under keel clearance

Both coefficients converge to zero in infinitely deep water conditions and have a linear correlation with the under keel clearance parameter. Consequently the model for a_H in the first quadrant is:

$$a_H = \left(x_1 \varepsilon^* + x_2 \varepsilon^{*2}\right) \frac{T}{h-T} \tag{9.46}$$

In the third and fourth quadrant a_H can be modelled as:

$$a_H = a_{H,deep} + \xi \frac{T}{h-T} \tag{9.47}$$

In all quadrants x_H shows a linear relationship with T/(h-T), see Figure 9.28 for an example in the third and the fourth quadrant.

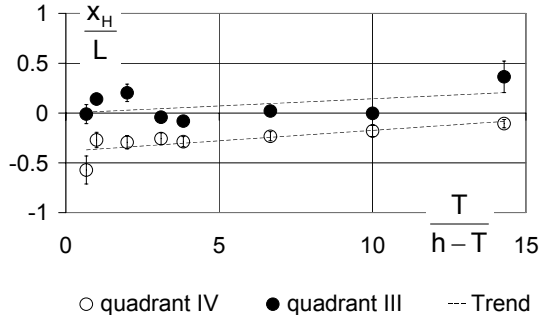

Figure 9.28. x_H in quadrants III and IV, ship model D.

As a result the following model is proposed:

$$x_H(\beta,\gamma) = x_{H,deep}(\beta,\gamma) + \xi(\beta,\gamma) \frac{T}{h-T} \tag{9.48}$$

where x_H moves more forward with decreasing under keel clearance. Only in the first quadrant a significant influence of β and γ has been observed.

9.3.4 Validation

For each under keel clearance, several validation runs have been carried out. During these captive model tests, a large range of kinematical and control parameters were covered, see 4.4.6.4. The output data of these runs have not been used during mathematical modelling; in this way, they could be utilized for validating the latter by comparison with the output of the mathematical models.

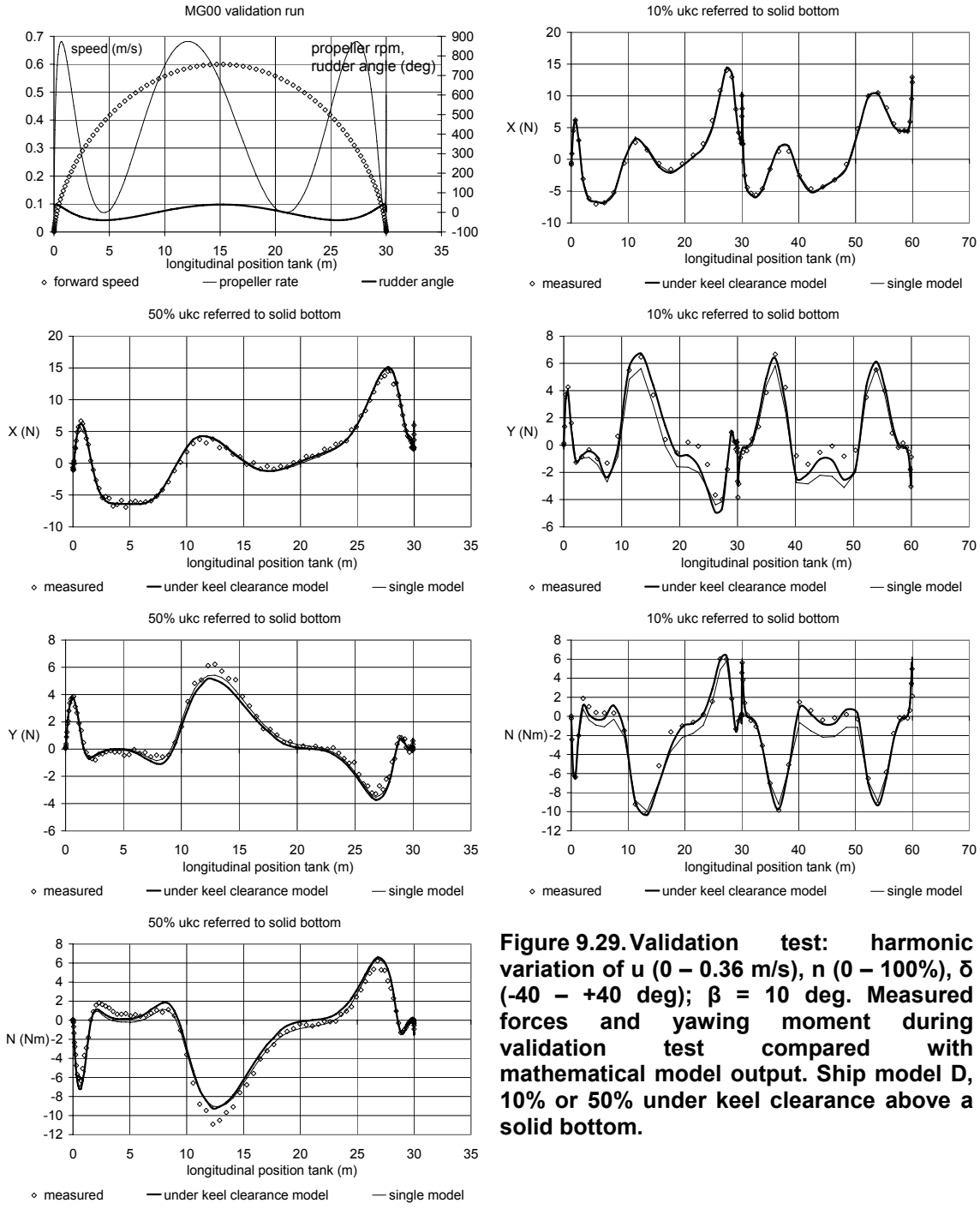

Figure 9.29. Validation test: harmonic variation of u (0 – 0.36 m/s), n (0 – 100%), δ (-40 – +40 deg); β = 10 deg. Measured forces and yawing moment during validation test compared with mathematical model output. Ship model D, 10% or 50% under keel clearance above a solid bottom.

Some examples are shown in Figure 9.29. The validation test measurements appear to be reproduced fairly well by the mathematical models. Moreover there

is no significant better prediction if for each under keel clearance a single set of coefficients is used. Of course, it would also be interesting to include full scale trials.

9.4 Conclusions

The effects of the under keel clearance on the manoeuvring behaviour of container vessels have been analyzed and compared to prior results:

- In the shallow water domain the forces acting on the hull are significantly influenced by the under keel clearance;
- The propeller thrust and torque increase in shallow water, but the increase of thrust is lost due to an increase of thrust deduction as well, consequently propeller action is less efficient in shallow water;
- The forces acting on the rudder are not affected by the under keel clearance, but the rudder induced lateral force on the hull increases, while its application point moves more forward with decreasing under keel clearance.

The shallow water effects were modelled for the 6000 TEU container vessel using linear and sometimes quadratic expressions as a function of an under keel clearance parameter. The mathematical models predict the forces acting on the ship fairly well[3] and can be extended to other container vessels. In general for the hull forces the same model – with different coefficients – can be applied to a 6000 and an 8000 TEU container ship.

[3] Based on the validation of model tests only.

9.5 References

[9.1] ANKUDINOV V.K., MILLER E.R., JAKOBSEN B.K, DAGGETT L.L. *Maneuvering performance of tug/barge assemblies in restricted waterways*, Proceedings MARSIM & ICMS 90, Tokyo, 1990, p 515-525.

[9.2] CLARKE D., GEDLING P., HINE G. *The application of manoeuvring criteria in hull design using linear theory*, RINA Transactions, **125**, 1983, p 45-68.

[9.3] CLARKE D. *The shallow water effect on linear derivatives*, Proceedings MCMC'97, Brijuni, 1997, p 87-92.

[9.4] CLARKE D., HORN J.R. *Estimation of hydrodynamic derivatives*, Proceedings 11th Ship Control Systems Symposium, Southampton, 1997, p 275-289.

[9.5] CRANE C.L. Maneuvering trials of 278000 tonnes DWT tanker in shallow and deep water, *Transactions SNAME*, **87**, New York, 1979.

[9.6] DELEFORTRIE G., VANTORRE M. *Modeling the maneuvering behavior of container carriers in shallow water.* Journal of Ship Research (Accepted for publication).

[9.7] GRONARZ A. *Numerical Simulation of the Ship's Motion in Manoeuvres with Special Consideration of the Dependency of the Water Depth, PhD dissertation*, Duisburg, 1997. (In German).

[9.8] GRONARZ A. *A mathematical model for manoeuvring simulation on shallow water.* Proceedings of the International Conference on marine simulation and ship manoeuvrability (MARSIM), Saint John's, 1993.

[9.9] HIRANO M., TAKASHINA J., MORIYA S., NAKAMURA Y. *An experimental study on manoeuvring hydrodynamic forces in shallow water*, TWSNA, Volume 69, 1985, p 101-110.

[9.10] INOUE S., HIRANO M., KIJIMA K. *Hydrodynamic derivatives on ship manoeuvring,* International Shipbuilding Progress, 28, No. 321, 1981.

[9.11] KIJIMA K., NAKIRI Y., TSUTSUI Y., MATSUNAGA M. *Prediction method of ship manoeuvrability in deep and shallow waters,* Proceedings of MARSIM & ICSM 90, Tokyo, 1990, p 311-318.

[9.12] KIJIMA K., NAKIRI Y., M. *On the practical prediction method for ship maneuverability in restricted water*, Transactions of the West Japan Society of Naval Architects, No. 107, 2004.

[9.13] KOBAYASHI E. *The development of practical simulation system to evaluate ship maneuverability in shallow water*, Proceedings, PRADS'95, 1995, p 1.712-1.723.

[9.14] LI M., WU X. *Simulation calculation and comprehensive assessment on ship maneuverabilities in wind, wave, current and shallow water,* Proceedings of MARSIM & ICSM '90, Tokyo, 1990, p 403-411, p 459-465.

[9.15] MILLWARD A. *The effect on water depth on hull form factor*, International Shipbuilding Progress, Vol. 36, No. 407, 1989, p 283-302.

[9.16] SADAKANE H., TODA Y., LEE Y.S. *The Simplified Formulas to Predict the Coefficient of Added Mass and Yaw Added Moment of Inertia of Ship in Shallow Water*, Journal of Japan Institute of Navigation, Vol.105, 2001, p11-20.

[9.17] SHENG Z.Y. *Contribution to the discussion of the Manoeuvrability Committee report*, Proceedings 16th International Towing Tank Conference, Leningrad, 1981.

[9.18] THE MANOEUVRING COMMITTEE. *Final Report and Recommendations to the 23rd ITTC.* Proceedings of the 23rd International Towing Tank Conference, Venice, 2002.

[9.19] VANTORRE M. *Manoeuvring coefficients for a container carrier in shallow water: an evaluation of semi-empirical formulae*, Mini Symposium on Prediction of Ship Manoeuvring Performance (Editor: Kijima, K.), Tokyo, 2001, p 71-81.

[9.20] VANTORRE M. *Roerkrachten in open water*. Onderzoek uitgevoerd op de sleeptank voor Manoeuvres in Ondiep Water van het Waterbouwkundig Laboratorium (Mod602) in het kader van onderzoeksproject RUG172L0992, Antwerpen, 2002. (In Dutch).

[9.21] VANTORRE M., ELOOT K., HEYLBROECK B. *Evaluation of mathematical models for propulsion and rudder forces by means of captive model tests with bulkcarriers in shallow water*. Manoeuvrability '95 (International Symposium on Manoeuvrability of Ships at Slow Speed), Ship Handling Research and Training Centre, Ilawa, Poland, Volume 1, 1995, p 39-54.

[9.22] YASUKAWA H. 1998 *Computation of effective rudder forces of a ship in shallow water*, Proceedings of Symposium of forces acting on a manoeuvring vessel (MAN98), Val de Reuil, 1998, p 125-133.

The sciences do not try to explain, they hardly even try to interpret, they mainly make models. By a model is meant a mathematical construct which, with the addition of certain verbal interpretations describes observed phenomena. The justification of such a mathematical construct is solely and precisely that it is expected to work.

John Von Neumann

CHAPTER 10

MODELLING THE MUDDY BOTTOM

10.1 Introduction

In the previous chapter a mathematical model that takes the under keel clearance effect into account has been developed. In this chapter an extension of this model will be presented in order to take the effect of a soft mud layer on the bottom into account. The extension of the mud related effects can be done in two ways:

- The hydrodynamically equivalent depth, i.e. the corresponding depth above a solid bottom that leads to the same forces, can be modelled;
- Additional forces that take the mud effect into account can be modelled.

Both ways will be used to build a bottom dependent model.

10.2 The hydrodynamically equivalent depth

With h_2 the thickness of the mud layer and h_1 the height of the upper lying water layer, the total depth can be written as:

$$h = h_1 + h_2 \tag{10.1}$$

The bottom material can vary from water over soft mud to consolidated mud. If the mud has large viscosity and density values, like sand or clay, the material will hardly move when a ship passes by and its top can be considered as the actual seabed. In this case the hydrodynamically equivalent depth h* is:

$$h^* = h_1 \tag{10.2}$$

On the other hand if the material is very fluid the mud layer cannot be considered as a solid bottom. In the limit condition of two equivalent water layers, the hydrodynamically equivalent depth is:

$$h^* = h_1 + h_2 = h \tag{10.3}$$

For intermediate situations a parameter Φ can be defined, so that:

$$h^* = h_1 + \Phi h_2 \leq h \tag{10.4}$$

Particular values for the parameter Φ are 0 (hard layer of thickness h_2) and 1 (watery layer of thickness h_2), Φ represents consequently the degree of watery behaviour of the bottom layer and is therefore called the fluidization parameter.

Intuitively the fluidization parameter of the mud covering the seabed depends on the following aspects:

- the rheological properties (e.g. viscosity) of the mud: a decrease of the latter means a more fluid mud layer and will logically result in an increased fluidization parameter;

- the under keel clearance referred to the mud-water interface: the fluidization parameter increases when the ship's keel is located closer to the mud or penetrates the mud. In these conditions the mud layer is stirred and will behave more fluidly.

In the following paragraphs the fluidization parameter will be modelled so that the mathematical model developed in Chapter 9 can be used to predict the manoeuvring behaviour in muddy navigation areas. The under keel clearance relationship was expressed as a function of h/T, T/(h-T) and L/(h-T). The aim is to use the same coefficients, but with the replacement of the real depth h by the hydrodynamically equivalent depth h* [1]. A virtual example is shown in Figure 10.1, where a real depth of 1.1T corresponds with a hydrodynamically equivalent depth of 1.045T.

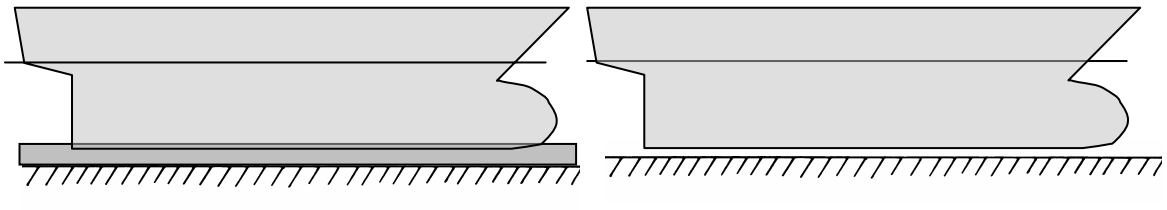

a. -1.1% of draft above a mud layer h2 (10% of draft above the solid bottom)

b. 4.5% of draft above the solid bottom.

Figure 10.1. Ship model D. Example of the hydrodynamically equivalent depth. Both conditions are hydrodynamically equal.

10.3 Modelling of the hull forces

10.3.1 The longitudinal force

10.3.1.1 Acceleration dependent terms

From Figure 6.16 it was concluded that when the ship's keel penetrates the mud layer, the value for the longitudinal acceleration derivative seemed to have the same value as in the deep water condition. Such is difficult to model with the hydrodynamically equivalent depth principle, therefore the second method of modelling additional forces will be used. Figure 10.2 represents the additional terms in muddy navigation areas. In the abscissa

$$\Pi_T = \frac{T - h_1}{T} \tag{10.5}$$

has been used to represent the penetration of the keel within the mud layer. A positive value of Π_T corresponds with a penetration of the keel into the mud.

[1] The hydrodynamically equivalent depth is a modelling concept. h* depends mostly on other kinematical parameters such as the drift angle, e.g. a ship navigating at a drift angle of 90° will have a different impact on the mud layer compared to the case of a drift angle of 0°.

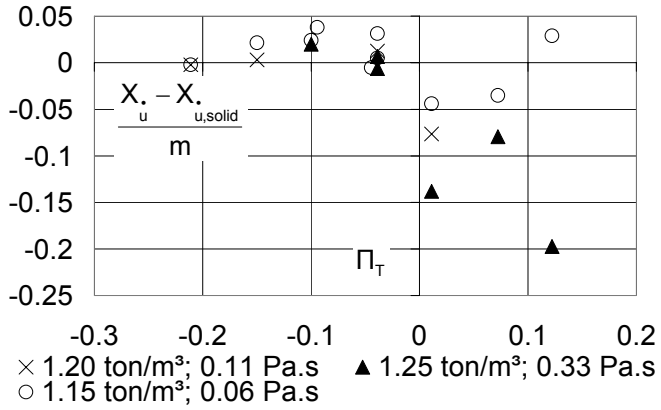

Figure 10.2. Ship model D. Rest fraction of the longitudinal acceleration derivative. Influence of the bottom condition.

A sharp increase of the acceleration derivative can be observed once the keel penetrates the mud layer. For mud layers of a lower density and viscosity the derivative returns to its initial state. It is expected that the same will occur with mud layers of higher density and/or viscosity, however, as there are no experimental results available with larger penetration ratios, the mathematical modelling will be restricted to the situations considered in the experimental program. With this restriction a linear tabulated relationship with the keel penetration parameter (10.5) and the mud viscosity can be used as a model:

$$\frac{X_{u} - X_{u,solid}}{m} = \xi_1(\Pi_T) + \mu'\xi_2(\Pi_T) \qquad (10.6)$$

In which:

- ξ_i are regression coefficients, tabulated for different values of Π_T;
- $X_{u,solid}$ is given by (9.10).

The dynamic viscosity of the mud layer μ' is used to denote the effect of the mud layer. The choice between density and viscosity is rather arbitrary as for the experimented mud layers higher density values correspond with higher viscosity values. However when comparing the mud layers that were carried out at the same density, but at a different viscosity, like:

- 0.11 and 0.19 Pa.s with 1.20 ton/m³;
- 0.28 and 0.33 Pa.s with 1.25 ton/m³;

it was observed that larger forces occurred at the higher viscosity levels. In these cases the viscosity values allow a better prediction of the manoeuvring behaviour. Moreover in 3.4.2 it was stated that viscosity acted as a depth reduction, so that the use of viscosity fits well in the concept of hydrodynamically equivalent depth.

Strictly speaking (10.6) is not non-dimensional, but has dimension Pa.s. Considering the fact that the viscosity has not been scaled during the

experimental testing, a non dimensional viscosity μ' (by dividing the viscosity by μ_{water}[2]) can be used, so that (10.6) has no dimension.

Expression (10.6) predicts the values in muddy areas very well, but should turn zero when navigating above a solid bottom. To do so for very thin mud layers a linear interpolation is proposed between (10.6) for the smallest experimented mud layer - 0.75 m - and zero for the solid bottom condition.

As mentioned in 6.3.1 additional inertia derivatives are needed when the ship penetrates mud layers of high viscosity. Figure 6.17 showed that these additional terms depend on the viscosity and the penetration of the mud layer, so that the following expression can be used:

$$X_{\dot{k}} = \left[\xi_1\left(\dot{k}\right) + \xi_2\left(\dot{k}\right)\mu' \right] \Pi \qquad (10.7)$$

In which $\dot{k}$ represents the accelerations $\dot{r}$, $\dot{v}$, $r\dot{r}$ or $v\dot{v}$. (10.7) is zero for negative values of Π and is valid for μ' > 158. Π is also a keel penetration parameter and is given by:

$$\Pi = \frac{T - h_1}{h_2} \qquad (10.8)$$

The keel penetration parameter can only be determined when a mud layer is present, but for a solid bottom condition its value is unimportant and for very thin mud layers it is unlikely that the ship will penetrate the mud layer. As $X_{\dot{k}}$ is zero for the mud layers of lower density, a linear interpolation between the highly viscous mud layers and the ones of low viscosity is proposed.

10.3.1.2 Velocity dependent terms

Drift function for the longitudinal force

The effect of the under keel clearance on the drift function for the longitudinal force is given in (9.12). Figure 10.3 gives an example for a drift angle of 90°. The resistance increases in muddy navigation areas and a hydrodynamically equivalent depth can be defined as shown in Figure 10.3. The fluidization parameter has been determined and is shown in Figure 10.4 for mud layers c2 and c3 (1.15 ton/m³ and 0.06 Pa.s) as a function of the keel penetration parameter (10.8). A linear relationship can be observed:

$$\Phi = a\Pi + \Phi_0 \qquad (10.9)$$

The fluidization parameter when the keel is on the water-mud interface Φ_0 and the slope a are different for each mud composition. A linear relationship with the mud viscosity can be used (see also 10.3.2.1):

[2] The viscosity of water at 15°C is 1.14E-03 Pa.s

$$\Phi(\beta) = \left[a_0(|\beta|) + \mu' a_\mu(|\beta|)\right]\Pi + \Phi_0(|\beta|) + \mu'\Phi_\mu(|\beta|) + \frac{h_2}{T}\Phi_h(|\beta|) \qquad (10.10)$$

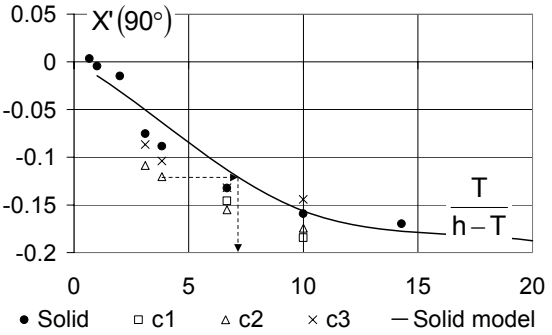

Figure 10.3. Ship model D. Longitudinal force at a drift angle of 90°. Influence of under keel clearance and bottom.

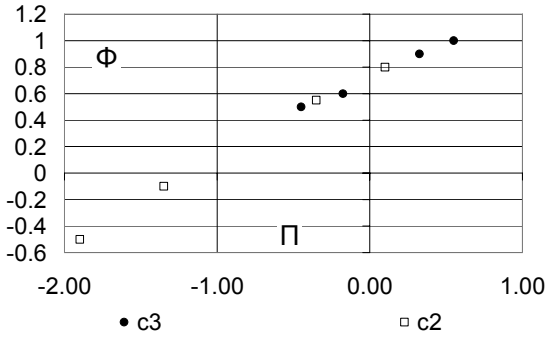

Figure 10.4. Ship model D. Fluidization parameter for the longitudinal force at a drift angle of 90°. Influence of keel penetration.

Note that the fluidization parameter in Figure 10.4 can reach negative values at higher under keel clearances above the mud layer. This can be explained due to the presence of the undulations of the interface that affect the manoeuvring behaviour of the ship. Consequently the hydrodynamically equivalent depth is smaller than the height of the water layer as if the solid bottom were located above the water-mud interface. On the other hand the effect on the forces is rather small, as the under keel clearance is larger in these conditions and thus T/(h-T) smaller.

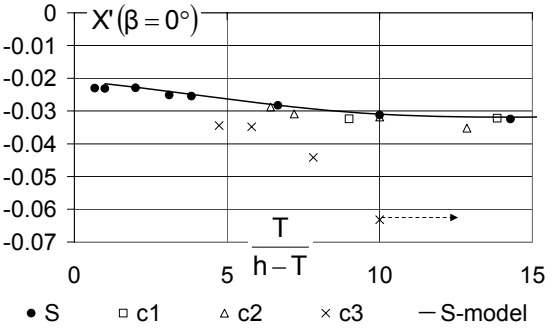

Figure 10.5. Ship model D. Longitudinal force at a drift angle of 0°. Influence of under keel clearance and bottom.

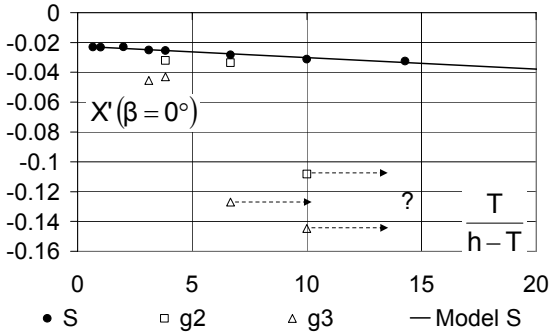

Figure 10.6. Ship model D. Longitudinal force at a drift angle of 0°. Influence of under keel clearance and bottom.

Figure 10.5 shows another example for a drift angle of 0°. X'(β=0°) does not seem to increase more when the under keel clearance is decreasing from 10% of draft until 7% of draft. A quadratic relationship as given in (9.12) results in a decrease of X'(β) when the under keel clearance decreases further:

- It is physically hard to explain why the ship resistance would decrease with decreasing under keel clearance;
- Accordingly the hydrodynamically equivalent depth concept to predict the longitudinal force cannot be applied.

As a consequence ξ_2 in (9.12) is chosen zero. Similar conclusions can be drawn for other drift angles, but even then there are conditions where the use of the hydrodynamically equivalent depth and the fluidization parameter only is not sufficient to predict the longitudinal force. This is especially the case where the ship penetrates into mud layers of a high viscosity and density, see the F^0 term in (3.1) and Figure 10.6.

In these cases an additional mud related term is needed as expressions (10.6) or (10.7):

$$F^0 = X'(|\beta|)_{mud} = [a_0(|\beta|) + \mu' a_\mu(|\beta|)]\Pi \tag{10.11}$$

which turns zero when the ship's keel does not penetrate into the mud. The model for X'(β) is then:

$$X'(|\beta|) = X'(|\beta|)_{deep} + \frac{T}{h^*(|\beta|) - T}\xi_1(|\beta|) + \left(\frac{T}{h^*(|\beta|) - T}\right)^2 \xi_2(|\beta|) + X'(|\beta|)_{mud} \tag{10.12}$$

where $X'(|\beta|)_{mud}$ is given by (10.11) and h* by (10.4) and (10.10).

Yaw and chi function for the longitudinal force

Figure 10.7 shows the under keel clearance effect on the longitudinal force at a yaw rate angle of 25°. As with the drift function an application of the hydrodynamically equivalent depth is not sufficient for accurate prediction of X'(γ) when the ship is navigating in contact with the mud layer. An additional mud related term is needed, as in (10.11):

$$X'(\gamma)_{mud} = [a_0(\gamma) + \mu' a_\mu(\gamma)]\Pi \tag{10.13}$$

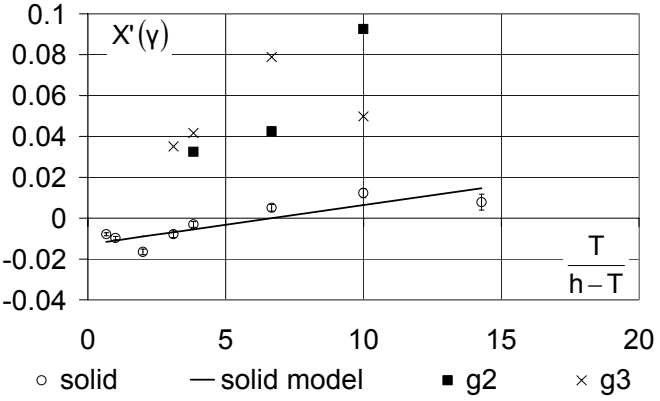

Figure 10.7. Ship model D. Longitudinal force at a yaw angle of 25°. Influence of under keel clearance and bottom.

The fluidization of the mud layer is given by:

$$\Phi(\gamma) = (a_0(\gamma) + \mu' a_\mu(\gamma))\Pi + \Phi_{00}(\gamma) + \frac{h_2}{T}[\Phi_{h0}(\gamma) + \mu' \Phi_{h\mu}(\gamma)] \tag{10.14}$$

The model for the yaw function for the longitudinal force is thus:

$$X'(\gamma) = X'(\gamma)_{deep} + \frac{T}{h^*(\gamma) - T}\xi(\gamma) + X'(\gamma)_{mud} \tag{10.15}$$

where $X'(\gamma)_{mud}$ is given by (10.13) and h* by (10.4) and (10.14).

For X'(χ) an analogous model can be built:

$$X'(\chi) = X'(\chi)_{deep} + \frac{T}{h^*(\chi) - T}\xi(\chi) + X'(\chi)_{mud} \tag{10.16}$$

With

$$X'(\chi)_{mud} = \left[a_0(\chi) + \mu' a_\mu(\chi)\right]\Pi \tag{10.17}$$

And h* a function of:

$$\Phi(\chi) = a_0(\chi)\Pi + \Phi_{00}(\chi) + \frac{h_2}{T}\Phi_{h0}(\chi) + \mu'\Phi_{0\mu}(\chi) \tag{10.18}$$

10.3.2 The sway force

10.3.2.1 Acceleration dependent terms

Sway added mass

Figure 10.8 represents the under keel clearance dependent model for the sway added mass. Again a hydrodynamically equivalent depth can be defined. The fluidization parameter has been determined for different mud layers and is shown on Figure 10.9.

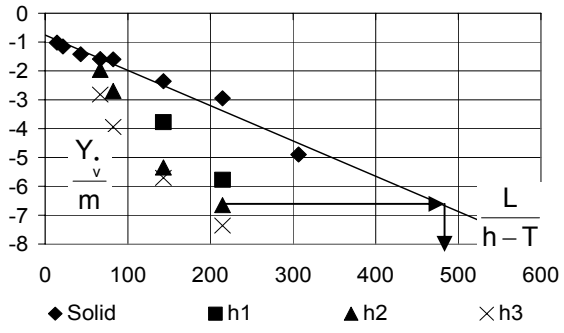

Figure 10.8. Sway added mass, ship model D, u > 0, 0 rpm. Illustration of the effect of the fluidization parameter.

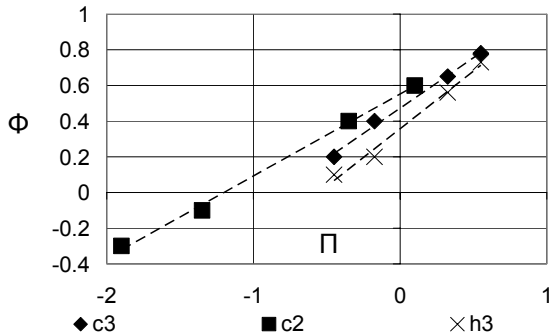

Figure 10.9. Fluidization for the sway added mass, ship model D, u > 0, 0 rpm.

The slope of the Φ(Π) characteristic is represented for different viscosities in Figure 10.10a. The relationship is obviously linear as it is for the relationship between fluidization parameter at Π=0 and the viscosity, see Figure 10.10b. The proposed model for the fluidization parameter is consequently:

$$\Phi = \left(a_0 + \mu' a_\mu\right)\Pi + \Phi_{00} + \mu'\Phi_{0\mu} + \frac{h_2}{T}\left[\Phi_{h0} + \mu'\Phi_{h\mu}\right] \qquad (10.19)$$

With (10.19) the hydrodynamically equivalent depth h* can be determined to predict the sway force using (9.15) with h* instead of h. For all the force components linear relationships between the fluidization parameter and the mud viscosity or the mud layer thickness can be observed.

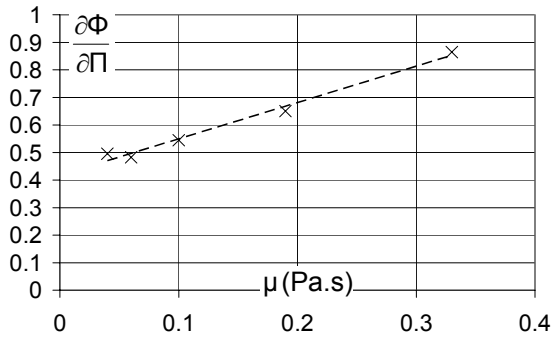

Figure 10.10a. Sway added mass, ship model D, u > 0, 0 rpm. Relationship between viscosity and the slope of the Φ(Π) characteristic for different mud layers.

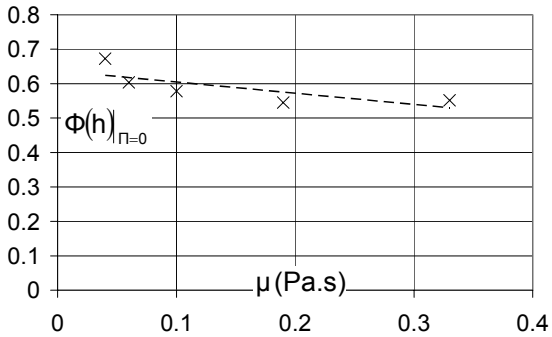

Figure 10.10b. Sway added mass, ship model D, u > 0, 0 rpm. Relationship between the viscosity and $\Phi(h)_{\Pi=0}$ for different mud layers.

Yaw acceleration derivative for the sway force

Figure 10.11 shows the yaw acceleration derivative for the sway force. Determination of the fluidization parameter results in graph 10.12a, which suggests the following model:

$$\Phi(\mathrm{sgn}(u)) = \left[a_0(\mathrm{sgn}(u)) + \mu' a_\mu(\mathrm{sgn}(u))\right]\Pi + \Phi_{00}(\mathrm{sgn}(u)) + \mu'\Phi_{0\mu}(\mathrm{sgn}(u)) + \frac{h_2}{T}\left[\Phi_{h0}(\mathrm{sgn}(u)) + \mu'\Phi_{h\mu}(\mathrm{sgn}(u))\right] \qquad (10.20)$$

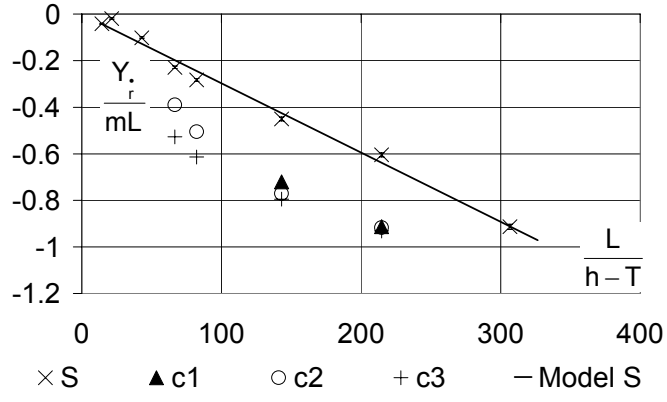

Figure 10.11. Yaw acceleration derivative for the sway force, ship model D, u > 0, 0 rpm, v=0. Influence of under keel clearance and bottom condition.

The yaw acceleration derivative can now be determined with (9.16), replacing h by h*. In Figure 10.12a two grey zones have been drawn. The darkest zone indicates the physical boundary of the fluidization parameter: the fluidization parameter can never be smaller than the keel penetration parameter, as this would result in a condition where the ship is navigating at a negative under keel clearance referred to a (virtual) solid bottom.

The percentage of fluidization, or the amount of material that is behaving like water, while the rest is behaving like solid, is represented in Figure 10.12b. A minimum seems to occur at small positive under keel clearances, which shows that the highest influence of the mud layer is found in these conditions. This is rather relative, as further penetration, though it will soften the effect of the mud, will have a more dominant effect on the under keel clearance dependent term.

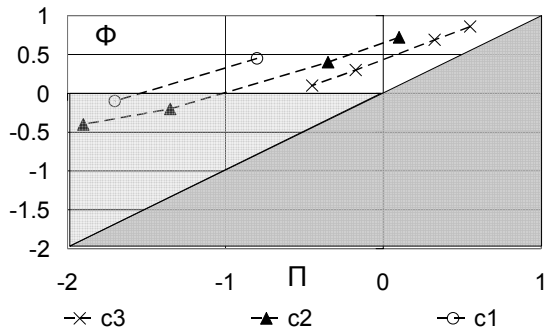

Figure 10.12a. Fluidization for the yaw acceleration derivative for the sway force, ship model D, u > 0, 0 rpm, v =0.

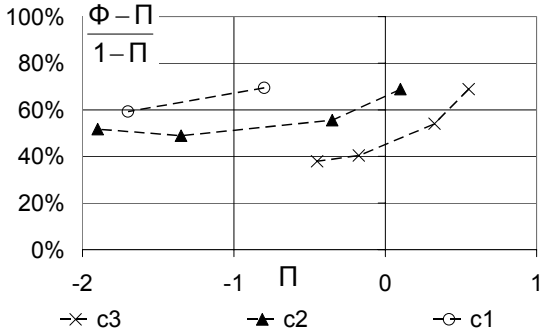

Figure 10.12b. Percentage of fluidization for the yaw acceleration derivative for the sway force, ship model D, u > 0, 0 rpm, v =0.

The lightest grey zone on Figure 10.12a indicates the zone where the hydrodynamically equivalent depth is smaller than the height of the water layer, which can be ascribed to the undulations of the interface as mentioned in 10.3.1.2. It can be expected that the fluidization parameter will not turn more negative when the under keel clearance referred to the mud increases, as the magnitude of the rising of the interface is limited and decreases with increasing under keel clearance. The suggestion is that a minimal fluidization parameter is obtained at Π = -2, which means that the distance between the top of the mud layer and the ship's keel is 2 times the thickness of the mud layer. From there on the fluidization parameter can linearly return to zero once Π = -4. This assumption is acceptable because:

- It corresponds either with a very large under keel clearance above a thick mud layer, so that the mud will probably not be affected by the passing ship and would behave as a solid bottom. The hydrodynamically equivalent depth is then equal to the height of the water layer. The possible error of the assumption is small as the under keel clearance related forces are already small;
- Or it corresponds with a small under keel clearance above a thin mud layer. In this case the undulations of the mud layer will be of no importance and it is unlikely that the manoeuvring behaviour would be affected. The possible error will also be small as a thin mud layer has only a small effect in the calculation of the hydrodynamically equivalent depth.

Of course the above assumptions can be applied to every force component of the ship.

10.3.2.2 Velocity dependent terms

Drift function for the sway force

Figure 10.13 shows an example of the drift function at a drift angle of 90°. As in the previous paragraphs the fluidization parameter can be determined using linear functions of viscosity and mud layer thickness. Although during regression analysis it seemed that more accurate results were obtained if the under keel clearance depended model (9.17) was replaced by a model that takes the square root of L/(h-T) into account.

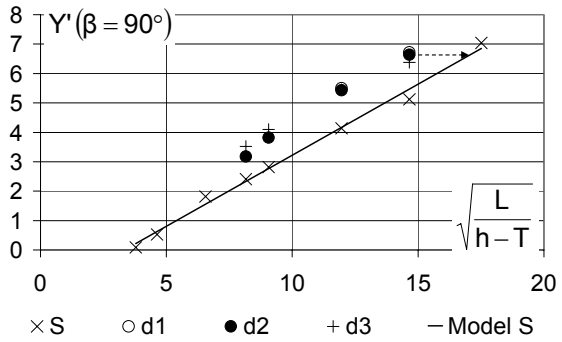

Figure 10.13. Drift function for the sway force. Ship model D, β = 90°.

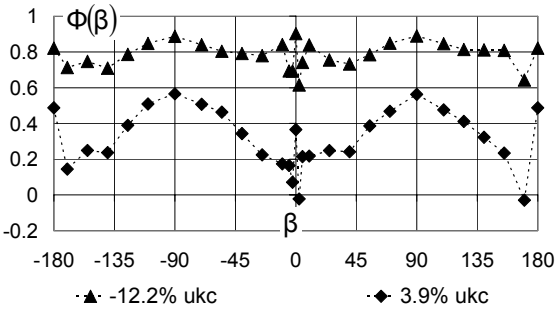

Figure 10.14. Fluidization function for the drift function of the sway force. Ship model D, mud layer b3.

The resulting model for the fluidization parameter is:

$$\Phi(\beta) = a(\beta)\Pi + \Phi_{00}(\beta) + \mu'\Phi_{0\mu}(\beta) + \frac{h_2}{T}\left[\Phi_{h0}(\beta) + \mu'\Phi_{h\mu}(\beta)\right] \qquad (10.21)$$

so that the drift function can be determined:

$$Y'(\beta) = Y'(\beta)_{deep} + \sqrt{\frac{L}{h^*(\beta) - T}}\xi(\beta) \qquad (10.22)$$

Although the model with the square root of the under keel clearance is more accurate, the reader should pay attention to the disadvantage that the under keel clearance independent term in (10.22) does not represent the drift function in deep water conditions anymore, see the topic concerning truncation in 9.3.2.4.

An example of the fluidization functions that were obtained through regression analysis is represented in Figure 10.14. Observe how the fluidization parameter is maximal at maximal drift, which can be ascribed to the fact that more mud will be likely to move and thus behave watery when a ship is subjected to pure sway.

Yaw function for the sway force

An example of the yaw function is given in Figure 10.15, with the corresponding determination of the fluidization parameter in Figure 10.16.

Again a similar model can be used for the fluidization parameter:

$$\Phi(\gamma) = a(\gamma)\Pi + \Phi_{00}(\gamma) + \mu'\Phi_{0\mu}(\gamma) + \frac{h_2}{T}\left[\Phi_{h0}(\gamma) + \mu'\Phi_{h\mu}(\gamma)\right] \qquad (10.23)$$

(9.18) used with the hydrodynamically equivalent depth h* allows the prediction of the yaw function for the sway forces in muddy areas.

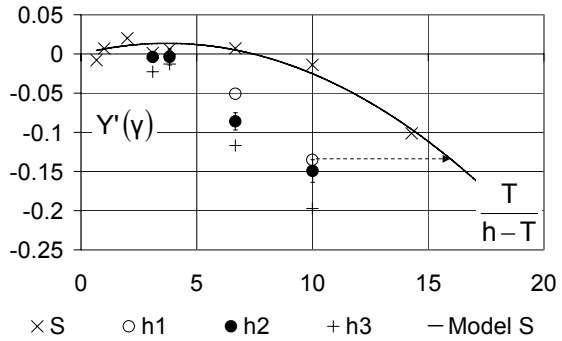

Figure 10.15. Yaw function for the sway force, ship model D, u > 0, 0 rpm, γ = -30°. Illustration of the effect of the fluidization parameter.

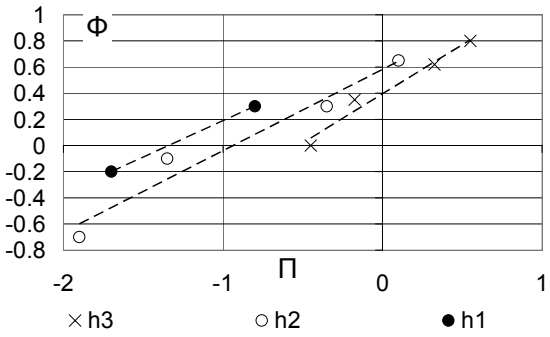

Figure 10.16. Fluidization for the yaw function for the sway force, ship model D, u > 0, 0 rpm, γ = -30°.

Chi function for the sway force

For the chi function a similar fluidization function can be built:

$$\Phi(\chi) = a(\chi)\Pi + \Phi_{00}(\chi)\left\{ + \mu'\Phi_{0\mu}(\chi) + \frac{h_2}{T}\Phi_{h0}(\chi)\right\} \qquad (10.24)$$

The terms between braces can be omitted as they have large standard deviations, which actually means that the fluidization does not depend significantly on the mud layer composition. With (9.19) the chi function can be determined.

10.3.3 The yawing moment

10.3.3.1 Acceleration dependent terms

Both the sway acceleration derivative and the yaw added moment of inertia use the same formulation for the fluidization parameter as for the sway force, see (10.19) and (10.20), but with different regression coefficients.

10.3.3.2 Velocity dependent terms

Drift function for the yawing moment

Paragraph 9.3.1.3 mentioned it was more convenient to model the under keel clearance effect of the application point of Y'(β) rather than modelling N'(β), but the model of the effect of the mud layer on the application point $x'_Y(\beta)$ does not

produce accurate results. The problem was solved by introducing a new model for the under keel clearance dependence:

$$N'(\beta) = N'(\beta)_{deep} + \sqrt{\frac{T}{h-T}}\xi_1(\beta) + \frac{T}{h-T}\xi_2(\beta) \qquad (10.25)$$

Figure 10.17 shows the motivation for using (10.25).

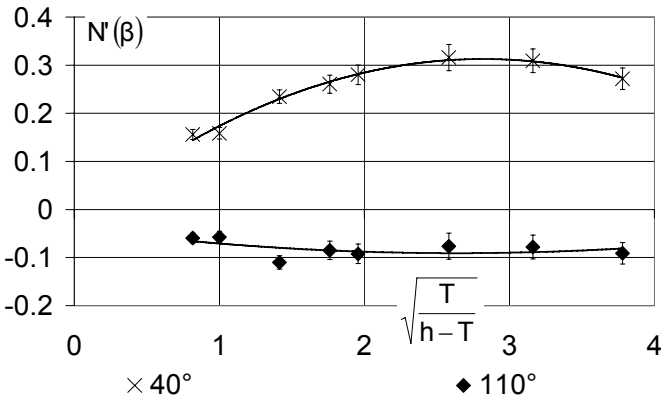

Figure 10.17. Drift function for the yawing moment, ship model D, 0 rpm, β = 40° and 110°.

The effect of the mud can be modelled using (10.25) with the hydrodynamically equivalent depth h* instead of the total depth h. h* is determined with the following fluidization parameter:

$$\Phi(\beta) = \left[a_0(\beta) + \mu' a_\mu(\beta)\right]\Pi + \Phi_{00}(\beta) + \mu'\Phi_{0\mu}(\beta) + \frac{h_2}{T}\Phi_{h0}(\beta) \qquad (10.26)$$

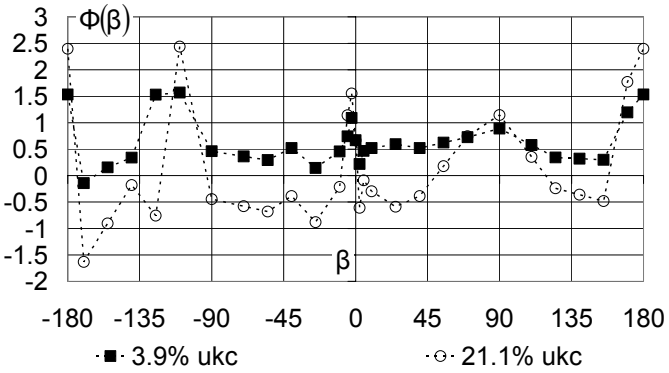

Figure 10.18. Drift function for the yawing moment, ship model D, 0 rpm, β = 40° and 110°. Under keel clearances referred to the top of a mud layer b2.

An example of the fluidization parameter is given in Figure 10.18. Special attention is given to the fact that the fluidization parameter has sometimes values larger than 1, which would physically mean that the hydrodynamically equivalent depth h* is larger than the total depth h. Those high fluidization parameters are the result of the regression analysis. Mostly they represent errors on small values as those that occur at 0° or 180° of drift. In other cases, like 125° of drift, the regression routine tries to soften the under keel clearance dependency when the measured force is lower than expected. It would be physically more correct if the fluidization parameter were limited to 1, but the author has chosen to give higher priority to a good fitting, as the final goal of the

mathematical model is an accurate manoeuvring behaviour in a ship manoeuvring simulator.

Furthermore the results are not symmetrical as they should be. This can be ascribed to the fact that for most drift angles the under keel clearance has little effect on the yawing moment, see for example β=110° in Figure 10.17. The value for fluidization parameter acting on the under keel clearance related terms will therefore be less significant, as is the difference between β=110° and β=-110° in Figure 10.18.

Yaw function for the yawing moment

Figure 10.19 represents the determined fluidization parameters for the thickest mud layers at a yawing angle of -40°. Once more a linear relationship between the fluidization parameter and the keel penetration parameter is possible. With regression analysis the following model is found:

$$\Phi(\gamma) = a(\gamma)\Pi + \Phi_{00}(\gamma) + \mu'\Phi_{0\mu}(\gamma) + \frac{h_2}{T}\left[\Phi_{h0}(\gamma) + \mu'\Phi_{h\mu}(\gamma)\right] \qquad (10.27)$$

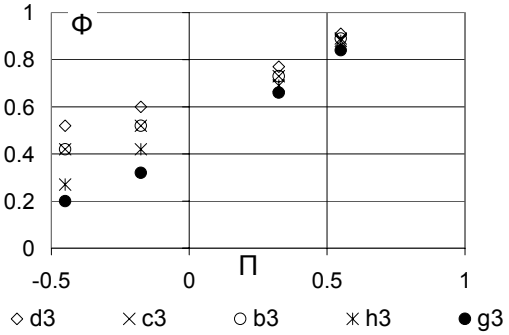

Figure 10.19. Yaw function for the yawing moment, ship model D, 0 rpm, γ = -40°. Fluidization parameter for the thickest mud layers.

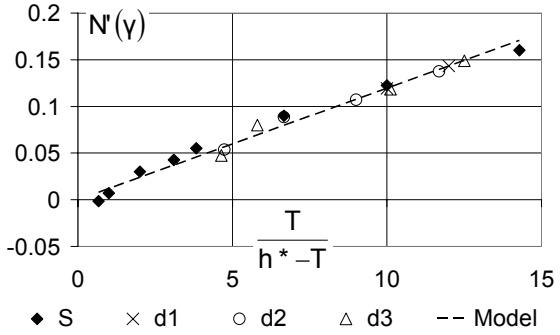

Figure 10.20. Yaw function for the yawing moment, ship model D, 0 rpm, γ = -40°. Evaluation of the model of hydrodynamically equivalent depth.

In Figure 10.19 a slight influence of the mud composition on the slope can be observed, which is not reflected in (10.27). On the other hand model (9.24), with the hydrodynamically equivalent depth, allows a very good prediction of the yaw function, as can be seen in Figure 10.20.

Chi function for the yawing moment

An analogous expression for the fluidization parameter can be built:

$$\Phi(\chi) = a(\chi)\Pi + \Phi_{00}(\chi) + \mu'\Phi_{0\mu}(\chi) + \frac{h_2}{T}\Phi_{h0}(\chi) \qquad (10.28)$$

With the definition of the hydrodynamically equivalent depth h*, (9.25) can be evaluated with good results in muddy navigation areas.

10.4 Modelling of the propeller forces

10.4.1 Thrust

10.4.1.1 Bollard pull

Equation (9.27) predicts the behaviour of the thrust in bollard pull conditions as a function of the under keel clearance. In order to be able to extend this model to the concept of hydrodynamically equivalent depth in muddy areas, the model has been represented in Figure 10.21 with some series in muddy areas. It can clearly be observed that the bollard pull thrust decreases significantly when a mud layer is present. The difference is such that no hydrodynamically equivalent depth can be defined to use (9.21) in muddy areas.

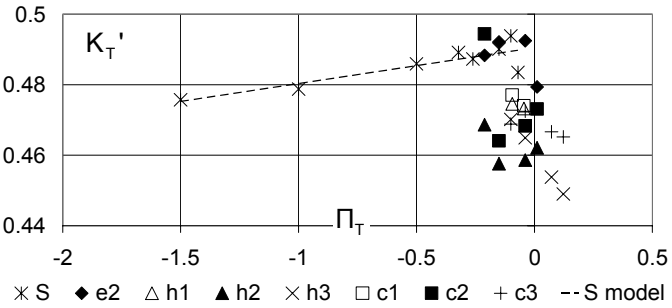

Figure 10.21. Thrust coefficient in bollard pull conditions as a function of the under keel clearance. Influence of the bottom condition, ship model D, positive propeller rate.

A redefinition of the model above a solid bottom is required. When the data points above a solid bottom are analysed in detail, one can detect a decrease of the thrust once the under keel clearance reaches a value of 7% of the ship's draught. With the further decrease of the bollard pull in muddy areas, this suggests the use of a quadratic model as a function of the under keel clearance, which is shown in Figure 10.22.

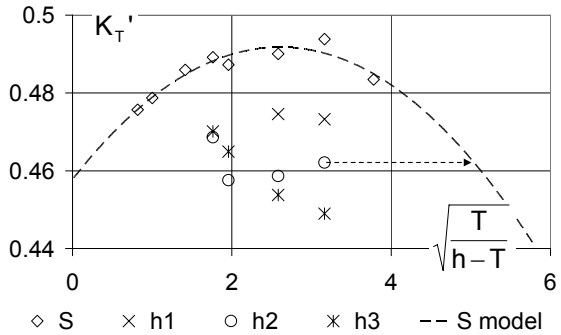

Figure 10.22. Thrust coefficient in bollard pull conditions as a function of the under keel clearance. Influence of the bottom condition, ship model D, positive propeller rate.

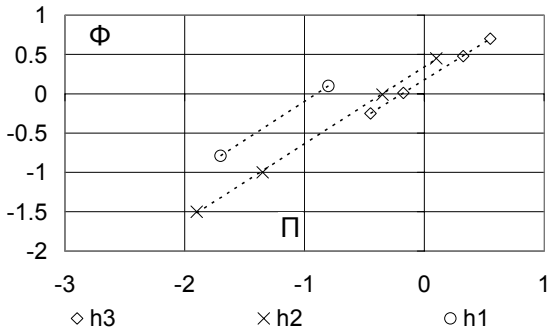

Figure 10.23. Thrust coefficient in bollard pull conditions. Fluidization parameter for mud layer h, ship model D, positive propeller rate.

(9.27) is then to be replaced by:

$$K_{(J=0)} = K_{(J=0,h^*=\infty)} + \sqrt{\frac{T}{h^*-T}}y_1 + \frac{T}{h^*-T}y_2 \qquad (10.29)$$

with h* the hydrodynamically equivalent depth, which can be defined by a fluidization parameter. When the muddy bottom is considered as an extrapolation of the solid bottom conditions[3], a fluidization parameter as shown in Figure 10.23 can be determined. Again an acceptable linear relationship with the keel penetration parameter and with the layer thickness can be observed.

The question arises which parameter should be used to model the mud composition. Both the mud viscosity and the mud density have been used to carry out regression analysis for the propulsion related forces, with more fruitful results when considering the mud density. This is not so astonishing as the propulsion behaviour in muddy areas is severely affected by the rising of the interface, see 6.4.2, which is a result of the differences in densities between the water and the mud layer. Introducing the non-dimensional density:

$$\rho^* = \frac{\rho_2 - \rho_1}{\rho_1} \tag{10.30}$$

the fluidization parameter for bollard pull thrust can be written as:

$$\Phi(\mathrm{sgn}(n)) = a(\mathrm{sgn}(n))\Pi + \Phi_{00}(\mathrm{sgn}(n)) + \frac{h_2}{T}\left[\Phi_{h0}(\mathrm{sgn}(n)) + \rho^* \Phi_{h\rho}(\mathrm{sgn}(n))\right] \tag{10.31}$$

as a linear relationship between the mud density and the fluidization can be observed, see Figure 10.24.

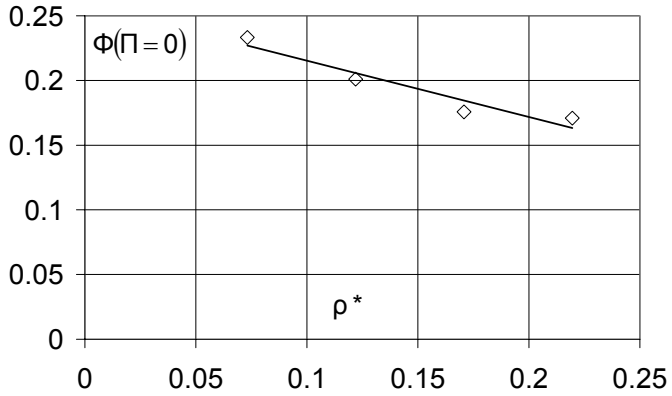

Figure 10.24. Bollard pull thrust, fluidization parameter for the thickest mud layers at zero keel penetration parameter, ship model D, positive propeller rate.

10.4.1.2 Wake factor

The $K_T(J')$ characteristic (9.28) has also been rewritten as:

$$K = K_{(J=0)} + \left[x_{2(h^*=\infty)} + \sqrt{\frac{T}{h^* - T}} x_1 \right] J' \tag{10.32}$$

The coefficient of J' has been represented in Figure 10.25 for different mud layers. The linear model above a solid bottom provides good results, but some

[3] Mathematically speaking two different fluidization parameters can be obtained, but from a physical point of view mud is considered as an extrapolation of a shallow water condition, and not of a deep water condition.

variations between the model and the data points can be observed. In fact, a zone of significance can be created, which contains all the data points above a solid bottom. This is the grey zone in Figure 10.25. All data points that are within this zone are not significantly different from the data points above a solid bottom. This is certainly the case for data points that represent conditions with highly viscous mud layers. There is no reason to reject the same model for these data points as for the ones above a solid bottom. In this case the hydrodynamically equivalent depth $h^* = h_1+h_2$, or:

$$\Phi = 1 \tag{10.33}$$

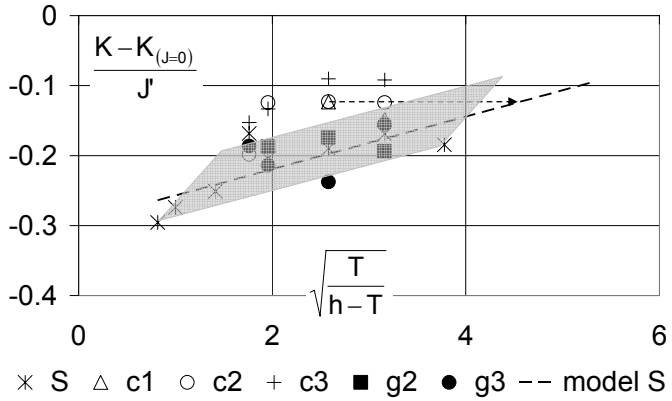

Figure 10.25. Coefficient of J' from (10.32), ship model D, influence of bottom condition.

The data points of mud layers of a lower viscosity are outside the boundaries of this zone. A fluidization parameter has to be defined to take the effects of the mud layer into account:

$$\Phi = \left[a_0 + \rho^* a_\rho\right]\Pi + \Phi_{00} + \rho^* \Phi_{0\rho} + \frac{h_2}{T}\left[\Phi_{h0} + \rho^* \Phi_{h\rho}\right] \tag{10.34}$$

With the fluidization parameters (10.33) and (10.34) the wake factors in muddy areas can be defined:

$$w(\varepsilon^*) = w(\varepsilon^*)_{(h=\infty)} + \sqrt{\frac{T}{h^* - T}}\xi(\varepsilon^*) \tag{10.35}$$

which replaces (9.31). Equation (9.32) remains valid for quadrants II, III and IV. The choice of equation (10.34) or (10.33) depends on the viscosity of the mud layer:

- For mud layers with a viscosity of 0.12 Pa.s or less (10.34) is used;
- For mud layers with a viscosity of 0.18 Pa.s or more (10.33) is used;
- For intermediate viscosities, a linear interpolation between (10.33) and (10.34) as a function of the mud viscosity is the most appropriate.

These values of the viscosity correspond with the definition of the critical viscosity to asses the undulations of the interface, see Chapter 5:

- Mud layers of a lower viscosity have their rising of the interface mostly near the ship's propeller. The calculation of the hydrodynamically equivalent depth corresponds with a density related fluidization parameter, which results in a hydrodynamically equivalent depth that is lower than the real depth. The wake factors increase and the thrust efficiency decreases.
- Mud layers of a higher viscosity have their rising usually amidships. The effect of the mud layer is restricted to bollard pull conditions. The influence of placing the propeller behind the ship's hull is equal to the influence of a solid bottom condition with depth $h = h^* = h_1+h_2$. The fluidization parameter for the wake factor is consequently 1.

10.4.2 Torque

10.4.2.1 Bollard pull

For bollard pull conditions (9.27) has been rewritten as:

$$K_{(J=0)} = K_{(J=0,h^*=\infty)} + \sqrt{\frac{T}{h^* - T}}\, y \qquad (10.36)$$

Figure 10.26 shows the torque coefficient in bollard pull conditions. A fluidization parameter can be determined, which is shown in Figure 10.27. Although the composition of the mud layer seems to influence the slope of the Φ(Π)-characteristic, this is not reflected in the regression model of the fluidization parameter, which is of the same form as (10.31).

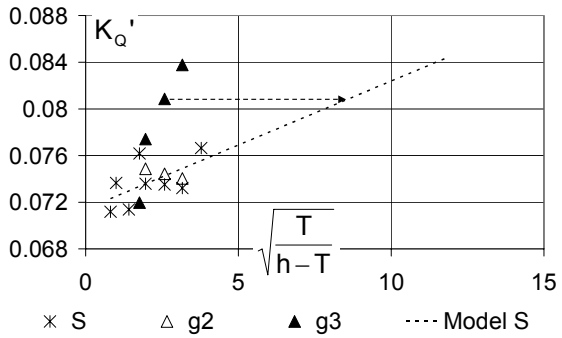

Figure 10.26. Torque coefficient in bollard pull conditions as a function of the under keel clearance. Influence of the bottom condition, ship model D, positive propeller rate.

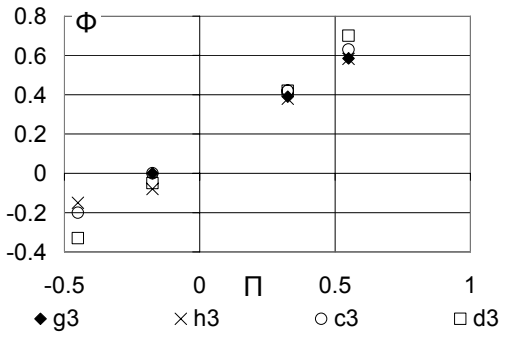

Figure 10.27. Torque coefficient in bollard pull conditions. Fluidization parameter for the thickest mud layers, ship model D, positive propeller rate.

10.4.2.2 Wake factor

The $K_Q(J')$ characteristic is like (10.32), but the fluidization parameter for the wake of the torque does not depend on the viscosity of the mud layer. For all mud layers a fluidization parameter has to be determined as given by (10.34). The wake factors for the torque can then be found using (10.35).

10.4.3 Thrust deduction

10.4.3.1 Bollard pull

The thrust deduction in bollard pull conditions does not seem to be significantly influenced by the mud composition or the mud layer thickness. Figure 10.28 shows the measured force versus the modelled one when (9.34) is used to predict the thrust deduction. A good correlation can be observed. Although some outliers occur for mud layer F, (9.34) can be used to predict the bollard pull thrust deduction above any bottom condition.

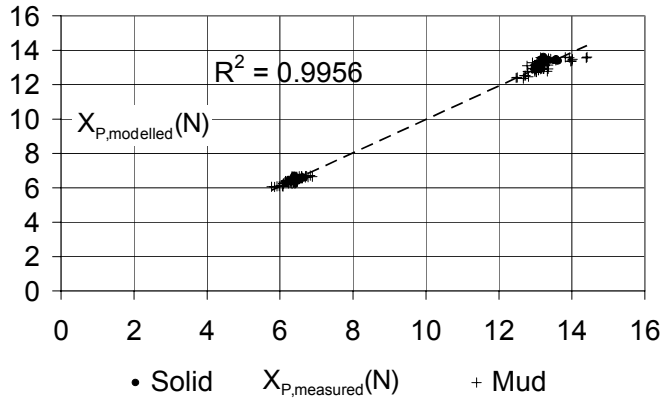

Figure 10.28. Measured propeller induced longitudinal force versus the modelled one, ship model D, positive propeller rate, bollard pull condition.

10.4.3.2 The four quadrants

The use of the principle of hydrodynamically equivalent depth h* was difficult to apply to the modelling of the thrust deduction factor, therefore the second method described in 10.1 will be used. Consider equation (9.35), which can be rewritten as:

$$t = t_{BP} + x_{solid}\left(\frac{h}{T}\right)\varepsilon^* + y_{solid}\left(\frac{h}{T}\right)\varphi^* \qquad (10.37)$$

A set of coefficients x_{mud} and y_{mud}, taking the mud layer characteristics into account, exists, so that

$$t = t_{BP} + \left[x_{solid} + x_{mud}\right]\varepsilon^* + \left[y_{solid} + y_{mud}\right]\varphi^* \qquad (10.38)$$

allows prediction of the thrust deduction in muddy navigation areas. Both x_{mud} and y_{mud} have been represented in Figure 10.29:

- When the ship navigates above the mud layer x_{mud} and y_{mud} are small;
- Once the keel penetrates the mud layer, larger values are reached, especially with highly viscous mud layers.

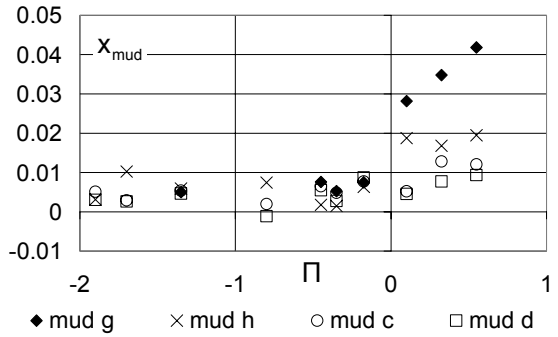

Figure 10.29a. x_{mud} from (10.38), ship model D, 1st quadrant.

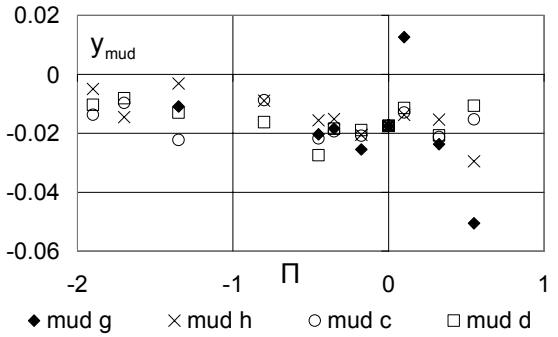

Figure 10.29b. y_{mud} from (10.38), ship model D, 1st quadrant.

When looking at the standard deviation of the coefficients during regression analysis, it seemed that x_{mud} and y_{mud} can be neglected when navigating at positive under keel clearance. This allows a simplification of the model, without jeopardizing the accuracy of prediction. If the ship penetrates the mud layer the following model is proposed:

$$k_{mud} = \Pi(k_1 + \mu' k_2) \tag{10.39}$$

with k_{mud} representing either x_{mud} or y_{mud}. This method can successfully be applied to the other quadrants as well. (9.37) and (9.38) for example can be written as (ε^* is expressed in degrees):

$$t = \left(\varepsilon^{*2} - 180^{\circ 2}\right)\left(x_{solid} + x_{mud}\right) + \left(\varepsilon^* + 180^{\circ}\right)\left(y_{solid} + y_{mud}\right) \tag{10.40}$$

$$t = t_{BP} + \left[x_{solid} + x_{mud}\right]\varepsilon^* + \left[y_{solid} + y_{mud}\right]\gamma^* \tag{10.41}$$

Some coefficients of (10.40-10.41) are represented in Figure 10.30.

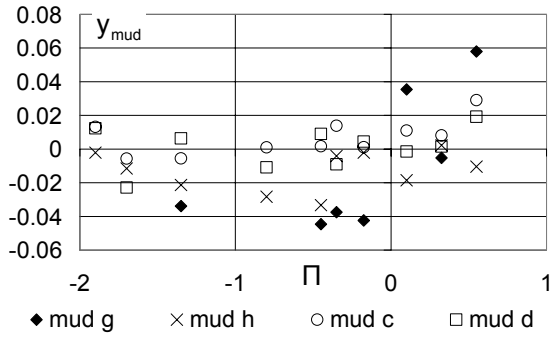

Figure 10.30a. y_{mud} from (10.40), ship model D, 3rd quadrant.

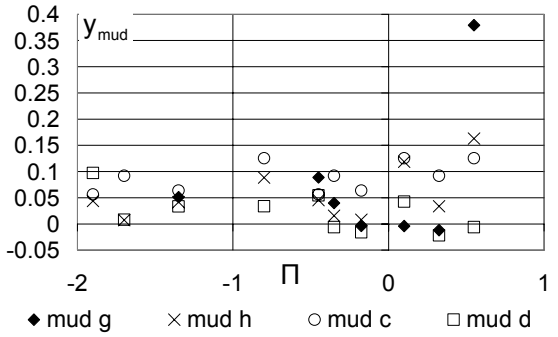

Figure 10.30b. y_{mud} from (10.41), ship model D, 4th quadrant.

The models to predict the thrust deduction in muddy navigation conditions are, in a nutshell:

- Quadrant 1:

$$t = t_{BP} + \left[x_1 - y_1 \frac{h}{T} + \Pi'(\alpha_1 + \mu'\beta_1) \right] \varepsilon^* + \left[x_2 + y_2 \frac{h}{T} - \Pi'(\alpha_2 + \mu'\beta_2) \right] \varphi^* \quad (10.42)$$
$$t_{BP} \le t < 1$$

- Quadrant 2:

$$t = (\varepsilon^* - 180°) \left(x + y \frac{T}{h-T} + \Pi'(\alpha - \mu'\beta) \right) \quad (10.43)$$
$$-1 < t \le 0$$

- Quadrant 3:

$$t = (\varepsilon^{*2} - 180°^2) \left(x_1 - y_1 \frac{T}{h-T} + \Pi'(\alpha_1 + \mu'\beta_1) \right) +$$
$$(\varepsilon^* + 180°) \left(x_2 - y_2 \frac{T}{h-T} + \Pi'(\alpha_2 + \mu'\beta_2) \right) \quad (10.44)$$
$$0 \le t < 1$$

- Quadrant 4:

$$t = t_{BP} + \left[-x_1 + y_1 \frac{T}{h-T} + \Pi'(\alpha_1 + \mu'\beta_1) \right] \varepsilon^* +$$
$$\left[x_2 + y_2 \frac{T}{h-T} - \Pi'(\alpha_2 - \mu'\beta_2) \right] \gamma^* \quad (10.45)$$
$$t_{BP} \le t < 1$$

In which:

- Π' = Π for $\Pi > 0$;
  = 0 for $\Pi < 0$;
- x_i, y_i, α_i and β_i are positive regression coefficients;
- ε^*, φ^* and γ^* are expressed in degrees.

10.4.4 Propeller induced sway force and yawing moment

10.4.4.1 Hydrodynamic inertia

First quadrant

The influence of the under keel clearance on the hydrodynamic inertia was modelled with (9.39). Figure 10.31 shows the fluidization parameter that can be determined to predict the propeller influence on the yaw acceleration derivative of the sway force. As always a linear model as a function of the keel penetration parameter is possible. Both for the sway acceleration and for the yaw acceleration of the sway force, the following model of the fluidization parameter can be used:

$$\Phi = \left[a_0 + \mu' a_\mu \right] \Pi + \Phi_{00} + \mu' \Phi_{0\mu} + \frac{h_2}{T} \left[\Phi_{h0} + \mu' \Phi_{h\mu} \right] \quad (10.46)$$

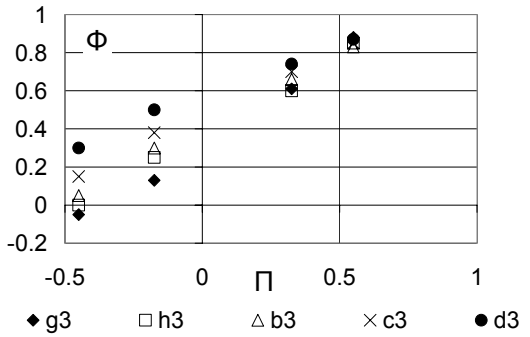

Figure 10.31. Fluidization parameter for the yaw acceleration derivative of the sway force, influence of propeller action, ship model D, 1st quadrant, thickest mud layers.

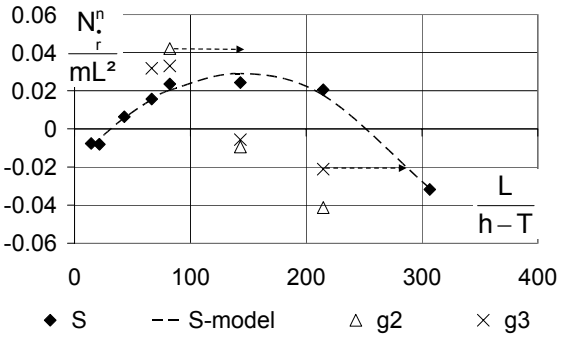

Figure 10.32. Yaw added moment of inertia, influence of propeller action, ship model D, 1st quadrant, thickest mud layers.

Figure 10.32 represents the yaw added moment of inertia due to propeller action. Above a solid bottom a linear model as a function of the under keel clearance was suggested, based on the assumption of unreliability of the measured value at the smallest under keel clearance. However, the measurements in muddy areas indicate that a quadratic model as a function of the under keel clearance is more appropriate:

$$N'^{n}_{r} = N'^{n}_{r\,deep} + \frac{L}{h^* - T}\xi_1 + \left(\frac{L}{h^* - T}\right)^2 \xi_2 \qquad (10.47)$$

The hydrodynamically equivalent depth h* can be determined with the following fluidization parameter:

$$\Phi = \left[a_0 + \mu' a_\mu\right]\Pi + \Phi_{00} + \frac{h_2}{T}\Phi_{h0} \qquad (10.48)$$

whose formulation is valid for both N'^{n}_{r} and N'^{n}_{v}. The under keel clearance dependence of the latter has still to be determined with (9.39).

Second quadrant

In the second quadrant the hydrodynamic inertia cannot be defined, due to the occurrence of oscillations. Their value is therefore set to zero, as possible effects are already included in the modelling of the oscillations.

Third quadrant

The effect of propeller action on the hydrodynamic inertia in the third quadrant, can only be analysed with the yaw acceleration, as no harmonic sway tests have been carried out in the third quadrant. Figure 10.33a shows the yaw acceleration derivative of the sway force. Again the measurements in muddy conditions show that a quadratic model as a function of the under keel clearance leads to better results. An analogous model as (10.47) will be used. Some fluidization parameters determined from this model are represented in Figure 10.33b. The model for the fluidization parameter is equal to (10.46).

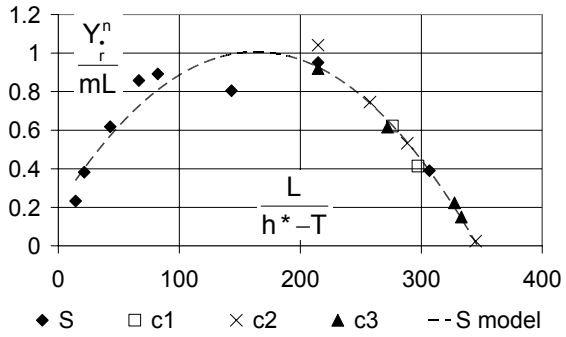

Figure 10.33a. Yaw acceleration derivative of the sway force, influence of propeller action, ship model D, 3rd quadrant, mud layer c.

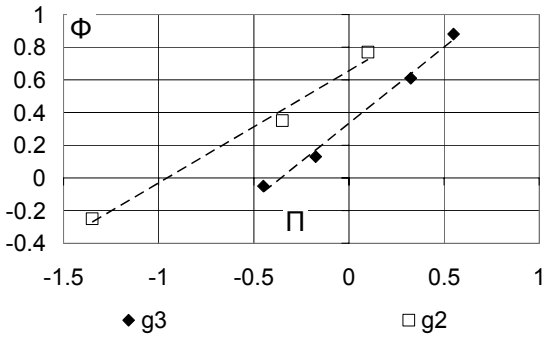

Figure 10.33b. Fluidization parameter for the yaw acceleration derivative of the sway force, influence of propeller action, ship model D, 3rd quadrant, mud layer g.

Unlike in the first quadrant, the under keel clearance effect on the yaw added moment of inertia in the third quadrant is linear. Figure 10.34 shows an example for the fluidization parameter. Some points have larger deviations from the proposed linear model, but the results are still acceptable. The model for the fluidization parameter is (10.46).

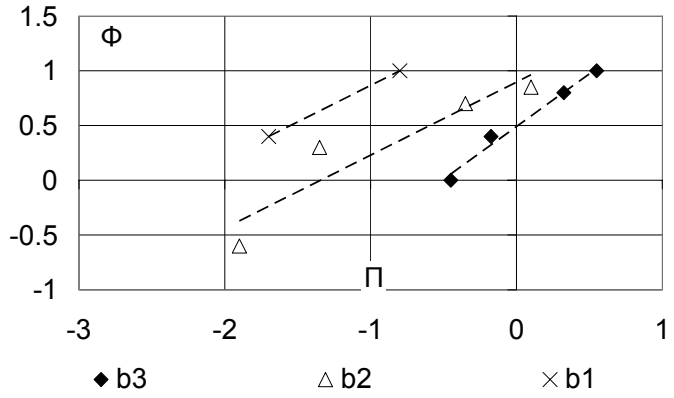

Figure 10.34. Fluidization parameter for the yaw added moment of inertia, influence of propeller action, ship model D, 3rd quadrant, mud layer b.

Fourth quadrant

The observations for the sway force are similar as in the third quadrant. The linear model as a function of the under keel clearance has to be changed to a quadratic one, with good results for the determination of the fluidization parameter, as shown in Figure 10.35. The same model as in the third quadrant will be used.

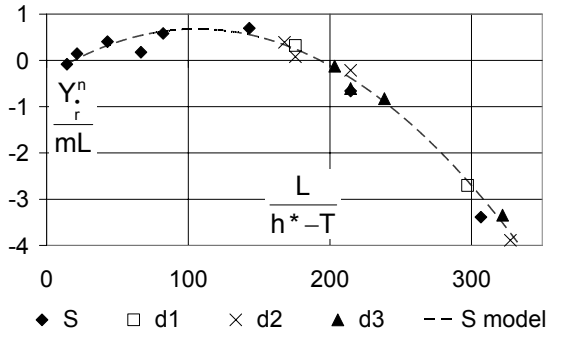

Figure 10.35a. Yaw acceleration derivative of the sway force, influence of propeller action, ship model D, 4th quadrant, mud layer d.

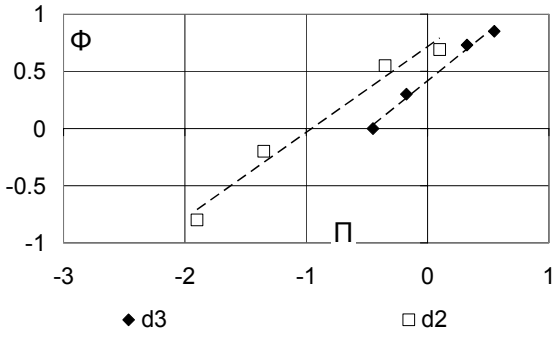

Figure 10.35b. Fluidization parameter for the yaw acceleration derivative of the sway force, influence of propeller action, ship model D, 4th quadrant, mud layer d.

Some complications occur when dealing with the yaw added moment of inertia in the fourth quadrant. Figure 10.36 represents the effect of propeller action on the yaw added moment of inertia. Considering the fact that the maximal non dimensional yaw added moment of inertia without propeller action has magnitude -0.3, propeller action leads to a total yaw added moment of inertia that reinforces the yaw acceleration, see Figure 10.37. This phenomenon can only be ascribed to the presence of oscillations.

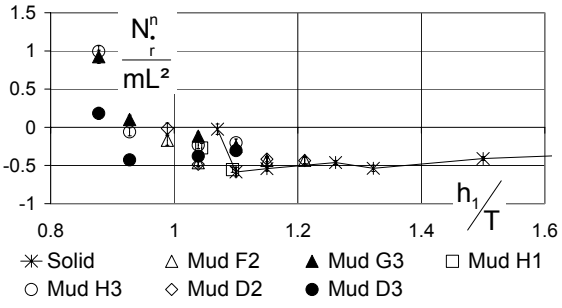

Figure 10.36. Yaw added moment of inertia, influence of propeller action, ship model D, 4th quadrant, influence of under keel clearance and bottom characteristics.

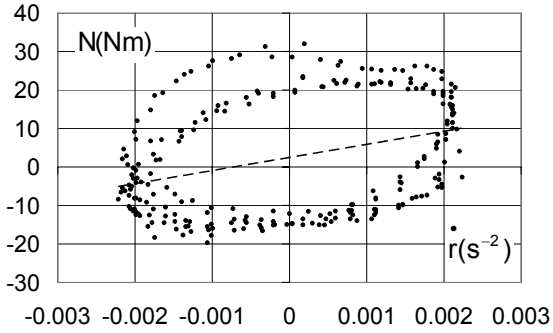

Figure 10.37. Yawing moment as a function of yaw acceleration, ship model D, 4th quadrant, mud g3, -12% under keel clearance.

Paragraph 6.4.4.6 stated that for sufficiently large yaw movements no oscillations occurred. This is when

$$\left|\dot{r}\right| \geq \dot{r}_{os,max} \text{ or } |r| \geq r_{os,max} \tag{6.36}$$

Apparently these limits depend on the bottom condition. When the ship navigates in contact with viscous mud layers oscillations are more likely to occur. The probability of oscillations depends thus on the under keel clearance into the mud and the composition of the mud, see Figure 10.38a. Furthermore the oscillations are not fully developed, which means that they correspond to the condition given between the two squares in Figure 6.52. This is also confirmed by the fact that no apparent oscillations occurred for the sway force.

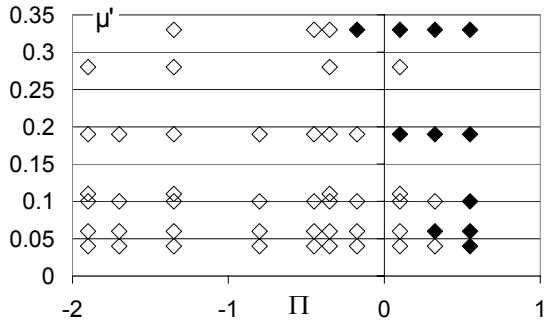

Figure 10.38a. Indication where oscillations (full symbols) occur for the yawing moment, ship model D, 4th quadrant, harmonic yaw movement with an amplitude of 15°.

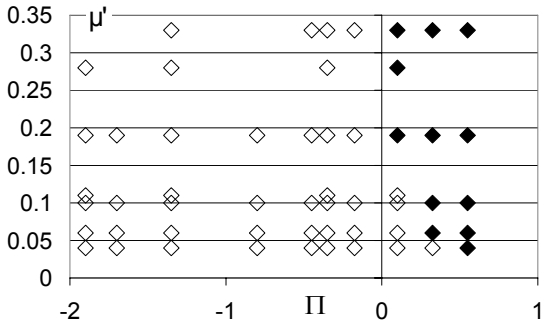

Figure 10.38b. Prediction where oscillations (full symbols) occur for the yawing moment, ship model D, 4th quadrant, harmonic yaw movement with an amplitude of 15°.

There are insufficient measured data to confirm the hypothesis, but it seems that the mud layer will only affect the upper limit (6.36), which can be rewritten as:

$$\left|\dot{r}\right| \geq \left(\dot{r}_{os,max} + \alpha\Pi'\mu'\right) \text{ or } \left|r\right| \geq \left[r_{os,max} + \beta\Pi'\mu'\right] \tag{10.49}$$

The coefficients α and β have to be determined empirically. This has been done by the assumption that a penetration with 7% of the ship's draught in mud layer d can be considered as a limiting condition for the occurrence of oscillations, when the ship carries out a harmonic yaw manoeuvre with an amplitude of 15°.

In the case of a solid bottom the minimal harmonic yaw amplitude to avoid oscillations had to be 10°. The prediction of oscillations with (10.49) is shown in Figure 10.39b. The differences between Figures 10.39a and 10.39b are acceptable. Due to these oscillation effects, the yawing moment related terms in the fourth quadrant will be determined with a fluidization parameter of 1. Whenever (10.49) is not valid, oscillations for the yawing moment will be applied as explained in 6.4.4.6.

10.4.4.2 Stationary force and moment

Figure 10.39a shows the stationary sway force due to propeller action in the first quadrant. It is a remarkable fact that, when the keel penetrates the mud layer, the forces, for a same under keel clearance referred to the solid bottom, are smaller in comparison with the solid bottom condition. As a result the fluidization parameter reaches values above one, see Figure 10.39b. A linear relationship with the keel penetration parameter can still be observed, so that the fluidization parameter can be written as:

$$\Phi(\beta,\gamma) = \left[a_0(\beta,\gamma) + \mu' a_\mu(\beta,\gamma)\right]\Pi + \Phi_{00}(\beta,\gamma) + \mu'\Phi_{0\mu}(\beta,\gamma) + \frac{h_2}{T}\left[\Phi_{h0}(\beta,\gamma) + \mu'\Phi_{h\mu}(\beta,\gamma)\right] \tag{10.50}$$

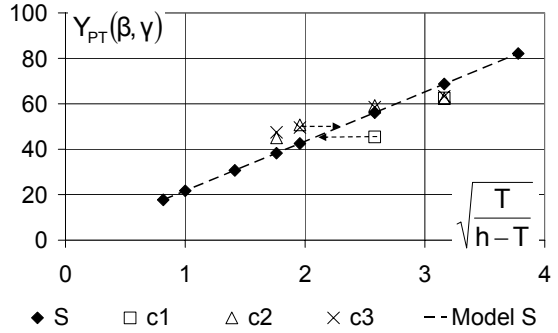

Figure 10.39a. Effect of the propeller action on the sway force $Y_{PT}(\beta,\gamma)$ in the first quadrant, ship model D, effect of solid bottom and mud layer c, β = 70°.

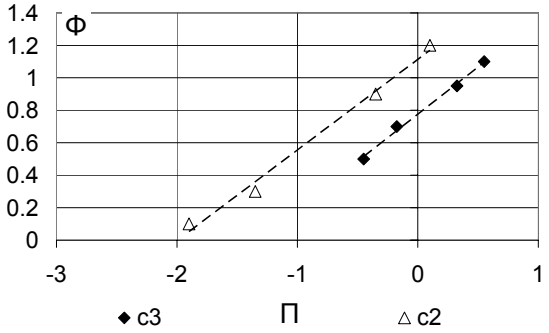

Figure 10.39b. Fluidization parameter the sway force $Y_{PT}(\beta,\gamma)$ in the first quadrant, influence of propeller action, ship model D, mud layer c, β = 70°.

Expression (10.50) can be used for all stationary forces and moments due to propeller action. An exception has to be made for the stationary moment due to yaw in the fourth quadrant. Because of the occurrence of oscillations, see 10.4.4.1, the fluidization parameter is always 1.

Another topic of interest is the under keel clearance dependence of the sway force due to drift action in the third quadrant. Instead of using model (9.40) it seemed more appropriate to use a quadratic model of the under keel clearance parameter, see Figure 10.40:

$$Y_{PT}(\beta) = \xi_1(\beta) + \sqrt{\frac{T}{h^* - T}}\xi_2(\beta) + \frac{T}{h^* - T}\xi_3(\beta) \qquad (10.51)$$

where the hydrodynamically equivalent depth is determined using a similar fluidization parameter as in (10.50). In all other cases (9.40) can be used to predict the behaviour as a function of the under keel clearance.

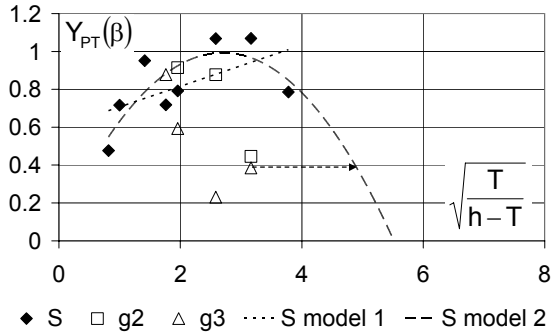

Figure 10.40a. Effect of the propeller action on the sway force $Y_{PT}(\beta)$ in the third quadrant, ship model D, effect of solid bottom and mud layer g, β = -155°.

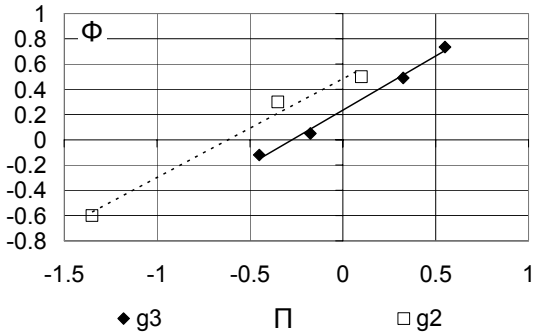

Figure 10.40b. Fluidization parameter for the sway force $Y_{PT}(\beta)$ in the third quadrant, influence of propeller action, ship model D, mud layer g, β = -155°.

10.4.4.3 Non stationary force and moment

The amplitude of the oscillations can be modelled in a similar way as the stationary forces. However, the formulation of the fluidization parameter can be simplified:

$$\Phi(\varepsilon^*) = a(\varepsilon^*)\Pi + \Phi_0(\varepsilon^*) + \mu'\Phi_\mu(\varepsilon^*) \qquad (10.52)$$

The frequency of the oscillations has been represented in Figure 10.41a as a function of the under keel clearance parameter, determined with the hydrodynamically equivalent depth h*. A good correlation can be obtained, where only in case of thick mud layers a fluidization parameter has to be determined, see Figure 10.41b. For thinner mud layers the hydrodynamically equivalent depth is equal to the real depth. For intermediate mud layers, a linear interpolation as a function of the mud layer thickness is proposed.

The same fluidization parameter can be determined for each mud layer composition, thus:

$$\Phi = a\Pi + \Phi_0 \qquad (10.53)$$

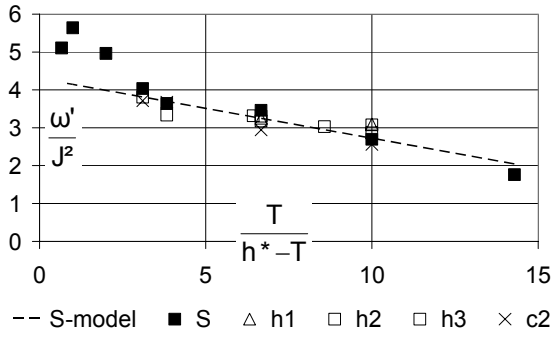

Figure 10.41a. Frequency of oscillations, ship model D, effect of solid bottom and mud layers h and c.

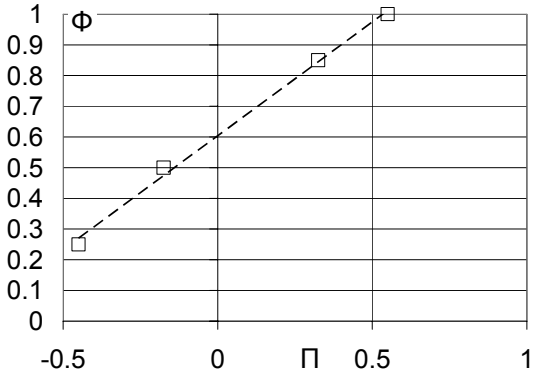

Figure 10.41b. Fluidization parameter for the frequency of oscillations, ship model D, mud layer h.

Again the phase angle of the oscillations is randomly distributed. The same average value above a solid bottom can be used in any condition.

10.5 Modelling of the rudder forces

10.5.1 Wake factors

The principle of hydrodynamically equivalent depth seemed difficult to be applied with (9.43). An alternative way of modelling the under keel clearance effect is:

$$w(\delta,\beta+\gamma)=\xi_1(\delta,\beta+\gamma)+\sqrt{\frac{T}{h^*-T}}\xi_2(\delta,\beta+\gamma) \qquad (10.54)$$

Model (10.54) gives good results in muddy areas as can be seen in Figure 10.42, where the principle of hydrodynamically equivalent depth allows a good fitting. The fluidization parameter is linear with the keel penetration parameter.

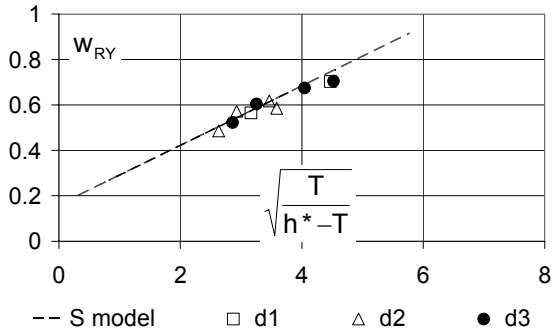

Figure 10.42a. Wake factor for the lateral rudder force, ship model D, effect of solid bottom and mud layer d. Rudder angle: -40°.

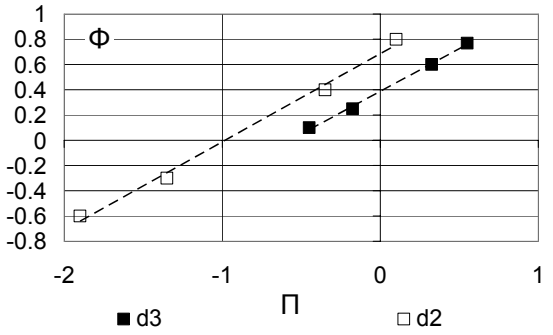

Figure 10.42b. Fluidization parameter for the wake factor for the lateral rudder force, ship model D, mud layer d. Rudder angle: -40°.

The wake factors of the rudder forces are highly affected by the wake factors of the thrust, consequently similar behaviour can be observed:

- The occurrence of the undulations, which are closely related to the mud density, affect the wake factors;
- As a result the fluidization depends on the density of the mud layer;
- The fluidization parameter depends also on the viscosity of the mud layer, where a same critical viscosity as for the wake factors for the thrust can be determined.

Consequently the fluidization parameter can be expressed as:

$$\Phi = \left[a_0 + \rho * a_\rho\right]\Pi + \Phi_{00} + \rho * \Phi_{0\rho} + \frac{h_2}{T}\left[\Phi_{h0} + \rho * \Phi_{h\rho}\right] \qquad (10.55)$$

The coefficients in (10.55) depend on a critical viscosity:

- For mud layers with a viscosity of 0.12 Pa.s a different set of coefficients is used in comparison with mud layers with a viscosity of 0.18 Pa.s or more;
- For intermediate viscosities, a linear interpolation between both sets of coefficients as a function of the mud viscosity is the most appropriate.

The above is valid for both the longitudinal rudder force and the lateral rudder force in the first quadrant. In the fourth quadrant (9.43) may be used, with the hydrodynamically equivalent depth h* equal to the height of the water layer h_1. Equally (9.44) can be used with h_1 instead of h to predict the behaviour in muddy areas.

10.5.2 Rudder induced forces

The a_H coefficient from equation (6.52) has been represented in Figure 10.43a for the fourth quadrant. The determination of the hydrodynamically equivalent depth with the fluidization parameter is still possible, although the results are more scattered, see for example Figure 10.43b.

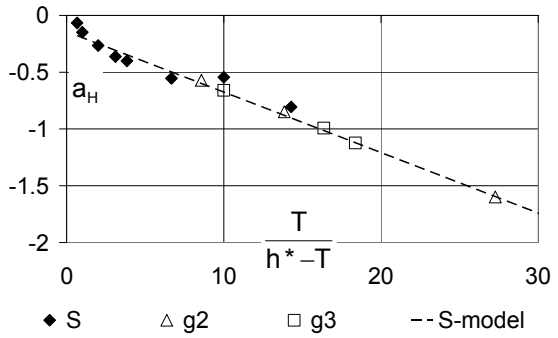

Figure 10.43a. Coefficient a_H, ship model D, effect of solid bottom and mud layer g, fourth quadrant.

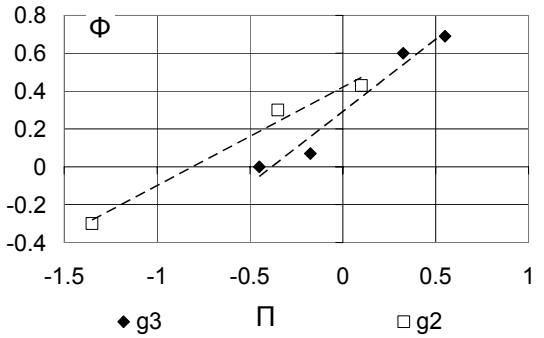

Figure 10.43b. Fluidization parameter for the coefficient a_H, ship model D, mud layer g, fourth quadrant.

For all the quadrants a_H can be determined with (9.47) with the hydrodynamically equivalent depth defined by the fluidization parameter:

$$\Phi(\beta,\gamma,\varepsilon^*) = \left[a_0(\beta,\gamma,\varepsilon^*) + \mu' a_\mu(\beta,\gamma,\varepsilon^*)\right]\Pi + \Phi_{00}(\beta,\gamma,\varepsilon^*) + \mu'\Phi_{0\mu}(\beta,\gamma,\varepsilon^*) + \frac{h_2}{T}\left[\Phi_{h0}(\beta,\gamma,\varepsilon^*) + \mu'\Phi_{h\mu}(\beta,\gamma,\varepsilon^*)\right] \quad (10.56)$$

Figure 10.44 represents the coefficient x_H from equation (6.53). In the first quadrant it can be concluded that the mud layer does not affect x_H significantly. The hydrodynamically equivalent depth can be considered equal to the total depth. The major deviations in deep water conditions are due to the smaller values of a_H; the absolute error is consequently small. The same conclusions are valid for the third quadrant.

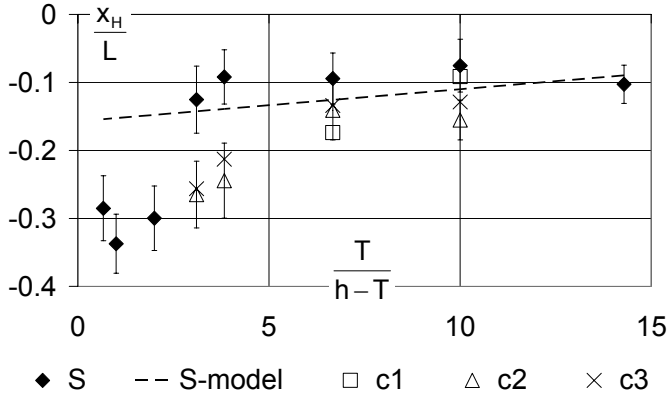

Figure 10.44. Coefficient x_H, ship model D, effect of solid bottom and mud layer c, first quadrant, β = 0°.

In the fourth quadrant a fluidization parameter is needed, see Figure 10.45.

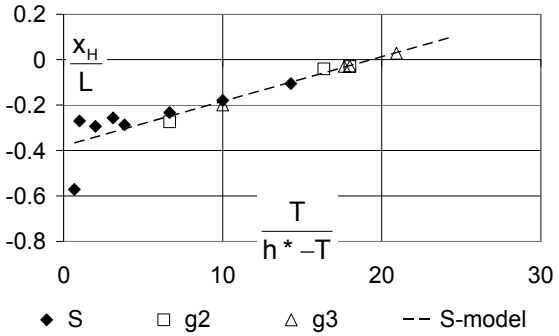

Figure 10.45a. Coefficient x_H, ship model D, effect of solid bottom and mud layer g, fourth quadrant.

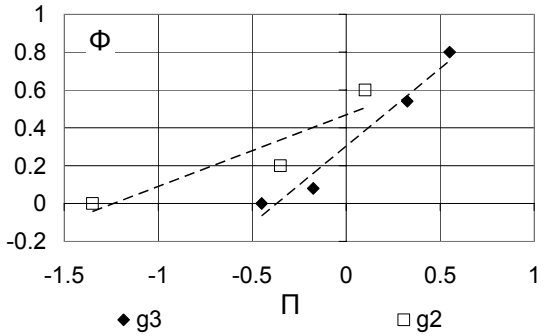

Figure 10.45b. Fluidization parameter for the coefficient x_H, ship model D, mud layer g, fourth quadrant.

In spite of the scattered results in Figure 10.45b, the following model for the fluidization parameter in the fourth quadrant can be used:

$$\Phi = \left[a_0 + \mu' a_\mu\right]\Pi + \Phi_{00} + \mu'\Phi_{0\mu} + \frac{h_2}{T}\left[\Phi_{h0} + \mu'\Phi_{h\mu}\right] \quad (10.57)$$

10.6 Validation

In this paragraph the results of the validation tests will be discussed. Two representative bottom conditions have been selected:

- -12% of under keel clearance in contact with mud layer g of 3/75 m thickness (viscosity: 0.33 Pa.s; density: 1250 kg/m³);
- 3.9% of under keel clearance above a mud layer c of 1.5/75 m thickness (viscosity: 0.06 Pa.s; density: 1150 kg/m³).

The discussion will focus on the differences in accuracy between model I, as described in Chapter 6, and model II, as described in Chapters 9 and 10. Figures 10.46-10.50 show the total measured forces in some of the validation tests in 4.4.7.4.

In most cases both mathematical models have an equal accuracy. Some major differences are:

- Figure 10.46: the lateral force has a small overshoot in model II for mud layer g;
- Figure 10.47: the yawing moment is slightly underestimated in case of model II;
- Figure 10.48: the yawing moment and sway force are underestimated for most series. The underestimation can be fully ascribed to an underestimation of the hull force. The only difference between Figures 10.47 and 10.48 is the sign of the drift angle. Although the forces have the same amplitude for both drift angles, which is physically acceptable due to the longitudinal symmetry of the vessel, the prediction is worse for a negative drift angle. In model I the prediction is better for the sway force, while the yawing moment is better predicted in model II.
- Figure 10.49: the odd evolution of the longitudinal force in case of mud layer g is better predicted with model II.
- Figure 10.50: a small overshoot can be observed for the yawing moment in case of model II.

The reader should be aware that, although in some cases model I provides better prediction, the overall prediction is acceptably well. Moreover model II uses roughly spoken only 10% of the total set of coefficients of model I to achieve the same level of accuracy. The mathematical model II is consequently positively validated with the validation tests.

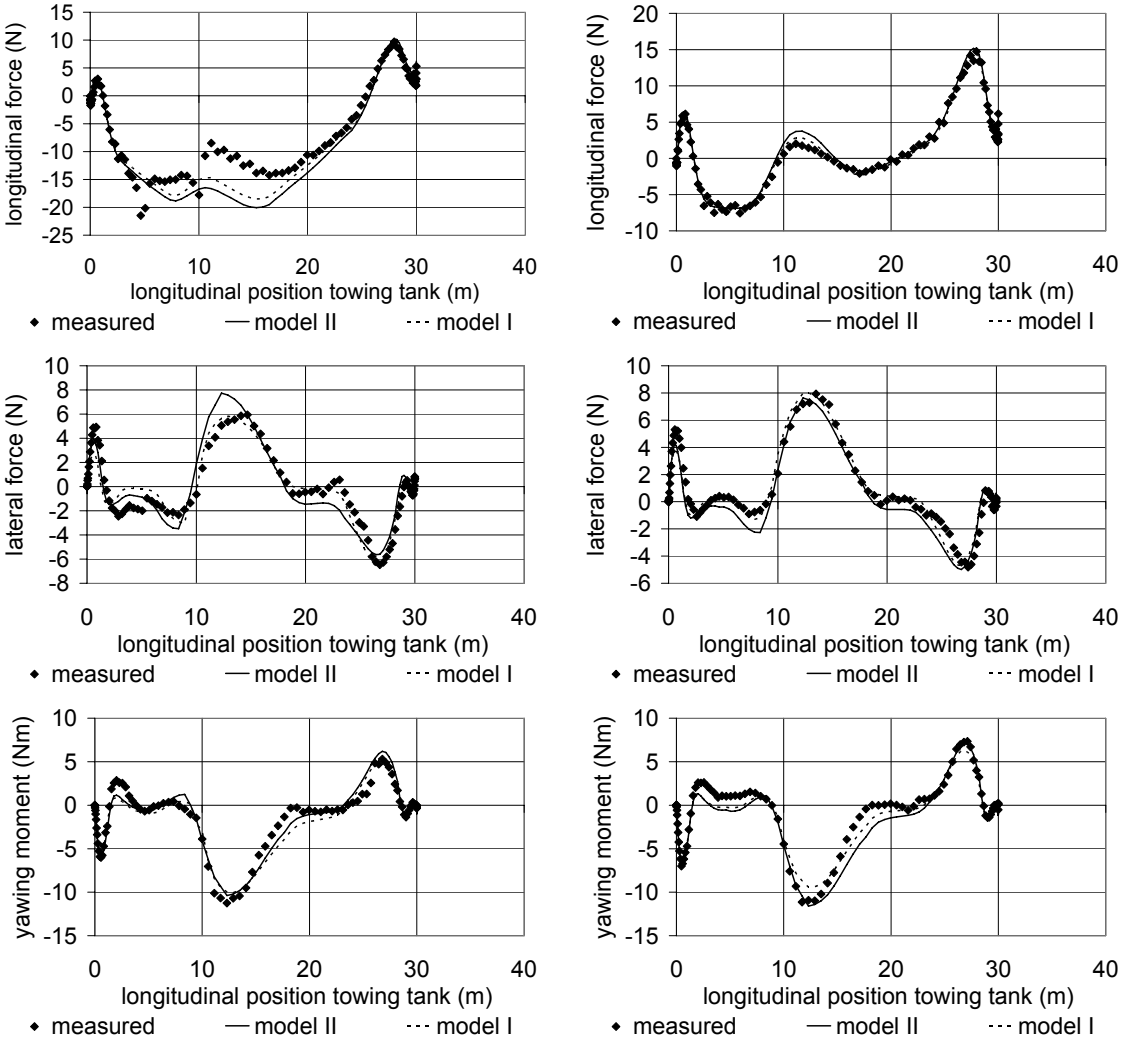

-12.2% under keel clearance in mud layer g3 3.9% under keel clearance above mud layer c2

Figure 10.46. Ship model D. Validation tests. Comparison between measured and modelled data. Validation 1 in 4.4.7.4.

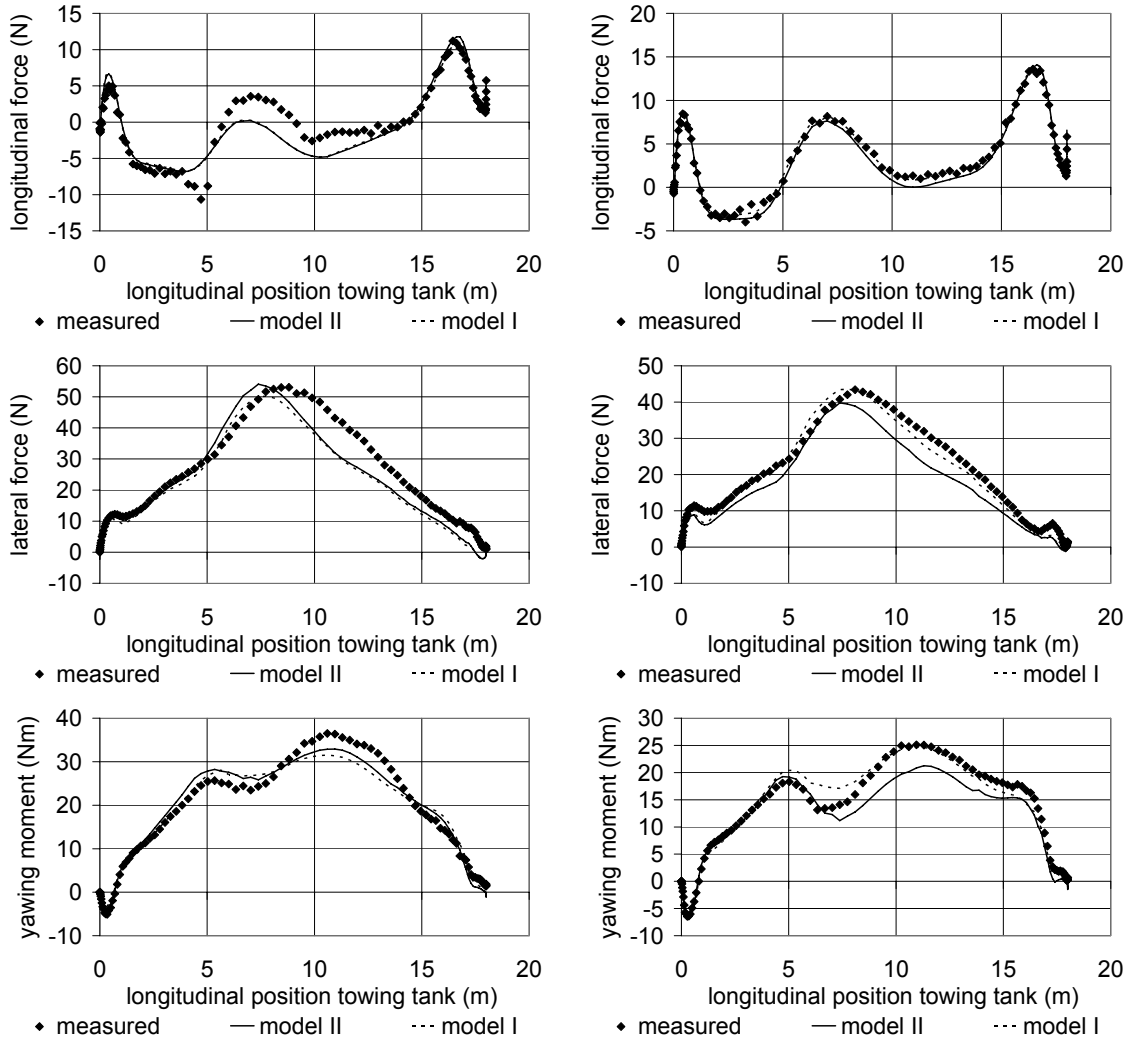

-12.2% under keel clearance in mud layer g3 3.9% under keel clearance above mud layer c2

Figure 10.47. Ship model D. Validation tests. Comparison between measured and modelled data. Validation 2 in 4.4.7.4.

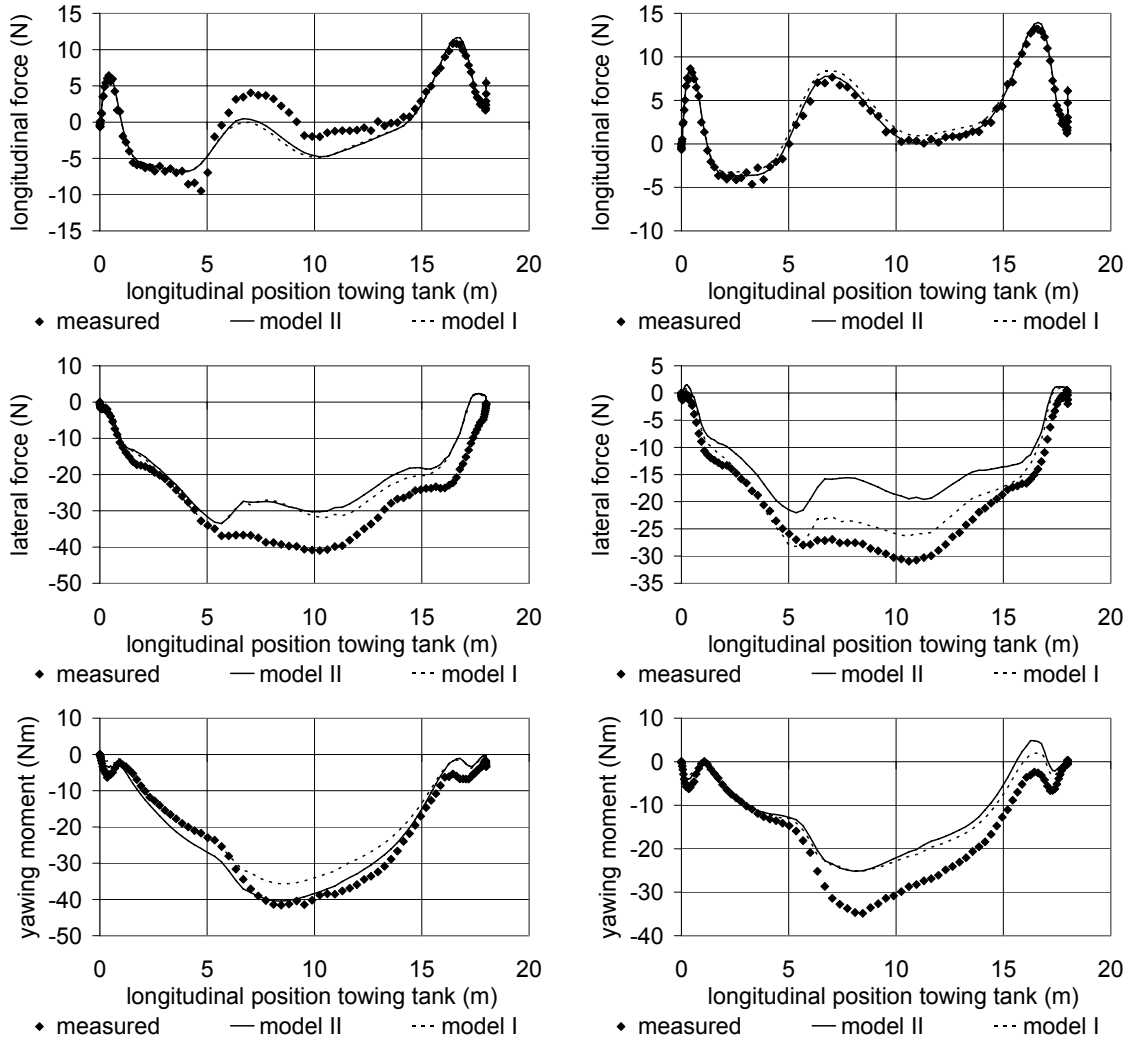

-12.2% under keel clearance in mud layer g3 3.9% under keel clearance above mud layer c2

Figure 10.48 Ship model D. Validation tests. Comparison between measured and modelled data. Validation 3 in 4.4.7.4.

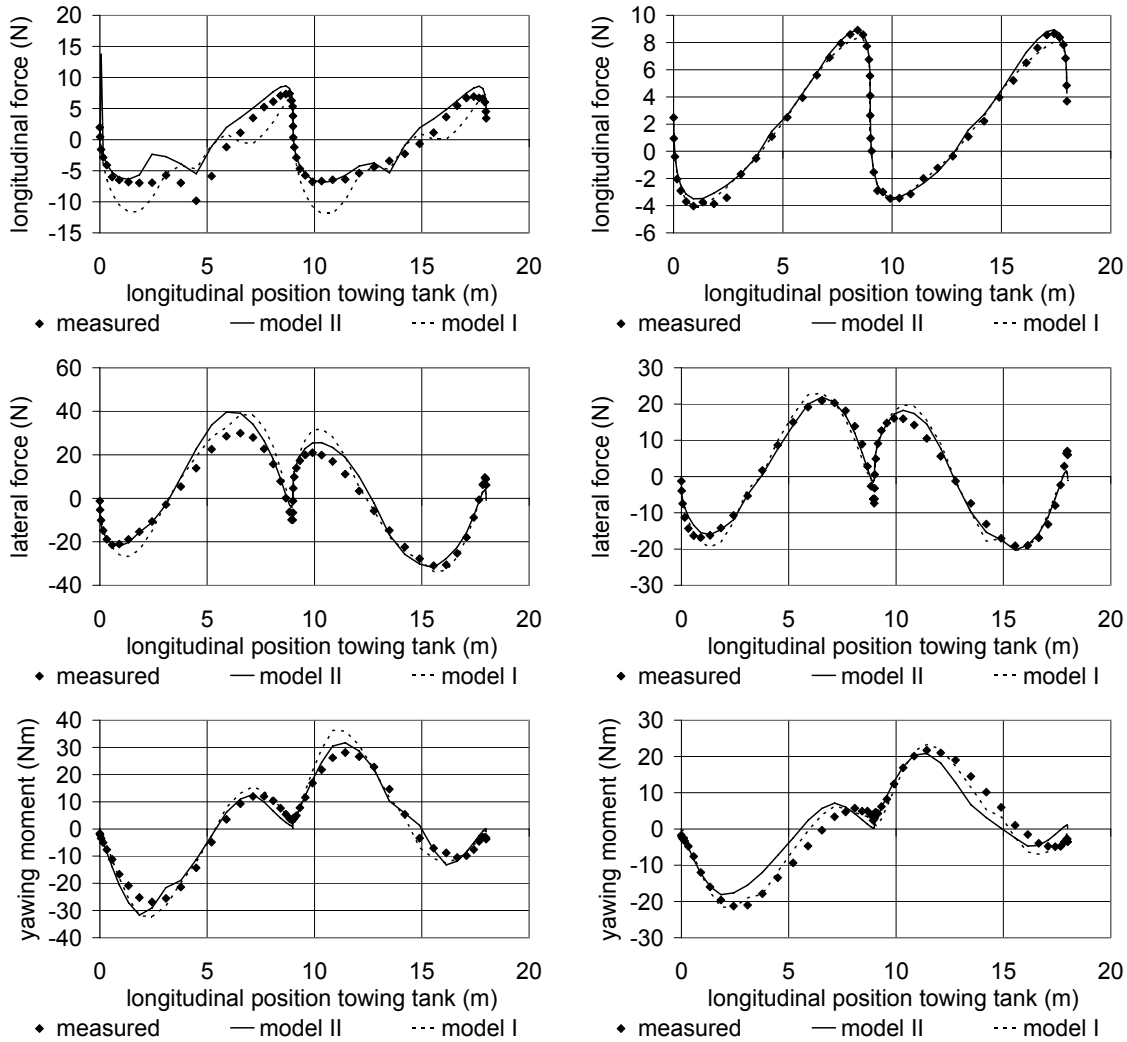

-12.2% under keel clearance in mud layer g3 3.9% under keel clearance above mud layer c2

Figure 10.49 Ship model D. Validation tests. Comparison between measured and modelled data. Validation 4 in 4.4.7.4.

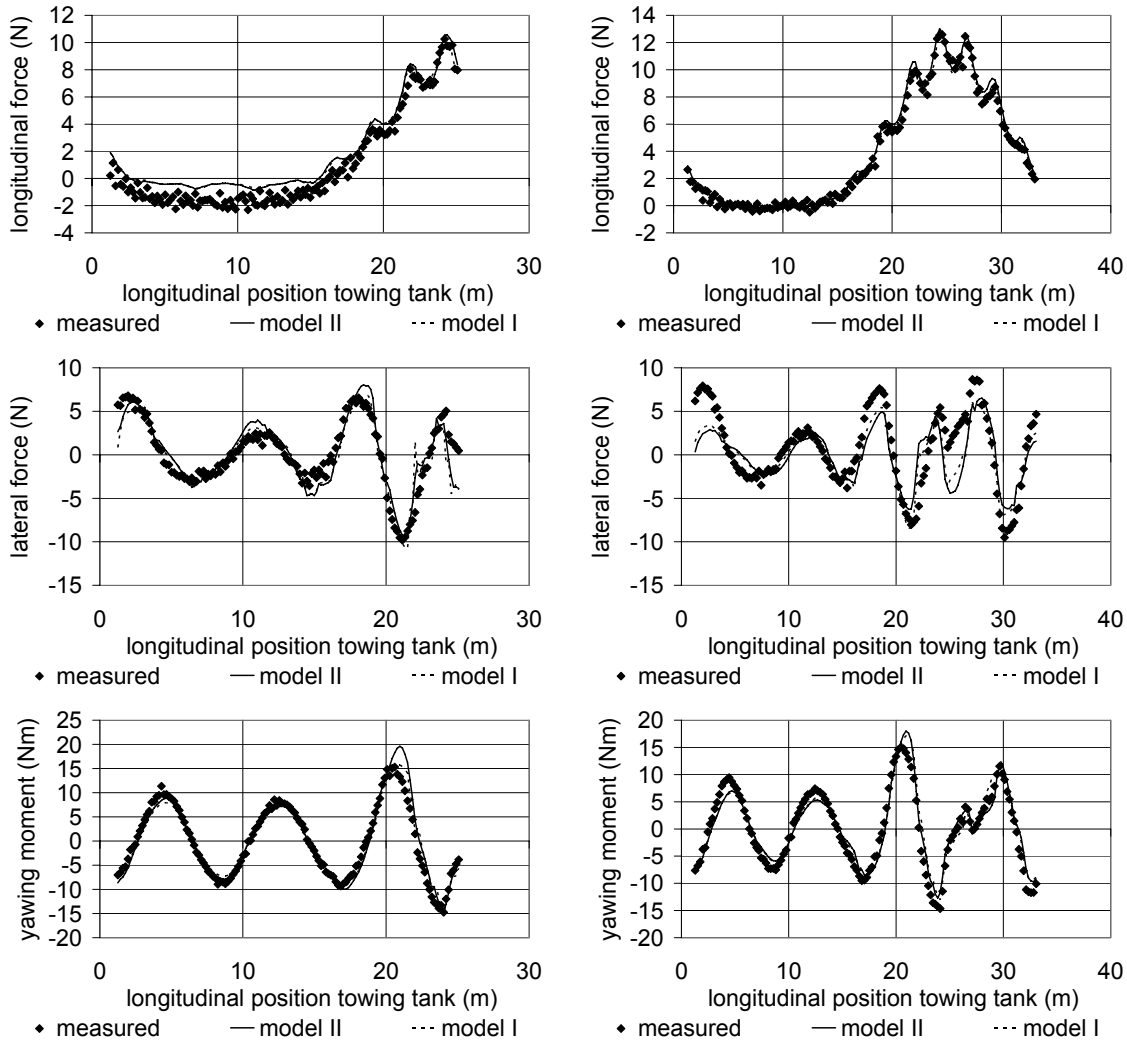

-12.2% under keel clearance in mud layer g3 3.9% under keel clearance above mud layer c2

Figure 10.50 Ship model D. Validation tests. Comparison between measured and modelled data. Validation 5 in 4.4.7.4.

10.7 Conclusions

The concept of hydrodynamically equivalent depth can be successfully applied to predict the forces on a manoeuvring container vessel in muddy areas. For any mud condition that is within the boundaries of the experimental program a fluidization parameter can be determined, which takes account of the amount of mud that behaves as water. The fluidization parameter can generally be written as:

$$\Phi = \left[a_0 + э\, a_э\right]\Pi + \Phi_{00} + э\, \Phi_{0э} + \frac{h_2}{T}\left[\Phi_{h0} + э\, \Phi_{hэ}\right] \qquad (10.58)$$

In which э represents a representative mud property. With this fluidization parameter the hydrodynamically equivalent depth can be determined using (10.4) to predict the manoeuvring behaviour. Chapter 11 will investigate whether the fluidization parameter can be used for mud conditions outside the experimental program.

You don't make progress by standing on the sidelines, whimpering and complaining. You make progress by implementing ideas.

Shirley Chisholm

CHAPTER 11

IMPLEMENTATION OF THE FLUIDIZATION MODEL

11.1 Introduction

In Chapters 7 and 8 simulation runs, carried out with the mathematical model as described in Chapter 6, have been discussed. The results of these simulation runs allowed a redefinition of the nautical bottom concept in the harbour of Zeebrugge. However, the bottom condition was initially constant throughout the harbour. This has been solved by implementing an algorithm that would allow transitions between different bottom conditions. Even in this case the possible conditions are restricted to the experimentally tested ones.

In Chapter 10 the hydrodynamically equivalent depth concept was introduced which allows the interpolation between the different mud layers. The new model was successfully validated using an independent set of captive model tests. As a consequence any bottom condition could possibly be modelled. On the other hand some obstacles remain:

- Can the fluidization model be applied to muddy layers whose parameters are outside the tested conditions? This is the case for a mud layer with one or more properties that are not between boundaries A and B in Table 11.1.

Table 11.1. Boundaries of the experimental program

Parameter	Boundary A	Boundary B
h_2	> 0.23 T	< 0.05 T
h_1	< 0.88 T	> 1.21 T
h_1+h_2	< 1.07 T	> 2.50 T
μ	> 0.33 Pa.s	< 0.04 Pa.s
ρ_2	> 1260 kg/m³	< 1100 kg/m³

- Can the principle of hydrodynamically equivalent depth be applied to other vessels (of a different type)?

This chapter will try to resolve the mentioned obstacles to allow a maximal implementation of the fluidization model.

11.2 Extrapolations

11.2.1 Bottom layer parameters beyond boundary A

Trying to predict the manoeuvring behaviour in case of denser or thicker mud layers in extremely shallow water is a difficult exercise. Figure 11.1 and 11.2 show some examples of forces that are determined when the fluidization model is applied without any assumptions.

The drift induced lateral force becomes an imaginary number for some drift angles - in Figure 11.1 represented as zero values - while the longitudinal force has overshoot values at some yaw angles. This is the consequence of the use of a linear model for the fluidization parameter. A decrease of Φ in the definition of the hydrodynamically equivalent depth:

$$h^* = h_1 + \Phi h_2 \tag{11.1}$$

results in a value of h* that is close to the ship's draught. Eventually, the keel clearance parameter:

$$\frac{T}{h^* - T} \tag{11.2}$$

will be infinite, resulting in overshoot values, before turning negative, which results in imaginary forces when the square root is taken from (11.2).

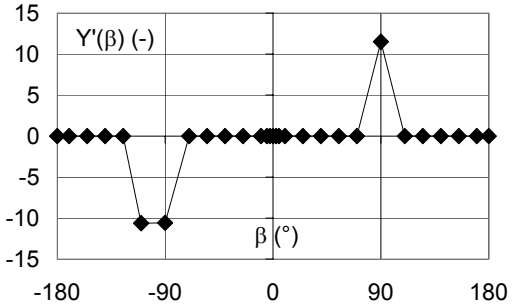

Figure 11.1. Ship D: drift induced lateral force, determined using (10.22), 32% ukc referred to the solid bottom, mud layer of 6 m thickness, mud c.

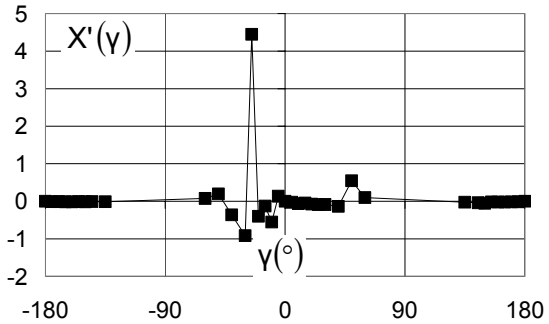

Figure 11.2. Ship D: yaw induced longitudinal force, determined using (10.15), -1.1% ukc in a mud layer with a thickness of 1.5 m and a viscosity of 0.50 Pa.s

It is clear that the definition of the fluidization parameter (10.58) is only valid within the scope of the experimental program. Other formulations have to be used in order to predict the manoeuvring behaviour in muddy areas, which parameters are beyond boundary A. This of course needs support from additional captive model tests in those conditions.

11.2.2 Bottom layer parameters beyond boundary B

This topic has already been introduced in 10.3.2.1. The value for the fluidization parameter turns negative for the largest negative keel penetration parameters that had been tested. The negative values for the fluidization parameters can be ascribed to the rising of the water mud interface, so that the hydrodynamically equivalent depth is even smaller than the height of the water layer.

Of course if the height of the water layer increases, the undulations will decrease when the mud layer thickness remains constant, see Figure 11.3 a-b or Chapter 5.

It is unlikely that the mud layer will still have a significant adverse effect on the manoeuvring behaviour. Therefore the assumption is made that a minimal fluidization parameter is obtained at Π = -2, which means that the distance between the top of the mud layer and the ship's keel is 2 times the thickness of the mud layer. From there on the fluidization parameter can linearly return to zero once Π = -4. When the clearance between the keel and the top of the mud

layer is large, the mud layer will not be affected by the passing ship. From the vessel's point of view the mud layer behaves then as a solid bottom. The same argumentation is valid when the thickness of the mud layer decreases, see Figure 11.3c.

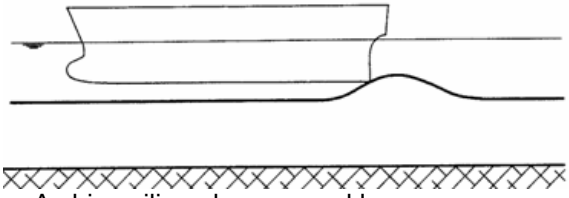

a. A ship sailing above a mud layer.

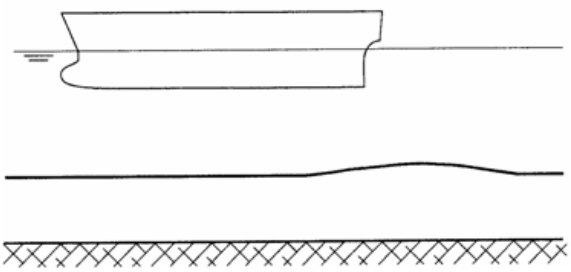

b. The same ship as in a. with a larger under keel clearance referred to the mud layer.

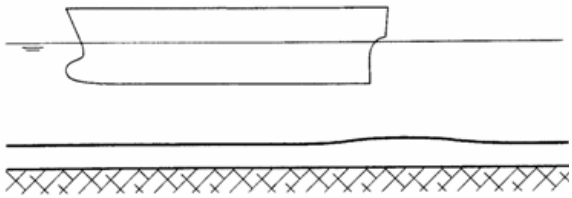

c. The same ship as in a. with a smaller mud layer.

Figure 11.3. Effect of increasing h_1 or decreasing h_2.

For mud layers of a very small viscosity and/or density a fluidization parameter can always be defined to predict the manoeuvring behaviour of the vessel. On the other hand the accuracy is uncertain:

- The model test programs described in Chapter 3 were all characterized by small values of the mud viscosity. Consequently higher undulations were observed, that would occur behind the stern at lower speeds, compared to the observations of the experimental program described in Chapter 4. The working conditions of rudder and propeller will be different than those predicted by the fluidization model;
- If the mud has the same viscosity and density as water, it still cannot be considered water, as the fluidization model takes undulations of the water mud interface into account. If in the limit two water layers of the same characteristics exist, they should be dealt as one water layer of thickness h_1+h_2 or the fluidization parameter should always equal unity;
- Additionally the specific case of fresh water above seawater cannot be dealt with this mathematical model, as typical for this case are the large internal waves that occur at the interface. Model tests in this condition were planned, but could not be executed due to the bulges that appeared on the tank floor during the experimental setup, see 4.5.

Finally it is worthwhile to mention that the keel penetration parameter turns infinite above a solid bottom. As in this case the fluidization parameter is always one, the value of the keel penetration parameter is unimportant and its determination should therefore be omitted.

11.2.3 Conclusions

The boundaries of the experimental program as described in Table 11.1 can:

- Mathematically be crossed in case of boundary B, but cannot be crossed for boundary A;
- Can physically be crossed in case of boundary B, but the reader should be aware of the assumptions made in 11.2.2.

Additionally, the reader should remember that the under keel clearance dependence is limited for water depths up till 2.5 times the ship's draught. In cases where the under keel clearance dependent terms are under a square root, truncation is needed to predict deep water conditions, as already stated in 9.3.2.4.

11.3 Application to other vessels

11.3.1 Introduction

Until now results have been discussed for a 6000 TEU container carrier, as most experimental data were available from this vessel type. However during the experimental program a larger container carrier (8000 TEU) and a bulk carrier have also been experimented in a limited number of muddy bottom conditions.

The question arises whether the fluidization parameters defined for the 6000 TEU container carrier can be applied to predict the manoeuvrability of the other vessel types. A first requisite of the fluidization model is that it can only be applied to a mathematical model that takes the under keel clearance effects into account as described in Chapter 9. For the bulk carrier only two solid bottom conditions are available: 10% and 15% of under keel clearance above a solid bottom. In case of the 8000 TEU container carrier three solid bottom conditions are available: 10%, 35% and 100% of under keel clearance. The muddy bottoms above which experiments have been carried out with those ships can be found in Appendix A.

The aim of this paragraph is to assess the applicability of the fluidization model to other vessels and not the determination of a complete mathematical model for those vessels types. In this case some assumptions can be made:

- The under keel clearance relationship is directly found through regression analysis of the regression coefficients of each mathematical model for a single under keel clearance and bottom condition as described in Chapter 6. Of course it is statistically more acceptable if new regression analyses were carried out starting from the measured data instead of the already modelled data. As a consequence the coefficients of the model of Chapter 6 can be considered the "real values".
- The applicability can be tested with some spot checks of relevant forces.

As only a few series above a solid bottom are known, the application of the fluidization parameter is significantly influenced by the accuracy of the under keel clearance related model.

11.3.2 Hull forces

11.3.2.1 Longitudinal force

The under keel clearance relationship for the resistance of the ship at a straight course is given by (9.12). Although the relationship is quadratic, the second order term can be omitted at zero drift angle, so that a model can be built for the two under keel clearances of the bulk carrier.

Table 11.2 gives some results for X'(β=0). A series for ship model D is included for comparison. The prediction accuracy is of the same order of magnitude for the three ship models.

Table 11.2 Comparison between the single model of X'(β=0) and the prediction with the fluidization parameter, which is determined with the regression coefficients of ship D.

series	real value	prediction	%
E, 0% ukc above mud g2	-0.070	-0.079	+13
E, -9.4% ukc in mud d3	-0.046	-0.036	-23
U, 3.9% ukc above mud d3	-0.031	-0.029	-7
U, 10% ukc above mud d3	-0.031	-0.028	-9
D, 10% ukc above mud d3	-0.031	-0.025	-20

11.3.2.2 Sway force

Table 11.3 represents an analogous analysis for the sway added mass. Again the prediction accuracy is of the same order for the three ship models.

Table 11.3 Comparison between the single model of Y_{vdot} and the prediction with the fluidization parameter, which is determined with the regression coefficients of ship D.

series	real value	prediction	%
E, 0% ukc above mud g2	-5.20	-4.32	-17
E, -9.4% ukc in mud d3	-3.79	-3.90	+3
U, 3.9% ukc above mud d3	-2.74	-2.95	+8
U, 10% ukc above mud d3	-2.09	-2.55	+22
D, 10% ukc above mud d3	-2.76	-2.20	-20

The drift function for the sway force is represented in Figure 11.4 for the three ship models above different bottom conditions. The accuracy of the fluidization model for ship U is fairly good. For ship model E some major deviations are observed for large drift angles when navigating astern. On the other hand one can notice that a severe asymmetry exists around a drift angle of 90° in case of the model of Chapter 6. Moreover only few data points were available when navigating astern with ship model E. Therefore the application of the fluidization model for model E also yields acceptable results.

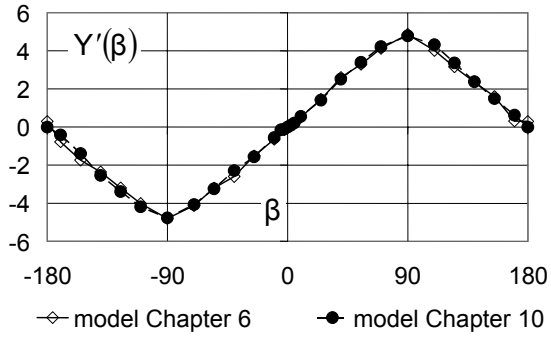

a. Ship model D, 10% of under keel clearance above mud d3.

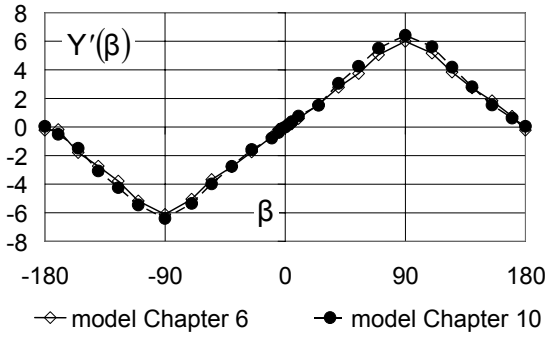

b. Ship model U, 3.9% of under keel clearance above mud d3.

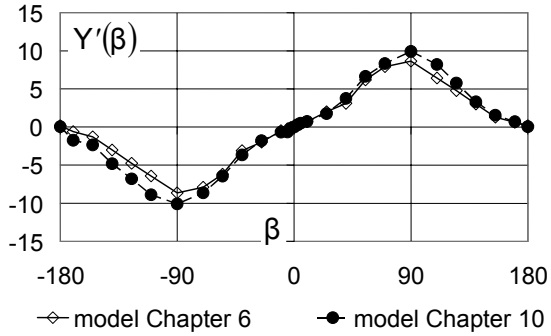

c. Ship model E, 0% of under keel clearance above mud g2.

Figure 11.4. Drift induced lateral force, influence of ship model.

11.3.2.3 Yawing moment

Table 11.4 represents some results for the yaw added moment of inertia. Most conditions have the same magnitude, although some relative large errors are observed for ship model U navigating at 10% of under keel clearance above mud d3. The absolute deviation for ship model E above mud g2 is also large.

Table 11.4 Comparison between the single model of N_{rdot} and the prediction with the fluidization parameter, which is determined with the regression coefficients of ship D.

series	real value	prediction	%
E, 0% ukc above mud g2	-0.212	-0.168	-21
E, -9.4% ukc in mud d3	-0.152	-0.170	+12
U, 3.9% ukc above mud d3	-0.089	-0.096	+8
U, 10% ukc above mud d3	-0.061	-0.085	+40
D, 10% ukc above mud d3	-0.063	-0.075	+20

11.3.3 Propeller forces

Figures 11.5 and 11.6 represent the wake factors for the propeller thrust and torque for the different vessel types. Although the undulations for ship model E reach their maximum mostly amidships, see Figure 5.25, the fluidization model is able to predict the wake factors very well. This is mainly due to the fact that the wake factors reach already large values above a solid bottom, due to the fuller hull form. The effect of the under keel clearance is consequently of minor importance and so is the effect of the fluidization parameter.

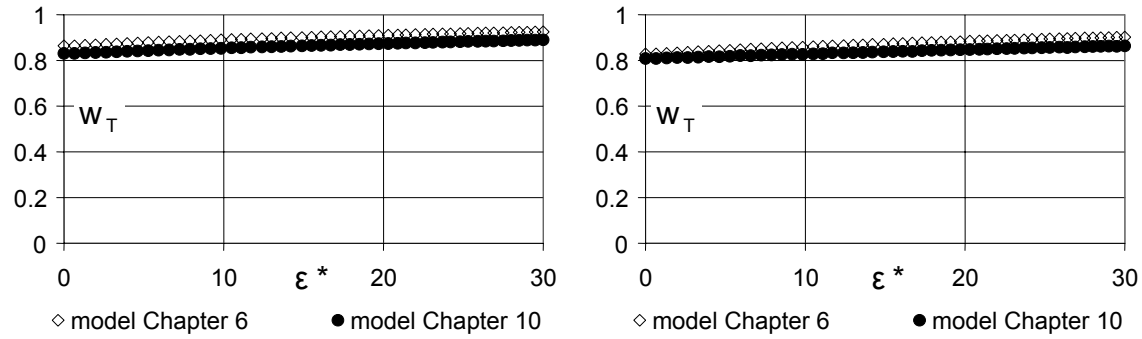

a. 0% of under keel clearance above mud g2 b. -9.4% of under keel clearance in mud d3

Figure 11.5. Wake factor for the propeller thrust, ship model E.

The wake factors for the propeller torque of ship model U are not predicted that well. It is not sure whether this can be ascribed to the fluidization model, because the wake factors for the three single under keel clearances are not linear with the under keel clearance parameter. If the largest under keel clearance is omitted an acceptable correlation is found between the two models.

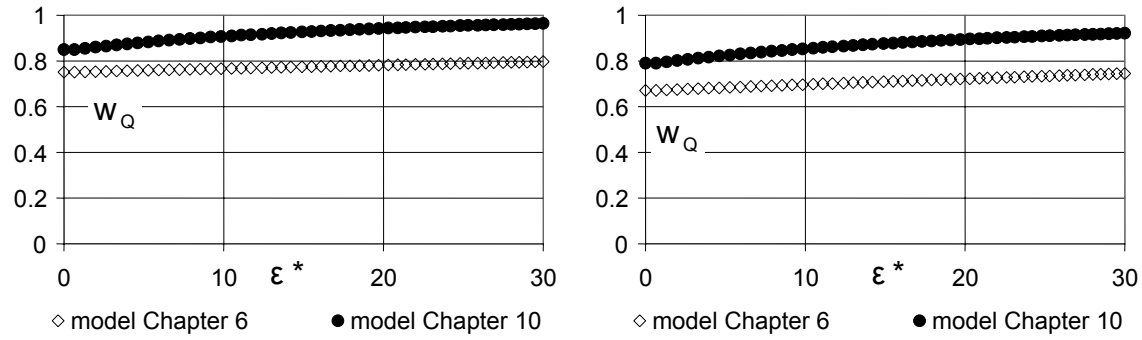

a. 3.9% of under keel clearance above mud d3 b. 10% of under keel clearance above mud d3

Figure 11.6. Wake factor for the propeller torque, ship model U.

11.3.4 Rudder forces

The wake factors for the rudder forces of the bulk carrier have always large values close to unity. The same conclusions as for the wake factors of the propeller can be formulated.

In case of ship model U the wake factors above the two tested muddy conditions are smaller than the wake factors above the corresponding solid bottom condition. This is the opposite effect compared to ship D. In this case the fluidization model of ship D cannot be applied. Again, this conclusion is only supported by the results of the available series.

11.3.5 Conclusions

The comparisons between the mathematical models with a single set of coefficients for each bottom condition and the mathematical models based on the fluidization parameter, with the regression coefficients from ship model D, give quite good results. Especially the hull force related coefficients are predicted fairly well. In case of propeller and rudder forces the deviations are larger, but still acceptable.

Although preference should be given to coefficients determined based on experimental results, it is not always possible to carry out model test experiments, especially when an artificial mud layer is involved. The comparisons in this section show that the fluidization coefficients determined for ship D can be applied to other vessel types without yielding major deviations in the forces. The only requisite is to have enough solid bottom results at different under keel clearances. In this case a fair prediction of manoeuvring behaviour in muddy areas can be achieved. Moreover it shows that the fluidization parameter is predominantly a mud dependent variable, describing how the mud behaves when a ship navigates above it, or penetrating it.

Enough research will tend to support your conclusions.

Arthur Bloch

CHAPTER 12

CONCLUSIONS AND FUTURE WORK

12.1 Conclusions

12.1.1 The nautical bottom concept

The nautical bottom concept, as defined by PIANC **[12.1]**:

The nautical bottom is the level where physical characteristics of the bottom reach a critical limit beyond which contact with a ship's keel causes either damage or unacceptable effects on controllability and manoeuvrability.

allows to determine the location of the bottom in muddy navigation areas in terms of manoeuvring behaviour. From the point of view of material characteristics the nautical bottom can be located at the rheological transition, which is the boundary between loose and stiff mud. However the rheological transition is difficult to measure in a continuous way, therefore the mud density is mostly used as a substitute. For the harbour of Zeebrugge, the critical limit was selected at a density of 1.15 ton/m³, based on density and rheology surveys carried out in the 1980s. However, mud is a time dependent suspension: as the characteristics can change in time, so will do the rheological transitions. This can be stated by the differences of rheological transition measured in the harbour of Zeebrugge during different campaigns.

12.1.2 Need for additional research

According to the definition of the nautical bottom by PIANC the manoeuvring behaviour of the vessels should be taken into account. In order to know how vessels react in muddy areas experimental research was needed. From 1976 till 1989 several research institutes carried out model tests involving muddy conditions. Those model tests were supported by a few full scale tests. The main results were that ship manoeuvring behaviour was significantly affected by the presence of a mud layer. Moreover the manoeuvring behaviour seemed to be affected by the observed undulations of the water mud interface. However, due to the limitations of the research programs, no general conclusions could be drawn. Therefore, additional experimental research was needed in order to redefine the nautical bottom in the harbour of Zeebrugge.

For this reason, a comprehensive research program was carried out at Flanders Hydraulics Research in the period 2001-2004, consisting of captive manoeuvring model testing in the *Towing tank for manoeuvres in shallow water (cooperation Flanders Hydraulics Research – Ghent University)* and real-time simulation runs. During the experimental research the real mud was substituted by an artificial mud layer, with constant density and viscosity values in function of the depth, in order to obtain controllable test parameters. A mathematical manoeuvring model was determined for a 6000 TEU container carrier in a large number of combinations of mud layer thickness, density, viscosity, and (positive and negative) under keel clearances with respect to the mud-water interface.

12.1.3 Simulation runs

With the mathematical model simulation runs have been carried out in 2004 and 2006 with the individual mathematical models valid for each combination of mud layer thickness, mud composition and under keel clearance. The fast-time simulations offered an insight of the manoeuvrability of the ship in muddy navigation areas, but the lack of a decisive human factor makes them unreliable to redefine the nautical bottom. During real-time simulations the nautical bottom criterion of the harbour of Zeebrugge could be redefined with the assistance of the Zeebrugge pilots. The critical density in the harbour of Zeebrugge is now determined at 1.20 ton/m³. This definition is not without limitations: the penetration of the vessel into lower density (up to 1150 kg/m^3) is constrained, depending on the available tug assistance:

- 12% of draft if two tugs of 60 ton bollard pull are available;
- 7% for two tugs of 45 ton bollard pull;
- 0% for 2 * 30 ton bollard pull and less.

It should be emphasized that these specific conclusions of the real-time simulations are only valid for deep-drafted 6000 TEU container carriers arriving at or departing from Zeebrugge harbour, as the mud characteristics, the environmental conditions (e.g. current) and harbour layout are typical for this area. The author also wishes to emphasize that the mud density is still no more than a substitute for the critical limit. A better critical limit should be based on the rheological transition.

12.1.4 The hydrodynamically equivalent depth

Starting from a newly built full four quadrants harbour manoeuvring model, which takes the under keel clearance effect referred to a solid bottom into account, it was possible to model the manoeuvring behaviour in muddy areas by replacing the real depth h by the hydrodynamically equivalent depth h*, which is a function of the ship's kinematical parameters.

If the height of the water layer is h_1 and the thickness of the mud layer h_2 there must exist a parameter Φ so that the hydrodynamically equivalent depth can be written as:

$$h^* = h_1 + \Phi h_2 \tag{12.1}$$

This parameter Φ equals 1 in case of a solid bottom, the hydrodynamically equivalent depth is in this case equal to the real depth. On the other hand if the mud layer can be considered as a stiff bottom, the hydrodynamically equivalent depth would be constrained to the height of the mud layer, thus Φ=0. For loose mud an intermediate value of Φ can be found to model the hydrodynamically equivalent depth. It is clear that less viscous mud will behave more as water, which leads to an increase of the hydrodynamically equivalent depth and consequently an increase of Φ, which is consequently called the fluidization parameter.

12.1.5 Effect of the undulations of the water-mud interface

Not only the viscosity of the mud layer is of importance, but also the density. The different densities between water and mud lead to undulations of the interface. Below a critical value of the viscosity, located in the range 0.13 - 0.18 Pa.s, the magnitude of the undulations increases significantly and the undulations reach their maximum in the vicinity of the propeller. At least this is the case for slender ship hulls, such as a container carrier. Fuller hull forms have their maximal undulation magnitude somewhere amidships.

The fact that the undulations reach their maximum near the propeller has an adverse effect on the inflow of the propeller, which can be seen in the increased values for the wake factors for the thrust. Consequently the propeller efficiency will be lower. On the other hand if the mud layer is more viscous, the wake factors for the thrust will be smaller, but contact between the propeller tip and the mud layer causes an increased propeller torque, and consequently also a decrease of propeller efficiency.

In some cases the presence of undulations yields values of the fluidization parameter that are less than 0, meaning that the hydrodynamically equivalent bottom is located above the top of the mud layer. The undulations have thus an adverse effect on the manoeuvring behaviour of the vessel, especially at very small positive under keel clearances referred to the water-mud interface.

The behaviour of the undulations also depends on the ship's speed and a significant influence of the viscosity can be observed. In previous research programs involving mud layers with much smaller viscosity, it has been observed that the undulations occurred behind the stern of the vessel above a certain critical speed. This could be confirmed by theoretical calculations, which however neglected the viscous effect. The deviation between theoretical calculations and the observations of the present research program, with larger mud viscosities, are as a consequence larger. Moreover, apart from some limited conditions of high speed and low density, the undulations always take place under the ship. The manoeuvring behaviour for the covered harbour speeds will therefore be affected in a similar way, having the advantage that no additional speed effect needed to be included in the model.

12.1.6 Implementation of the fluidization model

The fluidization parameter has been defined based on experimental results with a 6000 TEU container carrier, the standard type of vessel for the harbour of Zeebrugge at that time. However, the same set of coefficients can be used to model the behaviour of other deep drafted vessels as well, with a good degree of accuracy. Even fuller hull forms may be modelled with this set of coefficients. The effect of the undulations on the wake factors is small for this ship type, but due to the fuller hull form, wake factors are already large.

An extrapolation to thinner mud layers, or higher water layers is also possible, if at least an interpolation model is used. Mathematical extrapolations to lower densities and viscosities should be handled with care because the accuracy will

be less due to the different behaviour of the undulations. Extrapolations to thicker or more viscous and denser mud layers are not reliable, as they need support from additional model tests, but the realism of these conditions does not call for an urgent need to investigate more viscous or denser mud layers.

12.1.7 Current state of the art

This dissertation contains the latest advances in the domain of ship manoeuvring behaviour in muddy areas:

- It was the first time that such an extensive captive model testing program, in a wide variation of muddy navigation conditions, was carried out;
- With the results of this experimental program a four quadrant harbour manoeuvring model for container vessels navigating in muddy areas could be built. This was achieved in three steps:
    - A mathematical model with a single set of coefficients for each combination of under keel clearance and bottom characteristics was built;
    - The under keel clearance effect was taken into account in an extension of this model above solid bottom conditions;
    - Finally the effect of the mud layer could be modelled by the introduction of a fluidization parameter leading to a hydro-dynamically equivalent depth that replaced the real depth in the determination of the under keel clearance effect.
- With the first stage of this mathematical model both fast- and real-time simulation runs could be carried out leading to an optimisation of the nautical bottom criterion. The latter has a positive economic effect on the maintenance dredging program and the admittance policy of deep drafted container carriers to shallow water harbours without jeopardizing the safety.

12.2 Future work

12.2.1 Short term projects

From September 2005 till June 2008 the Maritime Technology Division of Ghent University carries out a research project, commissioned by Flanders Hydraulics Research, to validate the nautical bottom concept **[12.2]**. Some important tasks are:

12.2.1.1 Full scale measurements

In experimental research on model scale it is impossible to follow both Reynold's law and Froude's law. This yields an uncertainty for the frictional forces and the effect of the viscosity. In this dissertation the scaling effects have been taken into account with the ITTC1978 procedures, with an adaptation to take the effect of the mud layer into account. This adaptation is however a conservative approach that needs validation from tests on real scale. Some full

scale measurements have already been carried out, but still more are planned, as so far no valuable conclusions could be drawn.

12.2.1.2 Scaling to larger ships

Due to the increase of the vessel size as described in 1.1.1 the need for assessing their manoeuvring behaviour is always present. A scaling method has been developed to take the effects of the container carriers dimensions into account.

12.2.1.3 Effect of bow and stern thrusters

The real-time simulation runs were carried out with vessels that did not use their bow or stern thrusters as the effect of the mud layer on the thrusters' efficiency is unknown. A small experimental program is planned to assess the effect of the mud layer on those thrusters.

12.2.1.4 Additional simulation runs

With the new mathematical model, taking the fluidization parameter into account, additional fast- and real-time simulation runs will be carried out. Special attention should be paid to the effect of harsh weather conditions, shipping traffic and bank effects on the nautical bottom criterion.

It could also be interesting to carry out sensitivity analyses with the new model to see for instance which effect a change of viscosity or mud layer thickness has on the diameter of a turning circle or to analyse the effects of the extrapolations.

12.2.2 Long term projects

It would be interesting to include numerical, such as finite volumes, or theoretical calculations. A precious set of experimental captive manoeuvring tests can be used to fine tune such numerical models.

The mud layer in this thesis has been simplified to a fluid, having a constant density and viscosity in function of the depth. The research on the effect of stratification of the mud layer can be a challenge, especially from the experimental point of view. One research institute carried out model tests with a density gradient. A comprehensive model test program where the vessel manoeuvres above or in contact with mud layers having gradients is necessary to formulate an adequate model. Again this could be supported by theoretical or numerical calculations.

Finally the search for better survey techniques in muddy navigation areas should not be closed. It would be very useful if the rheological characteristics of the mud layer, and particularly the rheological transition, could be measured in a continuous way, as both echo sounding results and density values are only a surrogate to indicate the position of the rheological transition.

12.3 Epilogue

The size of the container carriers grows at an exponential pace. In 2001 a 300 m long 6000 TEU container carrier was the standard vessel for Zeebrugge. In the last week of 2006 the first container carrier of 367 m long entered the harbour, while in 2007 even a 400 m long container carrier is expected to call Zeebrugge harbour. The economic growth overtakes the experimental research. However it is the author's hope that this work has contributed in resolving the shallow water challenges mentioned in Chapter 1. This could not have been possible without the advances in computer and information technology, both in the field of automation of the experimental research as in the field of mathematical model calculations.

The understanding of the different shallow water challenges implemented into a ship manoeuvring simulator, will bring virtual reality closer to reality. A better understanding of the ship behaviour in confined conditions, will undoubtedly lead to an optimised admittance policy to any harbour. In this way, the understanding of the manoeuvring behaviour in muddy areas lead to an admittance of vessels having a larger draught and to an optimized maintenance dredging program.

12.4 References

[12.1] PIANC/IAPH. *Approach channels – A guide for design, Final report of the joint Working Group PIANC and IAPH, in cooperation with IMPA and IALA.* Supplement to PIANC Bulletin, No. 95, 1997, 108 pp.

[12.2] VANDER DONCKT S., DELEFORTRIE G., VANTORRE M. *Bepaling van de nautische bodem in de haven van Zeebrugge. Onderzoek nautische implicaties. Fase C: validatie concept nautische bodem. Vijfde interimrapport november 2006.* Research project UGent 174F5605, WL Mod. 582C. Ghent / Antwerp, 2006. (In Dutch).

APPENDICES

APPENDIX A: EXPERIMENTAL PROGRAM

Table A.1. Captive manoeuvring test program above a solid bottom

run	environment	ship	draught T (m)	water-depth h_1+h_2 (m)	under keel clearance (%T)
March 2001					
PA	VAST003	D	13.5	17.05	26.3
PB	VAST002	D	13.5	15.525	15.0
PC	VAST001	D	13.5	14.85	10.0
PI[1]	VAST000	D	13.5	14.445	7.0
PD	VAST004	D	13.5	17.825	32.0
QD	VAST004	E	15.5	17.825	15.0
QA	VAST003	E	15.5	17.05	10.0
August 2005					
PT	VAST005	D	13.5	20.25	50.0
PU	VAST006	D	13.5	27.0	100.0
PV	VAST007	D	13.5	33.75	150.0

Table A.2. Captive manoeuvring test program in muddy areas

run	environ-ment	mud density $\rho_2^{(N)}$ (t/m³)	ship	draught T (m)	water height $h_1^{(N)}$ (m)	mud thickn. $h_2^{(N)}$ (m)	total depth h_1+h_2 (m)	ukc bottom (%T)	ukc mud (%T)
January 2002									
PJ	SLIBE23	1.257	D	13.5	15.55	1.50	17.05	26.3	15.2
PK	SLIBE22	1.257	D	13.5	14.025	1.50	15.525	15.0	3.9
PL	SLIBE21	1.257	D	13.5	13.35	1.50	14.85	10.0	-1.1
PM	SLIBE24	1.257	D	13.5	16.325	1.50	17.825	32.0	20.9
March 2002									
PN	SLIBF24	1.206	D	13.5	16.325	1.50	17.825	32.0	20.9
PO	SLIBF23	1.206	D	13.5	15.55	1.50	17.05	26.3	15.2
PP	SLIBF22	1.206	D	13.5	14.025	1.50	15.525	15.0	3.9
PQ	SLIBF21	1.206	D	13.5	13.35	1.50	14.85	10.0	-1.1
May 2002									
PR*	SLIBG11	1.248	D	13.5	14.10	0.75	14.85	10.0	4.4
PS*	SLIBG12	1.248	D	13.5	14.775	0.75	15.525	15.0	9.4
June 2002									
QT*	SLIBG13	1.248	E	15.5	16.3	0.75	17.05	10.0	5.2
QU*	SLIBG14	1.248	E	15.5	17.075	0.75	17.825	15.0	10.2
June 2002									
QV	SLIBG24	1.248	E	15.5	16.325	1.50	17.825	15.0	5.3
QW	SLIBG23	1.248	E	15.5	15.55	1.50	17.05	10.0	0.0

[1] Was carried out in November 2003. *Only registrations of the interface.

run	environ-ment	mud density $\rho_2^{(N)}$ (t/m³)	ship	draught T (m)	water height $h_1^{(N)}$ (m)	mud thickn. $h_2^{(N)}$ (m)	total depth h_1+h_2 (m)	ukc bottom (%T)	ukc mud (%T)
October 2002									
PW	SLIBG23	1.248	D	13.5	15.55	1.50	17.05	26.3	15.2
PY	SLIBG22	1.248	D	13.5	14.025	1.50	15.525	15.0	3.9
PZ	SLIBG21	1.248	D	13.5	13.35	1.50	14.85	10.0	-1.1
September 2002									
RA	SLIBG32	1.248	D	13.5	12.525	3	15.525	15.0	-7.2
RB	SLIBG31	1.248	D	13.5	11.85	3	14.85	10.0	-12.2
RC	SLIBG33	1.248	D	13.5	14.05	3	17.05	26.3	4.1
RD	SLIBG34	1.248	D	13.5	14.825	3	17.825	32.0	9.8
August 2002									
SD	SLIBG34	1.248	E	15.5	14.825	3	17.825	15.0	-4.4
SC	SLIBG33	1.248	E	15.5	14.05	3	17.05	10.0	-9.4
November 2002									
SE	SLIBH14	1.207	E	15.5	17.075	0.75	17.825	15.0	10.2
SF	SLIBH13	1.207	E	15.5	16.3	0.75	17.05	10.0	5.2
November 2002									
RG	SLIBH12	1.207	D	13.5	14.775	0.75	15.525	15.0	9.4
RH	SLIBH11	1.207	D	13.5	14.10	0.75	14.85	10.0	4.4
December 2002									
RI	SLIBH23	1.207	D	13.5	15.55	1.50	17.05	26.3	15.2
RJ	SLIBH22	1.207	D	13.5	14.025	1.50	15.525	15.0	3.9
RK	SLIBH21	1.207	D	13.5	13.35	1.50	14.85	10.0	-1.1
RL	SLIBH24	1.207	D	13.5	16.325	1.50	17.825	32.0	20.9
December 2002									
SL	SLIBH24	1.207	E	15.5	16.325	1.50	17.825	15.0	5.3
SI	SLIBH23	1.207	E	15.5	15.55	1.50	17.05	10.0	0.0
February 2003									
RN	SLIBH33	1.207	D	13.5	14.05	3	17.05	26.3	4.1
RM	SLIBH34	1.207	D	13.5	14.825	3	17.825	32.0	9.8
RO	SLIBH32	1.207	D	13.5	12.525	3	15.525	15.0	-7.2
RP	SLIBH31	1.207	D	13.5	11.85	3	14.85	10.0	-12.2
April 2003									
RQ	SLIBB11	1.179	D	13.5	14.10	0.75	14.85	10.0	4.4
RR	SLIBB12	1.179	D	13.5	14.775	0.75	15.525	15.0	9.4
May 2003									
RV	SLIBB23	1.179	D	13.5	15.55	1.50	17.05	26.3	15.2
RU	SLIBB24	1.179	D	13.5	16.325	1.50	17.825	32.0	20.9
RW	SLIBB22	1.179	D	13.5	14.025	1.50	15.525	15.0	3.9
RX	SLIBB21	1.179	D	13.5	13.35	1.50	14.85	10.0	-1.1
August 2003									
RY	SLIBB32	1.179	D	13.5	12.525	3	15.525	15.0	-7.2
RZ	SLIBB31	1.179	D	13.5	11.85	3	14.85	10.0	-12.2
TA	SLIBB33	1.179	D	13.5	14.05	3	17.05	26.3	4.1
TB	SLIBB34	1.179	D	13.5	14.825	3	17.825	32.0	9.8

run	environ-ment	mud density	ship	draught	water height	mud thickn.	total depth	ukc	
								bottom	mud
		$\rho_2^{(N)}$ (t/m³)		T (m)	$h_1^{(N)}$ (m)	$h_2^{(N)}$ (m)	h_1+h_2 (m)	(%T)	(%T)
November 2003									
TE	SLIBC12	1.149	D	13.5	14.775	0.75	15.525	15.0	9.4
TF	SLIBC11	1.149	D	13.5	14.10	0.75	14.85	10.0	4.4
September 2003									
TG	SLIBC23	1.149	D	13.5	15.55	1.50	17.05	26.3	15.2
TH	SLIBC22	1.149	D	13.5	14.025	1.50	15.525	15.0	3.9
TJ	SLIBC24	1.149	D	13.5	16.325	1.50	17.825	32.0	20.9
TI	SLIBC21	1.149	D	13.5	13.35	1.50	14.85	10.0	-1.1
October 2003									
TL	SLIBC33	1.149	D	13.5	14.05	3	17.05	26.3	4.1
TK	SLIBC34	1.149	D	13.5	14.825	3	17.825	32.0	9.8
TM	SLIBC32	1.149	D	13.5	12.525	3	15.525	15.0	-7.2
TN	SLIBC31	1.149	D	13.5	11.85	3	14.85	10.0	-12.2
December 2003									
TO	SLIBD11	1.108	D	13.5	14.10	0.75	14.85	10.0	4.4
TP	SLIBD12	1.108	D	13.5	14.775	0.75	15.525	15.0	9.4
March 2004									
SQ	SLIBD13	1.108	E	15.5	16.3	0.75	17.05	10.0	5.2
SR	SLIBD14	1.108	E	15.5	17.075	0.75	17.825	15.0	10.2
April 2004									
SS	SLIBD24	1.108	E	15.5	16.325	1.50	17.825	15.0	5.3
ST	SLIBD23	1.108	E	15.5	15.55	1.50	17.05	10.0	0.0
January 2004									
TT	SLIBD23	1.108	D	13.5	15.55	1.50	17.05	26.3	15.2
TS	SLIBD24	1.108	D	13.5	16.325	1.50	17.825	32.0	20.9
TU	SLIBD22	1.108	D	13.5	14.025	1.50	15.525	15.0	3.9
TV	SLIBD21	1.108	D	13.5	13.35	1.50	14.85	10.0	-1.1
February 2004									
TW	SLIBD32	1.108	D	13.5	12.525	3	15.525	15.0	-7.2
TX	SLIBD31	1.108	D	13.5	11.85	3	14.85	10.0	-12.2
TY	SLIBD33	1.108	D	13.5	14.05	3	17.05	26.3	4.1
TZ	SLIBD34	1.108	D	13.5	14.825	3	17.825	32.0	9.8
April 2004									
SZ	SLIBD34	1.108	E	15.5	14.825	3	17.825	15.0	-4.4
SY	SLIBD33	1.108	E	15.5	14.05	3	17.05	10.0	-9.4
May 2004									
UA[2]	SLIBD31	1.108	U	14.544	12.766	3.232	15.998	10.0	-12.2
UB[2]	SLIBD32	1.108	U	14.544	13.494	3.232	16.726	15.0	-7.1
UC	SLIBD33	1.108	U	14.544	15.137	3.232	18.369	26.3	4.1
UD	SLIBD34	1.108	U	14.544	15.971	3.232	19.203	32.0	9.8

[2] Only registrations of the interface.

APPENDIX B: SHIP MODELS

B.1 Ship D: 6000 TEU container carrier

Quantity	Full scale values	Model values (scale 1/75)
	Ship dimensions	
L_{OA}	291.333 m	3.884 m
L_{PP}	289.804 m	3.864 m
B	40.252 m	0.537 m
D	22.8 m	0.304 m
T_{FP}	13.5 m	0.18 m
T_{AP}	13.5 m	0.18 m
T_M	13.5 m	0.18 m
	Additional ship data	
x_G	-7.633 m	-0.090 m
z_G	0 m	0 m
∇	94 165 m³	0.223 m³
C_B	0.5979	0.5979
I_{xx}	-	6.3097 kgm²
I_{yy}	-	222.1374 kgm²
I_{zz}	-	238.9599 kgm²
	Propeller data	
n_0	100 rpm	866 rpm
D_P	8.145 m	0.1086 m
pitch ratio	0.9696	0.9696
area ratio	0.8	0.8
	Rudder data	
A_R	60.964 m²	0.011 m²

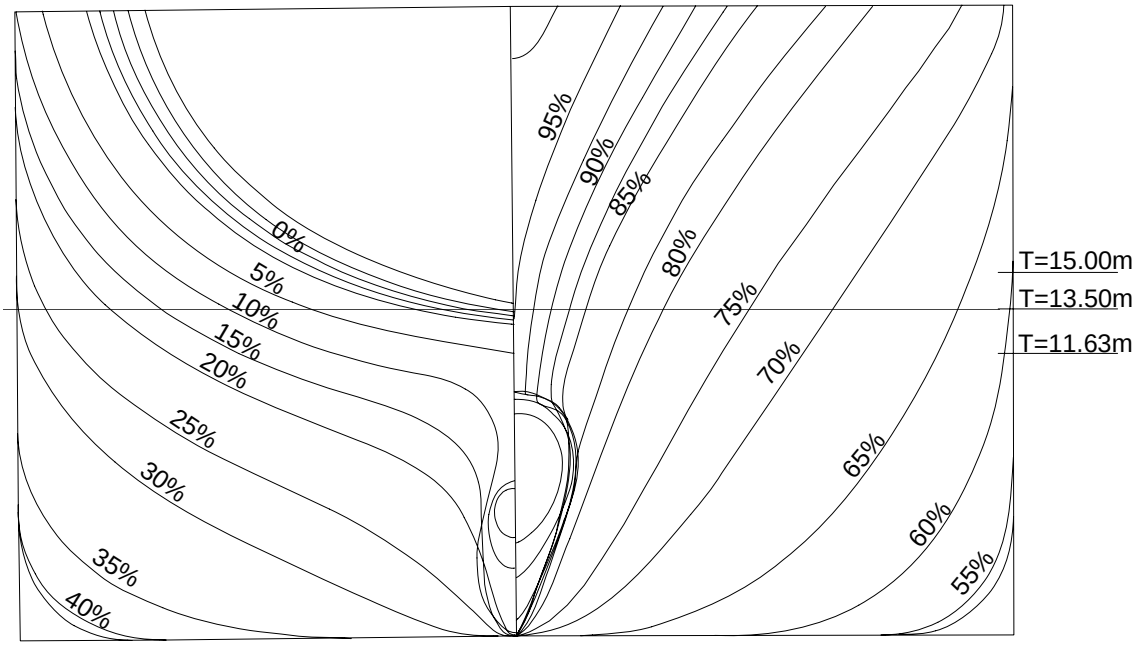

Figure B.1. Lines plan container carrier D.

B.2 Ship E: tanker model

Quantity	Full scale values	Model values (scale 1/75)
	Ship dimensions	
L_{OA}	302.647 m	
L_{PP}	286.765 m	3.824 m
B	46.765 m	0.624 m
D	30 m	0.400 m
T_{FP}	15.5 m	0.207 m
T_{AP}	15.5 m	0.207 m
T_M	15.5 m	0.207 m
	Additional ship data	
x_G	9.7147 m	0.1295 m
z_G	0.744 m	0.010 m
∇	169 649 m³	0.4021 m³
C_B	0.816	0.816
I_{xx}	-	19.169 kgm²
I_{yy}	-	321.8138 kgm²
I_{zz}	-	347.1201 kgm²
	Propeller data	
n_0	100 rpm	866 rpm
D_P	7.7325 m	0.1031 m
pitch ratio	0.6499	0.6499
area ratio	0.62	0.62
	Rudder data	
A_R	98.342 m²	0.0175 m²

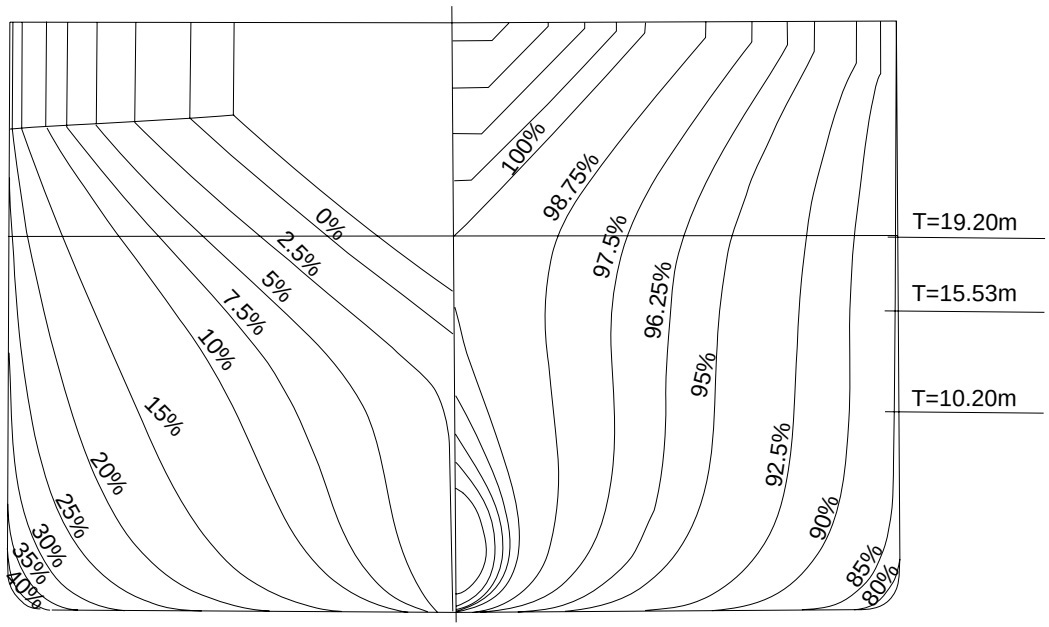

Figure B.2. Lines plan tanker model E.

B.3 Ship U : 8000 TEU container carrier

Quantity	Full scale values	Model values (scale 1/80)
	Ship dimensions	
L_{OA}	351.964 m	4.356 m
L_{PP}	331.765 m	4.106 m
B	42.824 m	0.53 m
D	26.745 m	0.331 m
T_{FP}	14.544 m	0.18 m
T_{AP}	14.544 m	0.18 m
T_M	14.544 m	0.18 m
	Additional ship data	
x_G	-0.626 m	-0.008 m
z_G	0 m	0 m
∇	135 232 m³	0.256 m³
C_B	0.6545	0.6545
I_{xx}	-	6.60 kgm²
I_{yy}	-	263.04 kgm²
I_{zz}	-	278.94 kgm²
	Propeller data	
n_0	100 rpm	899 rpm
D_P	8.46 m	0.1047 m
pitch ratio	1.0	1.0
area ratio	0.96	0.96
	Rudder data	
A_R	83.13 m²	0.0127 m²

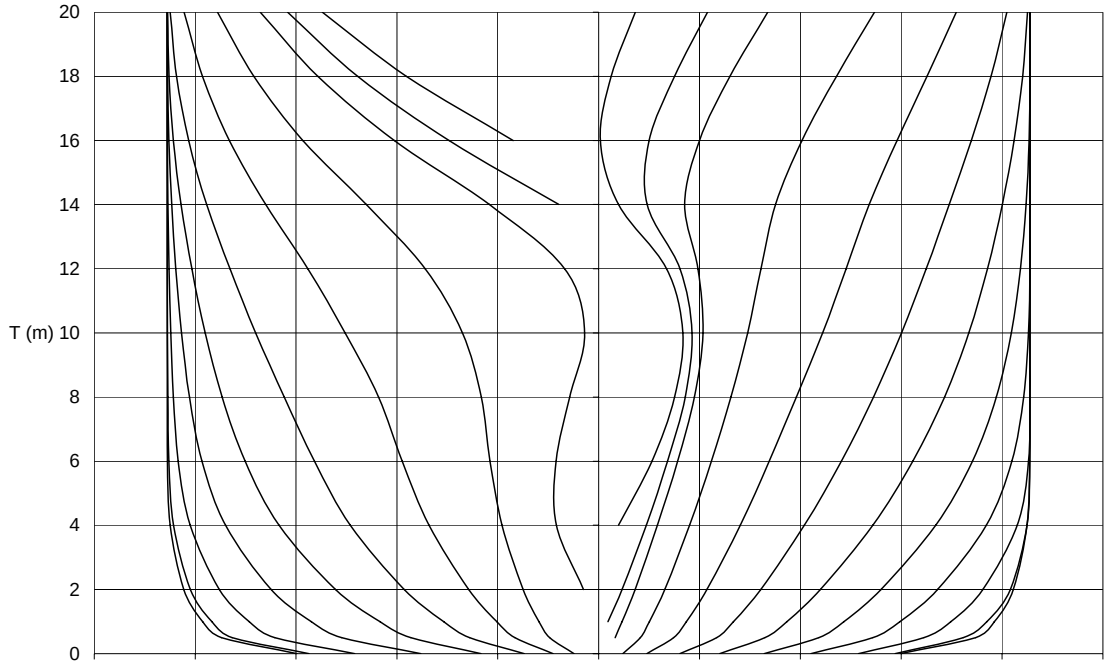

Figure B.3. Lines plan container carrier U. Lines are drawn each 5% of the ship's length. Additional lines at 2.5% L_{PP} and 97.5% L_{PP} are also included.

APPENDIX C: INFLOW SPEED OF THE RUDDER

C.1 First quadrant

An expression for the longitudinal inflow velocity at the rudder can be found by using the momentum theory **[C.3]**.

$$u_{RP} = u_{R0} + K_m u_P \left(\sqrt{1 + \frac{8K_T}{\pi J^2}} - 1 \right) \tag{C.1}$$

In which u_{R0} gives the inflow velocity without propeller action and u_P is the longitudinal velocity at the entrance of the propeller. The factor K_m takes the contraction of the propeller jet into account. **[C.1]** gives a value for K_m in function of $\frac{x_{RP}}{D_P}$, with x_{RP} the distance between the rudder axis and the propeller tip and D_P the propeller diameter.

Table C.1. Relationship between the parameter K_m and the distance between the rudder stock and the propeller tips.[C.1]

x_{RP}/D_P	0.00	0.25	0.50	0.75	1.00
K_m	0.50	0.79	0.88	0.94	0.96

The ratio $\frac{8K_T}{\pi J^2}$ in (C.1) can be written as $\frac{C_T}{\sin^2 \varepsilon}$, using the expressions in 6.4.1:

$$\frac{8C_T \frac{\pi}{8}\left(J^2 + (0.7\pi)^2\right)}{\pi J^2} = \frac{C_T\left((0.7\pi \tan\varepsilon)^2 + (0.7\pi)^2\right)}{(0.7\pi \tan\varepsilon)^2} = C_T \frac{1 + \tan^2\varepsilon}{\tan^2\varepsilon} = \frac{C_T}{\sin^2\varepsilon} \tag{C.2}$$

Both ratios are equal, but when the propeller rate reaches zero, J turns infinite, while sin ε becomes 1. The ratio $\frac{8K_T}{\pi J^2}$ decreases strongly when going from a small propeller ratio to zero rpm, while $\frac{C_T}{\sin^2\varepsilon}$ has a smoother course, without turning zero. A reason for the latter is that for the open water characteristic C_T is different from zero at zero propeller rate, due to the own resistance of the propeller.

The total inflow of the rudder is then given by a weighted average in function of η, the ratio propeller diameter – rudder height. η% of the rudder is within the propeller jet, while (1- η)% is outside the propeller jet.

$$u_R = \sqrt{\eta u_{RP}^2 + (1-\eta) u_{R0}^2} \tag{C.3}$$

If u_{RP} is replaced by (C.1), taking (C.2) into account:

$$\begin{aligned} u_R &= \sqrt{\eta\left[u_{R0} + K_m u_P\left(\sqrt{1+\frac{C_T}{\sin^2\varepsilon}} - 1\right)\right]^2 + (1-\eta)u_{R0}^2} \\ &= \sqrt{\eta\left[(1-w_R)u + (1-w_T)K_m u\left(\sqrt{\frac{\sin^2\varepsilon + C_T}{\sin^2\varepsilon}} - 1\right)\right]^2 + (1-\eta)[(1-w_R)u]^2} \\ &= (1-w_R)u\sqrt{\eta\left[1+\frac{1-w_T}{1-w_R}\frac{K_m}{\sin\varepsilon}\left(\sqrt{\sin^2\varepsilon + C_T} - \sin\varepsilon\right)\right]^2 + (1-\eta)} \end{aligned} \quad (C.4)$$

The last step is only valid when w_R is smaller than 1. Introducing ζ as:

$$\zeta = \frac{1-w_R}{1-w_T} \quad (C.5)$$

and k as:

$$k = \frac{K_m}{\zeta} \quad (C.6)$$

(C.4) can be rewritten as:

$$\begin{aligned} u_R &= (1-w_R)u\sqrt{\frac{\eta}{\sin^2\varepsilon}\left[\sin\varepsilon + k\left(\sqrt{\sin^2\varepsilon + C_T} - \sin\varepsilon\right)\right]^2 + (1-\eta)} \\ &= (1-w_R)\frac{u}{\sin\varepsilon}\sqrt{\eta\left[(1-k)\sin\varepsilon + k\left(\sqrt{\sin^2\varepsilon + C_T}\right)\right]^2 + (1-\eta)\sin^2\varepsilon} \end{aligned} \quad (C.7)$$

while (6.18) can be rewritten as:

$$\frac{u}{\sin\varepsilon} = u\frac{\sqrt{1+\left(\frac{u_P}{0.7\pi nD_P}\right)^2}}{\frac{u_P}{0.7\pi nD_P}} = u\frac{\sqrt{(0.7\pi nD_P)^2 + u_P^2}}{u_P} = \frac{\sqrt{(0.7\pi nD_P)^2 + u_P^2}}{1-w_T} \quad (C.8)$$

which is substituted in (C.7):

$$u_R = \zeta\sqrt{\left[\eta\left[(1-k)\sin\varepsilon + k\sqrt{(C_T + \sin^2\varepsilon)}\right]^2 + (1-\eta)\sin^2\varepsilon\right]\left[((1-w_T)u)^2 + (0.7\pi nD_P)^2\right]} \quad (C.9)$$

Equation (C.9) has been tested for several values of K_m in case of an under keel clearance of 26% above a solid bottom:

(A) $K_m = k = 0.94$;
(B) $K_m = k = 0.8$;
(C) $K_m = k$ = best fit, chosen by the regression model
(D) $K_m = \zeta k = 0.94$.

Option (D) is physically the most correct, but if the wake factor is determined using (C.9) with option (D), additional influence of the propeller loading on the wake factor must be included, see the large error bars in Figure C.1, which complicates the model.

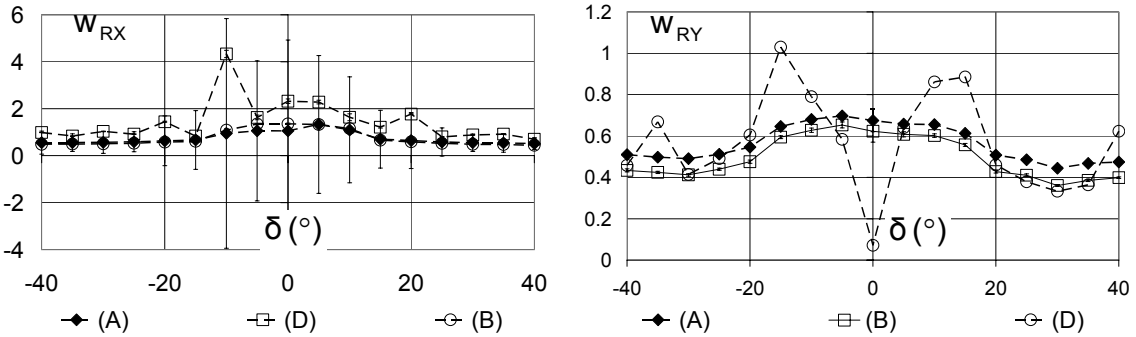

a. Longitudinal rudder force. b. Longitudinal rudder force.

Figure C.1. Wake factors for the different options to determine the longitudinal speed at the rudder, ship model D, 26% under keel clearance above a solid bottom, first quadrant, no drift nor yaw.

The simplification proposed by options (A) and (B) leads to acceptable results. Figure C.2 gives a comparison between measured and modelled rudder forces. The influence of using the correct option (D) will only have a marginal influence on the fitting of the values. The fitting seems to be better with smaller values of K_m. Indeed if the constant value is defined through regression analysis 0.79 seems to be the optimal value for F_X, while F_Y reaches an optimal fitting at K_m = k = 0.72.

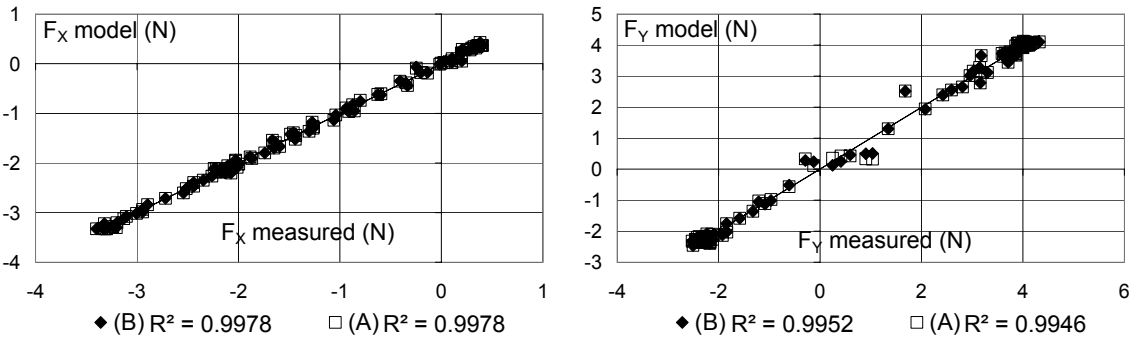

a. Longitudinal rudder force. b. Longitudinal rudder force.

Figure C.2. Comparison between measured and modelled rudder forces. Ship model D, 26% under keel clearance above a solid bottom, 40° drift angle, no yaw.

A good correlation is found between modelled and measured values with w_R modelled in function of the rudder angle. However, an influence of ε is still needed at the transition between quadrants IV and I, see (C.19) and (C.20).

C.2 Fourth quadrant

(C.9) is only valid in the first quadrant. In quadrant IV the ships sails astern with positive propeller rate. The sailing of the ship leads to a negative flow, while the propeller rate causes a positive flow. In addition eddies occur in the fourth quadrant because of the non stationary flow **[C.2]**. The eddies are mostly

oriented in such way they add a positive component to the inflow of the propeller. The net inflow of the rudder will be smaller than in the first quadrant, but still larger than in the other quadrants.

The largest possible inflow is needed to have an optimal rudder effectiveness. Assumed that the formation of eddies induces a significant positive inflow of the propeller, the following expression, based on the momentum theory, can be proposed:

$$u_{RP} = u_{R0} + K_m u_\infty = u_{R0} + K_m u_P \left(-\sqrt{1 + \frac{8K_T}{\pi J^2}} - 1 \right) \tag{C.10}$$

Where u_{R0} and u_P are strictly negative. Because w_T is zero in the fourth quadrant, $u_P = u < 0$. On the other hand if the inflow of the propeller is considered to be completely negative, the following can be used:

$$u_{RP} = u_{R0} + K_m u_P \left(-\sqrt{1 + \frac{8K_T}{\pi J^2}} + 1 \right) \tag{C.11}$$

(C.10) gives a overestimation of the inflow velocity of the rudder, while (C.11) underestimates it. The real inflow velocity will be between both values. In this case (C.10) will be chosen, which can be rewritten as:

$$u_{RP} = u_{R0} + K_m \left(\sqrt{u^2 \left(1 + \frac{8K_T}{\pi J^2} \right)} - u \right) \tag{C.12}$$

(C.12) takes account of the fact that $u < 0$, thus $u = -\sqrt{u^2}$. The fact that (C.10) predicts a too large inflow velocity can be seen from its value at zero ship speed, $\frac{8K_T}{\pi J^2} \Rightarrow 0$, consequently:

$$u_{RP} = (1 - w_R)u - 2K_m u > 0 \tag{C.13}$$

for all $0 < w_R < 1$. u_{RP} is thus always strictly positive. However in reality there is a possibility that a negative velocity u_{RP} is induced for low propeller rates **[C.2]**.

The total inflow of the rudder is given by a weighted average in function of η. Considering that $u_{R0} < 0$, the following expression can be used:

$$u_R = \sqrt{\eta u_{RP}^2 + (1-\eta) u_{R0} |u_{R0}|} = \sqrt{\eta u_{RP}^2 - (1-\eta) u_{R0}^2} \tag{C.14}$$

It can be proven with (C.12) that (C.14) has always a strictly positive value. (C.14) can be rewritten in function of the angle ε:

$$
\begin{aligned}
u_R &= \sqrt{\eta\left[u_{R0} + K_m|u|\left(\sqrt{1+\frac{C_T}{\sin^2\varepsilon}}+1\right)\right]^2 - (1-\eta)u_{R0}^2} \\
&= \sqrt{\eta\left[(1-w_R)u + K_m|u|\left(\sqrt{\frac{\sin^2\varepsilon + C_T}{\sin^2\varepsilon}}+1\right)\right]^2 - (1-\eta)[(1-w_R)u]^2} \\
&= (1-w_R)|u|\sqrt{\eta\left[1+\frac{1}{1-w_R}\frac{K_m}{\sin\varepsilon}\left(\sqrt{\sin^2\varepsilon + C_T} - \sin\varepsilon\right)\right]^2 - (1-\eta)}
\end{aligned}
\tag{C.15}
$$

with u, sin ε strictly negative and w_R smaller than 1. Making use of (C.5) and (C.6), with $w_T = 0$:

$$
\begin{aligned}
u_R &= (1-w_R)|u|\sqrt{\eta\left[1+\frac{k}{\sin\varepsilon}\left(\sqrt{\sin^2\varepsilon + C_T} - \sin\varepsilon\right)\right]^2 - (1-\eta)} \\
&= (1-w_R)|u|\sqrt{\frac{\eta}{\sin^2\varepsilon}\left[|\sin\varepsilon| - k\left(\sqrt{\sin^2\varepsilon + C_T} - \sin\varepsilon\right)\right]^2 - (1-\eta)} \\
&= (1-w_R)\frac{|u|}{|\sin\varepsilon|}\sqrt{\eta\left[|\sin\varepsilon| - k\left(\sqrt{\sin^2\varepsilon + C_T} - \sin\varepsilon\right)\right]^2 - (1-\eta)\sin^2\varepsilon} \\
&= (1-w_R)\frac{u}{\sin\varepsilon}\sqrt{\eta\left[(1-k)\sin\varepsilon + k\sqrt{\sin^2\varepsilon + C_T}\right]^2 - (1-\eta)\sin^2\varepsilon}
\end{aligned}
\tag{C.16}
$$

In which (C.8) can be substituted:

$$
u_R = (1-w_R)\sqrt{\left[\eta\left[(1-k)\sin\varepsilon + k\sqrt{(C_T + \sin^2\varepsilon)}\right]^2 - (1-\eta)\sin^2\varepsilon\right]\left[u^2 + (0.7\pi\, n D_P)^2\right]} \tag{C.17}
$$

The assumption that the wake factor for the propeller is zero in the fourth quadrant leads to the conclusion that with (C.17) the wake factor for the rudder angles should be zero **[C.2]**. However during regression analysis non-zero values are obtained. This is due to the overestimation of the inflow velocity.

Moreover (C.17) gives a discontinuity with the third quadrant. When the propeller rates decreases by 0.15 n_0 a linear interpolation between (C.18) and (C.22) yields however satisfactory results. The continuity between the first and the fourth quadrant can also be determined. At zero propeller rate, sin ε = -1, (C.17) is written as:

$$
u_R = (1-w_R)|u|\sqrt{\left[\eta\left[(k-1) + k\sqrt{(C_T+1)}\right]^2 - (1-\eta)\right]} \approx 0.4(1-w_R)|u| \text{ for model D} \tag{C.18}
$$

While in bollard pull conditions, u = 0, sin ε = 0, the following is found:

$$
u_R = 0.7\pi\, n D_P (1-w_R)\sqrt{[\eta k^2 C_T]} \tag{C.19}
$$

The formula for the first quadrant, (C.9), gives for bollard pull conditions:

$$u_R = 0.7\pi\, nD_P\zeta\sqrt{[\eta k^2 C_T]} \qquad (C.20)$$

The velocity in open water conditions, $w_R = 0 = w_T$, has no discontinuities. On the other hand when the rudder is located behind the ship, the assumption that k equals K_m leads to discontinuities between the first and the fourth quadrant. The differences in the resulting forces can be up to 20%.

Expression (C.17) has been used to model the inflow velocity in the first mathematical model as described in Chapter 6. To avoid the discontinuities a better expression has been found. It can be assumed that for equal propeller rates the inflow velocity in the fourth quadrant is never larger than the inflow velocity at the corresponding positive velocity in the first quadrant.

(C.17) always yields positive inflow velocities and is an overestimation of the real inflow velocity near the rudder. If the difference between (C.17) and (C.18) is considered, the inflow velocity at the rudder turns zero once the propeller rate turns zero. However the real value in this case is $(1\text{-}w_R)u < 0$. As a consequence the following model is proposed for the inflow velocity in the fourth quadrant:

$$u_R = (1-w_R)\begin{cases}\sqrt{\left[\eta\left[(1-k)\sin\varepsilon + k\sqrt{(C_T+\sin^2\varepsilon)}\right]^2 - (1-\eta)\sin^2\varepsilon\right]\left[u^2+(0.7\pi\, nD_P)^2\right]} - \\ |u|\sqrt{\left[\eta\left[(k-1)+k\sqrt{(C_T+1)}\right]^2-(1-\eta)\right]} + \\ u\end{cases} \qquad (C.21)$$

Rudder forces in the fourth quadrant have been modelled using (C.17) or (C.21). Again it has been assumed that $k = K_m$. Models were built for both k = 0.8 and k = 0.94, see Figure C.3.

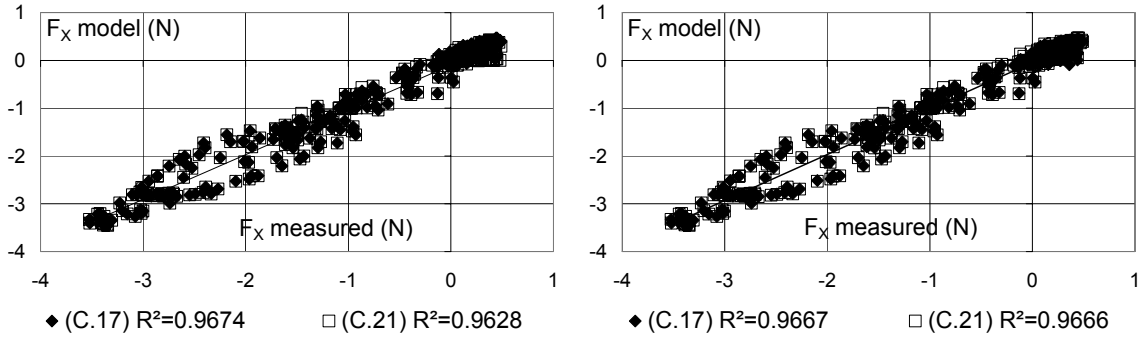

a. $K_m = k = 0.8$ a. $K_m = k = 0.94$

Figure C.3. F_X: ship model D, comparison between measured and predicted forces, 26% under keel clearance above a solid bottom, quadrant IV, different drift and yaw angles.

The differences between equations (C.17) and (C.21) are marginal. However when k = 0.8 negative wake factors are needed, k is therefore chosen to be

0.94. (C.21) is used for the mathematical models in Chapters 9 and 10. Moreover the wake factors due to rudder action in the fourth quadrant tend to zero, which approves the assumption that (C.21) gives a better approximation of the inflow velocity at the rudder.

The major part of the rudder inflow is due to propeller action. When the propeller pushes the water away from the rudder, which is the case in quadrants II and III, the inflow of the rudder, and consequently the forces acting on the rudder will be smaller. In quadrants II and III a more simplified formula to define the inflow velocity will be used. The inflow velocity u_R varies more or less linearly with the propeller rate n, so that:

$$u_R = \xi \times n + (1-w_R)u \qquad \text{(C.22)}$$

The wake factors in quadrant III are equal to those from quadrant IV, while the wake factors from quadrant II are equal to those from quadrant I. In this way all possible discontinuities between the quadrants are eliminated when (C.9), (C.21) and (C.22) are used to predict the inflow velocity.

C.3 Conclusions

In this appendix expressions to predict the inflow velocity at the rudder have been discussed. Some useful expressions have been found based on the momentum theory. Although some simplifications have been made a good correlation is found between the measured and the predicted values, with wake factors for the rudder forces that only depend on the rudder angle, and not on the propeller loading.

C.4 References

[C.1] BRIX J. (Editor). *Manoeuvring Technical Manual*. Seehafen Verlag GmbH, Hamburg, 1993.

[C.2] ELOOT K. *Selection, Experimental Determination and Evaluation of a Mathematical Model for Ship Manoeuvring in Shallow water.* Doctoral thesis, Ghent University, Faculty of Engineering, 2006, 414 pp.

[C.3] THE RESEARCH COMMITTEE OF DYNAMIC PERFORMANCE, MANOEUVRING AND CONTROL SECTION. *Prediction of manoeuvrability of a ship.* Bulletin of the Society of Naval Architects of Japan, No. 668, 1985.

APPENDIX D: EXECUTION OF REGRESSION ANALYSIS

D.1 Introduction

A considerable, and usually hidden, part of the research went to the execution of regression analysis. The large amount of data was not only a scientific challenge, but also a computational one. In this appendix the regression method and the corresponding software will be discussed.

D.2 Regression method

The core algorithm used to carry out the regression analysis is an efficient an stable trust region Levenberg-Marquardt method. The method has been described in **[D.1,D.2]**. The authors of the algorithm have also developed a software package called ODRPACK **[D.3,D.5]**. ODRPACK stands for *weighted orthogonal distance regression*, which is finding the parameters that minimize the sum of the squared weighted orthogonal distances from a set of observations to the curve or surface determined by the parameters. The package can also be used to solve the nonlinear ordinary least squares problem.

The original software **[D.5]** has been written in ANSI Fortran 77 subroutines, which are freely available for download. The author has upgraded the software to Fortran 95 code **[D.6]**, so that a better implementation and more modern coding style could be achieved.

In this paragraph a brief summary of the used regression model will be given, based on **[D.3]**. Let f be the model that defines the relationship between different variables. f can be either linear or nonlinear in its parameters β^*. One of the variables (measured force) is a response dependent upon the remaining variables (ship's speed, propeller rate, …), which are called the explanatory variables.

A mathematical model f gives the prediction of the response y in function of the explanatory variables x. The models are always explicit, i.e.

$$y \approx f(x;\beta^*) \tag{D.1}$$

y is assumed to be only approximately equal to $f(x;\beta^*)$ because of the possible measurement errors in both y (ε^*) and x (δ^*). (D.1) can therefore be rewritten as:

$$y = f(x+\delta^*;\beta^*) - \varepsilon^* \tag{D.2}$$

The problem is then find the unknown coefficients β^* so that the orthogonal distances from he curve $f(x;\beta)$ are minimized. This is accomplished by the minimization problem. Suppose there are n observations, the task is then to find:

$$\min_{\beta^*,\delta^*,\varepsilon^*} \sum_{i=1}^{n} \left(\varepsilon^{*2}_i + \delta^{*2}_i \right) \tag{D.3}$$

subject to the constraints

$$y_i = f(x_i + \delta^*_i; \beta^*_i) - \varepsilon^*_i \tag{D.4}$$

Eliminating ε^* from (D.3) using (D.4) leads to:

$$\min_{\beta^*,\delta^*} \sum_{i=1}^{n} \left(\left[f_i(x_i + \delta^*_i; \beta^*_i) \right] + \delta^{*2}_i \right) \tag{D.5}$$

which is the orthogonal distance regression (ODR) problem. The user must supply starting values for the coefficients β*. Good starting values are extremely important in order to have a convergent solution.

A major advantage of the ODRPACK is that the user can set boundaries for the coefficients β*. This feature resulted especially useful when determining physically acceptable fluidization parameters, see Chapter 10.

D.3 Software package

The different steps to be taken in the determination of the regression coefficients using (D.5) are:

- Select the response variable (the forces acting on the vessel in the horizontal plane: X, Y or N, the propeller thrust and torque or the forces acting on the rudder) in function of the explanatory variables (the velocities and accelerations in the horizontal plane, the propeller rate or the rudder deviation);
- Filter the data depending on the scope (model for one or more under keel clearances, for acceleration dependence or not, etc.);
- Define the regression model;
- Prepare the input files for the regression subroutines (response variable explanatory variables, starting values for the coefficients);
- Calculate;
- Read the coefficients with their standard deviations and write them in a standard result format. This can be preceded by one or more preliminary actions, such as performing interpolations.

To be able to manage this flow the author has written a comprehensive program in Visual Basic.NET **[D.4]**. The regression program itself is compiled from an update of **[D.5]**, written by the author, to Fortran 95. The resulting .exe regression routines can then be called by the Visual Basic.NET program.

In practice the dpt-files, see 1.2.1.2, or krt-files are read for one or more under keel clearances and/or bottom conditions. The data are stored into two-dimensional arrays. In case of the determination of the fluidization model, see

Chapter 10, those huge arrays needed a lot of computer memory. So, for future reference, a lot of computing time can be won by using a databank application.

D.4 References

[D.1] BOGGS P.T., BYRD R.H., SCHNABEL R.B. *A stable and efficient algorithm for nonlinear orthogonal distance regression.* SIAM Journal on Scientific and Statistical Computing, Volume 8, no 6, 1987, p 1052-1078.

[D.2] BOGGS P.T., BYRD R.H., DONALDSON J.R., SCHNABEL R.B. *Algorithm 676 – ODRPACK: software for Weighted Orthogonal Distance Regression.* ACM Transactions on Mathematical Software, Volume 15, n0 4, 1989, p 348-364.

[D.3] BOGGS P.T., BYRD R.H., ROGERS J.E., SCHNABEL R.B. *User's reference guide for ODRPACK Version 2.01. Software for Weighted Orthogonal Distance Regression.* U.S. Department of Commerce, National Institute of Standards and Technology, Center for Computing and Applied Mathematics, 1992, 113 pp.

[D.4] HTTP://MSDN.MICROSOFT.COM/VSTUDIO/

[D.5] HTTP://WWW.NETLIB.ORG/ODRPACK/

[D.6] HTTP://WWW.QTSOFTWARE.DE/DVF/DVF/INDEX.HTML

APPENDIX E: DISCUSSION ON SCALING EFFECTS

E.1 Introduction

In muddy areas not only the common scaling problem related to model testing exists, but also additional questions arise:

- What is the effect of the viscosity of the mud layer on the scalability?
- Have the undulations of the interface a (local) influence on the vessel's resistance?

This appendix provides a discussion concerning those topics.

E.2 Scaling

E.2.1 Reynolds or Froude

With the execution of model tests all variables need to be scaled. Different ways exist for scaling, one of them being Froude's law, i.e. the Froude numbers are equal for both the model (m) and the ship (S):

$$\frac{V_m}{\sqrt{gL_m}} = \frac{V_S}{\sqrt{gL_S}} \qquad \text{(E.1)}$$

This expresses mainly that the ratio between inertia and gravitation is equal both on model scale and on real scale. With (E.1) the other variables can be scaled:

- dimensions, risings, movements: nature value = λ (model value);
- surfaces: nature value = λ^2 (model value);
- Volumes, weights, forces: nature value = λ^3 (model value);
- Moments: nature value = λ^4 (model value);
- velocities: nature value = $\lambda^{½}$ (model value);
- propeller rates: nature value = $\lambda^{-½}$ (model value).

In the experimental research program, as described in Chapter 4, λ = 75 was determined as the scale factor. Another way of model testing is to follow Reynolds' law, i.e. the Reynolds numbers are equal for both the model (m) and the ship (S):

$$\frac{V_m L_m}{v_m} = \frac{V_S L_S}{v_S} \qquad \text{(E.2)}$$

(E.2) is equivalent with expressing that the ratio of inertia and viscous forces is equal for the model and the ship. With (E.2) the other variables can be scaled.

Considering that both model and ship navigate in the same fluid, one can determine that velocities have to be scaled according $1/\lambda$, or a model of scale 1/75 needs to be tested at 75 times the speed of the real vessel. This disadvantage and the fact that in ship hydrodynamics the presence of a free surface increases the importance of gravity forces make model testing using Froude's law a better option.

The neglect of Reynolds' law results in an erroneous scaling of the friction force. This friction is mainly of importance for the resistance of the ship. Indeed, the ship resistance can be written as a sum of **[E.9]**:

- Frictional resistance: the hull of the ship penetrates continuously the fluid, which has to be accelerated to maintain the boundary layer. The hull has to deliver continuously energy to the fluid;
- Viscous pressure resistance: the boundary layer changes the virtual form and length of the ship. As a consequence the pressure distribution along the ship changes;
- Wave making resistance: the energy needed to maintain the wave system on the water air interface.

In which the first two parts are viscous resistance parts (Reynolds), while the latter is related to gravity (Froude). The frictional resistance coefficient is not expected to change significantly as the under keel clearance becomes small **[E.3]**. This is based on the fact that the flow beneath a ship in shallow water conditions can be modelled as a Couette flow between two flat plates. The shallow water effect mainly consists in an increase of wave making resistance due to the changed wave pattern in shallow water. The increase in frictional resistance is principally due to the two-dimensional nature of the flow in shallow water, which confirms the observations of **[E.7]**.

In case of a mud layer the following can be added to the resistance:

- Undulations occur at the water mud interface as well, so an additional wave making resistance is generated;
- When the ship navigates in contact with the mud layer, the hull is in contact with two different fluids, this will have its effect on both the frictional and viscous pressure resistance;
- The undulations of the water mud interface cause a different speed distribution, see Figure 3.7, which can have an effect on the viscous resistance parts, even when the ship is not in contact with the mud layer.

As a consequence additional corrections are needed, even when there is no mud layer, which are based on the splitting up of the non-dimensional total resistance coefficient into a frictional part and a rest fraction, the latter being considered the same for the model and the ship. The 1978 ITTC Performance Prediction Method is hereby used.

It will be assumed that the shallow water effect on the frictional resistance coefficient as described in **[E.3]** is still valid above a mud layer, in spite of the fact that the top of a mud layer cannot be considered as a flat plate.

E.2.2 The 1978 ITTC Performance Prediction method [E.4]

General

The total measured resistance of the ship model when navigating ahead at constant speed and at zero drift angle can be written as:

$$C_{TM} = \frac{X'(\beta = 0°, 180°)}{S} LT \tag{E.3}$$

S is the wetted surface of the hull (m²).

The total resistance can be split into:

$$C_{TM} = (1+k)C_{FM} + C_R \tag{E.4}$$

With

- C_{FM}: the frictional resistance coefficient of the ship model (or of the ship: index S instead of M):

$$C_F = \frac{0.075}{\left(\log\frac{VL}{v} - 2\right)^2} \tag{E.5}$$

- k: the form factor, to be determined with model tests at a low Reynolds number or using the empirical formula of PROHASKA:

$$k = 0.11 + 0.128\frac{B}{T} - 0.0157\left(\frac{B}{T}\right)^2 - 3.10C_B\frac{B}{L} + 28.8\left(C_B\frac{B}{L}\right)^2 \tag{E.6}$$

- C_R: the coefficient of the rest fraction of the resistance

The total resistance of the ship can then be written as:

$$C_{TS} = (1+k)C_{FS} + C_R \tag{E.7}$$

Correction for any drift angle

The frictional resistance is considered of main importance in the longitudinal direction of the vessel. At a drift angle of +/- 90 degrees the movement of the ship is only lateral and no correction will be applied. For intermediate conditions, the following method can be used:

X'(β) can be written as:

$$X'(\beta) = \frac{X(\beta)}{\frac{1}{2}\rho LT(u^2+v^2)} = \frac{X(\beta)}{\frac{1}{2}\rho LTu^2(1+\tan^2\beta)} = \frac{X(\beta)}{\frac{1}{2}\rho LTu^2}\cos^2\beta \qquad \text{(E.8)}$$

The factor $\cos^2\beta$ can be used to apply the correction; it takes 1 for $\beta = 0°$ or 180° and zero for $\beta = 90°$, so that the correction can be applied as:

$$X'(\beta)_{corr} = \cos^2\beta\, X'(\beta)\frac{C_{TS}}{C_{TM}} + \sin^2\beta X'(\beta) = X'(\beta)\left(\frac{C_{TS}}{C_{TM}}\cos^2\beta + \sin^2\beta\right) \qquad \text{(E.9)}$$

E.2.3 The 1978 ITTC Performance Prediction method, applied to mud layers

In **[E.2]** a quick method has been used to correct the resistance only when a ship navigates in contact with the underlying mud layer. In this case a part of the wetted surface S_{water} is in contact with water, having a kinematical viscosity ν_{water}, while the other part S_{mud} is in contact with a mud layer having viscosity ν_{mud}. The calculation of the wetted surfaces S_{water} and S_{mud}, is based on the static draught. Due to squat and undulations of the interface, some minor differences can occur.

The two parts of the wetted surface that are in contact with different fluids will have a different frictional resistance. The frictional resistance coefficient can be written as:

$$C_F = \frac{0.075}{\left[\log\left(\frac{VL}{S}\left(\frac{S_{mud}}{v_{mud}} + \frac{S_{water}}{v_{water}}\right)\right) - 2\right]^2} \qquad \text{(E.10)}$$

In (E.10) a weighted average of the Reynolds number is thus determined to define the frictional resistance coefficient. This is as if the ship were in contact with one virtual fluid having the weighted viscosity. A better option would have been the determination of a weighted C_F:

$$C_{F,total} = C_{F,water}\frac{S_{water}}{S} + C_{F,mud}\frac{S_{mud}}{S} \qquad \text{(E.11)}$$

(E.10) and (E.11) generate resistance reductions of the same magnitude for mud layers of higher viscosity, but in case of lower viscosities a more significant reduction is yielded with (E.11).

E.3 Mud effects on resistance scaling

The use of the conservative approach (E.10) gave acceptable results for the Zeebrugge pilots during simulation runs, see Chapter 8. Nevertheless it should

definitely be confirmed by full scale measurements where the ship's speed is recorded so that the resistance can be derived.

Moreover (E.10) only takes the effect of the wetted surface in contact with the mud layer into account. In this paragraph the other effects of the mud layer on the resistance and the scaling will be discussed.

E.3.1 Additional wave making resistance

Several authors **[E.5, E.8]** put forward that the energy needed to invoke the undulations of the water mud interface will have a significant effect on the resistance, which can explain the S-curve (see for example Figure 3.3) for the speed-rpm relationship.

On the other hand the undulation still occurs at higher speeds **[E.6]**, but abaft the ship, so the same energy is still needed without an additional increase in resistance. Moreover the energy contained in the undulation at the water mud interface is proportional with the difference in densities between both fluids **[E.1]**, which is relatively small.

The drop in the speed rpm relationship in Figure 3.3 cannot be ascribed to an increased resistance due to the undulations of the water mud interface, as the contained energy is too small. Although it cannot explain this drop, there will be a small additional wave making resistance when navigating in muddy areas.

E.3.2 Effect of the vertical speed distribution

Together with the (small) additional wave making resistance, the resistance will change due to the different vertical distribution of the velocities. In **[E.6]** a method has been described to determine the resistance, based on a strip theory. The velocity for each strip of the vessel and the corresponding frictional force are determined based on the results of the model scale experiments at Flanders Hydraulics Research (3.2.2). This method implies that for any condition the profile of the interface has to be known.

E.4 Conclusions

The specific problems regarding scaling effects in muddy areas have been discussed. In this dissertation it is assumed that the frictional resistance coefficient can be determined using (E.10). This is a conservative approach that can be corrected once more results of full scale measurements are available. Furthermore the additional wave making resistance and the effect of the vertical speed distribution are assumed to be equal on both model scale and full scale. Following Froude's law the density and viscosity of the mud layer have to be equal for model and full scale.

E.5 References

[E.1] DALRYMPLE R.A., LIU PHILIP L.-F. *Waves over Soft Muds: A Two Layer Fluid Model.* Journal of Physical Oceanography, Volume 8, 1978, p. 1121-1131.

[E.2] DELEFORTRIE G., LAFORCE E., VANTORRE, M. *Bepaling van de nautische bodem in de haven van Zeebrugge: onderzoek nautische implicaties. Fase B: eigenlijke onderzoeksfase.* Final report. Research project UGent 51H01200, WL Mod. 582B. Ghent / Antwerp, 2004. (In Dutch).

[E.3] GOURLAY T. *Flow beneath a ship at small under keel clearance.* Journal of Ship Research, Vol. 50, No. 3, 2006, p 250-258.

[E.4] HTTP://ITTC.SNAME.ORG/

[E.5] KERCKAERT P., VANDENBOSSCHE D., MALHERBE B., DRUYTS M., VAN CRAENENBROECK K*. Maintenance dredging at the port of Zeebrugge: procedures to achieve an opertational determination of the nautical bottom*. KVIV Harbour Congress, 1988.

[E.6] LASURE K. *Invloed van los slib op weerstand en propulsie van een schip.* M. Sc. Thesis, Faculty of Engineering, Ghent University, Ghent, 1989. (In Dutch).

[E.7] SCHLICHTING O. *Schiffwiderstand auf beschränkter Wassertiefe: Widerstand von SeeSchiffen auf flachem Wasser*. Jahrbuch der Schiffbautechnischen Gesellschaft, Vol. 35, No. 127, 1934. (In German)

[E.8] SELLMEIJER R., VAN OORTMERSSEN G. *The effect of mud on tanker manoeuvres.* The Royal Institution of Naval Architects, Spring Meetings 1983, paper no. 7, 1983.

[E.9] VANTORRE M. *Maritieme hydrostatica en hydrodynamica II, Hoofdstuk 6: Scheepsweerstand*, M. Sc. Course, Ghent University, 2001. (In Dutch).

APPENDIX F: PORT MAP OF ZEEBRUGGE

PORT MAP

01"Zand" access channel
02 Wielingen dock
03 Albert II dock
04 Brittannia dock
05 Pierre Vandamme lock
06 Connection dock
07 Northern Inlet dock
08 Southern Canal dock
09 Visart lock
10 Baudouin canal
11 Projected Northern canal
12 Prince Albert dock
13 Prince Philip dock
14 Ferry dock
15 Leopold canal
16 Schipdonk canal

21 Western breakwater
22 Eastern breakwater
23 L.N.G.-dam
24 Leopold II-dam
25 Naval base

ROLL-ON/ROLL-OFF HANDLING

30 Toyota Terminal
31 C.T.O. - HNN terminal (Wielingen dock)
32 Sea-Ro Terminal - StoraEnso(Wielingen dock)
33 P&O Ferries Terminal
34 Superfast Terminal
35 Sea-Ro Terminal (Swedish Quay)
36 Sea-Ro Terminal (Hermes Quay-Brittannia dock-Minerva square)
37 Sea-Ro Terminal (Canada terminal)
38 CdmZ
39 Wallenius Wilhelmsen terminal
40 Sea-Ro Terminal
41 C.T.O. Terminal
42 C.T.O. Terminal
43 Roro terminal

CONTAINER HANDLING

45 APMT Container Terminal Albert II Dock South
46 OCHZ - HNN
47 Projected container terminal - HNN

GENERAL CARGO HANDLING

51 Multipurpose terminal C.T.O.
52 Fruit terminal B.N.F.W. (Sea-Invest)
53 Flanders Cold Center (Sea-Invest)
54 Tropicana

BULK HANDLING

61 Tameco
62 Nieuwpoortse Handelsmaatschappij
63 Alzagri
64 Seaport Shipping & Trading
65 Minne Port Services
66 Hanson

GAS

71 L.N.G. terminal (Fluxys)
72 Zeepipe-terminal (Statoil)
73Interconnector-terminal (Interconnector Baczee)
74 Peakshaving installation (Fluxys)

DISTRIBUTION

75Transportzone Zeebrugge (T.Z.Z.)
76 Bridgestone
77 European Fish Centre (E.F.C.) (Zeebrugse Visveiling ZV)

Planned Port Area
Industry
Existing waterways or docks
Waterways or docks planned or under construction
Residential areas

Roads
Railways
Natural gas pipeline
Wind turbines
Radar tower
Roro installations

Source: http://www.portofzeebrugge.be/images/plannen/havenplan2005_print_e.jpg